TERMINAL REPORT

Sago Project II.3:
Mapping Sago Habitats and Sago Suitable Sites Using Optical and Radar Image Analysis and Suitability Relationships

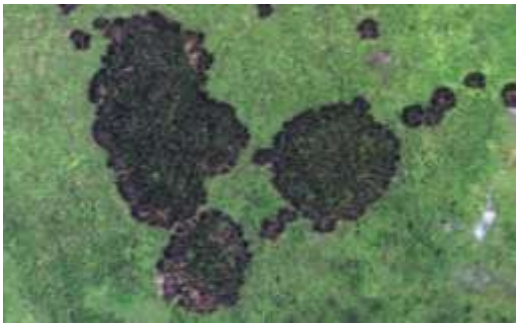




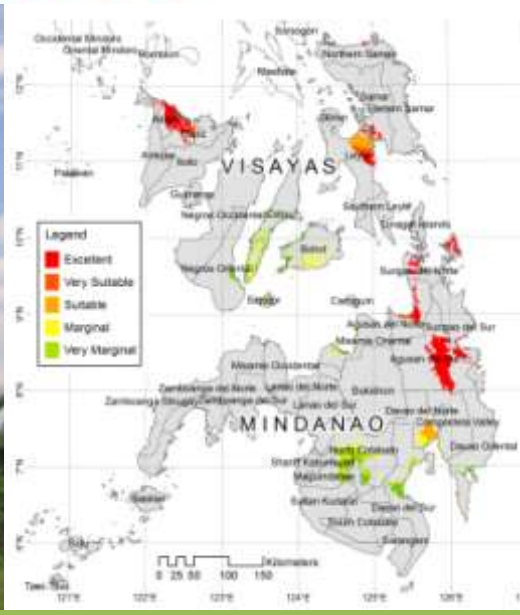

Training Center for Applied Geodesy and Photogrammetry

UNIVERSITY OF TH E PHILIPPINES
Diliman, Quezon City

Terminal Report

Sago Project II.3: Mapping Sago Habitats and Sago Suitable Sites Using Optical and Radar Image Analysis and Suitability Relationships

Engr. Jojene R. Santillan
(Project Leader)

Engr. Richelle L. Francisco
(Science Research Specialist I, Jan. – July 2012;
Science Research Specialist II, July – Oct. 2012)

For. Jezleer T. Montajes
(Science Research Specialist I, July – Dec. 2012;
Science Research Associate, Jan – June 2013)

Ms. Ma. Elena C. Ignacio
(Project Staff, L2)

Training Center for Applied Geodesy and Photogrammetry
University of the Philippines
Diliman, Quezon City
(Implementing Agency)

Philippine Council for Industry, Energy and Emerging Technology Research and Development
Department of Science and Technology
(Funding Agency)

January 1, 2012 – June 30, 2013
(Period of Implementation)

Summary

Program Title:	Sago Bioresource Assessment for Sustainable Industry Utilization Using Remote Sensing Geospatial Analyses and Suitability Relationships
Project Title:	II.3 Mapping Sago Habitats and Sago Suitable Sites Using Optical and Radar Image Analysis and Suitability Relationships
Project Leader:	Engr. Jojene R. Santillan
Research Staff:	Engr. Richelle L. Francisco (Science Research Specialist I, Jan. – July 2012; Science Research Specialist II, July – Oct. 2012) For. Jezleer T. Montajes (Science Research Specialist I, July – Dec. 2012; Science Research Associate, Jan – June 2013)
Project Staff L2:	Ms. Ma. Elena C. Ignacio
Implementing Agency:	Training Center for Applied Geodesy and Photogrammetry University of the Philippines, Diliman, Quezon City
Cooperating Agencies:	1. Caraga State University 2. University of the Philippines-Mindanao
Duration of the Project:	January 1, 2012 – June 30, 2013
Source of Fund:	Philippine Council for Industry, Energy and Emerging Technology Research and Development, Department of Science and Technology (PCIEERD DOST)

Acknowledgements

The Philippine Council for Industry, Energy and Emerging Technology Research and Development – Department of Science and Technology (PCIEERD DOST) is gratefully acknowledged for the funding and numerous supports to the project. We are grateful to its former and current Executive Directors, Dr. Amelia P. Guevara and Dr. Rowena Cristina L. Guevara, for trusting us in undertaking this research. We also acknowledge the assistance of Engr. Nelson Beniabon, Ms. Claire Reyes and Ms. Mary Joy Buitre of DOST PCIEERD for all their assistance.

We also acknowledge the contribution of Dr. Enrico C. Paringit of the UP Department of Geodetic Engineering & Training Center for Applied Geodesy and Photogrammetry. His effort to gather researchers from UP Mindanao, Caraga State University and UP Diliman was very instrumental in the conceptualization of this project

We are also thankful for the field work assistance of the Sago Project II.2 team of Caraga State University namely, Engr. Meriam Makinano-Santillan (Project Leader), Engr. Michelle V. Japitana (Project Staff, L2), Engr. Arnold Apduhan (Research Assistant) and their students namely Arthur M. Amora, Linbert Cutamora, Dylan Dikraven Galavia and Cherry Bryan G. Ramirez.

We are grateful to Dr. Dulce M. Flores of UP Mindanao for inspiring us and for sharing her knowledge about the Sago palm and all the food and non-food uses that can be derived from the starch of this palm. We also thank her for accommodating us when we visited Argao, Cebu last August 2012.

The UP Mindanao project team of Dr. Nilo P. Oponda and Mr. Adrian Almeria is also acknowledge for sharing their ground truth data of Sago palm stands in La Paz and Veruela, Agusan del Sur. We thank Dr. Oponda, Dr. Flores and Dr. Anna Novero and their teams for accommodating us when we visited UP Mindanao last February 2013.

The National Mapping and Resource Information Authority (NAMRIA) is also acknowledged for providing the ALOS AVNIR-2 images used in this study. The Envisat ASAR data was provided by the European Space Agency through Category 1 Project No. 11044. ASTER GDEM used in this project is a product of METI and NASA.

We would like to acknowledge the administrative support and cooperation of the UP Department of Geodetic Engineering & Training Center for Applied Geodesy and Photogrammetry through its Chairman and Director, Dr. Ariel C. Blanco and its Administrative Officer, Ms. Ellen Cruz-Ignacio.

Lastly, the Project Leader, Engr. Santillan, extends his appreciation to the project researchers, Engr. Richelle L. Francisco and For. Jezleer T. Montajes, for their important contributions in the implementation and completion of this project.

Table of Contents

List of Figures

List of Tables

List of Abbreviations

ALOS	Advance Land Observing Satellite
ANN	Artificial Neural Network
ASAR	Advanced Synthetic Aperture Radar
ASTER	Advanced Spaceborne Thermal Emission and Reflection Radiometer
AVNIR-2	Advanced Visible and Near Infrared Radiometer type 2
DEM	Digital Elevation Model
Envisat	Environmental Satellite
ESA	European Space Agency
ETM+	Enhanced Thematic Mapper plus
GDEM	Global Digital Elevation Model
GLOVIS	Global Visualization Viewer
GIS	Geographic Information System
HSM	Habitat Suitability Modeling
MLC	Maximum Likelihood Classifier
NAMRIA	National Mapping and Resource Information Authority
NDVI	Normalized Vegetation Index
OLI	Operational Land Imager
ROI	Region of Interest
RS	Remote Sensing
SAR	Synthetic Aperture Radar
SRTM	Shuttle Radar Topography Mission
SVM	Support Vector Machine
VNIR	Visible Near Infra-red
WV-2	Worldview-2

Abstract

The Sago Project II.3 is part of a program funded by PCIEERD DOST, entitled “Program II: Sago Bioresource Assessment for Sustainable Industry Utilization Using Remote Sensing Geospatial Analyses and Suitability Relationships”. The combined outputs of the three projects under this program aim to provide a better assessment of Sago palm availability in Visayas and Mindanao by mapping their actual location, distribution and availability and identifying the basic characteristics of their habitats and environment. This will then lead to the assessment on the potential yield and bioresource availability of Sago for sustainable industry utilization. Among the three projects, Project II.3 provides location and areal statistics of existing Sago palm habitats as well as areas that are suitable for Sago palm propagation in Visayas and Mindanao.

The project was conducted through an integrated approach utilizing optical and radar remotely-sensed images and use of statistical and GIS-based suitability analysis. Field measured spectral reflectance of Sago palms and other palm species were analyzed to obtain information necessary for their detection and identification in medium and high resolution optical images. Medium resolution images such as Landsat 7 ETM+, ALOS AVNIR-2 and Envisat ASAR were then analyzed to detect possible locations of Sago palm habitats in various provinces in Visayas and Mindanao. The areas to look for Sago palm habitats were narrowed down through the use of species distribution modeling which considerably reduced areal coverage of image analysis while maintaining acceptable accuracy of detecting actual locations of Sago palm.

The detected possible locations of Sago palms in Visayas and Mindanao were examined with the aid of data from field surveys, and recent high resolution Worldview-2 images (purchased and those available in Google Earth) for their confirmation if they are indeed Sago palms or just results of misclassifications. Refinements in the extents of Sago palm stands were done during this stage.

Sago palm stands were confirmed in 4 provinces in Visayas and 13 provinces in Mindanao, with a total aggregated area of 914.04 hectares. In Visayas, all the confirmed Sago palm stands have an aggregated area of 252.87 hectares. Sago palms were found to be most abundant in Leyte (215.70 has.), followed by Cebu (19.54 has) and Aklan (17.59 has). None of the confirmed Sago palms in Visayas are within protected areas.

In Mindanao, all the confirmed Sago palm stands have an aggregated area of 661.17 hectares. Of this, 337.92 hectares are within protected areas, majority of which is found in Agusan del Sur, specifically in the La Paz and Bunawan municipalities. In these municipalities, 337.87 hectares of Sago palm stands are within the Agusan Marsh Wild Life Sanctuary. At the provincial level, Agusan del Sur has the highest total aggregated area of confirmed Sago palm stands (570.29 has), followed by Agusan del Norte (44.81 has), Sulu (19.67 has), Maguindanao (17.68 has), and Davao Oriental (2.72 has).

Habitat suitability analysis of Sago palms in Visayas and Mindanao was aided by exploratory statistical analysis that determined the biophysical and bioclimatic characteristics of known Sago palm habitats. The information derived from the statistical analysis was then used in conjunction with bioclimatic models to create suitability rules that are then used to search for

lands in Visayas and Mindanao where Sago palms can grow at a spatial resolution of one hectare (100 m x 100 m). The suitability map that was generated has a prediction accuracy of 93.52%. Based on the suitability map, a total of 999,491 hectares of lands in Visayas and Mindanao were found to be biophysically and bioclimatically “suitable” for growing Sago palms. Of this, 415,260 hectares have “excellent” suitability while 104,020 hectares are “very suitable”. The municipalities with confirmed Sago palm stands and with "very suitable" to “excellent” suitabilities were also identified in Visayas and Mindanao. If Sago palms are to be mass propagated, then these municipalities should be targeted since in these municipalities there is proof that Sago palms can actually grow. In Visayas, majority of these municipalities are in Leyte and Aklan. In Mindanao, majority are found in Agusan del Sur, Agusan del Norte, Surigao del Sur and Surigao del Norte.

Chapter 1. Introduction

1.1 Background

The Sago palm (*Metroxylon sagu Rottb.*), as shown in Figure 1 and Figure 2, is well known for its rich starch contents [**1**] and as a significant source of other raw materials of high economical value [**2**]. Although the initial waiting period is long (up to 10 years for the plant to be harvestable), Sago is considered to be the highest starch producer at 25 tons per hectare per year [**3**]. It is now grown commercially in Malaysia, Indonesia and Papua New Guinea for production of Sago starch and/or conversion to animal food or fuel ethanol [**4**]. The largest Sago palm plantation can be found in Sarawak, Malaysia wherein between 30,000 to 50,000 tons of Sago starch have been exported annually, procuring incomes of between US$3.4 million to US$10.8 million [**3**].

Figure 1. Stands of Sago palms as photographed in Argao, Cebu on August 11, 2012.

Aside from its economic benefits and as potential source of raw material for biofuel production, there are also environmental benefits in the propagation of Sago palms. Its large fibrous root system traps silt loads and removes pollutants, faecal contaminants, and heavy metals [**5**]. Sago forest also acts as an excellent carbon sink for carbon sequestration, thereby mitigating the greenhouse effect and global warming arising from the release of carbon dioxide into the atmosphere due to industrialization, and increase in the number of motorized vehicles [**5**] [**6**]. Throughout the years, interest in Sago palm has increased considerably because of its advantages of being economically acceptable, relatively sustainable, environmentally friendly, uniquely versatile, vigorous, and promotes socially stable agroforestry systems [**1**], [**6**].

In the Philippines, the mass propagation and commercial utilization of Sago palm has gained interest from the government in planning to develop and sustain a large-scale Sago starch industry that can supply raw materials for food and non-food uses, as well as for production of high value products such as ethanol and lactic acid. To be able to compete in the world market, the Philippines has to increase its supply of Sago through the development of plantation-scale Sago production [**7**]. However, information on the present location and distribution of Sago palms is incomplete, and it cannot be ascertained whether there is enough supply of Sago to drive and sustain a large scale Sago starch industry. Therefore, mapping the location of existing Sago palms is necessary in order to determine current supply as well as to characterize its habitat. Once these characteristics have been identified, it is then possible to locate other areas that have the same habitat characteristics for Sago palms to grow.

Figure 2. Stands of Sago palms as photographed in Bunawan, Agusan del Sur on May 9, 2012.

Large clusters of Sago palms have been reported to exist in marshlands and other wetlands of Mindanao and in some islands in the Visayas. A thorough mapping of the locations of these clusters is not only difficult due to in-accessability; it is also expensive especially when done using conventional field mapping techniques. The use of remote sensing data and GIS techniques is considered to be the best alternative. While several studies have been reported to have used remote sensing techniques in mapping forest resources and agricultural crops (e.g., [**8**], [**9**]), nothing have been published so far that relates to the use of appropriate techniques in mapping the distribution of the Sago palm. All literatures pertaining to the location, extent and distribution of Sago palms are indicative of using conventional field survey mapping methods [**10**]. This situation opens up several opportunities for the adoption of existing RS-based techniques as starting point for mapping

of the Sago palm in RS images, which could lessen logistical and practical difficulties that are often encountered when using conventional field surveys, especially in inaccessible areas.

1.2 Previous study on Sago Palm Distribution Mapping and Suitability Analysis in Mindanao

A previous research project conducted by UP-Mindanao entitled “Program I: Conservation of a Bioresource - Project I.1 Assessing the Sago Bioresource in Mindanao Using Remote Sensing Technology” [**11**] looked into the location and distribution of Sago palm in Mindanao through the use of Remote Sensing and GIS technologies. The research project was able to identify 86,000 hectares of Sago stands in the provinces of Agusan del Norte and Agusan del Sur. The research was also able to identify suitable (850,000 has.) and probable (700,000 has) areas in Mindanao where Sago stands could be found. While the results of the research is very promising, the methodology employed was limited by several factors, among them: (i.) the use of not up-to-date satellite images which were contaminated with clouds and shadows which limited the Sago detection in areas not covered by clouds and shadows; (ii.) insufficiency in the number of ground truth samples to completely cover the land cover of interest which is the Sago palm; (iii). the spectral characteristics were not examined and it was not definite whether the spectral signatures of Sago stands and other land cover types as derived from the satellite images are unique to each land cover; and (iv.) the model used in the Sago suitability analysis assumes a linear weighted relationship between the presence of Sago and the factors considered (land cover, soil type and elevation). The suitability analysis also neglected to include some of the important factors that may affect the presence or absence of Sago palm in the area such as slope, rainfall, and soil moisture. Also, analysis of the spectral response of Sago palm was not done. The spectral response analysis is a very good and useful technique in order to discriminate Sago palm from other palm trees/plants.

Refinements in the employed methodology by the use of up-to-date medium to high resolution optical and radar images will generate more reliable estimate on the location, extent and distribution of Sago habitats.

The use of suitability relationships or rules in mapping Sago habitats using information on biophysical and bioclimatic at the actual locations of Sago palms will also provide relevant information not only on where Sago habitats thrive, but also on the type of biophysical and climatic conditions the Sago palms are well-suited. This information could then be used in conducting suitability analysis for mass propagation of Sago palms in Visayas and Mindanao.

1.3 The Sago Program II and Purpose of Project II.3

A new research program entitled “Sago Bioresource Assessment for Sustainable Industry Utilization Using Remote Sensing Geospatial Analyses and Suitability Relationships” was funded by DOST PCIEERD to conduct further assessment of Sago Palm distribution not only in Mindanao but also in Visayas. This program can be considered as a follow-up and refinement (in terms of methodologies) of the Sago Project I.1 conducted earlier by UP Mindanao. Program II consisted of 3 projects namely:

- Project II.1: GIS-Assisted Assessment on the Potential Yield and Bioresource Availability of Sago in the Wild for Sustainable Industry Utilization (Implementing Agency: UP Mindanao)
- Project II.2: Biophysical, Structural and Spectral Characterization of Sago and Its Environment (Caraga State University)
- Project II.3: Mapping Sago Habitats and Sago Suitable Sites using Optical and Radar Image Analysis and Suitability Relationships (this project)

The combined outputs of the three projects under Program II aim to provide a better assessment of Sago palm availability in Visayas and Mindanao by mapping their actual location, distribution and availability and identifying the basic characteristics of their habitats and environment. This will then lead to the assessment on the potential yield and bioresource availability of Sago for sustainable industry utilization. The inter-relationships among the three projects are shown in Figure 3.

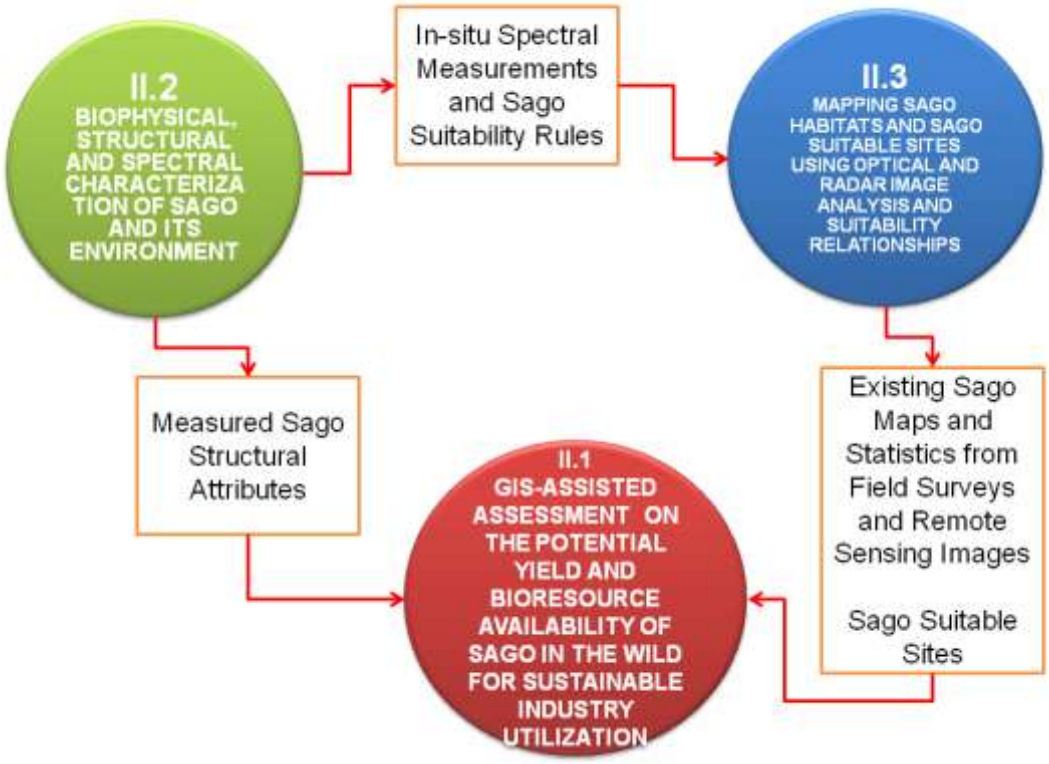

Figure 3. Interrelationships among the 3 projects under Sago Program II.

Among the three projects, Project II.3 provides location and areal statistics of existing Sago palm habitats as well as areas that are suitable for Sago palm propagation in Visayas and Mindanao.

Figure 4. Map showing the provinces in Visayas and Mindanao covered in Sago palm mapping.

1.4 Objectives

In general, this component project will conduct mapping of Sago habitats in Visayas and Mindanao (Figure 4) using an integrated approach utilizing optical and radar remotely-sensed images and use of statistical and GIS-based suitability analysis.

The specific objectives are:

i.) to analyze field measured spectral reflectance of Sago palms and other palm species to obtain information necessary for its detection and identification in medium and high resolution optical images; (this activity is done together with Sago Project II.2)

ii.) to analyze medium resolution optical and radar images for the detection and mapping possible locations of Sago palm habitats;

iii.) to confirm and refine the detected possible locations of Sago palms through the use of high resolution optical satellite images aided by field surveys;

iv.) to conduct habitat suitability analysis to derive suitability rules for mapping potential sites where Sago palm could be cultivated for mass production purposes; (this activity is done together with Sago Project II.2); and

v.) to generate thematic maps and tables containing information on the location, distribution and areal extent of Sago habitats as well as the location of sites suitable for mass propagation of the Sago palm.

1.5 Expected Outputs

At the end of this project, the following outputs will be produced:

i.) Maps showing the most recent location and distribution of Sago palm in Visayas and Mindanao;

ii.) Tabular data of estimates on the area of existing Sago habitats mapped in Visayas and Mindanao, including a list (at provincial, municipal and barangay levels) of the locations where the Sago palm habitats are located; and

iii.) Thematic maps showing the location of lands in Visayas and Mindanao that were found suitable for mass propagation of the Sago palm.

1.6 Project Significance and Target Beneficiaries

This component project will address the need by the Philippine government for timely and accurate information on the present location, distribution and extent of Sago palm stands in Visayas and Mindanao. With the thematic maps indicating the location and extent of Sago habitats derived from this project, assessments could then be made for its conservation and to determine whether there is enough supply of Sago to drive and sustain a large scale Sago starch industry.

The following are some of the beneficiaries of the project outputs, and how they may benefit from the outputs of the project:

a. The Philippine Government - the reliable and up-to-date information generated by this project will aid the government in creating plans for the development and sustainability of the Sago starch industry, as well as in drawing efforts for the conservation and mass propagation of the Sago palm.
b. The Sago starch industry - the information on the distribution and abundance of Sago palms will help the industry determine whether there is enough supply of Sago palms necessary for large scale Sago starch industry.
c. Researchers – the thematic maps derived will assist researchers in studying the geography and socio-economic aspects of the Sago palm in Visayas and Mindanao.

Biotechnology researchers will also be guided where to get samples for their research that will explore other potentials of the Sago palm.

d. LGUs - the information generated from this study will be useful for the LGUs as basis for planning and development activities to attract investments in the Sago starch industry.
e. Local community - the results of this project will inform the local community if their barangays have lands suitable for Sago palms that they can propagate that could then provide them livelihood and economic opportunities.

Chapter 2. Literature Review

2.1 Studies on Sago palm and its distribution in the Philippines

In recent years, considerable progress has been made in researches on the Sago palm (e.g., [**2**], [**12**], [**13**], [**14**], [**15**]) and its relevant environmental and socioeconomic conditions (e.g., [**16**], [**17**], [**18**], [**5**]). In spite of such progress, much remains unexplored regarding this underutilized plant resource, one of which is on the accurate mapping of its location and distribution, a basic information needed for exploring its full economic potential, and transforming it into a well-accepted industrial raw material [**1**].

In the Philippines, very few studies have been reported that explore the utilization of Sago palms as an important bioresource, including the determination of the location and distribution of these palms throughout the country (e.g., [**19**], [**10**], [**20**], [**21**], [**22**], [**23**], [**24**], [**25**]). Majority of these studies indicated that Sago palms are mostly located in Visayas and Mindanao, specifically in Northern Mindanao and in Aklan, Cebu and Leyte in Eastern and Central Visayas regions. While most of these studies provide an indication of where the Sago stands are, more accurate and up-to-date information on the exact area and distribution of the remaining Sago stands is still lacking.

2.2 Satellite remote sensing approaches in mapping resources

Satellite remote sensing (RS) technology has been extensively used to provide accurate and timely information describing the nature and extent of land resources and changes over time [**8**], [**26**]. Imageries from satellite RS platforms provide valuable sources of land-cover and other information related to topography, and surface conditions especially in areas which are difficult to monitor and could be very expensive when using conventional techniques [**27**]. For example, RS data and techniques can address the data needs of ecological studies from broad spatial extents that cannot be collected using field-based methods, which include identifying and detailing the biophysical characteristics of species' habitats, predicting the distribution of species and spatial variability in species richness [**28**].

Moderate resolution images from optical sensors such as those obtained by the Landsat satellite sensors (Multispectral scanner, Thematic Mapper, and Enhanced Thematic Mapper plus) have been widely used in land resources mapping such as land cover classification and change analysis [**29**], remote monitoring of tropical forest environments [**30**], mapping forest structures and biomass estimation [**31**], [**32**], [**33**]; and several applications in agriculture that includes agricultural area mapping [**34**], [**35**], [**36**], and crop mapping, management and yield estimations [**9**]. Recently, the availability of high resolution optical satellite images have shown excellent potential to extend satellite RS beyond what has been possible with aerial photography and moderate resolution satellite data, and had become of great interest to resource managers as a way to create timely and reliable assessments of land and water resources at a local scale [**37**]. With the use of appropriate image analysis techniques, very high resolution satellite images such as those acquired by IKONOS, Quickbird and Worldview, have been found useful in detailed mapping of forest cover and forest structure parameters [**38**], [**39**], [**40**]; species-level mapping of vegetation

habitats [**41**], [**42**]; and cropland extraction [**43**], [**44**], crop classification and mapping of their agro-environmental associated measures [**45**].

The disadvantages, however, of using optical satellite RS images in land resources mapping, specifically in forestry and agricultural mapping applications, is its restricted spectral range which in turn also restricts the amount of detail that could be extracted from the images and may induce misclassification errors due to similarities in spectral signatures of objects being mapped; the slow turnaround time, and inadequate repeat coverage is another limitation of optical RS technology [**46**] . Another limiting factor is the presence of clouds and shadows that often mask large parts of the images, thus reducing the amount of available data and prevent contiguity in time and in space [**47**]. The presence of clouds severely limits the regular exploitation optical satellite RS images in various application fields [**48**]. It is in these situations that the use of radar images, particularly, synthetic aperture radar (SAR) images are often advantageous because of its capability of not being affected by cloud cover or haze, as optical sensors are, and operate generally independent of weather conditions [**49**]. SAR data are also sensitive to dielectric and geometrical properties of vegetation, and are thus more directly related to measurements of vegetation parameters than optical data, which mainly respond to chemical properties of the vegetation constituents [**50**]. It is possible also to obtain from the SAR images information about the trunk structure (height, radius, dielectric constant), the understory structure (shape and size of components, their dielectric constant and orientation), and the forest floor, in addition to the canopy, because long wavelengths are used during image acquisitions [**51**].

Several studies have been successful in utilizing SAR images for estimating forest stand attributes [**52**], [**53**], and in agricultural applications such as rice crop growth mapping [**54**], and crop type mapping and condition assessment [**55**]. However, depending on the kinds of terrain cover types, the information provided by the SAR data alone may be not sufficient for a detailed analysis. A possible solution to this problem may be derived from the integration of SAR data with optical data (or multisensor data) of the same site acquired at a same or different time through image fusion [**56**]. This approach has been applied in land cover mapping in general [**57**], and in such specific applications to map deforestation and secondary growth forest using multiple polarization SAR and Landsat ETM+ optical images with more than 90% mapping accuracies [**58**]; to discriminate forest type using SAR and Landsat MSS images [**59**]; and for delivering operational annual crop inventories [**60**]. The synergistic combination of optical and radar RS images through image fusion techniques has resulted to an improved mapping accuracy [**56**] because information relevant for the desired mapping output has been combined resulting to a single image that is more informative than any of the input images, which is basically a combination of spectral responses from the optical images and image textures from the SAR images [**61**].

An added value of utilizing RS technology in resource mapping is the possibility of obtaining several levels of information from the RS images. In forest resource assessment, satellite remote sensing may be used to provide three levels of information [**8**]. The first level refers to the spatial extent of forest cover, the second level comprises information on forest type, and the third level provides information on the physical and biochemical properties of forests. There are currently two approaches of relating RS data to biophysical variables. In physical modeling, canopy radiative transfer processes are simulated mathematically with valuable insights into the fundamental factors driving the relationships between RS data and vegetation biophysical and biochemical properties [**62**], [**63**]. However, this approach is

hindered by factors such as the canopy heterogeneity, dynamic characteristics of the canopy optical properties and external effects such as atmospheric scattering and absorption [**8**]. An alternative approach that is more operational is empirical modeling, whereby the quantitative relationship between RS data (and various derivatives, e.g., vegetation indices) and ground-based biophysical and biochemical property data is calibrated by interrelating known coincident observations of the RS and ground data through statistical regression [**8**]. The use of radiometrically and atmospherically corrected RS data to develop an empirical model allows its application at other spatial and temporal resolutions to generate the necessary information on biophysical and biochemical properties as well as the overall distribution of the resource being mapped.

The empirical model developed through RS data – ground data calibration can also serve as an additional tool in predictive vegetation mapping. Predictive vegetation mapping can be defined as predicting the geographic distribution of the vegetation composition across a landscape from mapped environmental variables [**64**]. Computerized predictive vegetation mapping is made possible by the availability of digital maps of topography and other environmental variables such as soils, geology and climate variables, and geographic information system software for manipulating these data. Especially important to predictive vegetation mapping are interpolated climatic variables related to physiological tolerances, and topographic variables, derived from digital elevation grids, related to site energy and moisture balance. Predictive vegetation mapping is founded in ecological niche theory and gradient analysis, and driven by the need to map vegetation patterns over large areas for resource conservation planning, and to predict the effects of environmental change on vegetation distributions [**64**].

2.3 Habitat Suitability Modeling and Analysis

Habitat suitability modeling (HSM) and analysis a technique for predicting the suitability of habitat for a given species based on known affinities with environmental parameters [**65**]. It is often used to produce probability maps depicting the likelihood of occurrence of certain species and to find out the landscape properties of preferred habitats [**66**]. Predictive vegetation mapping, as discussed in the previous section, is an example of HSM.

According to Hirzel and Le Lay [**67**], habitat suitability models (HSMs) are based upon the theory that the presence of a species in a location obeys three constraints (i) the local environment allows the population to grow, (ii) the interactions with other local species (predation, competition, mutualism, etc.) allow the species to persist, and (iii) the location is actually accessible, given the dispersal abilities of the species. These constraints determine the geographical distribution of the species. It follows that, theoretically, it is possible to reconstruct a realized ecological niche for a species from the environmental variables measured at the locations it occupies. This reconstruction and the spatial predictions derived from it are the goals of HSM.

HSMs work by statistically relating field observations to set of environmental variables, presumably reflecting some key factors of the niche, like climate, topography, geology or land-cover [**68**]. Spatial predictions indicating the suitability of locations for a target species are then produced. Different types of modelling techniques are used to fit

different types of biological information recorded at each sample site: (1) presence-only: occurrences of the target species are recorded; (2) presence/absence: each sample site is carefully monitored so as to assert with sufficient certainty whether the species is present or absent [**68**].

2.3.1 Statistical Tools in Habitat Suitability Modeling and Analysis

Multivariate statistical tools such as logistic regressions, Gaussian logistic regressions, discriminant analyses, Mahalanobis distances and artificial neural networks, are commonly used to formalize the link between the species and their habitat, in particular to quantify the parameters of HSMs. According to Hirzel et al. [**69**], these methods share largely similar principles:

- The study area is modeled as a raster map composed of *N* adjacent isometric cells;
- The dependent variable is in the form of presence/absence data of the focal species in a set of sampled locations;
- Independent eco-geographical variables (EGV) describe quantitatively some characteristics for each cell such as topography (altitude, slope), ecological data, or human superstructures (e.g., distance to nearest town, road density);
- A function of the EGV is then calibrated so as to classify the cells as correctly as possible as suitable or unsuitable for the species.

Among the method mentioned, logistic regression analysis is the most popular [**69**]. Binary logistic regression in conjugation with GIS and spatial data has been successfully used by several studies in plant distribution modeling (e.g. [**70**]; [**71**], [**72**]). Through their use of logistic regression, locations of suitable habitat for the target species were identified. Logistic regression was implemented by Padalia et al [**70**] in a GIS to predict the suitable habitats for endangered plant species, *Pittosporum eriocarpum* Royle, in the Himalayan region using a dataset consisting of land-cover, topography (altitude, slope) and soil characteristics. Morissette et al [**72**] successfully integrated satellite data and tens of thousands of field sampling points through logistic regression modeling to create a 90% accurate national-scale map of habitat suitability for tamarisk (*Tamarix* spp, salt cedar), a high-priority invasive species.

While multivariate statistical tools such as logistic regression approach have been successful in a number of HSM studies, their usage becomes problematic when only presence data are available. In this case, the modeler is prompted to first create “pseudo-absences”, a common procedure to overcome the lack of true absence data to facilitate the use of group discrimination methods such as logistic regression [**73**]. This is usually achieved by randomly choosing point locations in the region of interest and treating them as absences [**74**]). Essentially, pseudo-absences are meant to provide a comparative data set to enable the conditions under which a species occurs to be contrasted against those where it is absent [**75**].

Warton and Shepherd [**74**] saw problems of the approach in terms of model specification, interpretation, and implementation. For these authors, a sounder model

specification would involve constructing a model for the observed data only, rather than generating new data prior to constructing a model. In addition to this, interpretation of the result is difficult because some model parameters are a function of the number of pseudo-absences and their location. More importantly, implementation of the approach is problematic because it is unclear how pseudo absences should be chosen, and one can obtain qualitatively different results depending on the method of choice of pseudo absences [**74**].

2.3.2 Habitat Suitability Modeling using Presence-only Data

Sampling the presence/absence data is a crucial part of the HSM process since the sample must be unbiased to be representative of the whole population [**69**]. In particular, absence data are often difficult to obtain accurately. A given location may be classified in the "absence" set because (i.) the species could not be detected even though it was present, (ii.) the species is absent even though the habitat is suitable, or (iii.) the habitat is truly unsuitable for the species [**69**]. In the case when presence-only data is available, use of the pseudo-absence approach and selecting localities for model parameterization is a very important decision as the selection may influence model parameterization and thus, can influence the appropriateness and accuracy of the model prediction when extrapolating the species distribution across time and space [**75**].

Several presence-only models, also called predictive distribution models, are available to circumvent the difficulties of using the presence/absence or presence/pseudo-absence approach in HSM. With these models, the occurrence datasets served as the dependent variable and the selected environmental variables as the predictors. Some of these models are Bioclim [**76**], Domain [**77**], ENFA [**78**] and Maxent [**79**], [**80**]. The methods implemented in these models do not require an explicit quantification of absence to formulate a predicted distribution model [**81**].

Bioclim, Domain and Maxent models have been described in Hernandez et al. [**81**] as follows:

- Bioclim: this "boxcar" environmental envelope algorithm identifies locations that have environmental values that fall within the range of values measured from the occurrence dataset. The area, often termed the "core bioclimate", represents the 5–95 percentile limits and is calculated by disregarding 5% of the lower and higher values of each climatic index thereby attempting to reduce the impact of outliers.

- Domain derives a point-to-point similarity metric to assign a classification value to a potential site based on its proximity in environmental space to the most similar occurrence. The Gower metric, which is the sum of the standardized distance between two points for each predictor variable, is used to quantify the similarity between two sites. The standardization is achieved using the predictor variable range at the presence sites to equalize the contribution from each predictor variable. Similarity is then calculated by subtracting the distance from 1. The maximum similarity between a candidate point and the set of known occurrences is assigned to

each grid cell within the study area; these similarity values are degrees of classification confidence.

- Maxent utilizes a statistical mechanics approach called maximum entropy to make predictions from incomplete information. Maxent estimates the most uniform distribution (maximum entropy) across the study area given the constraint that the expected value of each environmental predictor variable under this estimated distribution matches its empirical average (average values for the set occurrence data).

On the other hand, ENFA or Ecologic Niche Factor Analysis is built upon the concept of ecological niche wherein factor analysis is implemented as a means to compare in multidimensional space of ecological variables, the distribution of the localities where the focal species was observed to a reference set describing the whole study area [**69**]. The first factor extracted maximizes the marginality of the focal species, defined as the ecological distance between the species optimum and the mean habitat within the reference area. The other factors maximize the specialization of this focal species, defined as the ratio of the ecological variance in mean habitat to that observed for the focal species. Eigenvectors and eigenvalues are readily interpreted and can be used to build habitat-suitability maps. This approach is recommended in situations where absence data are not available (many data banks), unreliable (most cryptic or rare species), or meaningless (invaders) [**69**].

Bioclim, Domain, ENFA and Maxent have been used in a number of species distribution modeling and habitat suitability analysis with considerable success. Some of the applications of Bioclim include predicting current and future distributions of butterfly species [**82**] and modeling potential distribution of willows in Canada [**83**]. On the other hand, the Domain model has successfully been used by several researchers to model potential distribution of plant species (e.g., [**77**]; [**84**]; [**85**]; [**86**]; [**87**]) owing to the fact the model is easily implemented and performs well with limited site data. Vargas et al. [**87**] used Domain in modeling the potential distribution of 36 endemic and 47 non-endemic species of Anthurium (Araceae) in Ecuador based on mean annual temperature and humidity. Their results indicate the location of the most important region for endemics and a belt of potential high diversity of Anthurium. Maxent was used by Heumann et al. [**88**] in modeling crop suitability for upland and lowland crops, including rice varieties, although model results varied between datasets due to the high sensitivity of the model to the distribution of observed crop locations in geographic and environmental space. Evangelista et al. [**89**] used Maxent modeling technique to model potential beetle distributions and forest vulnerability by fitting it with occurrence points and current climate data. Kumar and Stohlgren [**90**] used Maxent with 91% success rate to predict potential suitable habitat for *Cancomyrica monticola*, a threatened and endangered new species in New Caledonia. The approach presented appears to be promising for predicting suitable habitat for threatened and endangered species with small sample records and can be an effective tool for biodiversity conservation planning, monitoring and management.

Chapter 3. Scientific Basis and Theoretical Framework

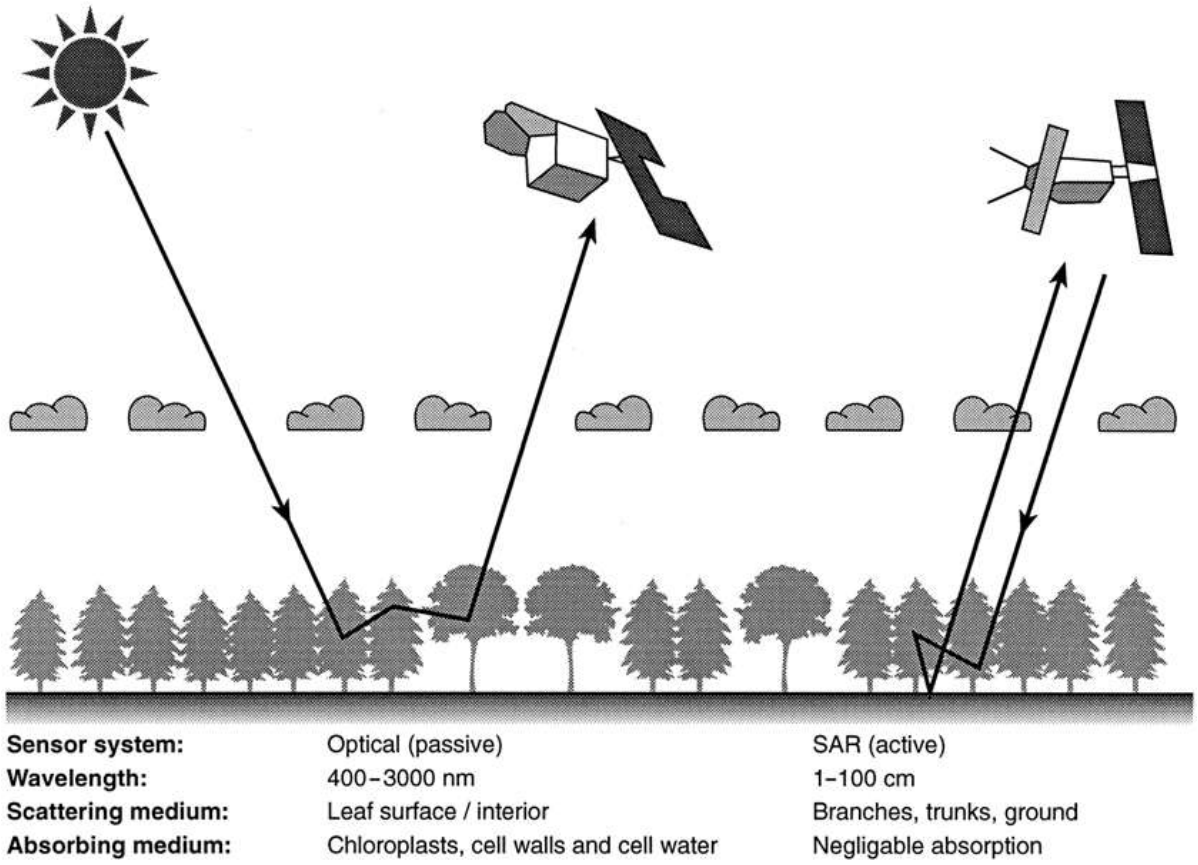

Figure 5. Satellite remote sensing using optical and synthetic aperture radar (SAR) sensors. Illustration from [**8**].

3.1 Scientific Basis

The RS-based mapping of Sago habitats will make use of an existing framework on satellite remote sensing for forest resource assessment recently presented by Boyd and Danson [**8**], and as illustrated in Figure 5.

The framework is based on the fact that, like all forest resources applications of remote sensing, the measurement of Sago habitats from RS images relies on the interaction of electromagnetic radiation with the target and analysis of the returned signal by a sensor. The sensor can be of two kinds: optical sensors and SAR systems. The former measure reflected radiation in one or more discrete wavebands located in the spectral range 400-3000 nm, whereas the latter measure backscattered microwave radiation at wavelengths between 1 cm and 1000 cm. Optical wavelengths are several orders of magnitude smaller than the leaves and branches that make up a Sago palm canopy and, consequently may be both absorbed and scattered by these components. In the case of the longer microwave wavelengths, scattering from leaves, branches, trunks and ground is the dominant

mechanism. It follows that optical remote sensing systems may provide information on the amount of foliage and its biochemical properties whereas the SAR systems provide information on woody biomass and forest structure. Moreover, remote sensing instruments are imaging devices that may provide additional spatial information related to the three-dimensional structure. Extracting information on resources such as the Sago palm depends on the use or development of techniques to infer the desired resource information from the remotely sensed data acquired by the optical and SAR systems.

The use of fine spatial resolution optical sensors can be compromised by their relatively high cost, large data volumes and low frequency of data acquisition, compounded further particularly by cloud cover. The use of SAR systems affords the certainty of cloud free data. While both systems can provide information of the distribution of Sago palms through application of image analysis tools such as classification algorithms with the aid of ground truth datasets, the synergy of both optical and SAR sensors may provide improved delineation of Sago palms from other land-cover types. Synergy allows for the exploitation of exclusive information on the Sago and non-Sago provided by the different spectral data collected by different sensors. The cloud penetrating capability of SAR sensors allows areas that have missing optical data to be included in the analysis.

The collection of Sago in-situ spectral reflectance on-site as well as data on the biophysical, structural, climatic and environmental of Sago stands and habitats is important in the use or development of techniques to infer Sago palm distribution from optical and SAR images. The field-measured spectral reflectance of Sago stands and habitats may be related with the measured biophysical, structural, climatic and environmental conditions. The resulting empirical model will then serve as a set of relationships that can be applied to the optical and SAR images to map the distribution of Sago habitats, and to generate spatially-distributed map of Sago palm biophysical and structural attributes. Using the same concept behind predictive vegetation mapping, suitability rules can also be developed using the same datasets used in empirical modeling, and to apply this rules on available datasets of biophysical, climatic and environmental conditions so that the potential sites where Sago palm could be cultivated for mass production purposes can be located.

3.2 Theoretical Framework

The detection of Sago habitats and determination of Sago suitable sites is not a straight forward task because of several factors that needs to be considered.

First, information on actual conditions of Sago stands must be measured on the ground to determine their degree of detectability on RS images. Their environmental conditions must be also understood so that we could gain insights on the factors that affect their growth and the site conditions that they are well-suited.

This project worked upon a framework (Figure 6) wherein spectral, structural, biophysical and climatological characteristics of Sago and non-Sago as measured on the ground, where applicable, will be interrelated with their corresponding characteristics in high resolution and medium resolution optical and radar satellite images. These empirical relationships will be applied to RS images so that information on location, extent and distribution of Sago stands could be mapped out. Empirical relationships will also provide the

degree of contribution of biophysical and climatologically factors in finding locations where Sago can be mass propagated.

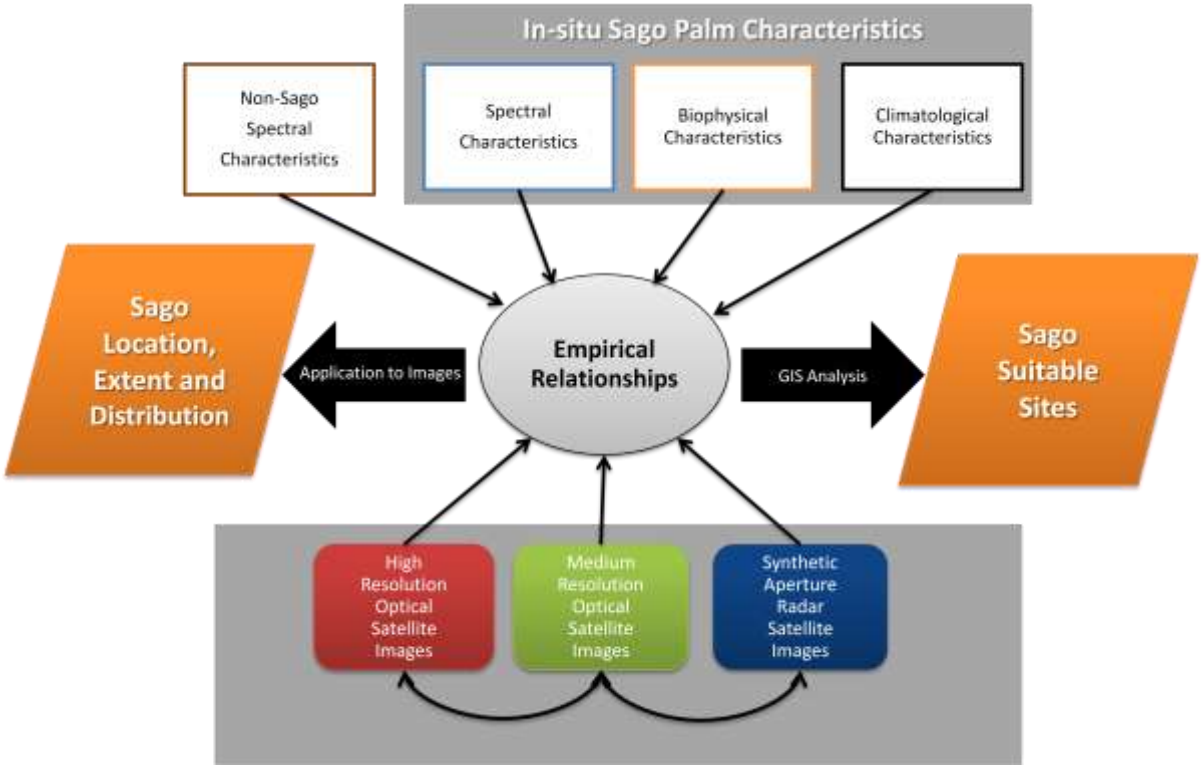

Figure 6. Theoretical framework for Sago palm detection in satellite images and finding Sago suitable sites.

Chapter 4. Overview of Project Methodology

This project was implemented through a combination of field surveys, statistical analysis, potential distribution mapping, optical and radar (SAR) image analysis, and habitat suitability analysis (Figure 7) to come up with the thematic maps and figures on the present location, extent, abundance and distribution of Sago palms in Visayas and Mindanao, as well as maps and figures of areas suitable for Sago palm propagation.

Overviews of the project activities are presented in the next sections, with detailed discussions in the following chapters.

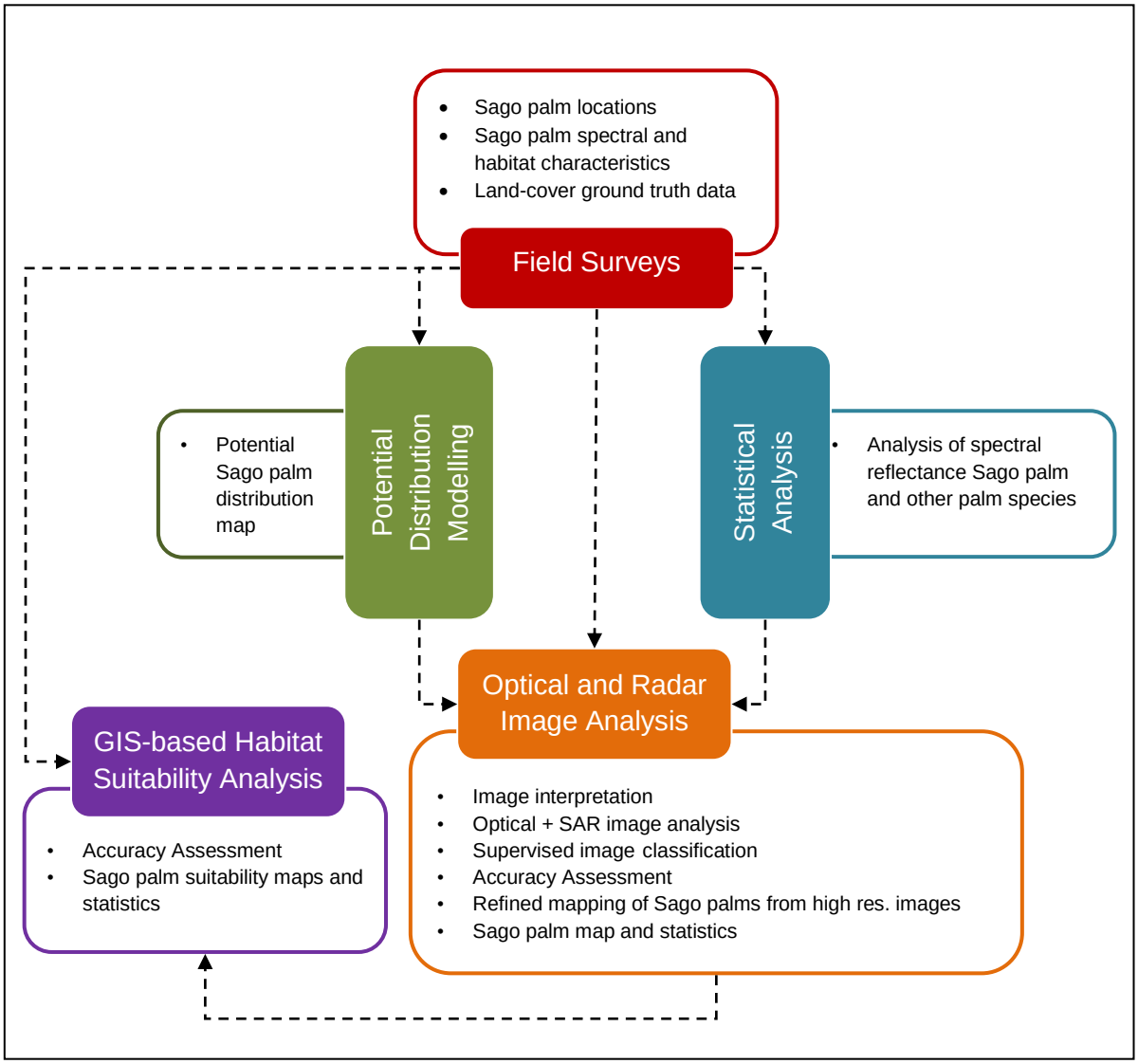

Figure 7. Flowchart summarizing the project's methodology.

4.1 Field Surveys

Field surveys were conducted in the Visayas and Mindanao provinces where Sago palms have been reported to exist (for example in the reports of [**10**], [**11**], [**19**], [**21**], [**22**] , [**23**], and [**24**]).

In Visayas, these provinces included Aklan, Cebu and Leyte. In Mindanao, the provinces included Agusan del Norte, Agusan del Sur, Davao del Norte, Davao del Sur, Davao Oriental, Compostela Valley, Misamis Oriental, and Misamis Occidental. Field surveys were made together with the Sago Project II.2 team.

The purpose of the field surveys are:

1. To gather information on the geographic locations of existing Sago palm stands, including conduct of perimeter surveys of visited stands;
2. To conduct in-situ measurements of Sago spectral reflectance and structural attributes, including biophysical characteristics of their habitats (conducted by Sago Project II.2 team);
3. To conduct spectral reflectance measurements of non-Sago palms such as coconut, nipa, and oil palm (conducted by Sago Project II.2 team);

Field surveys in the provinces that were along the way e.g., Antique (in the Visayas) and Bukidnon (in Mindanao) were also conducted but mainly as reconnaissance of Sago palm stands to verify if they also exist in these provinces.

Detailed discussions of field surveys of existing Sago palm stands are presented in Annex 1 of this report.

4.2 Statistical Analysis of Spectral and Radar Backscatter Data

Together with Sago Project II.2, the spectral reflectance data of Sago palm and other palm vegetation was analyzed to ascertain on which part of the electromagnetic spectrum the Sago palm is more distinguishable from other palm vegetation. The analysis was made using the in-situ spectral reflectance data that has been resampled to match the spectral response of the ALOS AVNIR-2, ASTER VNIR, Landsat 7 ETM+, Landsat 8 OLI and Worldview-2. The resampled data here is considered as the resulting reflectance values as if they were measured by the 3 optical satellite imaging sensors without atmospheric effects. This will help in the interpretation and analysis of medium (e.g., ALOS AVNIR-2, Landsat 7 ETM+) and high resolution (Worldview-2) optical satellite images, specifically in selecting which band to use when mapping Sago palms using these images.

The same analysis was also conducted using reflectance data extracted from medium resolution images. The aims is to reveal the bands of the optical sensors that could best discriminate Sago from other land-cover classes

An analysis of backscattering characteristics of Sago and other land-cover types was also conducted. The analysis aims to assess if a SAR image acquired by Envisat ASAR sensor can be useful in detecting and discriminating Sago palms from other land-cover types.

All these analyses are part of satisfying the project's number one objective. Details are presented in Chapter 5, 6 and 7.

4.3 Potential Sago Palm Distribution Mapping

Mapping very specific vegetation such as the Sago palm using satellite images could be an arduous task especially if the coverage is very large such as Visayas and Mindanao. If mapping is to be done using medium resolution satellite images such as ALOS AVNIR-2 (which is 70 x 70 km), the number of image scenes to be processed will range from 60 to 100. For Landsat 7 ETM+, there will be around 20 scenes to analyze.

Although satellite remote sensing has been known to be a useful platform for mapping land-cover in wide areas, the process of applying it for Sago palm mapping maybe counter-productive. This is because this vegetation species is not widely distributed as compared to other species (e.g., coconut). There might be a scenario when one or more images of an area have been acquired and processed but later on it was found that Sago palm cannot exist in this area because the conditions is not suitable. This leads to waste of time and resources. A better approach would be to avoid processing satellite images where Sago palms are unlikely to be found and focusing only on areas that Sago palms are likely to exist. In this project, potential distribution mapping was first conducted to identify areas in Visayas and Mindanao where Sago palms are likely to occur.

Details of the Sago palm distribution mapping as an important activity prior to satellite image analysis is discussed in Chapter 8.

4.4 Sago Palm Mapping using Optical and Radar Satellite Images

A three stage mapping approach was implemented in this study to derive detailed maps and statistics of Sago palms. The first step is potential distribution mapping (as discussed in the previous section). The second step is mapping possible Sago palm locations in medium resolution optical and radar images (Landsat 7 ETM+, ALOS AVNIR2, Envisat ASAR) within the areas identified through potential distribution mapping. Finally, the detected possible locations of Sago palms are examined through the use high resolution optical satellite images. The last step are the refinements in the extent of Sago palm stands. From this refinement, the final maps and statistics of existing Sago palms were prepared.

Details are presented in Chapters 9, 10 and 11.

4.5 Sago Palm Habitat Suitability Analysis

Habitat suitability analysis was conducted primarily to search for lands in Visayas and Mindanao where Sago palms can grow based on biophysical and bioclimatic factors. A one hectare (100 m x 100 m) mapping unit was utilized upon the assumption that 1 ha corresponds to the unit of decision making for agricultural or forestry management [**91**].

The suitability analysis consisted of finding suitable areas based on biophysical characteristics, and finding suitable areas based on bioclimatic characteristics. More details are presented in Chapter 12.

Chapter 5. Analysis of In-Situ Spectral Reflectance of Sago Palms and Other Palms Species: Implications for their Detection in Optical Satellite Images[1]

This chapter presents a discussion on the analysis of spectral reflectance data of Sago palm and other palm vegetation such as coconut, oil palm and nipa, to ascertain on which part of the electromagnetic spectrum the Sago palm is more distinguishable from other palm vegetation. The analysis was made using both in-situ spectral reflectance data and reflectance data that has been resampled to match the spectral response of the 4 bands of ALOS AVNIR-2, 3 bands of ASTER VNIR, 4 bands of Landsat 7 ETM+, 5 bands of Landsat 8, and 8 bands of Worldview-2. The resampled data here is considered as the resulting reflectance values as if they were measured by the 4 optical satellite imaging sensors free from atmospheric effects. This will help in the interpretation and analysis of medium (ALOS AVNIR-2, ASTER VNIR, Landsat) and high resolution (Worldview-2) optical satellite images, specifically in selecting which band to use when mapping Sago palms using these images.

5.1 In-Situ Spectral Reflectance Measurement

In-situ reflectance spectral data used in the analysis was collected in tandem with Sago Project II.2. The data consisted of reflectance spectra of Sago palm and other palm species which have similar leaf structures to those of Sago palms (coconut, oil palm and nipa). The sampling sites are unique stands of these four species. For Sago palm, the reflectance spectra measured were those of its different growth stages (rosette, bole formation, inflorescence and fruit ripening; see Figure 10 and Table 2).

At each sampling site, the amount of electromagnetic radiation (i.e. radiation from the sun) reflected by palm vegetation was measured using the Ocean Optics™ USB4000-VIS-NIR Miniature Fiber Optic Spectrometer. The sensor detects and records data with spectral range from 345 nm to 1047 nm. In order to measure the spectra of Sago palms and that of other palms, the set-up is composed of the sensor, mounted in an improvised pole, attached to fiber optic cable and is positioned just above the canopy. The spectrometer is connected to a laptop computer that performs the scanning procedure, displays the plot of the observed reflectance and stores the reflectance data. Figure 11 illustrates the set-up of the in-situ spectral measurement.

At each site, five trials with each consisting of 25 consecutive measurements of reflected canopy radiation were conducted. To determine the percentage of radiation coming from the sun that has been reflected by a palm vegetation, it is necessary to measure also how much radiation is reflected by a reference standard. This was done by doing another set of 25 measurements of radiation reflected by a white reference panel before and right after measuring reflected radiation by palm vegetation. The white reference panel used is the Ocean Optics™ WS-1-SL White Reflectance Standard with Spectralon which approximately

[1] *This chapter presents a more updated analysis of what was previously conducted by Sago Project II.2. The results discussed here will differ from what has been reported by Sago Project II.2 in their terminal report.*

reflects 99% of incoming radiation with wavelengths ranging from 400-1500 nm. The average of the measurements, noted here as $R_{reference}$, were then taken at each trial. With this setup, the percentage reflectance of a palm vegetation is obtained by dividing the reflected radiation from a palm (R_{canopy}) with the reflected radiation from the reference panel ($R_{reference}$) x 100. It was assumed that the incoming radiation from sun was the same during measurement of R_{canopy} and $R_{reference}$. At each site, the average of the five trials was then used in the analysis.

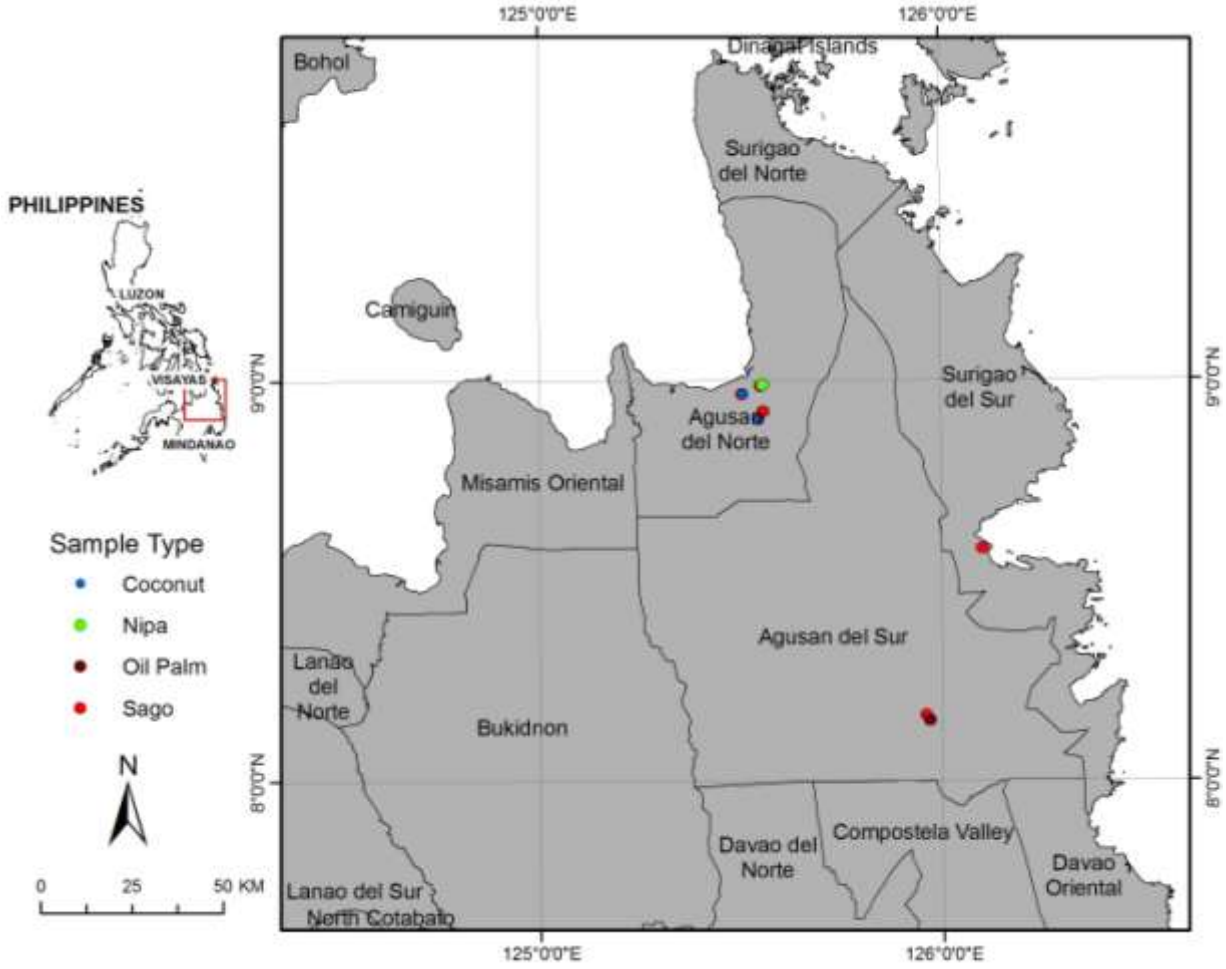

Figure 8. Map showing the sampling sites of in-situ reflectance of Sago palm, coconut, oil palm and nipa.

Figure 9. Pictures of Sago palm, coconut, oil palm and nipa.

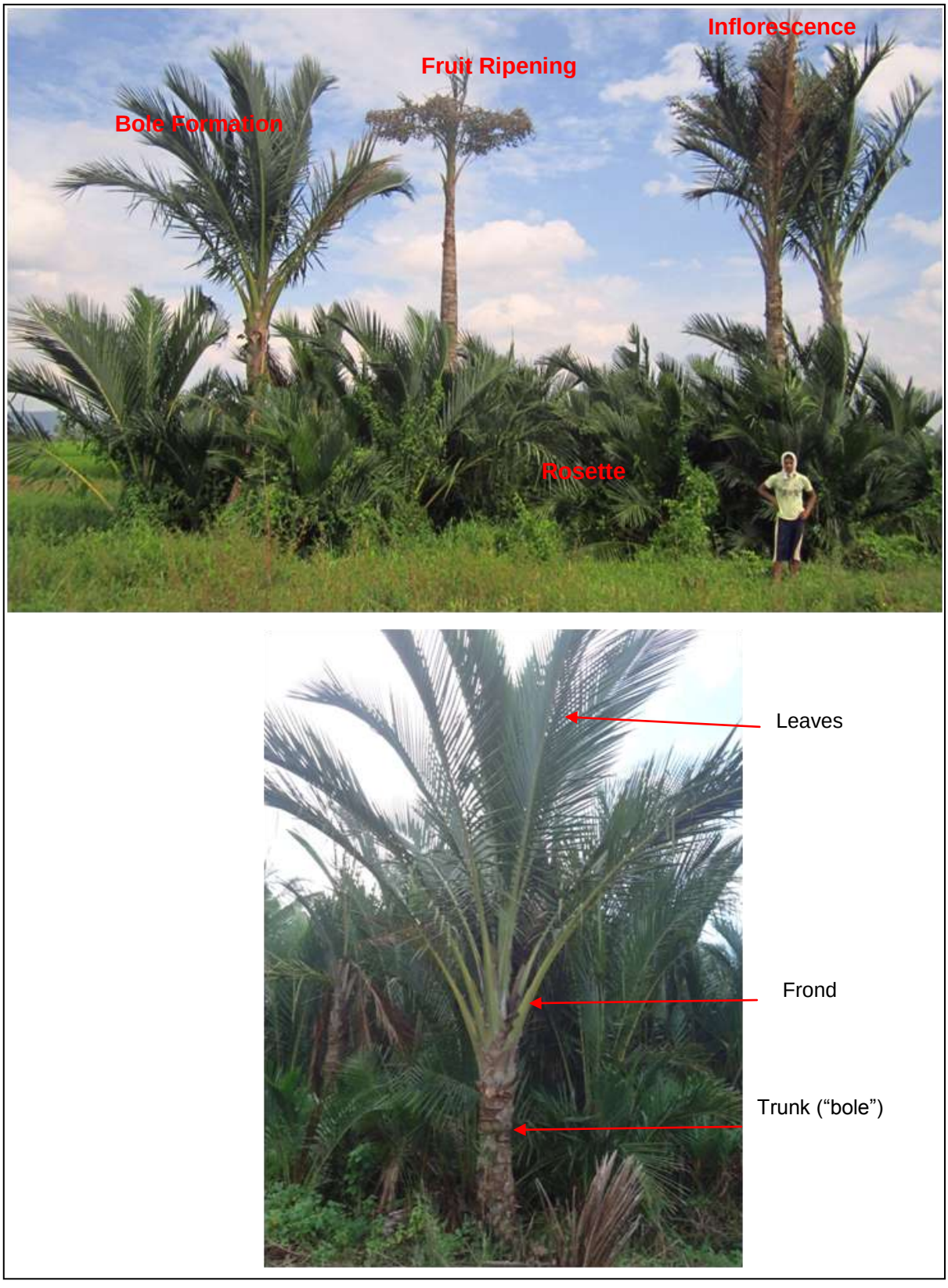

Figure 10. Above photo: A cluster of Sago palms showing different growth stages. Below photo: A Sago palm in bole formation stage, with some of its parts indicated. Below photo courtesy of Project II.2.

Figure 11. The set-up of the in-situ spectral reflectance measurement conducted in tandem with Sago Project II.2. The set-up is in a stand of Sago palm in rosette stage.

Figure 12. To measure the reflected radiation on top of the Sago palm, the fiber optic sensor is attached to a very long pole.

Figure 13. Most of the time, it is necessary to use a ladder in order to reach the top of mature Sago palms.

Table 1. Number of sampling sites for reflectance measurements.

Palm species	Number of Sites (Samples)	No. of Trials Per Site	No. of Measurements per Trial
Coconut	9	5	25
Nipa	7	5	25
Oil Palm	5	5	25
Sago (total):	31	5	25
- *At rosette stage*	*9*	*5*	*25*
- *At bole formation stage*	*12*	*5*	*25*
- *At inflorescence stage*	*5*	*5*	*25*
- *At fruit ripening stage*	*5*	*5*	*25*

Table 2. Description of Sago palm growth stages (Source: [**4**]).

Stage	Approx. Age, in no. of months from seeding	Description
Rosette	0 - 45	A period characterized by relatively little growth. During this period the plant forms a total of about 90 fronds.
Bole Formation	46 - 100	The bole elongates to maximum height and produces one frond per month. Plants during this stage have a total of about 24 fronds and 54 frond scars on the bole and are producing a high amount of starch.
Inflorescence	101 - 113	The plant forms two fronds per month, the rate of starch accumulation starts to decrease, and the starch moves from the lower to the upper bole. It is in this stage that flowers emerge. Palms are harvested for starch during this and the next period.
Fruit Ripening	114 - 137	The stage when the flowers have been converted into fruits. When the fruits have fully ripened, the plant's life cycle is completed because the starch in the trunk has already been exhausted to produce the seeds.

5.2 In-Situ Spectral Reflectance of Sago Palm at Different Growth Stages

Figure 14 shows the average in-situ spectral reflectance curves of Sago palm at different growth stages, including the average of all samples (regardless of growth stage).

At the visible portion of the electromagnetic spectrum (400-700 nm), it appears that reflectance of Sago palm increases as they grow old. Sago palms in rosette stage have the lowest reflectance while those in fruit ripening stage have the highest reflectance. In the infra-red region (beyond 700 nm), this trend is reversed (i.e., decreasing reflectance as they grow old).

These observations can be explained by their appearance and leaf composition. As shown previously in Figure 10 and as described in Table 2, Sago palms in rosette stage

have more fronds and leaves. This number decreases as they grow old. Because of this, there is high rate for which incident light/radiation at visible range will be absorbed rather than reflected by younger Sago palms, especially in the blue (~450-500 nm) and red (~650-700 nm) regions. Younger Sago palms have low reflectance in both the blue and red regions of the spectrum, due to absorption by chlorophyll for photosynthesis. Their reflectances peak at the green region which gives rise to their green color.

For later stages, especially the fruit ripening stage, there is high reflectivity in both the green and red regions due to lesser number of leaves, presence of fruits, and exposure of trunks and fronds (without leaves). Because of this, they appear less green than the younger Sago palms.

In the near infra-red (NIR) region, younger Sago palms have higher reflectance than older ones. This is again due to the presence of leaves of younger Sago palms. As reported in several remote sensing literatures, the reflectance of vegetation is much higher in the NIR than that in the visible region due to the cellular structure in the leaves. Since older Sago palms have lesser leaves, it follows that they also have lower number of cellular structures than can reflect radiation at these wavelength range.

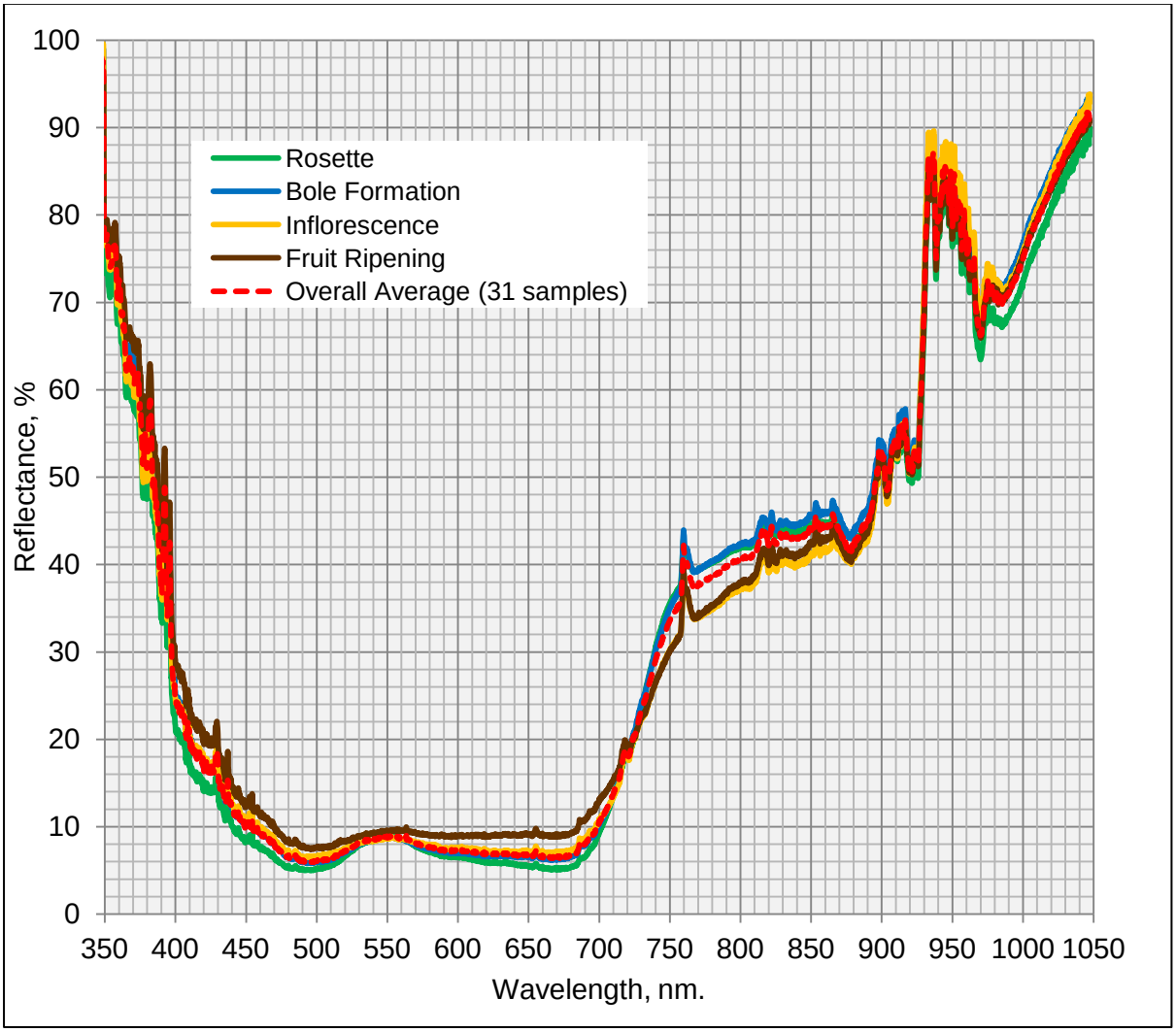

Figure 14. Average in-situ spectral reflectance curves of Sago palm at different growth stages.

If the spectral reflectance curves are to be used for distinguishing growth stages of Sago palm, the blue and red regions are the best portions, especially those at the 400-500 nm and at 650-700. However, the degrees of separability at these regions are quite low due to nearness of reflectance values. All growth stages are indistinguishable at the wavelengths less than 400 nm, at 550 nm, at 720 nm, and at wavelengths greater than 900 nm. Greatest separability was found at 770 nm but only between two groups of growth stages: rosette-bole formation and inflorescence-fruit ripening. This means that Sago palms in rosette and bole formation stages can be distinguished from those in inflorescence and fruit ripening stages. This information is helpful in finding appropriate bands of available optical satellite sensors for distinguishing Sago palm growth stages.

5.3 In-Situ Spectral Reflectance of Sago and Other Palm Vegetation

Figure 15 shows the average in-situ spectral reflectance of Sago and other palms, including the 95% confidence interval of the mean.

The graph indicates that in general, all palms have lower reflectance in the blue and red regions but higher reflectance in the green region. The graph shows several portions of the electromagnetic spectrum where Sago palm is distinguishable from other palms. The most obvious is at 550 nm, at 770, at 800, and at 875 nm. At these portions, Sago palm has the lowest reflectance while nipa has the highest. In between are coconut and oil palm. However, the Sago palm's average reflectance curve cannot be considered unique. Looking at the 95% confidence intervals, the Sago palm's reflectance is slightly contaminated by those of Oil palm but not by coconut and nipa. Based on this data, there is high discrimination of Sago palm from nipa and coconut but relatively low discrimination from oil palm specifically at 400-700 nm region. In the NIR region, specifically at 750-800 nm, the Sago palm's average reflectance is almost the same as the lower 95% CI of oil palm, while the Oil palm's average reflectance is almost the same as the upper 95% CI of Sago palm. Considering only the average reflectance, the NIR region, specifically at 770, 800 and 875 nm, provides the best wavelengths where Sago palm can be distinguished from other palms. However, the validity of this result when applied in analyzing optical satellite remote sensing images must be evaluated since the bands of the sensors does actually equate to a specific wavelength but to a range of wavelengths. Also, the conditions during the in-situ reflectance measurements are different from the condition when the satellite images were acquired. Moreover, reflectance values measured by satellite sensors are also affected by atmospheric effects which will make the in-situ spectral reflectance very different from the image-base reflectance.

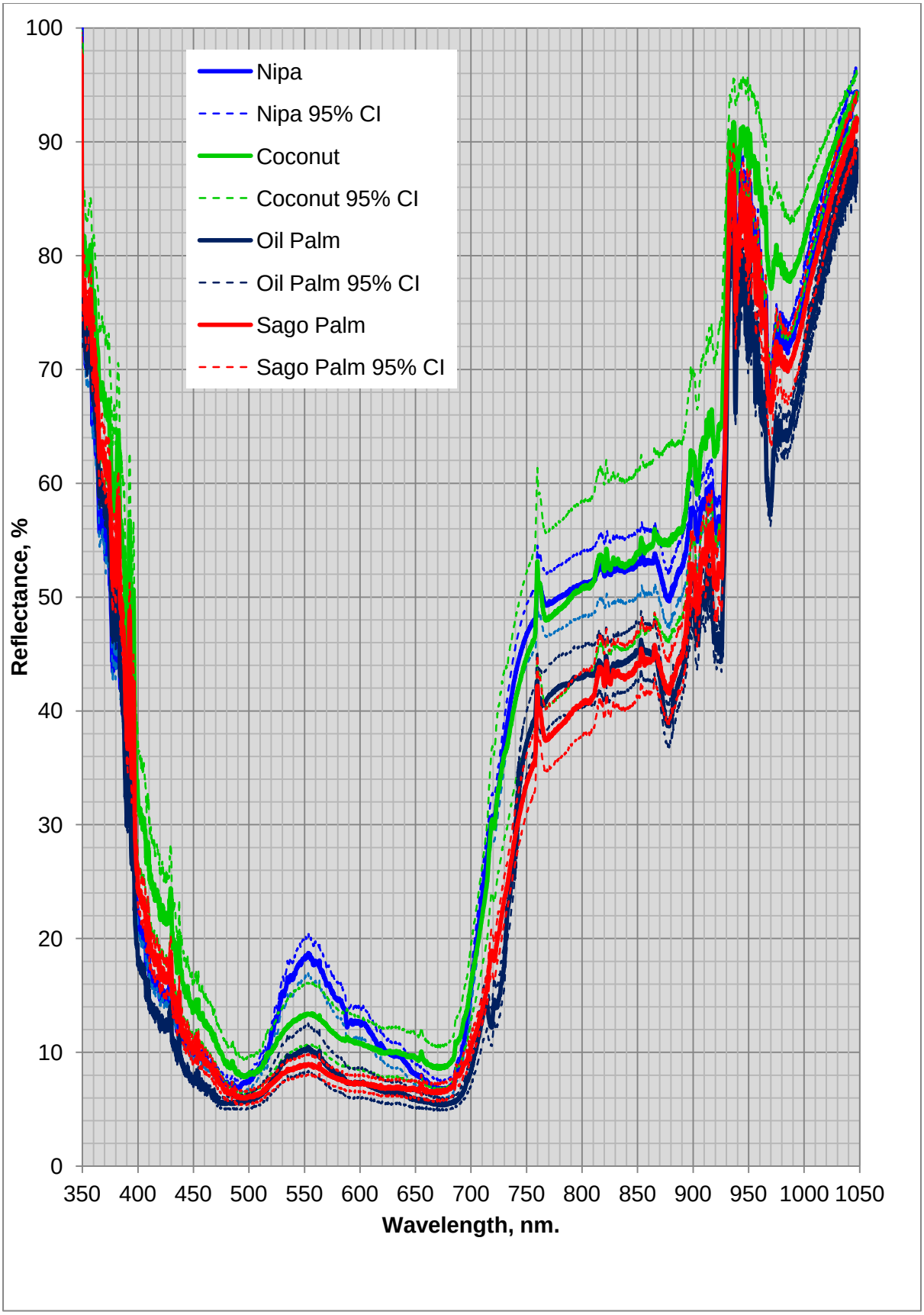

Figure 15. Average in-situ spectral reflectance of Sago and other palms, including the 95% confidence interval of the mean.

5.4 Using Resampled In-situ Reflectance to Simulate Sensor-specific Reflectance of Sago and Other Palms

The in-situ reflectance curves of Sago and other palms can be resampled to simulate reflectance values as if they were measured by the optical satellite imaging sensors namely Landsat 7 ETM+, Landsat 8 OLI, ALOS AVNIR-2, ASTER VNIR, and Worldview-2. Some call this as resampling to match the spectral response of the four sensors. Landsat 8 OLI resampling was also included although the actual analysis of images acquired by this new sensor (imagery available by April 2013 onwards) were not made. The resampling will help in the interpretation and analysis of images acquired by these sensors, especially on which bands the palms are distinguishable from each other. The resampled values are assumed to be free from atmospheric effects. Salient features of these sensors are listed in Table 3.

Table 3. Description of optical sensors considered in this study.

Satellite and Sensor	Spatial Resolution	No. of Optical Bands	Band No.	Band Names	Band Wavelength Range, nm	Central Wavelength, nm
Landsat 7 ETM+[2]	30 m	7[2]	1	Blue	450 - 520	482.5
			2	Green	520 - 600	565
			3	Red	630 - 690	660
			4	Near Infrared	770 - 900	825
			5	SWIR 1	1,550 - 1,750	1,650
			7	SWIR 2	2,080 - 2,350	2,220
Landsat 8 OLI	30 m	7	1	Coastal aerosol	433 - 453	443
			2	Blue	450 - 515	482.6
			3	Green	525 – 600	561.3
			4	Red	630 – 680	654.6
			5	NIR	845 – 885	864.6
			6	SWIR 1	1,560 – 1,660	1,609
			7	SWIR 2	2,100 – 2,300	2,201
ASTER VNIR	15 m	3	1	Green	520 -600	556
			2	Red	630 – 690	661
			3	NIR	760 – 860	807
ALOS AVNIR-2	10 m	4	1	Blue	420 – 500	460
			2	Green	520 – 600	560
			3	Red	610 – 690	650
			4	NIR	760 - 890	825
Worldview-2	2 m	8	1	Coastal blue	400-450	425
			2	Blue	450-510	480
			3	Green	510-580	545
			4	Yellow	585-625	605
			5	Red	630-690	660
			6	Red Edge	705-745	725
			7	Near infrared 1	770-895	832.5
			8	Near infrared 2	860-1,040	950

[2] Landsat 7 ETM+ Band 6 does not provide reflectance values but brightness temperatures, hence was not included.

The resampling of the in-situ reflectance curves was done using ENVI 5 software (Spectral Library Resampling) with the aid of relative spectral response functions of the four sensors. The spectral response function defines the spectral sensitivities of a sensor's band to reflected light. By characterizing the sensor's sensitivities, it allows the calculation of band values from any given spectral content of light reflected by an object back to the sensor (in this case the palm vegetation). The band values are calculated by integrating the RSRF over the in-situ reflectance spectra. Figure 17 to Figure 20 show the RSRFs of the four sensors overlaid with the reflectance spectra of Sago and other palms. From these graphs, the band or group of bands of a particular sensor that Sago palm can be discriminated from other palms can easily be identified. The graphs can also be used as initial assessment tool in determining if a particular sensor is suitable for discriminating Sago palms from other palms.

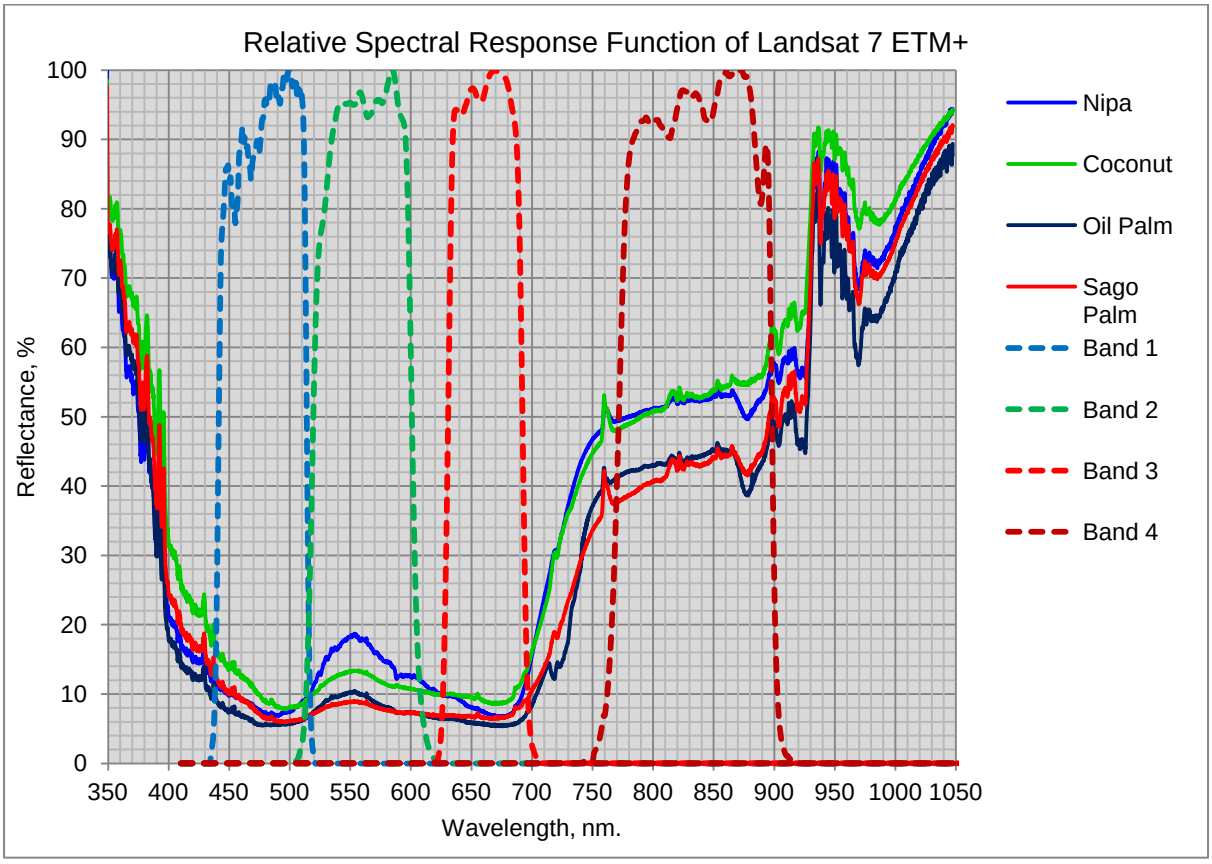

Figure 16. Relative spectral response functions (RSRF) of Landsat 7 ETM+ Bands 1-4 shown together with the in-situ spectral reflectance of Sago and other palms. The RSRF of Bands 5 and 7 are not shown as they are beyond the NIR wavelength range.

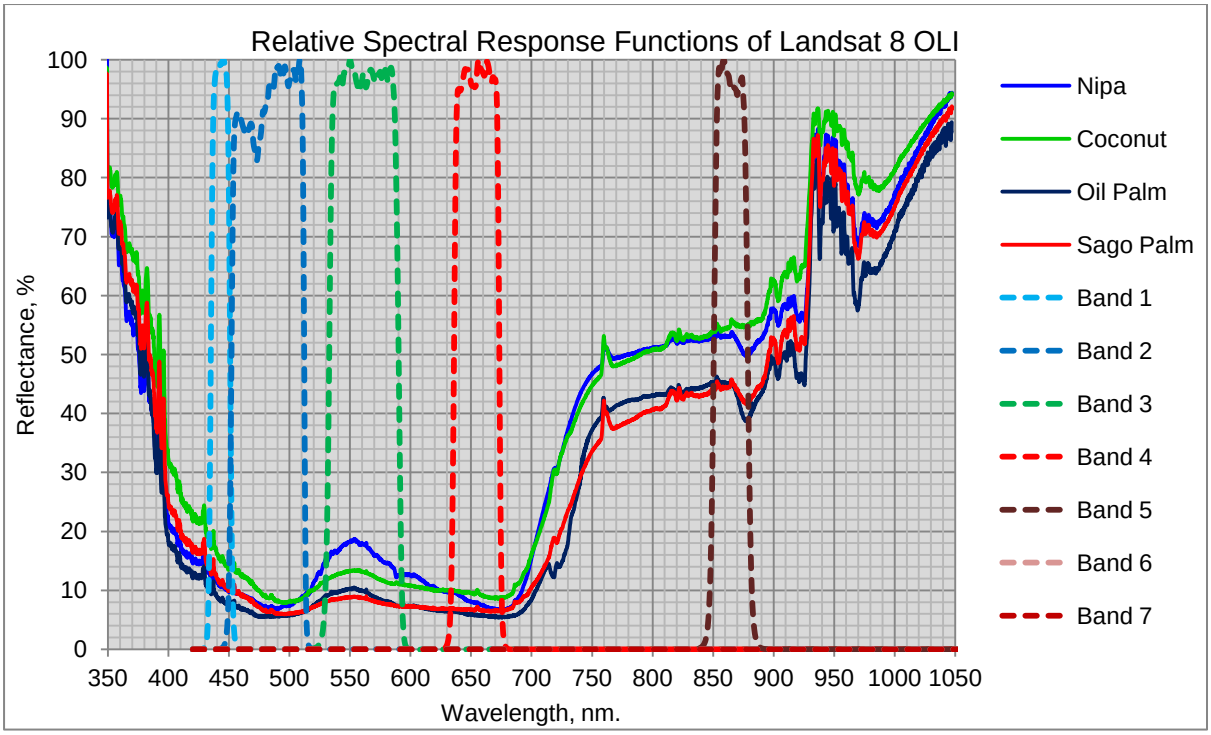

Figure 17. Relative spectral response functions (RSRF) of Landsat 8 OLI Bands 1-5 shown together with the in-situ spectral reflectance of Sago and other palms. The RSRF of Bands 6 and 7 are not shown as they are beyond the NIR wavelength range.

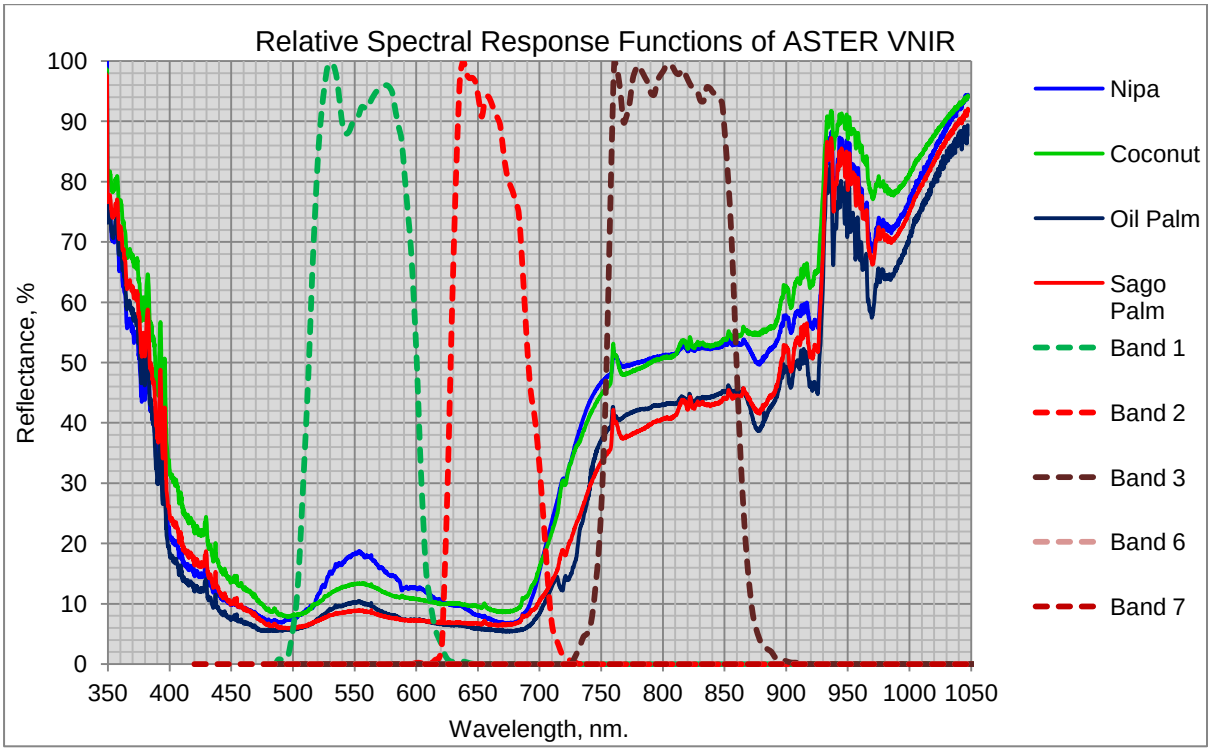

Figure 18. Relative spectral response functions (RSRF) of ASTER VNIR shown together with the in-situ spectral reflectance of Sago and other palms.

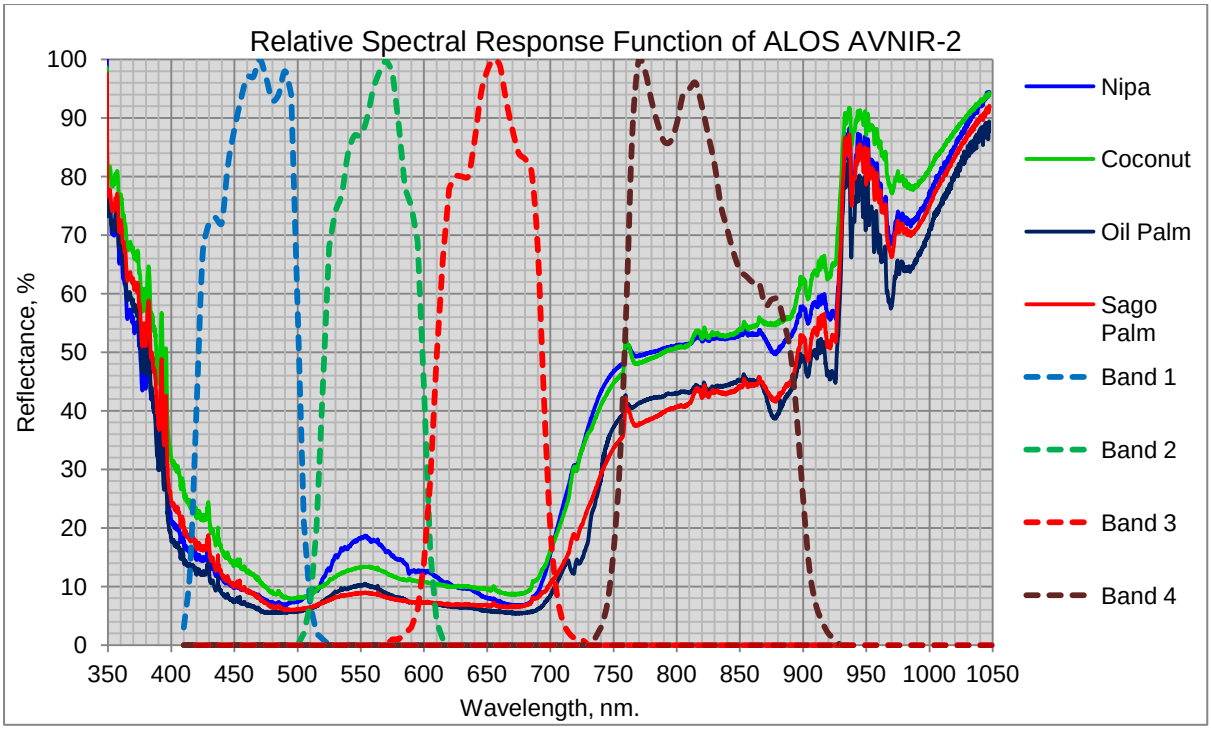

Figure 19. Relative spectral response functions (RSRF) of ALOS AVNIR-2 shown together with the in-situ spectral reflectance of Sago and other palms.

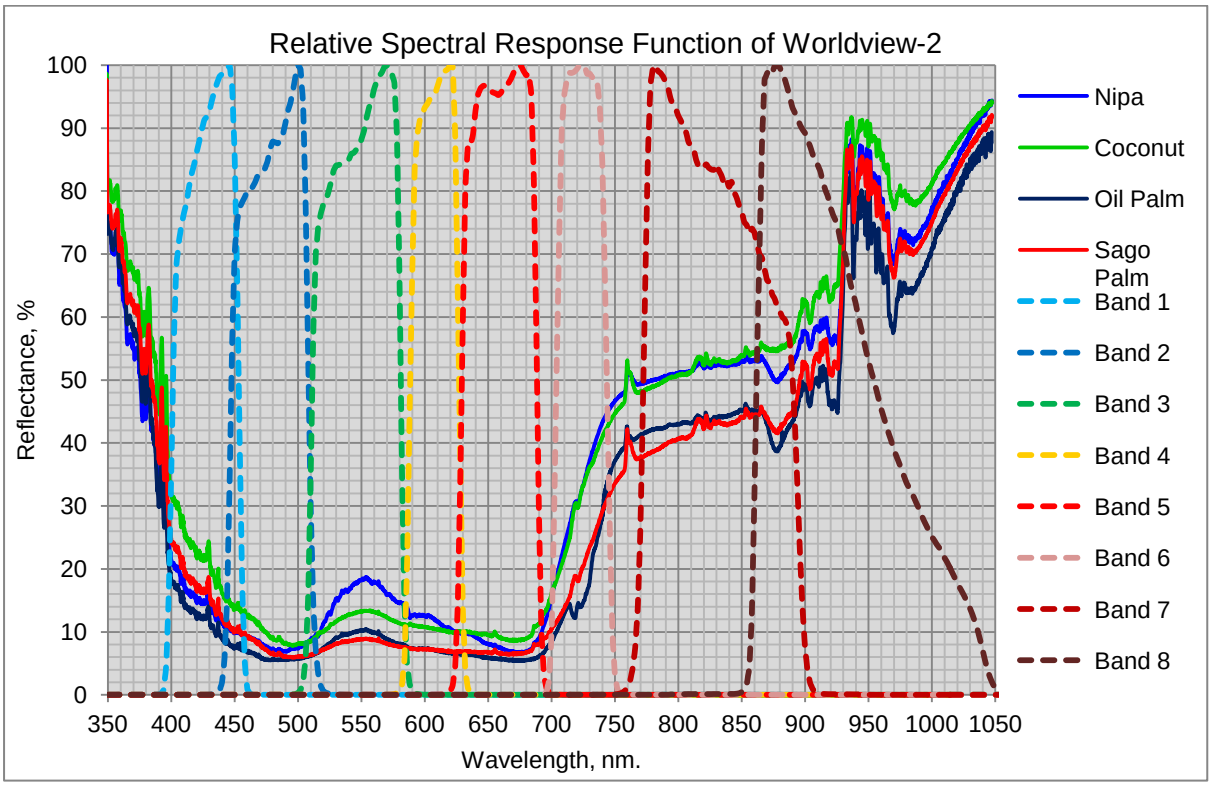

Figure 20. Relative spectral response functions (RSRF) of Worldview-2 shown together with the in-situ spectral reflectance of Sago and other palms.

5.4.1 Resampled Palm In-situ Reflectance in Landsat 7 ETM+ Bands

Figure 21 shows the resampled in-situ reflectance values of Sago and other palms in Bands 1-4 of Landsat 7 ETM+. The reflectance values of Sago palm appear to be similar to that of oil palm in Bands 2, 3 and 4. There is slight difference in reflectance values of Sago palm to those of other palms in Bands 2 and 4. Looking at the differences in reflectance values of Sago with those of other palms (Figure 22), it appears that none of the four bands of Landsat 7 ETM+ is suitable to discriminate Sago with other palms if they are to be used individually.

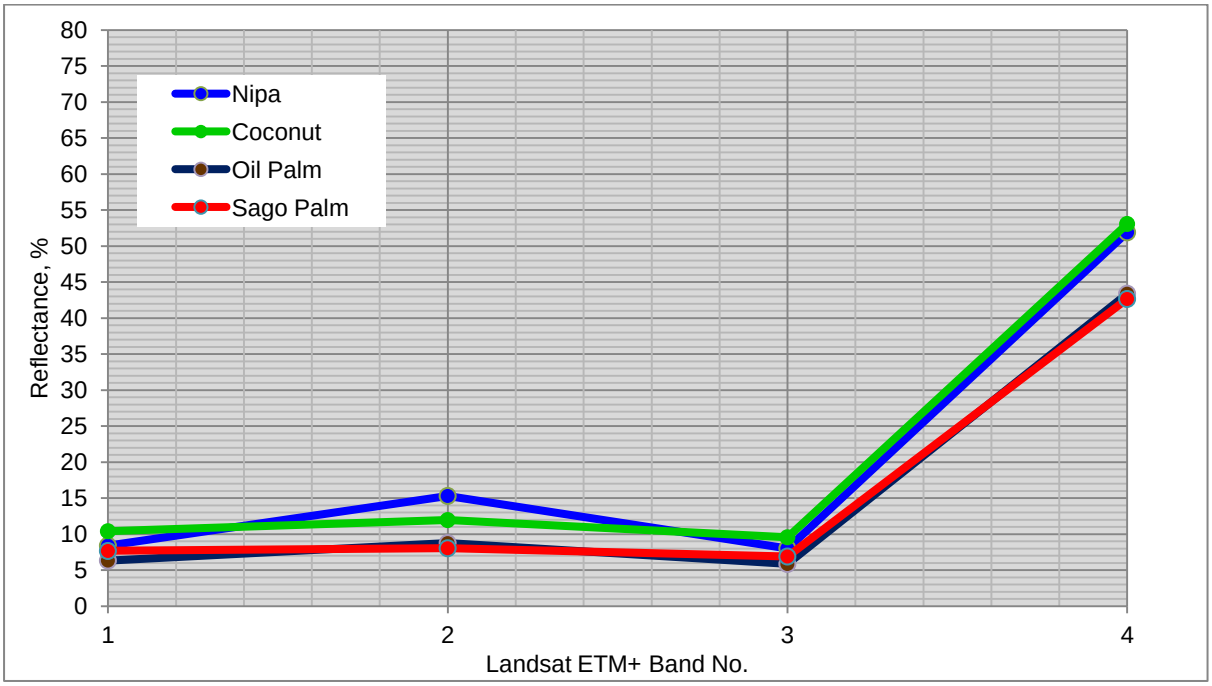

Figure 21. Resampled in-situ reflectance values of Sago and other palms in Bands 1-4 of Landsat 7 ETM+.

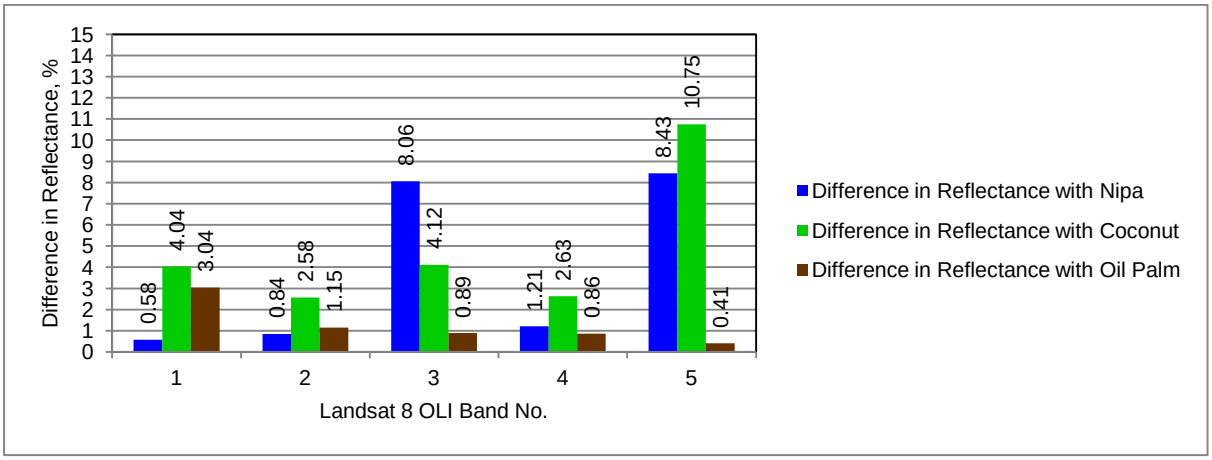

Figure 22. Difference in resampled in-situ reflectance of Sago with those of other palms in Bands 1-4 of Landsat 7 ETM+.

5.4.2 Resampled Palm In-situ Reflectance in Landsat 8 OLI Bands

Figure 23 shows the resampled in-situ reflectance values of Sago and other palms in Bands 1-5 of Landsat 8 OLI. The reflectance values of Sago palm appear to be similar to those of nipa in Band 1, and to oil palm in Bands 3 and 5. There is slight difference in reflectance values of Sago palm to those of other palms in Bands 2 and 4. Looking at the differences in reflectance values of Sago with those of other palms (Figure 24), it appears that Bands 2 and 4 are the only bands useful to discriminate Sago with other palms but the minimum differences is very low. At Band 2, Sago palm's reflectance differs to that of coconut by 2.58%, to oil palm by 1.15%, and to nipa by 0.84%. At Band 4, the difference is 2.63% with coconut, 1.21% with nipa, and 0.86% with oil palm. Based on this data, it shows that Landsat 8 OLI bands, just like Landsat 7 ETM+, may not be suitable to discriminate Sago with other palms if they are to be used individually.

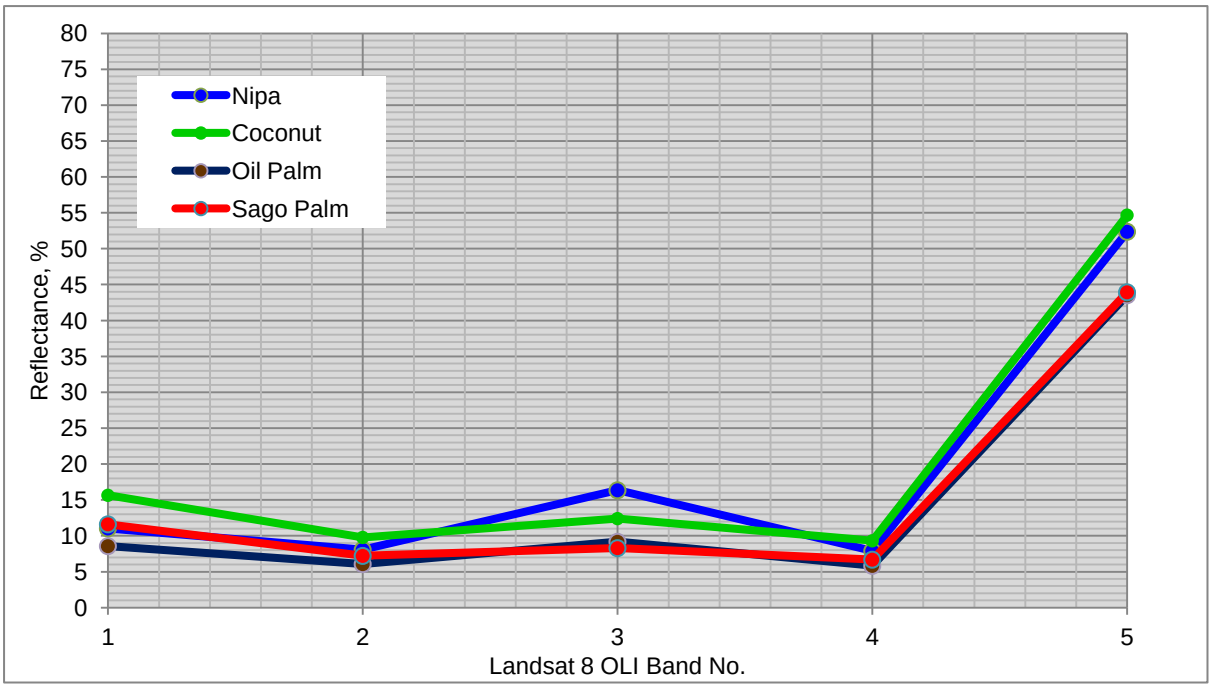

Figure 23. Resampled in-situ reflectance values of Sago and other palms in Bands 1-5 of Landsat 8 OLI.

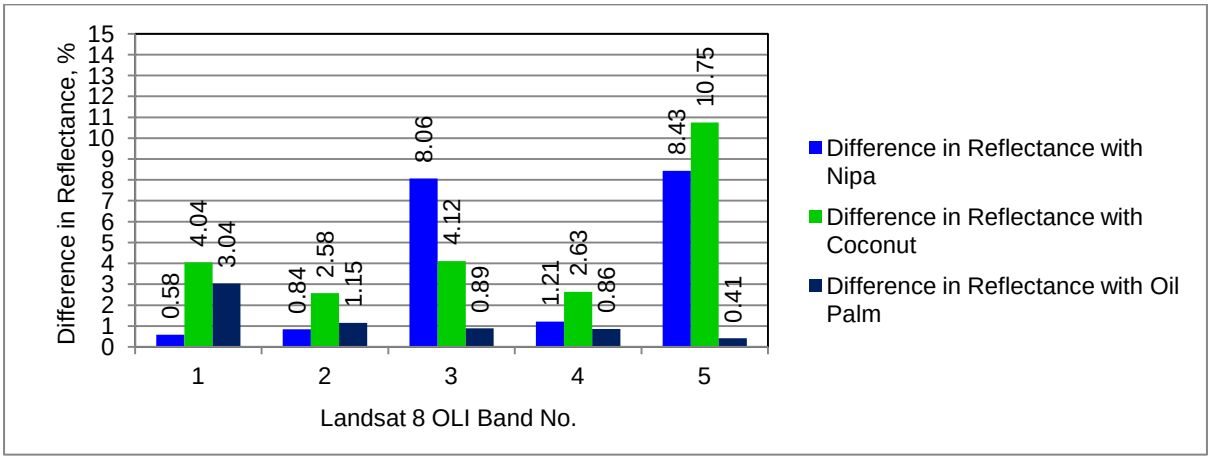

Figure 24. Difference in resampled in-situ reflectance of Sago with those of other palms in Bands 1-5 of Landsat 8 OLI.

5.4.3 Resampled Palm Reflectance in ASTER VNIR Bands

Figure 25 shows the resampled in-situ reflectance values of Sago and other palms in Bands 1-3 of ASTER VNIR. The reflectance values of Sago palm appear to be similar to those of oil palm in Band 1. In Bands 2 and 3, the reflectance values of Sago palm appear to be dissimilar with the other palms. Looking at the differences in reflectance values of Sago with those of other palms (Figure 26), it appears that Bands 2 and 3 are useful to discriminate Sago with other palms with the differences greater than 1%. In Band 3, there is large separability between reflectance values implying that Sago palm can be best discriminated in this band.

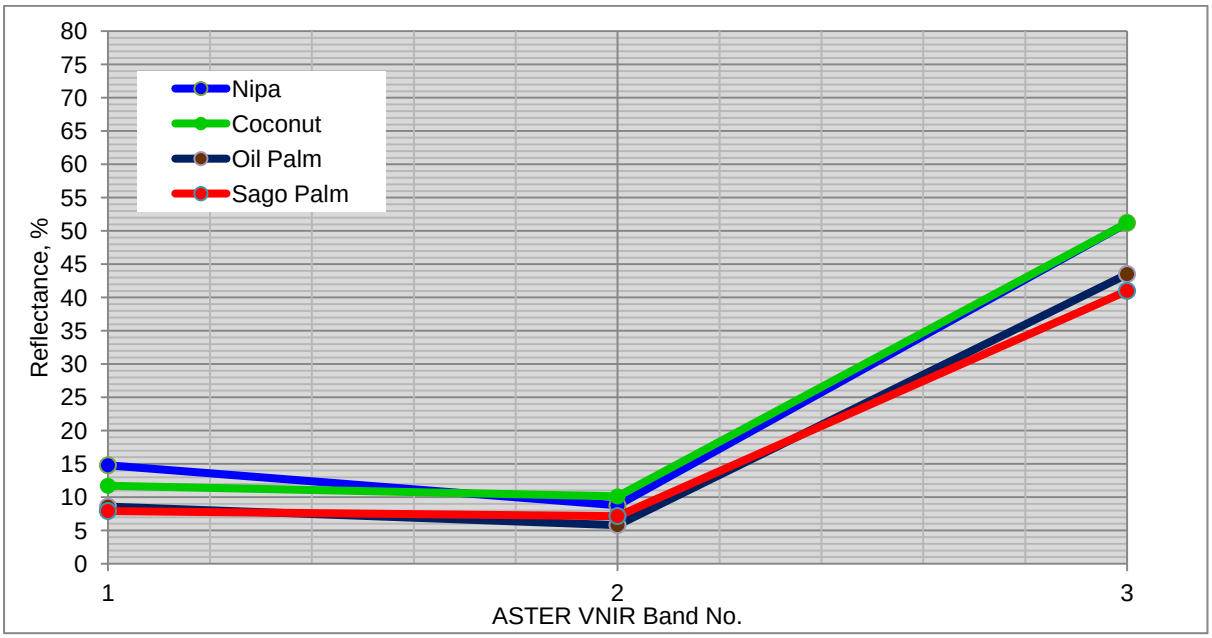

Figure 25. Resampled in-situ reflectance values of Sago and other palms in Bands 1-3 of ASTER VNIR.

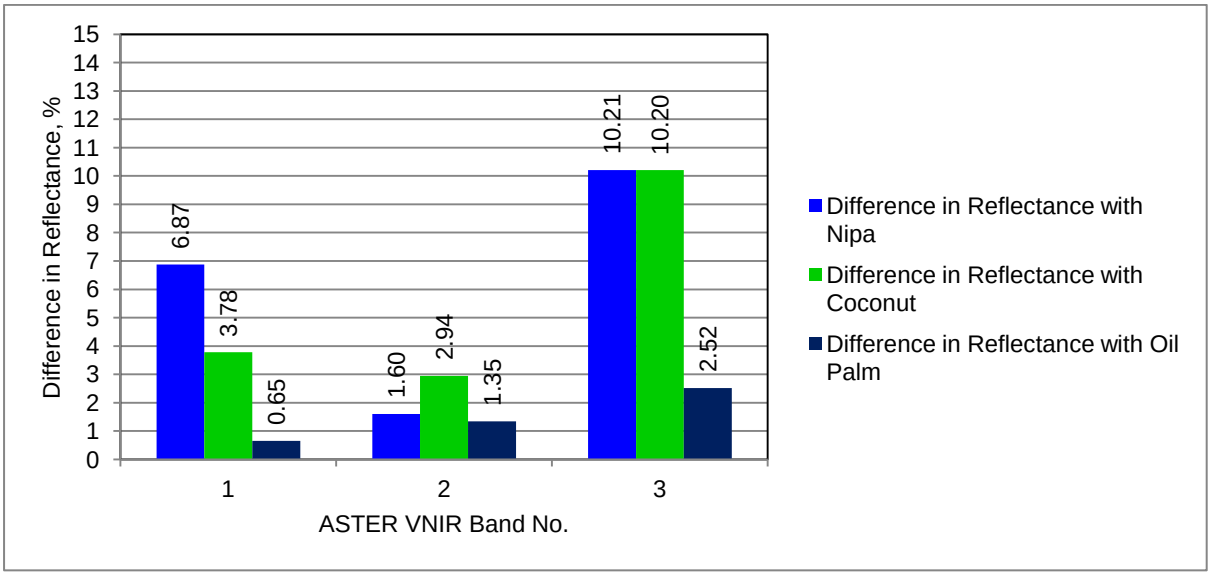

Figure 26. Difference in resampled in-situ reflectance of Sago with those of other palms in Bands 1-3 of ASTER VNIR.

5.4.4 Resampled Palm Reflectance in ALOS AVNIR-2 Bands

Figure 27 shows the resampled in-situ reflectance values of Sago and other palms in Bands 1-4 of ALOS AVNIR-2. The reflectance values of Sago palm appear to be similar to those of oil palm in Bands 2 and 3. In Bands 1, the reflectance of Sago palm has value nearer to that of Nipa. Looking at the differences in reflectance values of Sago with those of other palms (Figure 26), it appears that ALOS AVNIR-2 bands 1-3 may not be suitable to discriminate Sago with other palms if they are to be used individually. In Band 4, there is better separability between reflectance values implying that Sago palm can be best discriminated in this band.

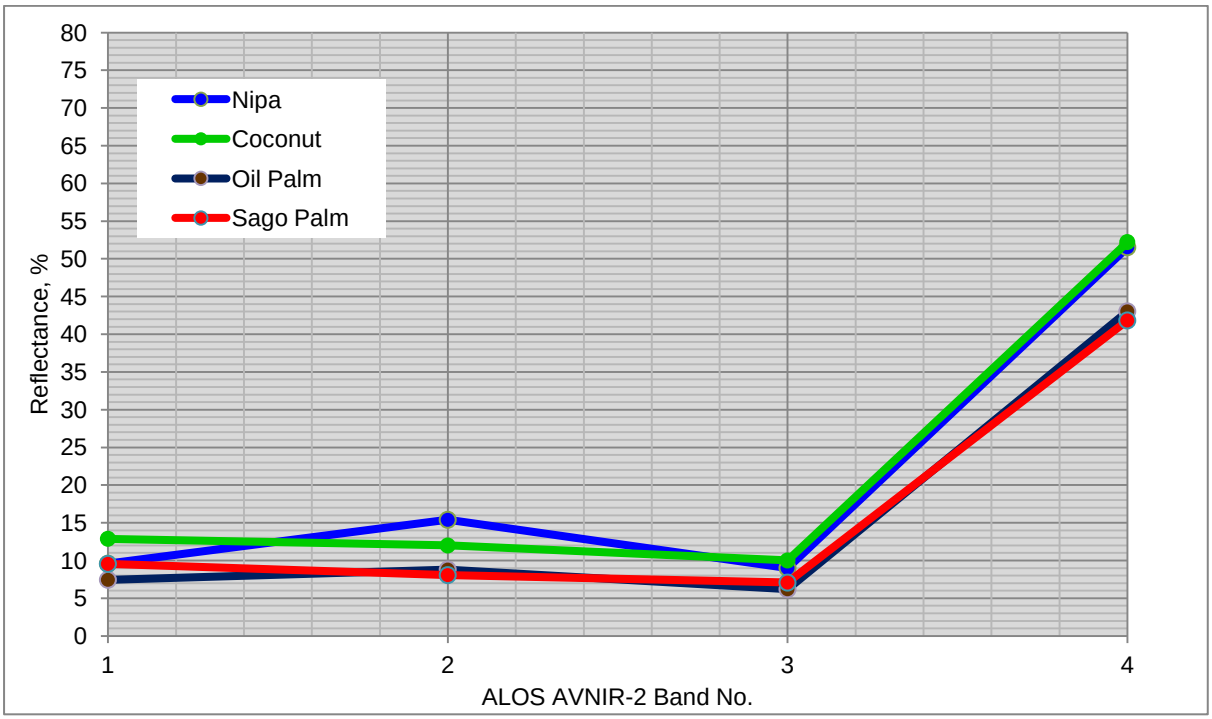

Figure 27. Resampled in-situ reflectance values of Sago and other palms in Bands 1-4 of ALOS AVNIR-2.

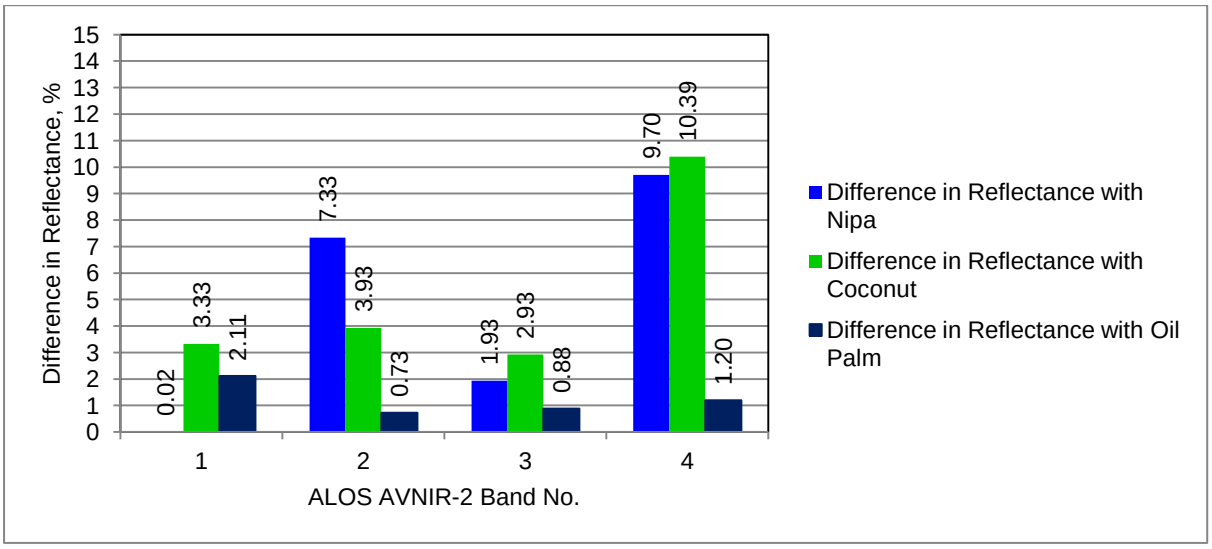

Figure 28. Difference in resampled in-situ reflectance of Sago with those of other palms in Bands 1-4 of ALOS AVNIR-2.

5.4.5 Resampled Palm Reflectance in Worldview-2 Bands

Figure 29 shows the resampled in-situ reflectance values of Sago and other palms in Bands 1-8 of Worldview-2. Compared to the other 3 sensors, there are several bands of Worldview-2 that are useful in discriminating Sago from other palms. These bands are 1, 6, 7 and 8. The greatest difference in reflectance values can be found in Band 8 followed by Band 6 (Figure 28).

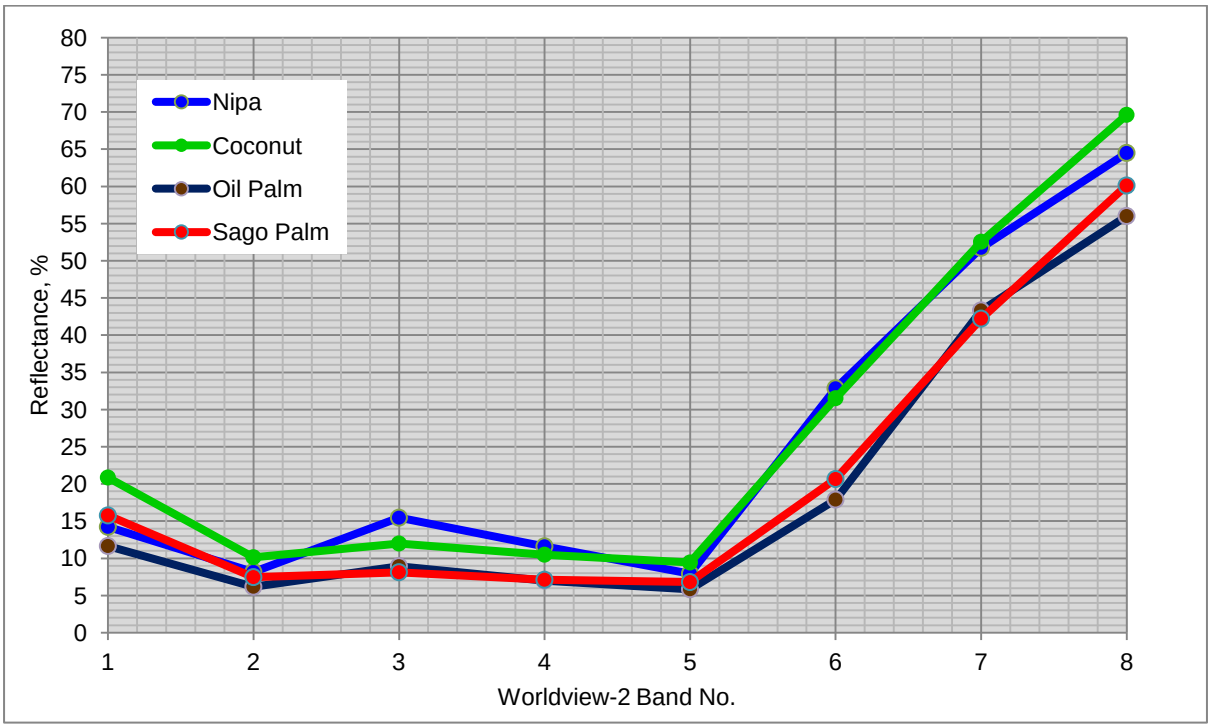

Figure 29. Resampled in-situ reflectance values of Sago and other palms in Bands 1-8 of Worldview-2.

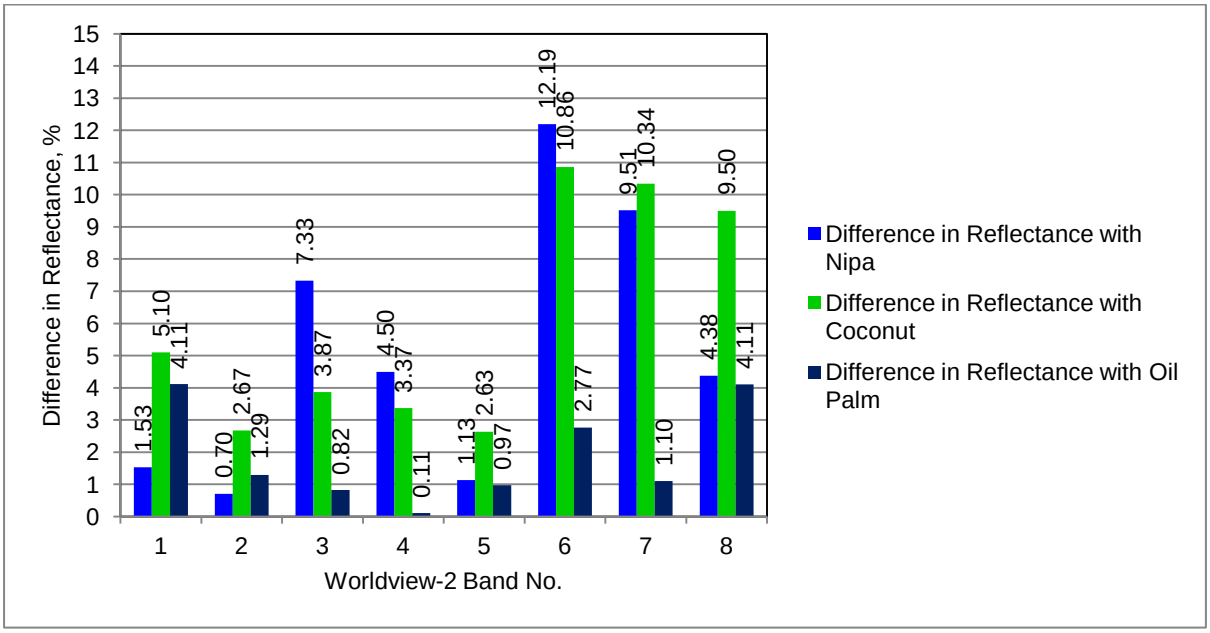

Figure 30. Difference in resampled in-situ reflectance of Sago with those of other palms in Bands 1-8 of Worldview-2.

5.5 Chapter Conclusions

In this chapter, important information with regards to differences in spectral reflectance of Sago and other palms in the visible to near infra-red region of the electromagnetic spectrum was revealed. The analysis of the reflectance spectra measured from the field showed that the blue and red regions are the best portions, especially those at the 400-500 nm and at 650-700, in distinguishing growth stages of Sago palm. The two groups of growth stages: rosette-bole formation and inflorescence-fruit ripening can be distinguished at 770 nm.

Further analysis of reflectance spectra showed that in general, Sago, coconut, nipa and oil palms have lower reflectance in the blue and red regions but higher reflectance in the green region. There were several portions of the electromagnetic spectrum where Sago palm is distinguishable from other palms. The NIR region, specifically at 770, 800 and 875 nm, provides the best wavelengths where Sago palm can be distinguished from other palms.

The resampling of the in-situ reflectance spectra to match the spectral response of optical sensors namely, Landsat 7 ETM+, Landsat 8 OLI, ASTER VNIR, ALOS AVNIR-2 and Worldview-2 made possible the analysis of the differences in reflectance values of Sago and other palms in different bands of the sensors. Results showed that both Landsat 7 ETM+ and Landsat 8 OLI bands may not be suitable to discriminate Sago with other palms if they are to be used individually. The differences of Sago palm's reflectance values with those of the other palms were very low in bands 1-5 of Landsat 8 OLI. On the other hand, Sago palm can be best discriminated in Band 3 of ASTER VNIR because of large differences in reflectance values. For ALOS AVNIR-2, all of its four bands appear to be not suitable to discriminate Sago with other palms if used individually. This observation is the same with that of Landsat 7 ETM+ and Landsat 8 OLI. It suggest that if images acquired by either Landsat 7 ETM+, Landsat 8 OLI, ALOS AVNIR-2 and even ASTER VNIR are to be used to detect Sago palms, the use of single band may not provide good results. The use of all bands (and maybe some derivatives such as NDVI) may be helpful to successfully detect Sago palms by discriminating them from other palm vegetation.

A more interesting result was obtained with the analysis of Worldview-2 reflectance values of Sago and other palms. Compared to the other 3 sensors, there were four bands that appear to be useful in discriminating Sago from other palms: Bands 1, 6, 7 and 8. It is in these bands that the large differences in reflectance values were obtained.

In all the optical sensors, it was very evident that the resampled reflectance of Sago palm is similar with those of Oil palm. This is similar to what can be observed even if the spectral reflectance curves of these two palms have not yet been resampled. As far as spectral reflectance information is used, this similarity can greatly affect the discrimination of Sago palm from oil palms in any of the images such as misclassifying oil palms as Sago palm or vice-versa.

The knowledge learned is this chapter is useful in the actual analysis of optical satellite images, specifically in determining which band to include or to exclude, or whether to use all bands of a sensor in discriminating and mapping Sago palms using the images. An important matter not discussed in this chapter is the consistency of the patterns obtained in the analysis of in-situ reflectance values with those obtained from the images (i.e., image-

based reflectance values). Another matter not done is the comparison between the palm reflectance values with non-palm vegetation. Although it was shown that Sago palms are distinguishable from other palms, it was not established if they are also distinguishable from other types of vegetation. This will be addressed through image-based spectral reflectance analysis (Chapter 6).

Chapter 6. Analysis of Image-derived Spectral Reflectance of Sago and Other Vegetation Types

In this chapter, the analysis presented in the previous chapter is extended to cover non-palm vegetation types and other land-cover classes. Instead of in-situ reflectance data, reflectance data derived from Landsat 7 ETM+, and ALOS AVNIR-2 were used. The analysis focused only on these two sensors as their images were the ones used in the actual mapping of Sago palms.

Visited locations of Sago palm and other land-cover types were used to aid in collecting reflectance data from the satellite images. It was also aided by high resolution images available in the Google Earth application.

Table 4. List of land-cover classes used in the image-based spectral reflectance analysis.

Name	Description
Barren areas	Denuded mountain areas, bare exposed soils (other than unplanted croplands). Also include unpaved roads. May include very thin patches of grassland.
Built-up areas and other impervious surfaces	Residential, commercial and industrial areas as well as other man-made features such as roads and bridges, majority of which have impervious surfaces. Exposed river beds and rocks in mountain are also included in this class.
Cropland - Unplanted, dry	Comprised of areas used for agriculture but not yet planted and dry.
Cropland - Unplanted, wet	Comprised of areas used for agriculture but not yet planted and wet.
Cropland - Planted	Comprised of areas used for agriculture but already planted (e.g., fields planted with rice, corn, etc.)
Grassland	Areas where the vegetation is dominated by grasses and other herbaceous (non-woody) plants.
Palm - Sago	Tracts of land containing Sago.
Palm - Banana	Tracts of land containing banana.
Palm - Coconut	Tracts of land containing coconut.
Palm - Nipa	Tracts of land containing nipa.
Palm - Oil	Tracts of land containing oil palm.
Other non-palm vegetation - Mangroves	Mangrove forests
Other non-palm vegetation - Marsh	Marshy vegetation (e.g., those found in the Agusan Marsh; usually shrubs and trees submerged in water)
Other non-palm vegetation - Shrubs and trees	Densely vegetated areas, especially of the vegetation type found in forested areas (e.g., wooded vegetation). Also includes trees planted in parks and recreational areas, in residential areas and along the road. This type does not include grasslands, mangroves and palm vegetation.
Water bodies	Sea, lakes, reservoirs, rivers and streams.

The aim of the analysis is to further evaluate the spectral characteristics of Sago palm and its difference from those of other land-cover types. The outcome of the analysis will assist in wide-area mapping Sago palms using Landsat 7 ETM+ and ALOS AVNIR-2.

6.1 Spectral Reflectance Derived from Landsat 7 ETM+ Image

Spectral reflectance of Sago palm and other land-cover classes were extracted from a Level 1T (terrain-corrected) Landsat 7 ETM+ image covered under the World Reference System (WRS)-2 path 112 row 54. The image was downloaded from the USGS Global Visualization Viewer (GLOVIS, http://www.glovis.usgs.gov/). The image was acquired on September 14, 2008 and contains the provinces of Agusan del Norte, Agusan del Sur, and Surigao del Sur as well as portions of Surigao del Norte, Davao Oriental, Compostela Valley, Bukidnon and Misamis Oriental (Figure 31). The image has gaps due to the Scan-Line Corrector (SLC) error of the Landsat ETM+ sensor. Some portions of the image are also covered by clouds. Nonetheless, this image was still selected because it contains representative locations of all the land-cover classes listed in Table 4.

Prior to extraction of land-cover reflectance values, the image underwent radiometric calibration and atmospheric correction using ENVI 5 software. The radiometric calibration consisted of converting the pixel values (in Digital Number, DN) to top-of-atmosphere (TOA) or at-sensor radiance (W/m^2sr^{-1}) and TOA reflectance. The TOA reflectance values were then corrected for atmospheric effects through dark object subtraction by band minimum. The image was then checked for geometric accuracy using 9 control points (mostly road intersections) collected from 1:50,000 NAMRIA topographic maps. The total root mean square error (RMSE) of the comparison of the UTM 51 WGS 1984 coordinates of the control points in the image and in the topographic map was found to be less than 15 meters. The image was no longer subjected to geometric correction by georeferencing since the rule-of-thumb of total RMSE ≤ 0.5 pixel (15 m) was satisfied.

The numbers of pixels collected per land-cover type from the Landsat ETM+ image are summarized in Table 5. For each land-cover type, the average image reflectance per band were computed and plotted in Figure 32. The values were plotted as bar graphs instead of line graphs to improve clarity and to easily show the differences in reflectance values. The average values of NDVI (multiplied by 100) are also plotted as additional information. NDVI was computed as (Band 4 - Band 3)/(Band 4 + Band 3).

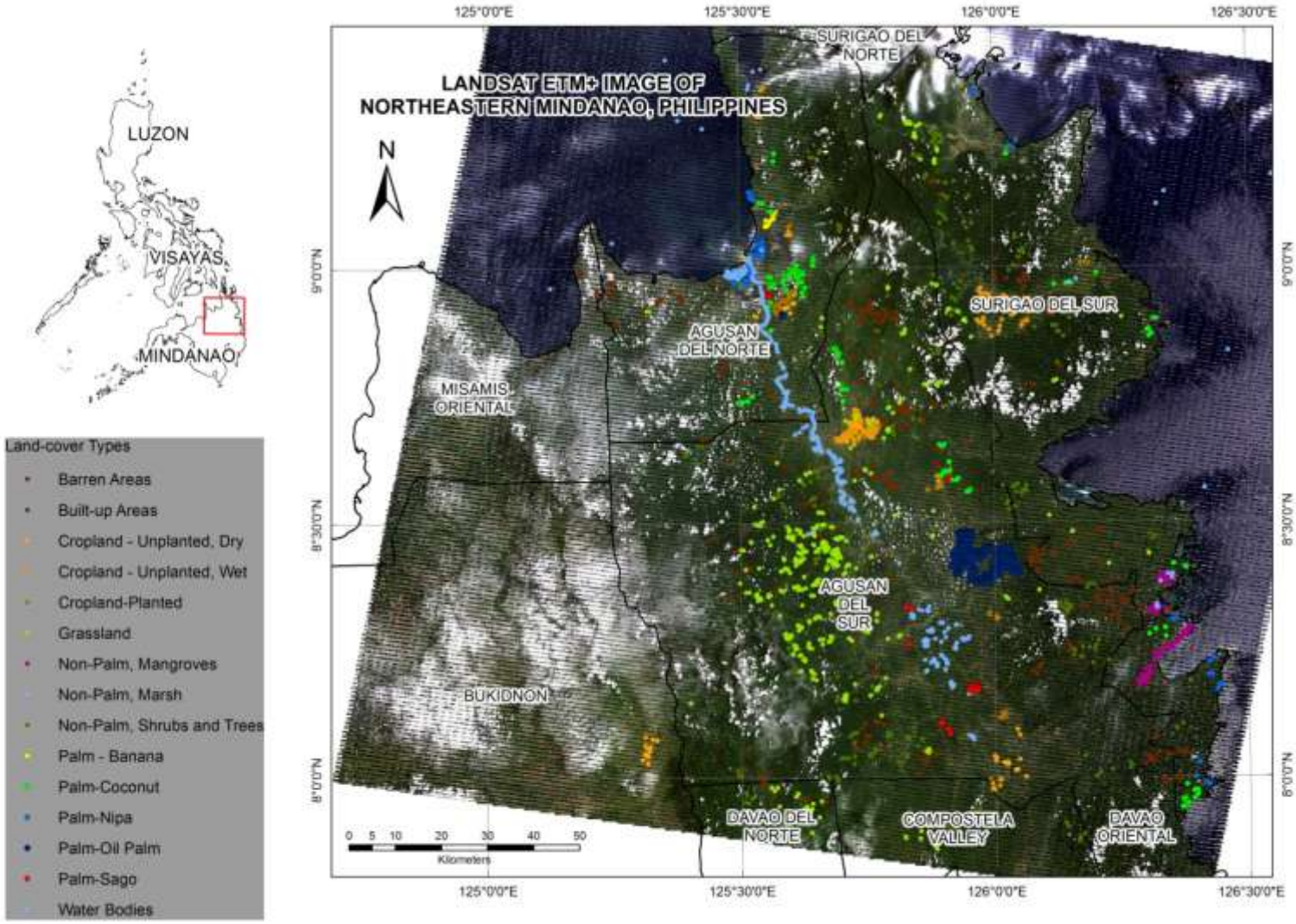

Figure 31. The Landsat ETM+ image acquired on September 14, 2008 including the locations of pixels of land-cover types used in spectral analysis.

Table 5. Number of pixels collected per land-cover type from the Landsat ETM+ image.

Name	Number of Pixels
Barren areas	2,160
Built-up areas and other impervious surfaces	2,444
Cropland - Unplanted, dry	1,752
Cropland - Unplanted, wet	1,924
Cropland - Planted	1,913
Grassland	1,851
Palm - Sago	1,046
Palm - Banana (growth stage unknown)	1,324
Palm - Coconut	1,300
Palm - Nipa	652
Palm - Oil Palm	9,620
Other non-palm vegetation - Mangroves	1,762
Other non-palm vegetation - Marsh	760
Other non-palm vegetation - Shrubs and trees	14,682
Water bodies	2,222

It can be seen in Figure 32 that in bands 1-3 (blue, green and red), reflectance values of all land-cover types except for built-up areas are low with majority of the land-cover types having reflectance values less than 10%. In these bands, reflectance of Sago palm is almost similar to those of other palms, especially to that of oil palm. In band 4, pronounced differences in reflectance values can be observed. In this band, Sago palm can be discriminated from other land-cover types except from coconut. The difference in reflectance values between the two is less than 1%. Better differences in reflectance values among the land-cover types can be found in Band 5. In this band, Sago palm can be discriminated from other palms, with differences between reflectance values greater than 1%. In Band 7, very low reflectance values were observed for all vegetation classes (<5%). In this band, Sago palm cannot be discriminated from nipa due to almost similar reflectance values. In general, it can be seen that there is no band that Sago palm can be uniquely discriminated from other land-cover types both palm and non-palm. In terms of NDVI, there are great differences in values between the land-cover types. Among the palms, oil palm has the highest average NDVI followed by Sago while nipa has the lowest. It appears that NDVI can be useful in discriminating Sago palm other vegetation types. In all the bands including NDVI, Sago palm can be discriminated form non-vegetation classes (barren areas, built-up, water, unplanted cropland). Just like in the analysis of in-situ reflectance, if images acquired by Landsat 7 ETM+ are to be used to detect Sago palms, the use of all bands (and maybe some derivatives such as NDVI) may be helpful to successfully detect Sago palms by discriminating them from other palm and non-palm vegetation instead of individual use of any of the bands.

The image-derived reflectance values of Sago and other palms appear to be lower than their resampled in-situ reflectance values (presented earlier in Figure 21). This is due to several reasons such as the spatial resolution of the image, difference in locations of the in-situ reflectance data, and the use of more number of image-derived samples. Failure to completely correct the atmospheric effects in the image (such as haziness in some portions and presence of cloud shadows) may be another factor.

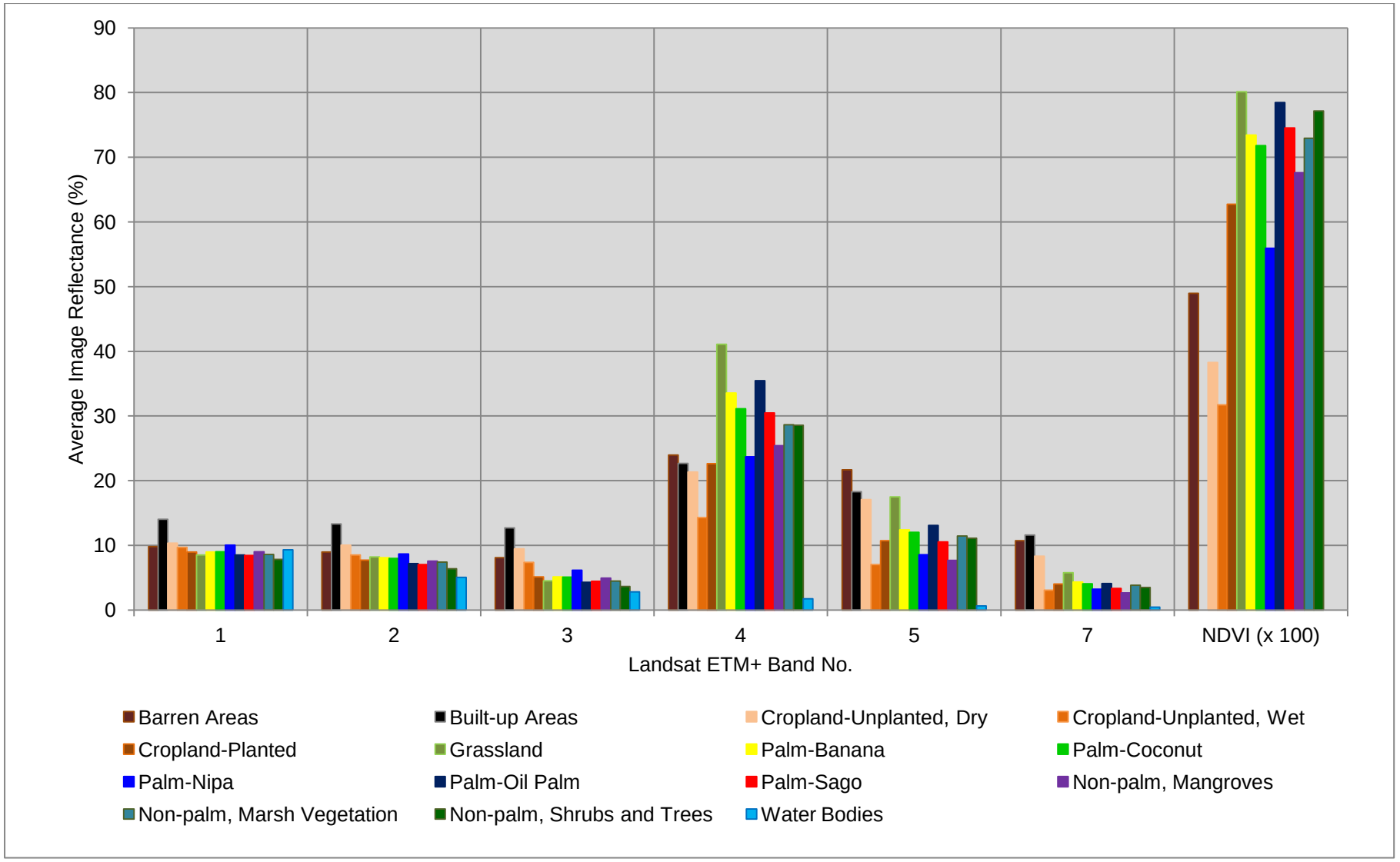

Figure 32. Average reflectance in Bands 1-5 and 7 of Landsat 7 ETM+ including the average NDVI of various land-cover types.

6.2 Spectral Reflectance Derived from ALOS AVNIR-2 Images

Spectral reflectance of Sago palm and other land-cover classes were extracted from three ALOS AVNIR-2 images acquired in 2009 and 2010 (Table 6; Figure 33). Each image is approximately 70 x 70 km in dimension. The images were obtained from the NAMRIA.

Table 6. List of ALOS AVNIR-2 images used for extraction of image-based reflectance of various land-cover types.

Image Index No.	Area Covered	Date of Acquisition
P42	Agusan del Norte, Misamis Oriental	October 4, 2010
Q43	Agusan del Norte, Agusan del Sur, Surigao del Sur	September 14, 2009
R44	Agusan del Sur, Surigao del Sur, Compostela Valley, Davao Oriental	July 16, 2010

Similar to the Landsat 7 ETM+ image, the ALOS AVNIR-2 images also underwent radiometric calibration and atmospheric correction using ENVI 5 software. The radiometric calibration consisted of converting the pixel values (in Digital Number, DN) to top-of-atmosphere (TOA) or at-sensor radiance (W/m^2sr^{-1}). The TOA radiances were then converted to surface reflectance and corrected for atmospheric effects using the Fast Line-of-Sight Atmospheric Analysis of Spectral Hypercubes (FLAASH). Initially, the images were already geo-referenced but there were offsets found when comparing the coordinates of control points from NAMRIA topographic maps with their corresponding coordinates in the image. Hence, each image was geometrically corrected using 9 control points (mostly road intersections) collected from 1:50,000 NAMRIA topographic maps with total RMSE ≤ 0.5 pixel.

The numbers of pixels collected per land-cover type from the ALOS AVNIR-2 images are summarized in Table 7. Representative samples of land-cover types were collected in images where they are found to be dominant. For each land-cover type, the average image reflectance per band were computed and plotted in Figure 34. The values were plotted as bar graphs instead of line graphs to improve clarity and to easily show the differences in reflectance values. The average values of NDVI (multiplied by 100) are also plotted as additional information. NDVI was computed as (Band 4 - Band 3)/(Band 4 + Band 3).

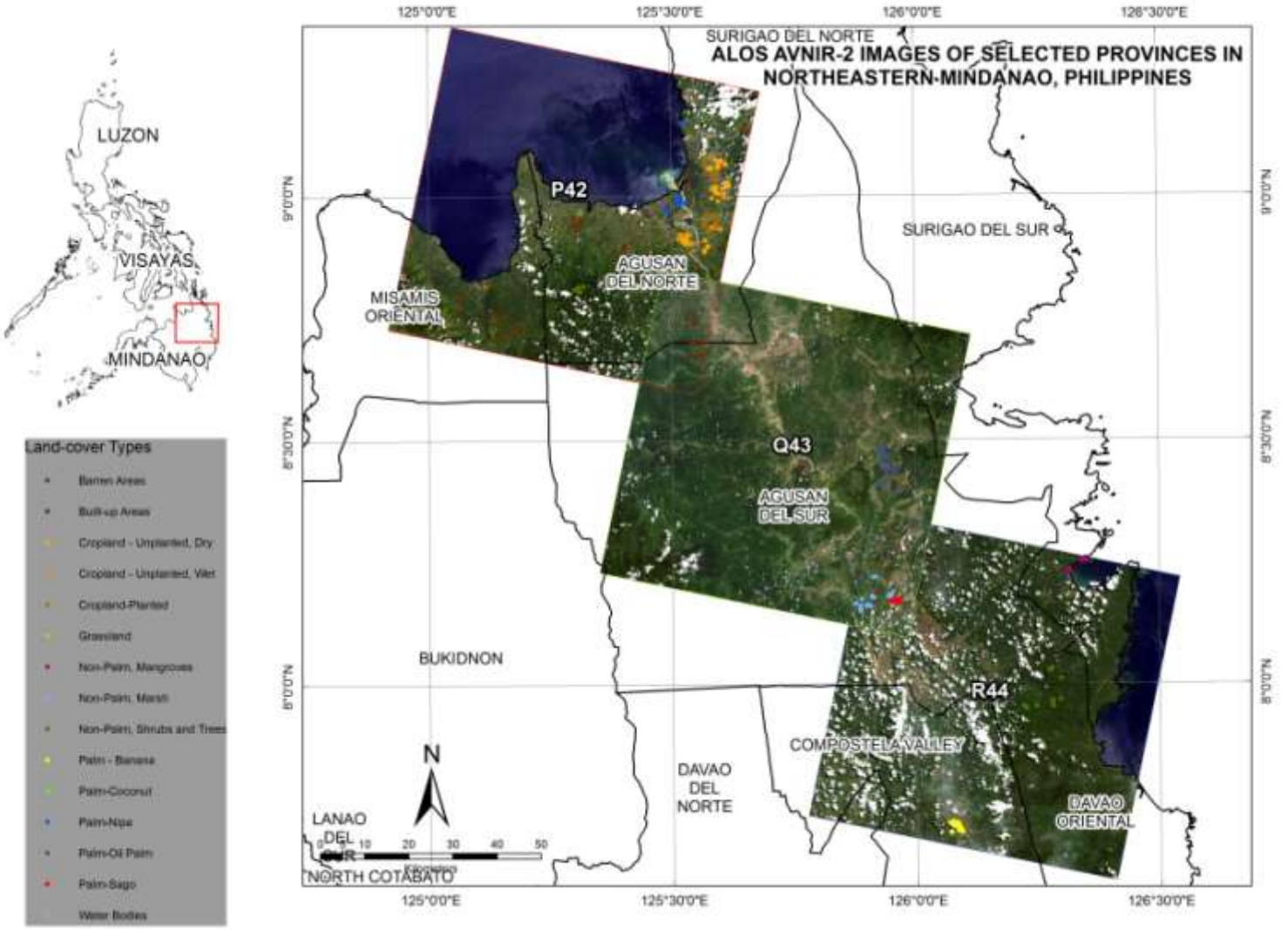

Figure 33. The ALOS AVNIR-2 images including the locations of pixels of land-cover types used in spectral analysis.

Table 7. Number of pixels collected per land-cover type from the ALOS AVNIR-2 images.

Name	Number of Pixels	Source Image Index No.
Barren areas	920	P42
Built-up areas and other impervious surfaces	1,265	P42
Cropland - Unplanted, dry	2,051	P42
Cropland - Unplanted, wet	1,032	P42
Cropland - Planted	1,216	P42
Grassland	1,024	R44
Palm - Sago	1,307	R44
Palm - Banana	2,112	R44
Palm - Coconut	1,763	P42
Palm - Nipa	1,119	P42
Palm - Oil Palm	4,935	Q43
Other non-palm vegetation - Mangroves	1,137	R44
Other non-palm vegetation - Marsh	4,713	R44
Other non-palm vegetation - Shrubs and trees	4,594	R44
Water bodies	12,516	P42

Based on the graph, the following are the observations: in bands 1 and 2, similarities in reflectance values of Sago and other vegetation are evident. In these bands, Sago palm's reflectance value closely resembled that of nipa. In band 3, a decreasing trend in reflectance values can be observed for all palms. Among the palms, banana has the highest reflectance value and Sago palm has the lowest. Difference in reflectance values of Sago palm from other land-cover types can be observed also. In band 4, higher reflectance values were observed for grassland and banana. Surprisingly, Sago palm has the third highest reflectance value in this band and has greater difference with other vegetation. This result is similar to what has been observed during the analysis of resampled in-situ reflectance of Sago palm (as discussed earlier in section 5.4.4). In terms of NDVI, Sago palm has the highest among the palms, and can be said to be different from NDVI of other land-cover types except for Shrubs and Trees.

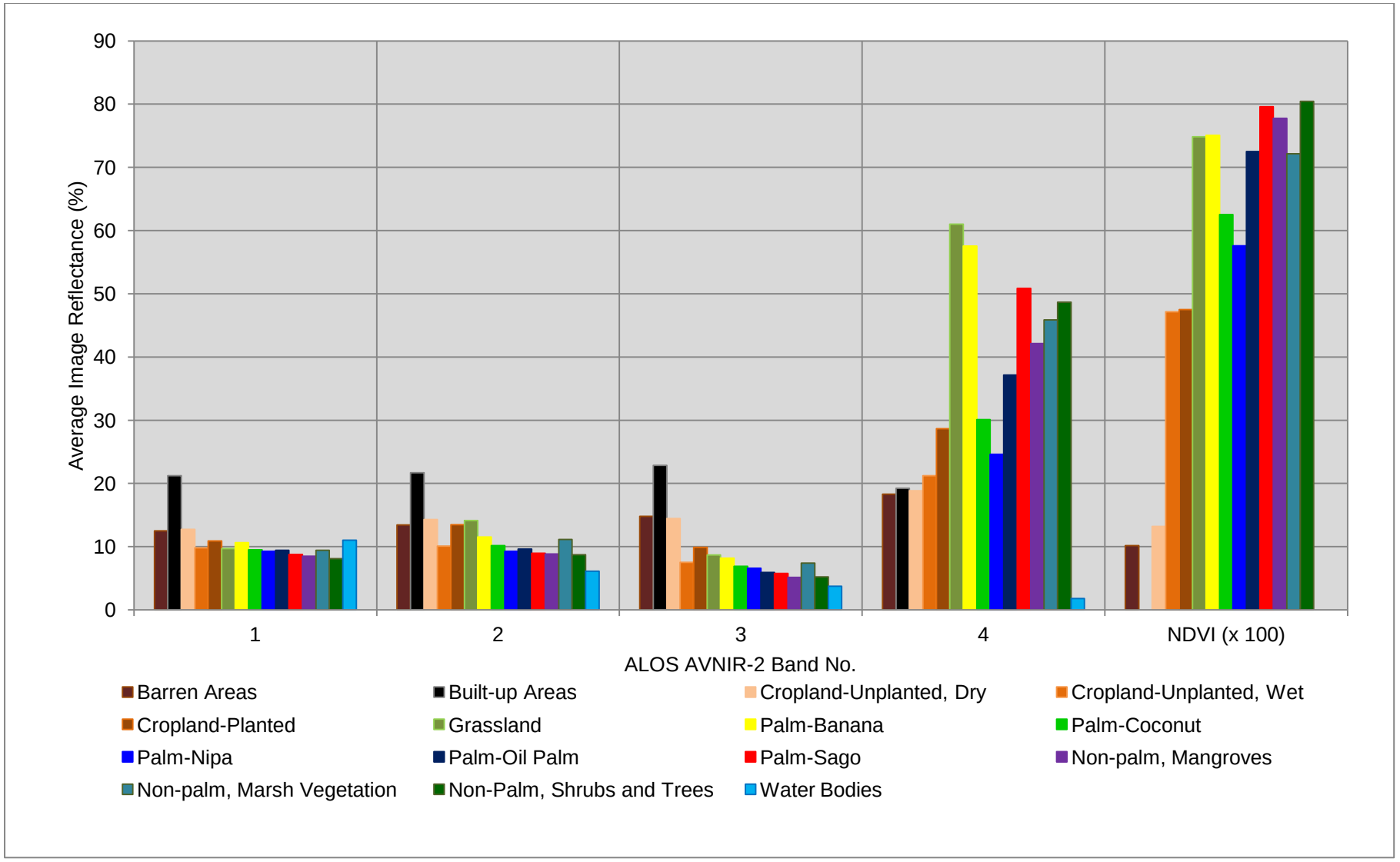

Figure 34. Average reflectance in Bands 1-4 of ALOS AVNIR-2 and NDVI of various land-cover types.

6.3 Discussion and Conclusions

It can be noticed that the average reflectance values derived from ALOS AVNIR-images are higher than what was derived from Landsat 7 ETM+ image. Also, the differences in reflectance values are more apparent in ALOS AVNIR-2 than in Landsat 7 ETM+. One factor that may have contributed to this is the higher spatial resolution of the ALOS AVNIR-2 images which is 10x10 m. Because of this, the reflectance values extracted were more precise because the inclusion of other land-cover types in pixel is minimized. In a Landsat 7 ETM+ image pixel of 30x30 m, several land-cover classes may exist other than the target land-cover type. This in turn affected the reflectance values. Another factor is the differences in locations of the samples used, and the differences in the dates of acquisitions of the images.

The analysis presented in this chapter is more of visual, and mainly focused on the interpretation of average reflectance values. While the analysis revealed some bands of sensors that could best discriminate Sago from other land-cover classes, it needs further analysis through actual image analysis. In land-cover type discrimination/classification using satellite images, supervised classification algorithms are available such as the Maximum Likelihood Classifier to automatically classify a pixel into any of the land-cover types based on statistics coming from sample areas (or training regions of interests). During this process, all or combinations of the bands of a sensor are utilized as inputs. Choosing which band combinations to use can be aided by what has been learned in this chapter.

Chapter 7. Backscattering Characteristics of Sago Palms and Other Land-cover Types: Analysis based on Envisat ASAR image

This chapter presents an analysis of backscattering characteristics of Sago and other land-cover types. The analysis aims to assess if a SAR image acquired by Envisat ASAR sensor can be useful in detecting and discriminating Sago palms from other land-cover types.

7.1 Background on Envisat ASAR

The Advance Synthetic Aperture Radar (ASAR) sensor is a high-resolution imaging radar onboard the Envisat (Environmental Satellite) that was operated by the European Space Agency (ESA). The Envisat was launched on 1 March 2002 into a Sun synchronous polar orbit at an altitude of 790 km. It orbits the Earth in about 101 minutes with a repeat cycle of 35 days. Contact with the satellite was lost on 8 April 2012. On May 9, 2012, ESA formally announced the end of Envisat's mission [**92**].

According to its dedicated website [**93**], Envisat ASAR operates in the C Band (5.7 cm wavelength) and in 5 distinct Measurement Modes: Image Mode (IM), Alternating Polarization Mode (AP), Wide Swath Mode (WS), Global Monitoring Mode, or Wave Mode. Images can be acquired at incidence angles ranging from 15 to 45 degrees, and with choice of 5 polarization modes: horizontal (HH), vertical (VV), or cross (HV, VH). The radiometric resolution is from 1.5 to 3.5 dB with accuracy within 0.65 dB. A single Envisat ASAR scene (IM) is 56 km by 100 km. A processed IM image can have a pixel resolution of 12.5 x 12.5 m.

7.2 Envisat ASAR Test Image and Processing

Figure 35 shows the Envisat ASAR image used in the analysis. The image was acquired on November 15, 2010 at 13:42:13 UTC (or 9:42:13 PM in the Philippines) in IM with HH polarization while the satellite was in ascending mode (incidence angle ranging from 19.2 to 26.7 degrees). This data was provided as a Level 1P product by the ESA under Category 1 Project No. 11044. The image was processed using the Next ESA Tool Box (NEST) version 4C-1.1 in order to generate a radiometrically calibrated and orthorectified sigma nought, σ^0(dB) (also called backscattering or normalized radar cross-section) image in UTM 51 WGS 1984 projection. The order of the steps employed are: (1) refining the orbit state vectors in the product's metadata through application of the DORIS precise orbit file generated by the Centre for Traitement Doris Poseidon and Delft University; (2) radiometric calibration to convert the DN values (amplitude) to radar backscatter or sigma nought (σ^0) in linear scale; (3) de-speckling using the Enhanced/Refined Lee filter; (4) terrain correction using rigorous SAR simulation where a 3-arcsecond SRTM DEM was utilized; (5) radiometric normalization; and (6) computation of backscattering coefficients from the linear scaled and normalized σ^0. The equations used in each step and other details are available in the NEST documentation available at http://nest.array.ca/web/nest/documentation.

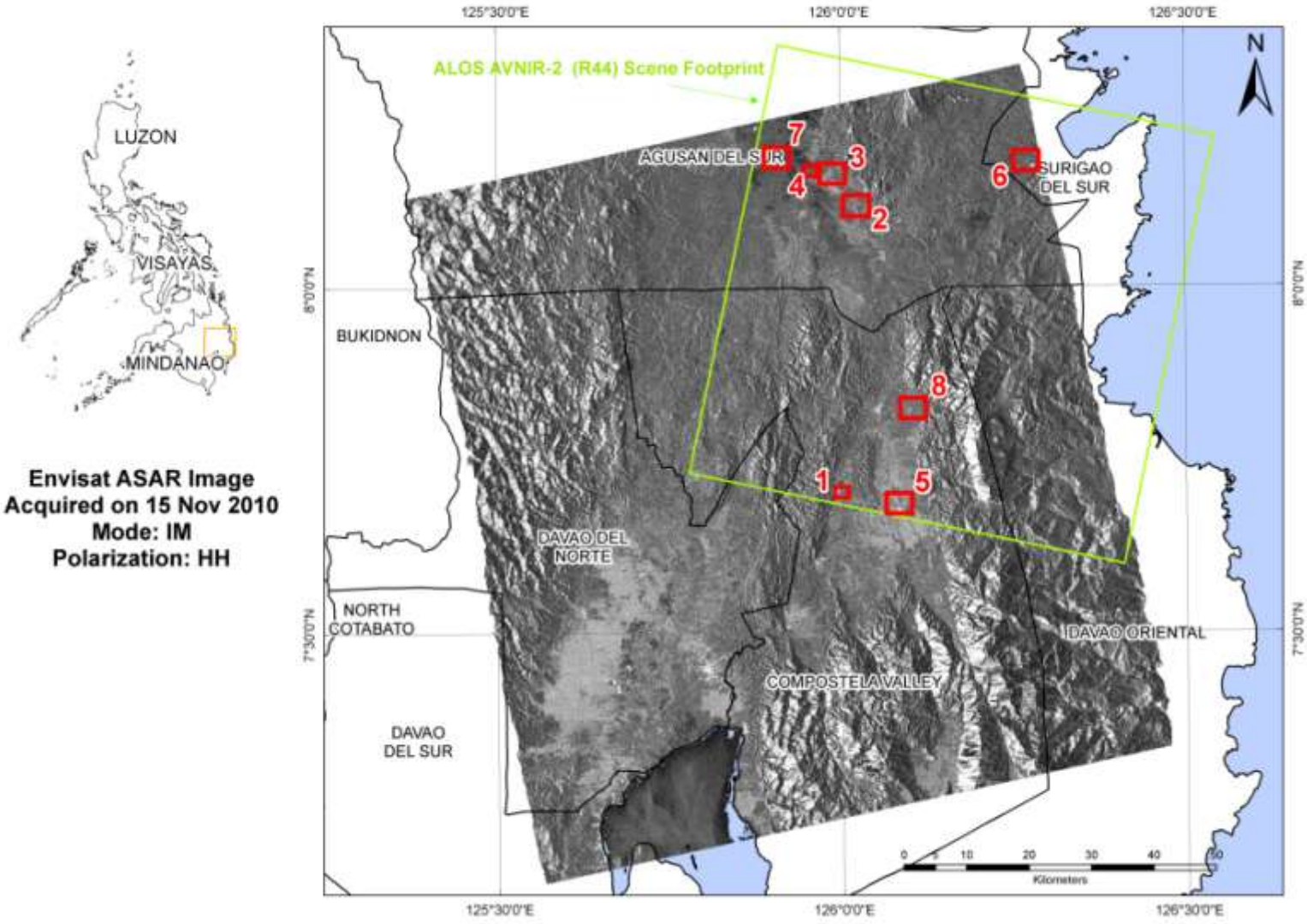

Figure 35. The Envisat ASAR IM test image shown here with the scene footprint of ALOS AVNIR-2 image with index no. R44. The red rectangles (with numbers) indicates locations of imagettes of the SAR image as presented in the following figures.

7.3 Extraction of Backscattering Coefficients

Pixels representing various land-cover classes were identified in the Envisat ASAR image through the use of ground truth data from the field surveys and with the help of ALOS AVNIR-2 (R44) image and high resolution Google Earth images. A series of imagettes are shown in Figure 36, Figure 37, Figure 38 and Figure 39 to illustrate how the land-cover classes appear in the Envisat ASAR image as well as their appearance in a true-color ALOS AVNIR-2 image. The locations of these imagettes are indicated in Figure 35.

The number of pixels randomly collected for each land-cover class was limited to 500 to make a fair analysis and comparison of the backscattering coefficients. Pixels representing nipa were not collected as the collection focused only on the portion of the Envisat SAR image overlapping with the ALOS AVNIR-2 image. Ground truth data of nipa in this portion of the image was not available.

Basic statistics of the backscattering coefficients of the land-cover classes were then computed. These include the mean, minimum, maximum, standard deviation, standard error, and 95% confidence interval of the mean.

To evaluate how different the backscattering coefficient of Sago palm is from other land-cover types, an Analysis of Variance (ANOVA) was employed. First, the ANOVA was used to test if significant differences (at 95% confidence level) exist between the mean backscattering values of the land-cover classes. If such difference exist, the next step employed was the use of Tamhane's T2 (an ANOVA posthoc test) [**94**] to identify which of the land-cover classes have significant differences with their mean backscatter values. In particular, Tamhane's T2 was employed to check if the computed differences between the means of Sago palm with those of other land-cover classes are significant at 95% confidence levels. The analysis was done using SPSS version 16.

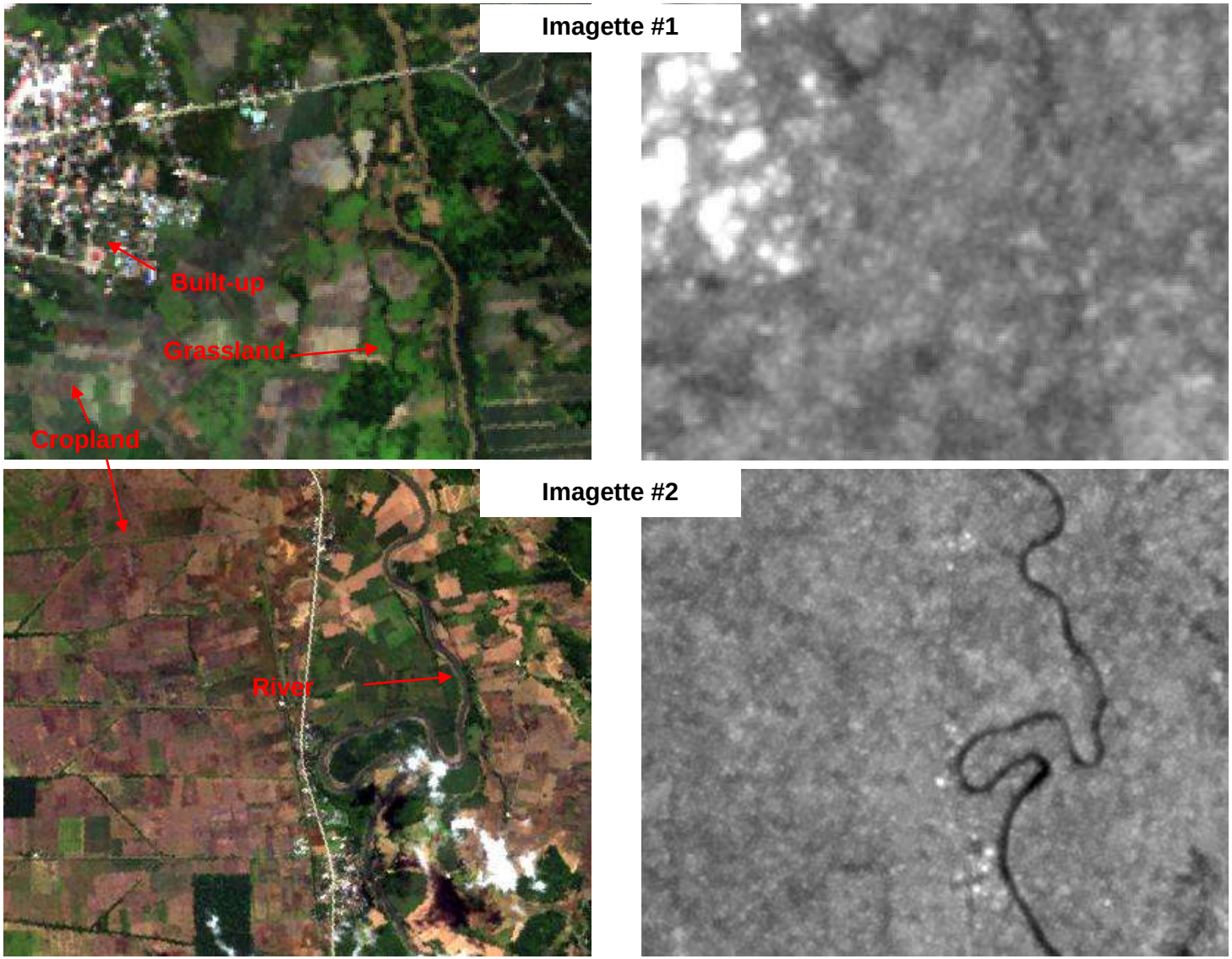

Figure 36. Imagettes 1 and 2 of ALOS AVNIR-2 (left) and the corresponding Envisat ASAR imagettes (right). (Shown not to scale.)

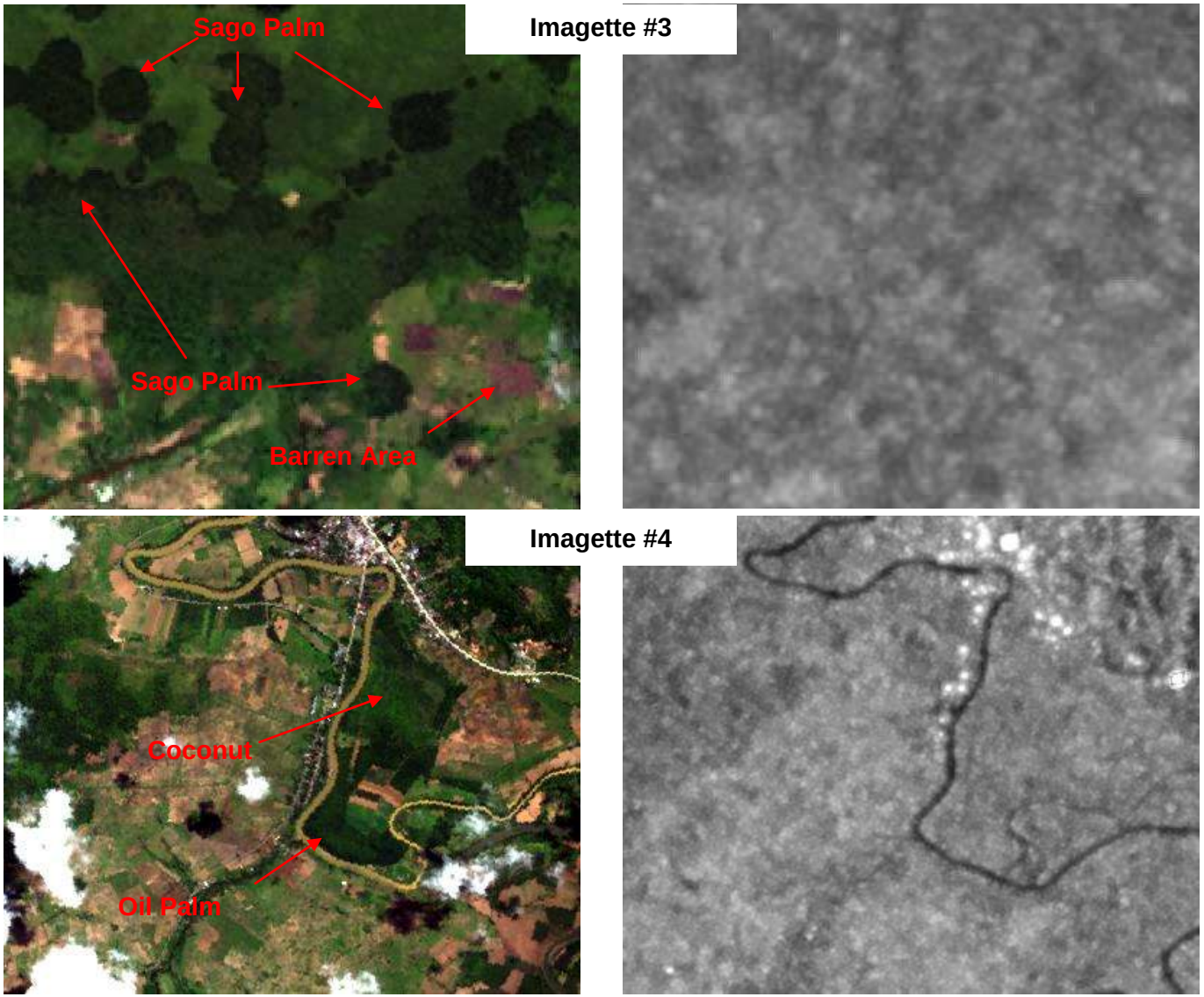

Figure 37. Imagettes 3 and 4 of ALOS AVNIR-2 (left) and the corresponding Envisat ASAR imagettes (right). (Shown not to scale.)

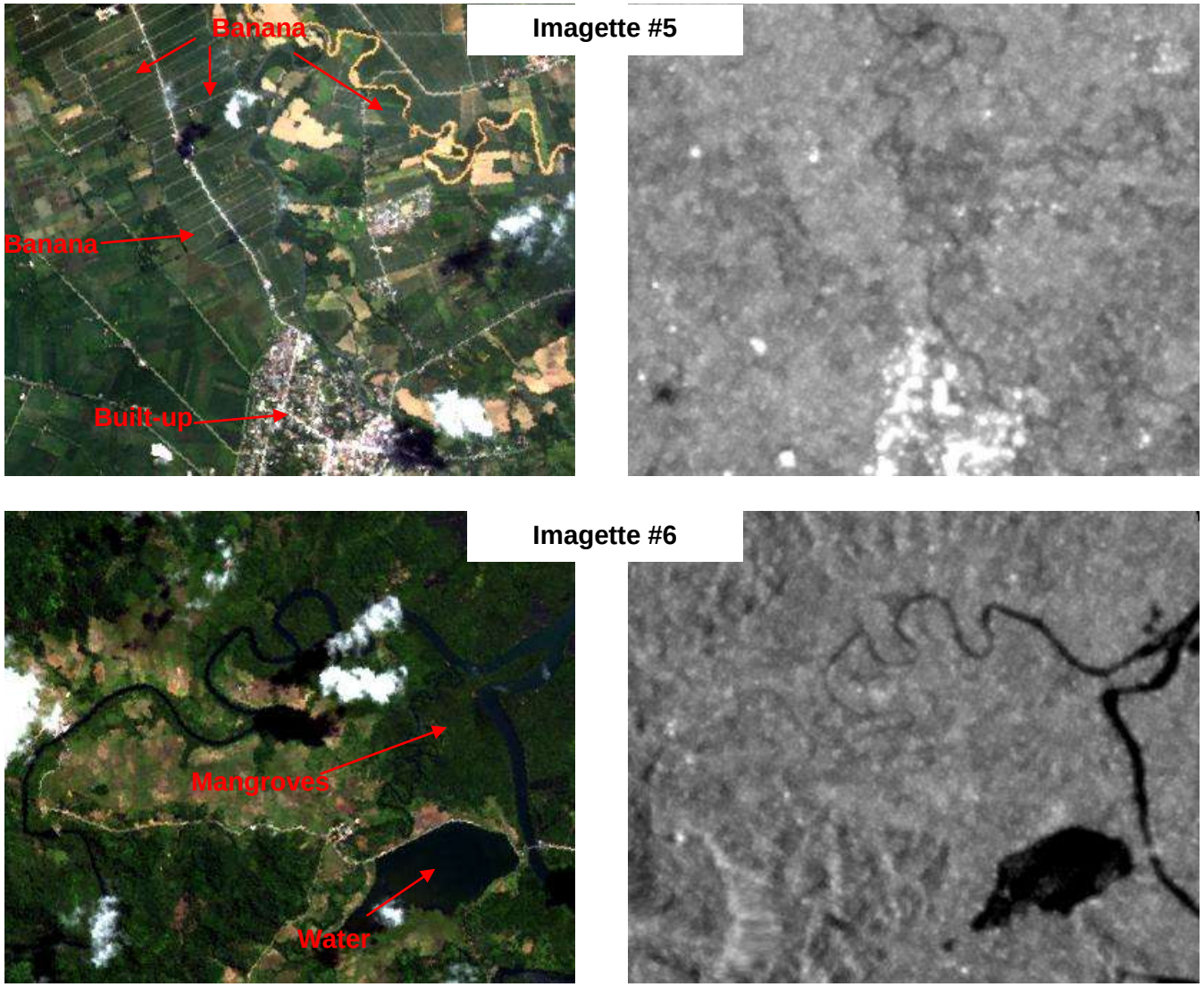

Figure 38. Imagettes 5 and 6 of ALOS AVNIR-2 (left) and the corresponding Envisat ASAR imagettes (right). (Shown not to scale.)

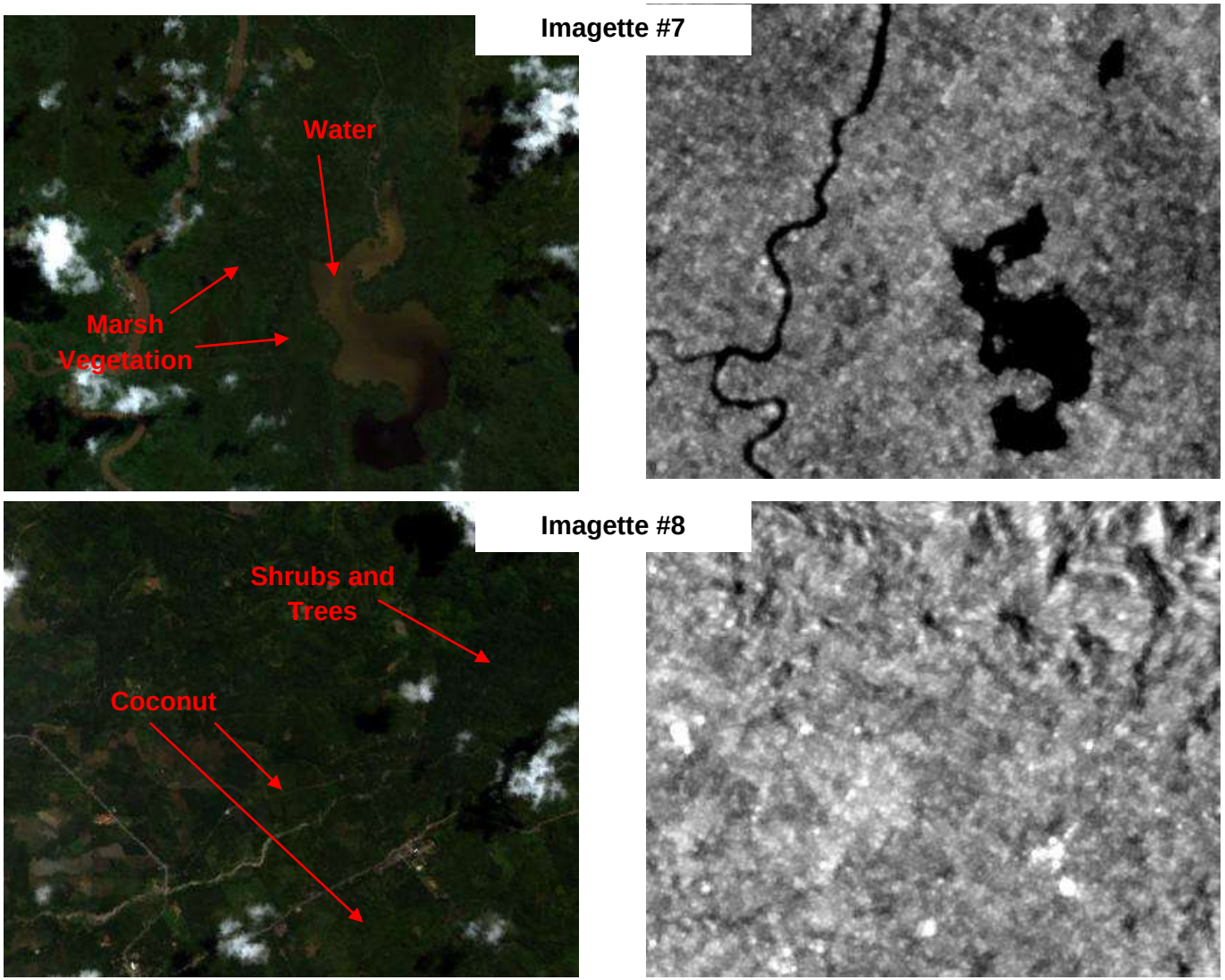

Figure 39. Imagettes 7 and 8 of ALOS AVNIR-2 (left) and the corresponding Envisat ASAR imagettes (right). (Shown not to scale.)

7.4 Results and Discussion

7.4.1 Comparison of backscattering values

Based on the imagettes presented, it can be observed that most of the land-cover classes are not discernible from the Envisat ASAR image. Except for built-up areas, water bodies and banana, the rest of the land-cover classes did not possess recognizable patterns in the image.

The statistics of extracted backscattering values of the land-cover types are summarized in Table 8 and in Figure 40.

Table 8. Backscatter statistics (in dB) of land-cover types extracted from Envisat ASAR image.

Class Name	Minimum	Maximum	Mean	Standard Deviation	Standard Error	95% Confidence Interval	Upper CI	Lower CI
Built-up Areas	-8.82	12.10	-0.38	4.34	0.19	0.38	0.00	-0.76
Cropland	-8.01	-1.53	-4.95	1.04	0.05	0.09	-4.86	-5.04
Grassland	-9.46	-2.62	-6.82	1.19	0.05	0.10	-6.72	-6.93
Palm-Banana	-5.35	-1.20	-3.32	0.82	0.04	0.07	-3.24	-3.39
Palm-Coconut	-8.72	-1.11	-5.19	1.37	0.06	0.12	-5.07	-5.31
Palm-Sago	-10.31	-4.99	-7.65	0.96	0.04	0.08	-7.56	-7.73
Palm-Oil Palm	-8.36	-3.01	-5.25	0.92	0.04	0.08	-5.17	-5.33
Non-Palm, Mangroves	-8.36	-3.58	-6.06	0.89	0.04	0.08	-5.98	-6.14
Non-Palm, Shrubs and Trees	-9.29	-2.29	-6.87	1.43	0.06	0.13	-6.74	-6.99
Non-Palm, Marsh	-12.88	-5.94	-9.93	1.00	0.04	0.09	-9.85	-10.02
Water	-21.13	-5.72	-15.81	2.89	0.13	0.25	-15.55	-16.06

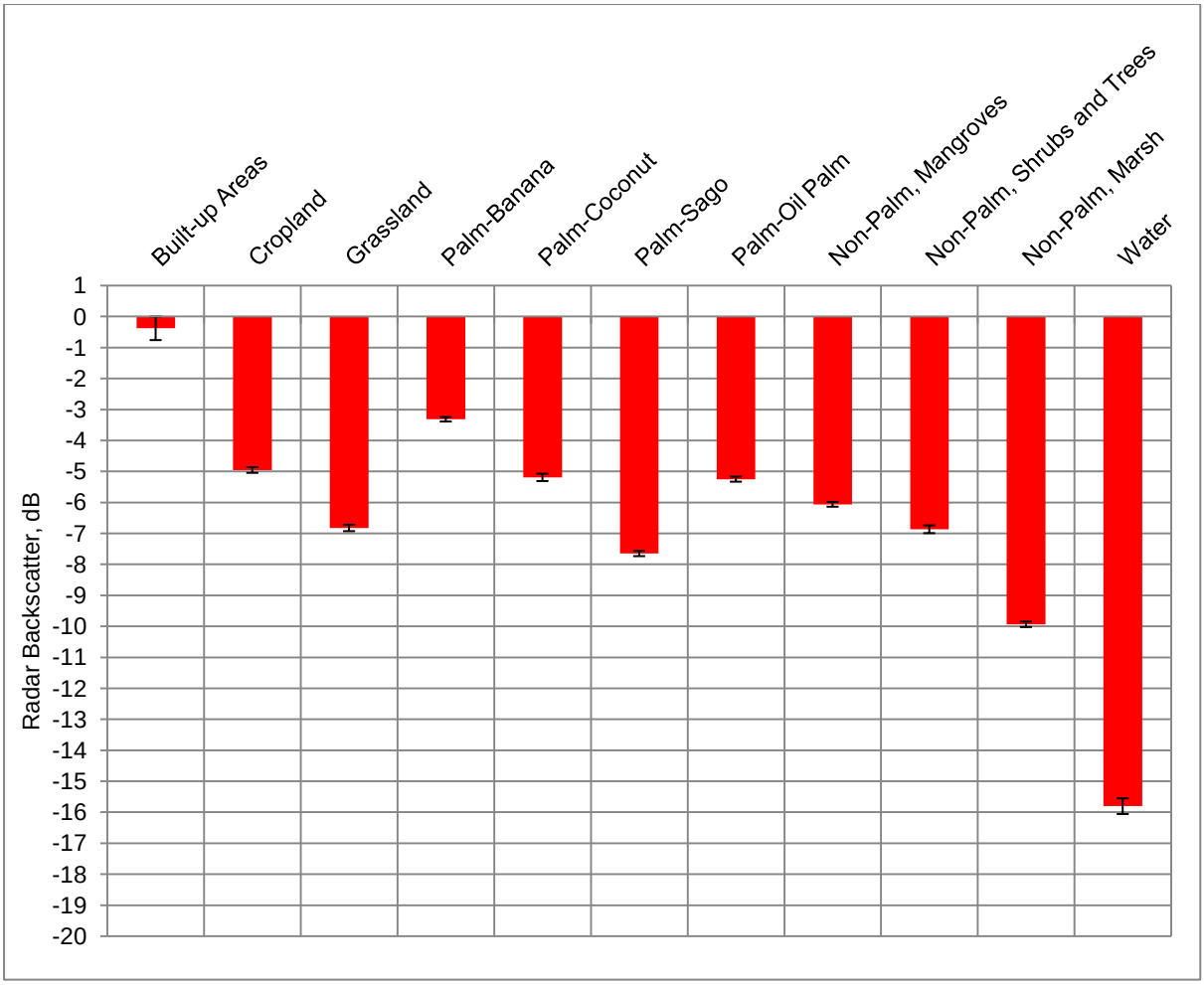

Figure 40. Bar chart of average Envisat ASAR backscatter of Sago palm and other land-cover types, including the 95% confidence intervals of the means (shown as error bars).

Built-up areas have the highest backscattering coefficient making them appear brightest in the image. This is due to the corner-reflector or double-bounce effect where the radar pulse bounces off the horizontal ground towards the target (built-up areas), and then reflected from one vertical surface of the target back to the sensor [**95**]. The basic statistics shown in Table 8 and the graph in Figure 40 confirm this observation.

Among the vegetation types, banana has the highest average backscattering value. The banana samples used in the analysis were obtained from a plantation in Compostela Valley. Being a plantation, the high radar backscatter or return may have been due to their fairly homogenous characteristic which also translates to homogenous tone in the Envisat ASAR image. Their homogeneity is confirmed by their low standard deviation (0.82) compared to the other land cover types. Aside from homogeneity, the large leaves of banana are another contributor to its high backscatter [**96**].

On the hand, water has the lowest backscattering since most of the incident radar pulses are specularly reflected away from the sensor, especially that the samples taken were obtained from calm water bodies.

The land-cover with second lowest backscatter is marsh vegetation. This is expected as this vegetation is mostly submerged in water. Surprisingly, Sago palm came as third to have the lowest backscattering values. Trees and other vegetations are usually moderately rough on the radar wavelength scale. Hence, they appear as moderately bright features in the image [**95**].

In the case of Sago palm, its appearance is darker than other vegetation types such as cropland, shrubs and trees, grassland, mangroves, coconut and oil palm. What makes it darker is perhaps the presence of standing water underneath its canopy which has been observed during the field surveys in Bunawan, Agusan del Sur (the location of the samples used in the analysis). It has been reported that for *C*-band radar, high backscattering should be expected for a vegetation with high moisture (due to humid or saturated soil) and rough canopy structure. But for wetlands with no woody plants the increase in specular scattering caused by standing water tends to decrease radar backscattering [**97**]. On site, Sago palm stands have a rough canopy structure due to presence of many fronds and leaves, with young Sago palms having the most number of the fronds and leaves. Only Sago palms in bole formation and later stages have woody materials that when compared to younger palms (rosette stage) is not significant in terms of quantity. Moreover, standing water is a usual characteristic of Sago palm stands. These perhaps explain the low backscattering of Sago palms in an Envisat ASAR IM Image.

7.4.2 Uniqueness of Sago palm's backscattering with other land-cover types

Table 9 summarizes the results of the ANOVA of the mean values of backscattering coefficients of the land-cover types. The computed *F* value of 2,227.174 has a *p* value of 0.000 which is below the critical *p* value of 0.05. This established that there is significant difference between the land-cover mean backscattering coefficients.

Table 9. Result of one-way ANOVA on the mean backscattering coefficients of land-cover classes.

Comparison of Mean Backscatter Coefficients	**Sum of Squares**	**Degrees of Freedom**	**Mean Square**	**F**	***p* value**
Between Land-cover Classes	76,685.040	10	76,68.504	2,227.174	0.000
Within Land-cover Classes	18,899.472	5,489	3.443		
Total	95,584.512	5,499			

Figure 41 shows the differences between the mean backscattering coefficients of Sago palm with other land-cover types. The Tamhane's T2 test result shown in Table 10 indicates that the mean backscattering coefficient of Sago is significantly different from those of other land-cover types ($p<0.05$ at 95% confidence level). This result is crucial and significant in considering the use of Envisat ASAR images in detecting Sago palms and discriminating them from other land-cover types.

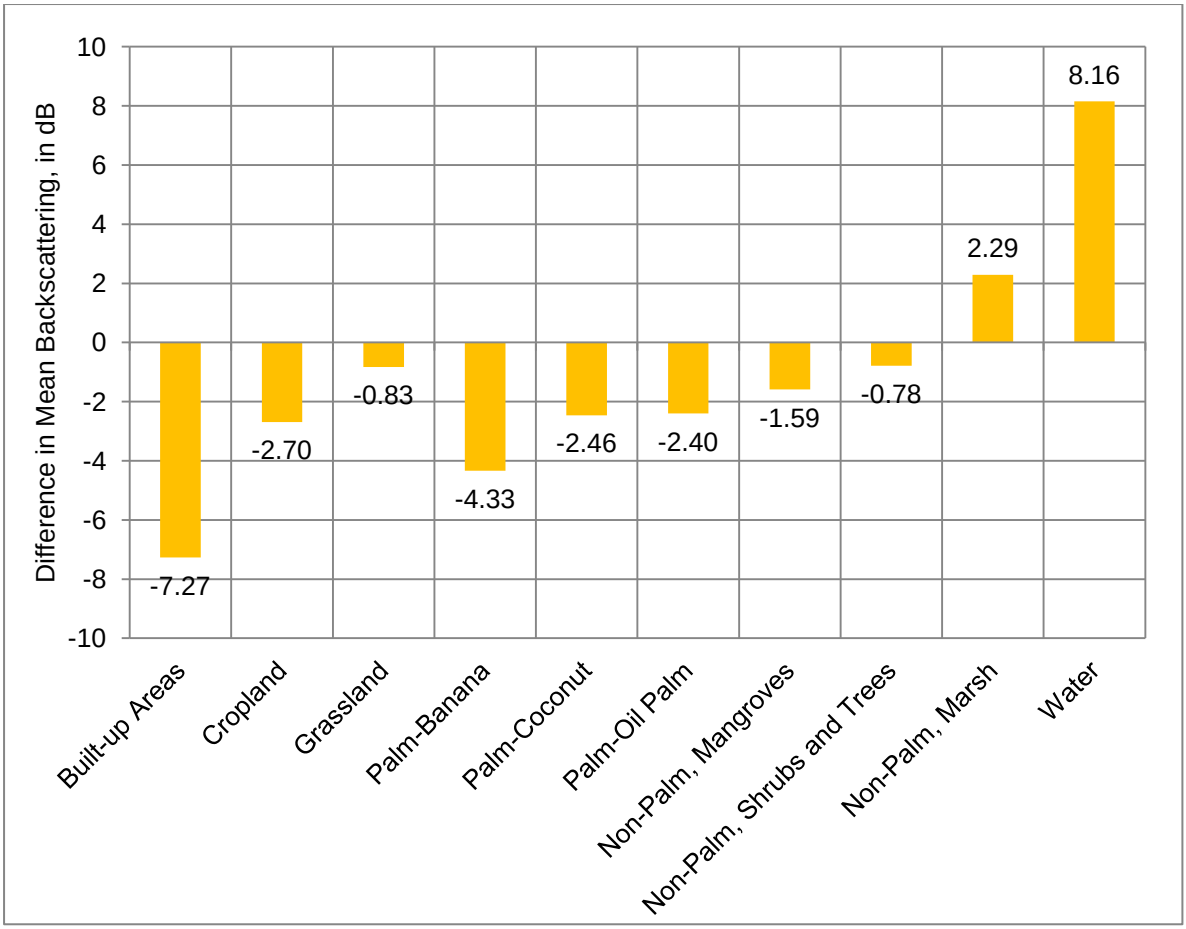

Figure 41. Differences between the mean backscattering values of Sago palm with means of other land-cover types.

Table 10. Results of Tamhane's T2 test on mean differences.

Land-cover Type	Land-cover Type Compared to:	Difference in Mean Backscattering values	Std. Error	*p* value	95% CI Lower Bound	95% CI Upper Bound
Sago Palm	Built-up Areas	-7.27	0.20	0.00	-7.93	-6.61
	Cropland	-2.70	0.06	0.00	-2.91	-2.49
	Grassland	-0.83	0.07	0.00	-1.05	-0.60
	Palm-Banana	-4.33	0.06	0.00	-4.52	-4.14
	Palm-Coconut	-2.46	0.08	0.00	-2.71	-2.21
	Palm-Oil Palm	-2.40	0.06	0.00	-2.60	-2.20
	Non-Palm, Mangroves	-1.59	0.06	0.00	-1.78	-1.39
	Non-Palm, Shrubs and Trees	-0.78	0.08	0.00	-1.04	-0.53
	Non-Palm, Marsh	2.29	0.06	0.00	2.08	2.49
	Water	8.16	0.14	0.00	7.70	8.61

7.5 Chapter Conclusions

The basic statistics and the ANOVA analysis revealed that it is possible to identify land-cover types according their backscattering values in an Envisat ASAR IM image. The statistics suggest better discrimination of Sago palm from other land-cover types due to its relatively low but unique mean backscattering value which is significantly different from those of other land-cover types.

The method to do the classification of this kind of image may be hard to find considering that there is only a single band to work upon. Other researchers have utilized a multi-temporal approach wherein SAR images acquired at different times or periods were stacked and subjected to classification using available classifiers such as Maximum Likelihood, Artificial Neural Network, and Support Vector Machine. Many researchers also made use of the rich information provided by a SAR image by fusing them with optical satellite images prior to classification with the notion that better results can be obtained in terms of accuracy. In this study, both are tried, and the details are presented in Chapter 10.

Chapter 8. Potential Distribution Modelling of Sago Palm as an Important Activity Prior to Satellite Image Analysis

Sago palms are considered to be very uncommon in the Philippines. In fact, there were only very few locations in Visayas and Mindanao where Sago palms have been reported to exist. Many areas remain to be explored. In this case, the use of satellite remote sensing becomes a convenient tool because of its wide coverage. But mapping very specific vegetation such as the Sago palm using satellite images could be an arduous task especially if the coverage is very large such as Visayas and Mindanao. If mapping is to be done using Landsat images, about 20 scenes are needed to be processed, with land area within the images totaling to 147,000 km^2. Satellite remote sensing has been known to be a useful platform for mapping land-cover in wide areas, but the process of applying it for Sago palm mapping maybe counter-productive considering that this vegetation species is not widely distributed as compared to other species (e.g., coconut). There might be a scenario when one or more images of an area have already been acquired and processed but later on it was found that Sago palm cannot exist in this area because of unsuitable conditions. This may lead to a waste of time and resources. A better approach would be to avoid processing satellite images where Sago palms are unlikely to be found and focusing only on areas that Sago palms are likely to exist.

This chapter discusses the use of species distribution modeling (SDM) as an important procedure prior to actual use of satellite images in mapping uncommon vegetation species such as the Sago palm. Here, SDM together with location data of Sago palms are used to identify areas where the species are likely to occur. The likelihood of occurrence is computed based on the degree of similarity of bioclimatic conditions of a certain location to those of where Sago palms that have been actually found. The importance of SDM is evaluated in terms of reducing the areal coverage to be subjected to image analysis, and the expected mapping accuracy and errors of omission when the approach is to be utilized.

8.1 Species Distribution Modeling by Similarity of Bioclimatic Conditions

SDM is based upon the theory that presence of a species in a location obeys three constraints (i) the local environment allows the population to grow, (ii) the interactions with other local species (predation, competition, mutualism, etc.) allow the species to persist, and (iii) the location is actually accessible, given the dispersal abilities of the species [**67**]. These constraints determine the geographical distribution of the species. It follows that, theoretically, it is possible to reconstruct a realized ecological niche for a species from the environmental variables measured at the locations it occupies. For this work, SDM of Sago palm was implemented using the DOMAIN model [**77**]. This model derives a point-to-point similarity metric to assign a classification value to a potential site based on its proximity in environmental space to the most similar occurrence. The Gower metric,

$d_{AB} = \frac{1}{p}\sum_{k=1}^{p}\frac{|A_k - B_k|}{range(k)}$, which is the sum of the standardized distance between two points for each predictor variable, is used to quantify the similarity between two sites. The standardization is achieved using the predictor variable range at the presence sites to equalize the contribution from each predictor variable. Similarity is then calculated by subtracting the distance from 1 and multiplying by 100. The maximum similarity between a candidate point and the set of known occurrences is assigned to each grid cell. DIVA GIS version 7.5 [**98**] was used to implement the DOMAIN model using values of 19 WorldClim bioclimatic variables at selected Sago palm locations. WorldClim, which can be obtained at http://www.worldclim.org/, is a set of 19 global climate layers (climate grids with resolution of ~900 x 900 m) depicting temperature and precipitation that can be used for mapping and spatial modeling in a GIS or with other computer programs [**99**]. In DIVA GIS, the Domain procedure calculates the Gower distance statistic between each cell on the map and each point, using the values of the 19 climate variables. The distance between point A and grid cell B for a single climate variable is calculated as the absolute difference in the values of that variable divided by the range of the variable across all points. The Gower distance is then the mean over all climate variables.

8.2 Sago Palm Actual Location Data

Point location data of Sago palms were obtained from a series of field surveys conducted between February - December 2012 in several provinces in Visayas and Mindanao, and enhanced through digitizing from available high resolution Worldview-2 satellite images.

To make the analysis more realistic, only Sago palm location data in areas where it has been explicitly reported to exist were used, which are in Aklan, Cebu and Leyte (in the Visayas), and in the provinces of Agusan del Norte, Agusan del Sur, Davao del Norte and Davao del Sur (in Mindanao). The rationale behind this is that initially information about the location of Sago palms in other areas aside from those already reported is still unknown - that remote sensing is yet to be used to find them. And since the area covered is large, identifying locations with similar bioclimatic conditions is necessary is minimize the number of images and the effort needed in image analysis.

A total of 181 location points (randomly selected and unique in 900 x 900m grid cells of the WorldClim layers) were utilized in the DOMAIN analysis. Another set consisting of 376 randomly selected locations (independent from the DOMAIN set) were utilized to validate the potential distribution maps (at varying degrees of similarity), specifically to check if how many Sago palm locations may be omitted if the image analysis will only focus on areas identified by the DOMAIN model as bio-climatically similar. The validation points are located in different provinces including those provinces where Sago palm location data has not been used in the DOMAIN analysis.

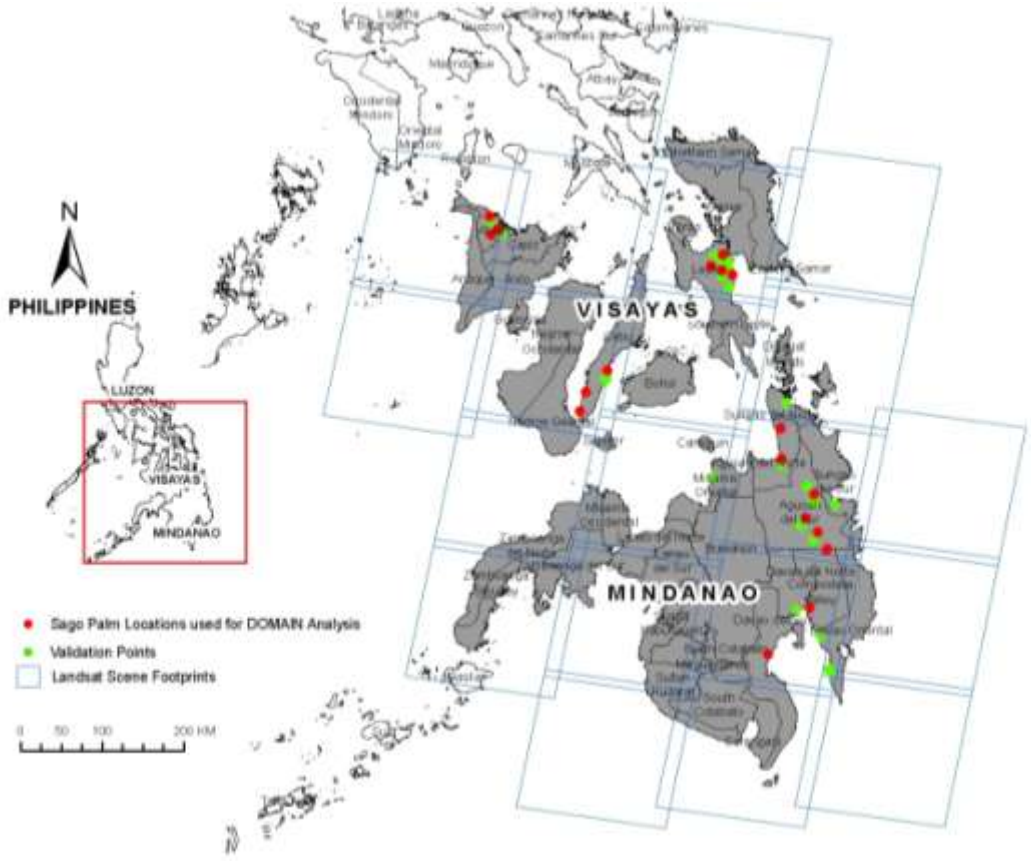

Figure 42. Map showing the Sago palm locations used in potential distribution modeling using DOMAIN and for validation of results. Note that for clarity of presentation, the point locations shown in the map have been generalized to avoid overlapping of points. A single point may contain several more locations.

8.3 Results and Discussion

The similarity index map derived using the DOMAIN model for Visayas and Mindanao is shown in Figure 43. Since the percentage values indicates the similarity in the bioclimatic conditions of a certain location to those in the actual locations of Sago palms, the likelihood of finding a Sago palm increases as the similarity index increases. As the similarity index increases, the area where Sago palm is likely to occur decreases (Figure 44, Figure 45).

If the similarity index is to be used as basis to locate specific areas where remote sensing image analysis is to be employed, the accuracy to completely map actual Sago palm locations will decrease when a higher similarity index is selected. As shown in Figure 46, a similarity index cut-off of greater than or equal to 86% will still provide 100% correct prediction of Sago palm locations even though there is a significant decrease in land area. The accuracy decreases to 99% when the similarity index is greater than or equal to 87%, and this continues to decrease until the accuracy is only 50% when the similarity index is 100%. This pattern is expected as the area where Sago palm is likely to occur becomes more specific and the conditions now equate to the bioclimatic conditions at the observed locations. For classifications requiring only a minimum of 85% accuracy, a similarity index cut-off of 95% can be chosen (i.e., to select areas with 95-100% index).

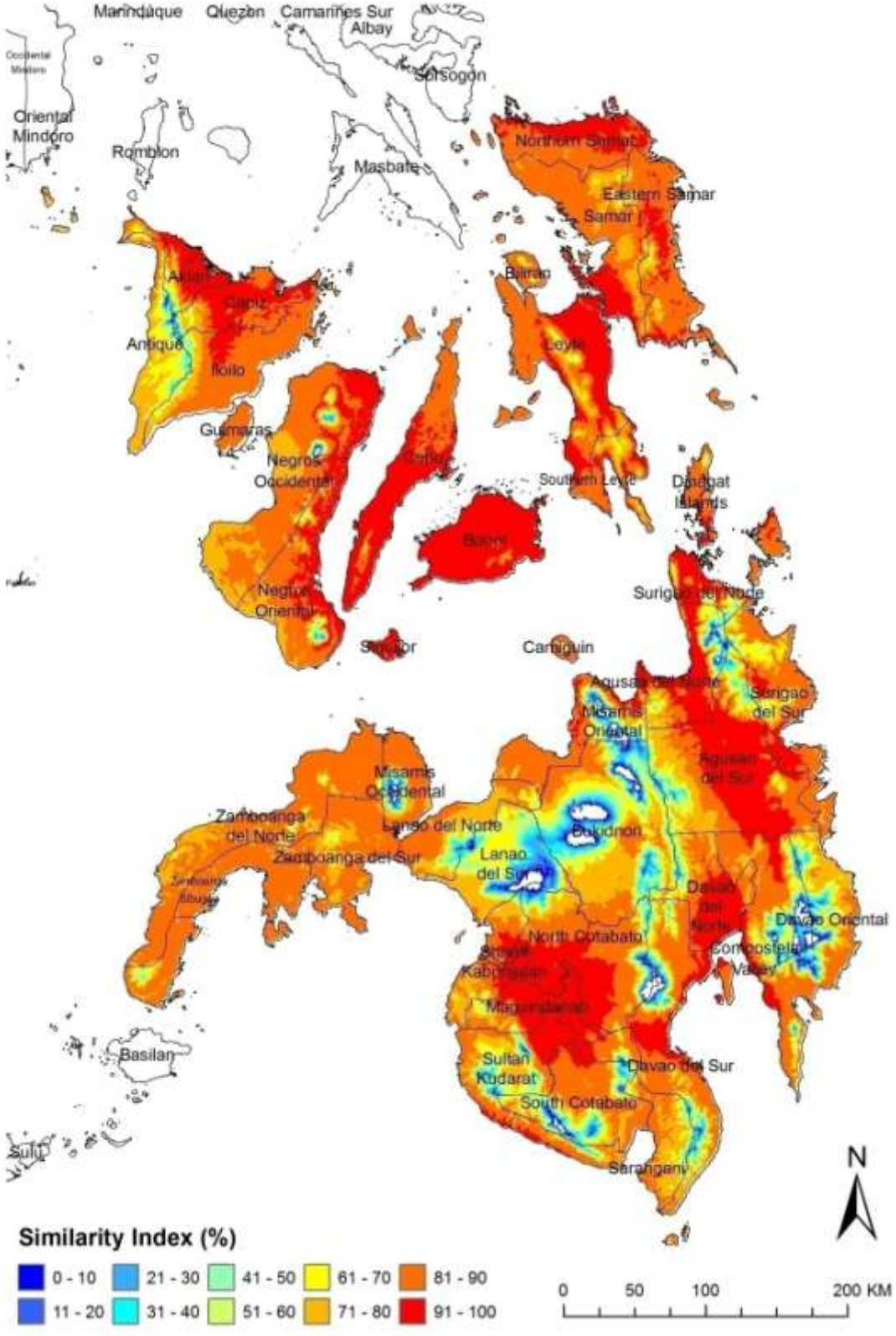

Figure 43. Similarity index map derived using the DOMAIN model which is indicative of the likelihood of occurrence of Sago palms.

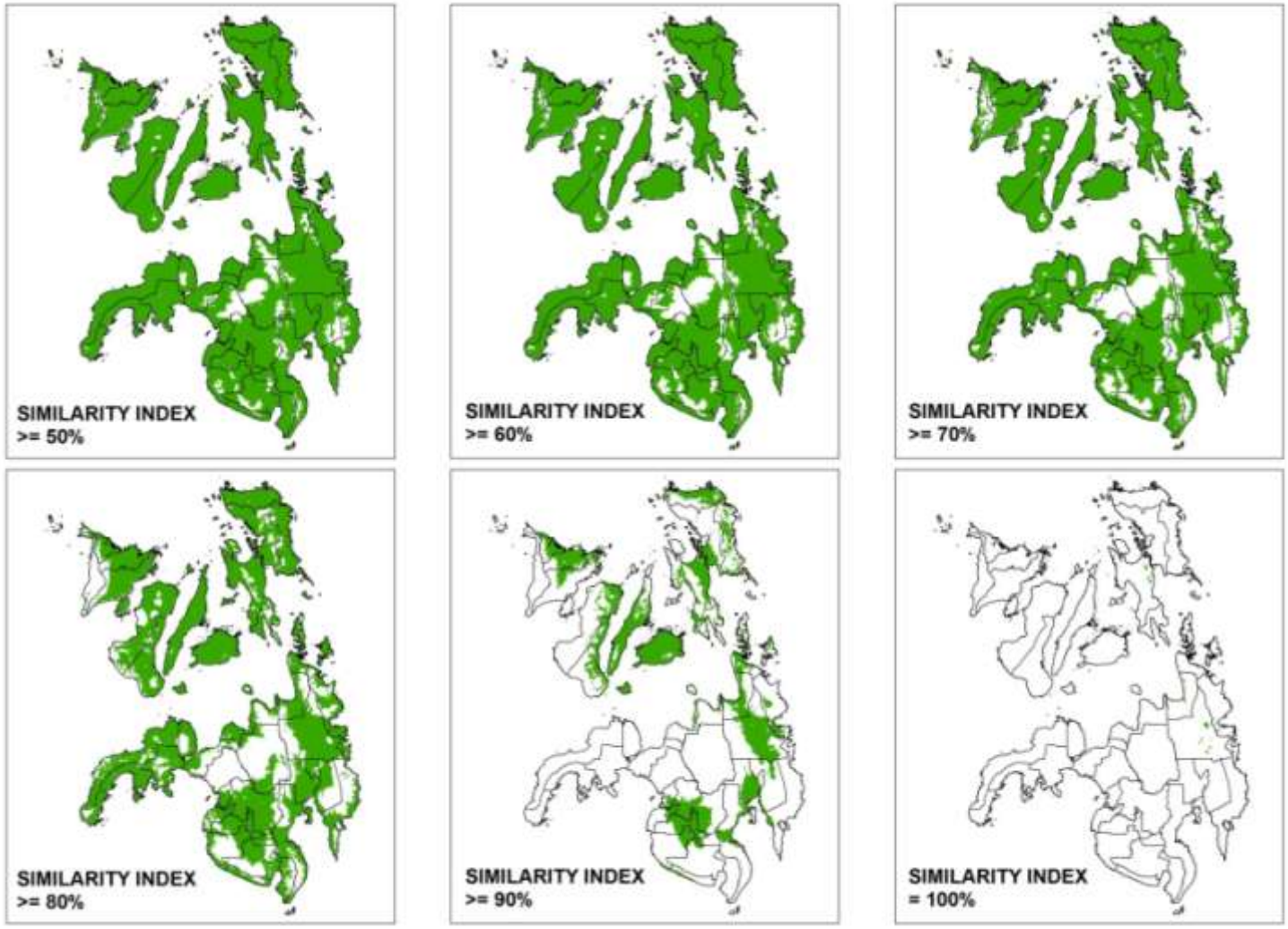

Figure 44. Series of maps showing locations at different similarity index cut-offs which are useful in selecting areas where images can be analyzed to detect Sago palms.

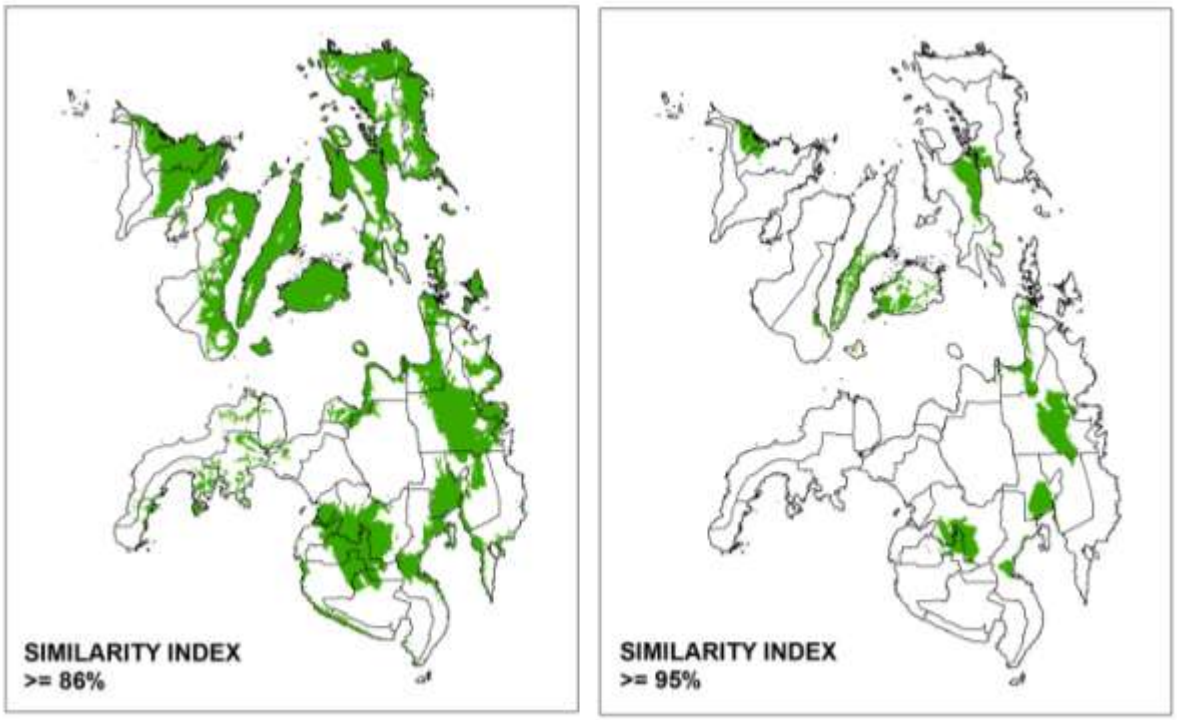

Figure 45. Maps showing locations at similarity index cut-offs of 86% and 95%.

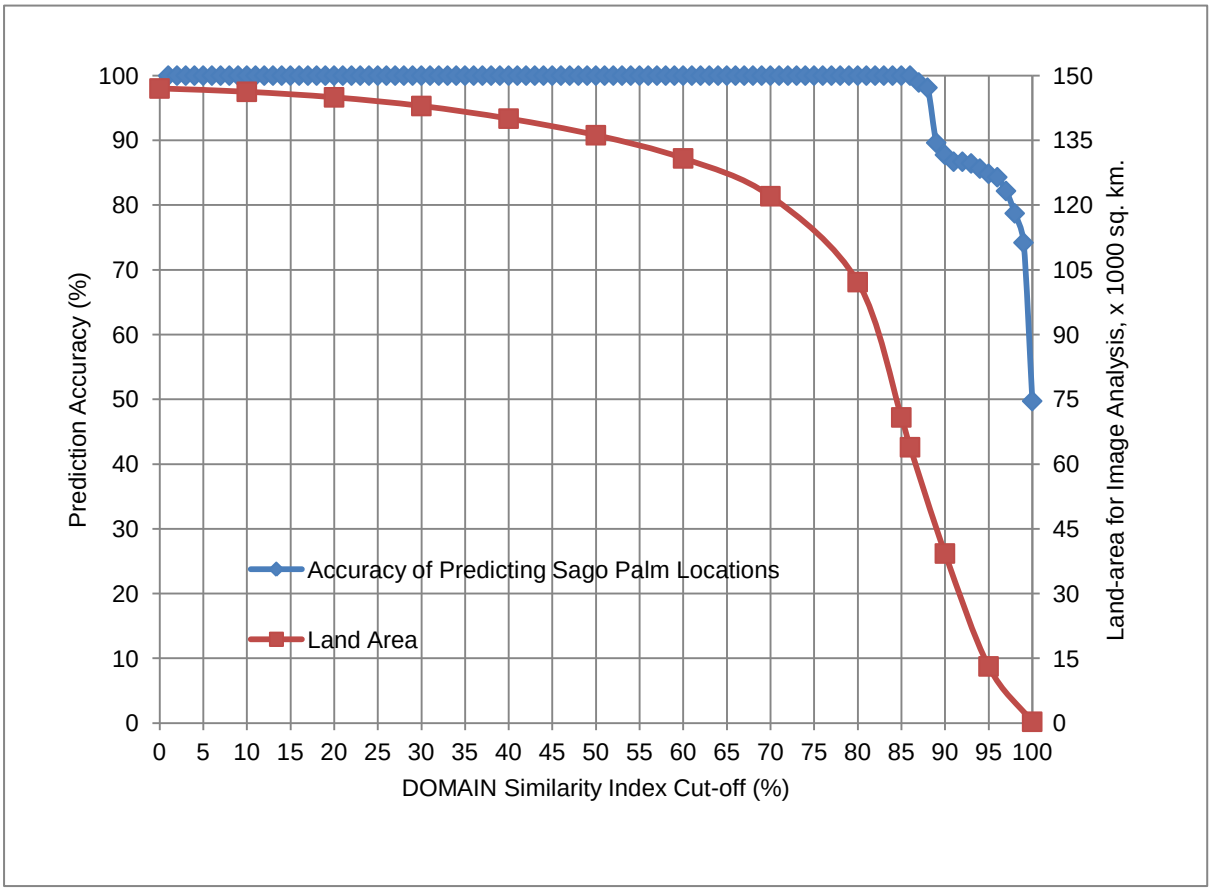

Figure 46. Graph showing accuracy of predicting Sago palm locations and land area for image analysis in various percentages of similarity index.

It can be observed that there will be a considerable decrease in land area when species distribution modeling using the DOMAIN model is employed prior to image analysis. The original area of 147,000 km^2 is greatly reduced to ~64,000 km^2 when only those areas with 86% similarity index are chosen (Figure 45). This translates to more than 200% reduction in coverage area for image analysis which is good in terms of resources and time management. A 95% similarity index cut-off which could provide at least 85% accuracy in detecting Sago palms will only require ~13,000 km^2 of land area to be analyzed.

8.4 Chapter Conclusions

It was shown that employing SDM using the DOMAIN model can be a valuable procedure prior to employing remote sensing image analysis to map uncommon vegetation species such as the Sago palm. The SDM approach was found to considerably reduce areal coverage of image analysis while maintaining acceptable accuracy of detecting actual locations of Sago palm. As the approach only targets locations where there is high likelihood of occurrence of a species, it reduces the number of images to analyze and can save time and resources.

The similarity index map with 86% cut-off was utilized in mapping Sago palms using Landsat 7 ETM+, ALOS AVNIR-2, and Envisat ASAR. Details are discussed in Chapter 9 and Chapter 10.

Chapter 9. Evaluation and Application of Landsat 7 ETM+ Images in Mapping Sago Palm Locations

This chapter presents an evaluation and application of Landsat ETM+ images in mapping possible locations of Sago palms. The terms “possible locations” are used here to indicate that the pixels identified in the images may or may not contain Sago palm stands. This is in consideration of the classification errors and inadequacy of the image spatial resolution of 30 m for mapping Sago palms that are less than 30 x 30 m in size.

The first major section presents a case study/evaluation of the image as input to Maximum Likelihood classification. The remaining sections show the application of the images in mapping possible locations of Sago palms in pre-selected locations in Visayas and Mindanao as earlier determined through potential distribution modeling.

9.1 Case Study: Sago Palm Detection through Maximum Classification of Landsat ETM+ image

This case study aims to determine the accuracy of detecting Sago palms locations through Maximum Likelihood classification of Landsat ETM+ image. The Maximum Likelihood classifier (MLC) is a parametric classifier based on statistical theory with the assumption that spectral signatures of the land-cover classes are normally distributed [**100**]. MLC quantitatively evaluates both the variance and covariance of the class spectral signatures [**101**] and based on the evaluation, discriminant functions for each class are developed and used to classify an unknown pixel. The basic parameters of the MLC are the class mean vector and the class covariance matrices. These parameters are usually obtained from pixels representative of land-cover classes in an image. A thorough discussion of the MLC can be found in [**102**]. The MLC has been widely used in land-use/land-cover classification of remotely sensed images [**101**].

9.1.1 Datasets Used

The analysis, using Envi 5 software, utilized the 14 September 2008 Landsat 7 ETM+ image that was previously used in the image reflectance analysis (Chapter 6). In addition to the 6 reflectance bands (bands 1-5 and 7), the brightness temperature (band 6) was also utilized together with a normalized differenced vegetation index (NDVI) computed using bands 4 an 5, and a Shuttle Radar Topography Mission (SRTM) digital elevation model (DEM). The stacked vector approach [**103**] is adapted to incorporate these multi-source data into the classification process. It is a straightforward approach where the data from each source are treated as augmented dimensions of an input data vector. The incorporation of the three additional data in image classification has been found by other researchers to increase classification accuracy. NDVI and DEM in particular can account for the rugged topography so as to eliminate the presence or absence of certain classes in some elevation zones, and can reduce the impact of shadows and to enhance the separability among various vegetation classes [**103**], [**104**].

The brightness temperature image (referred hereafter as “TEMP”) has values in Kelvin (K) with pixel resolution of 30 m, while the DEM have elevation values in meters at resolution of 90 m. To make these two datasets compatible with the scale of the reflectance bands (0 to1) and NDVI (-1 to 1), their pixel values were divided by 1000. The NDVI, TEMP and DEM bands were then stacked and co-registered with the bands 1-5 and 7. During the layer stacking, the pixel resolution of DEM was resampled to 30 m. The stacked dataset consisted of 9 layers.

9.1.2 Selection of Samples for Classifier Training and Accuracy Assessment

In this case study, the evaluation of Landsat 7 ETM+ image was focused only on discriminating Sago palms from other vegetation types. The detection of non-vegetation features (built-up, unplanted cropland, barren land, etc) was not done as it was already established in Chapter 6 that Sago palms reflectance characteristic can be fairly discriminated from these features.

Representative groups of pixels (or Regions of Interests, ROIs) were collected in the image for each vegetation-cover type (Table 11) that will be used for training the classifier. The collection of ROIs was assisted by high resolution images provided by the Google Earth application. Data from field surveys conducted between February – August 2012 in the study area were used as guide in identifying Sago palms and other land-cover types in the image. The number of pixels collected for each class were more than the practical minimum of 10*N (where N = maximum number of input bands = 9), in order to have as many training pixels as possible that will ensure proper estimation of the parameters of the Maximum Likelihood classifier, as well as to ensure that its assumption of normal distribution is satisfied [**105**].

Table 11. Number of pixels collected for classifier training and accuracy assessment.

Vegetation Class Name	No. of Pixels
Classifier Training	
Cropland - Planted	1,931
Grassland	1,851
Palm - Sago	1,046
Palm - Banana	1,324
Palm - Coconut	1,300
Palm - Nipa	652
Palm - Oil	9,620
Other non-palm vegetation - Mangroves	477
Other non-palm vegetation - Marsh	1,762
Other non-palm vegetation - Shrubs and trees	14,682
Classification Accuracy Assessment	
Sago	387
Non-Sago	1,161

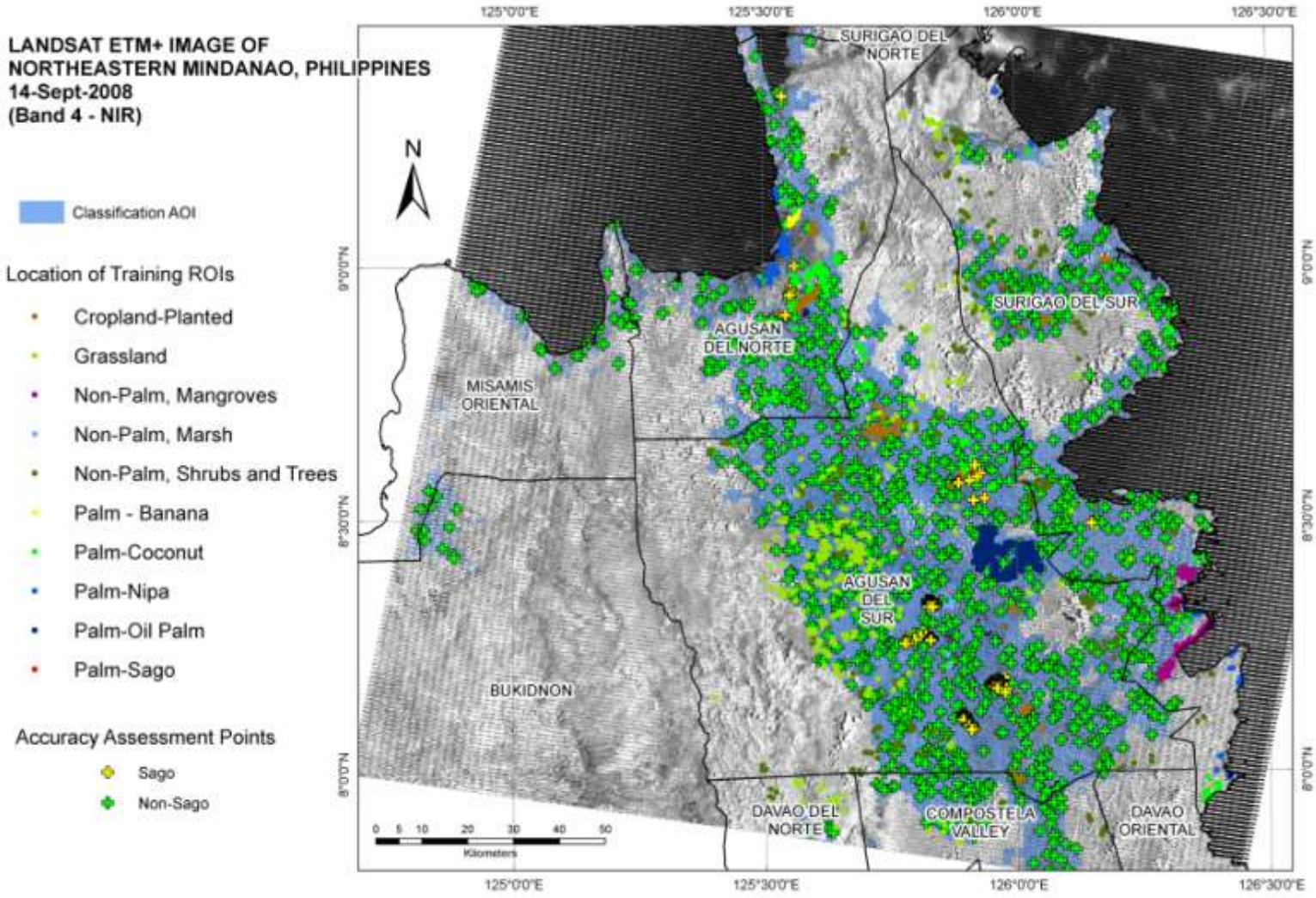

Figure 47. Band 4 of the Landsat 7 ETM+ image shown overlaid with the locations of the training and accuracy ROIs, including the classification area of interest.

An independent set of pixels representing Sago and Non-Sago were collected to assess the accuracy of the Maximum Likelihood classifier in detecting Sago palms from other vegetation classes. ROIs representing various vegetation classes were no longer collected since the analysis will not involve their accurate detection in the image as individual classes. As will be shown later, the resulting classification image were simplified into Sago and Non-Sago only. The Sago ROIs were collected based on data collected from the field surveys. A total of 387 pixels were selected. It was ensured that each of these pixels are not the same with the pixels earlier collected for classifier training. On the other hand, the Non-Sago ROIs were collected randomly within the classification area of interest using the Random Point Generator extension of Arcview GIS 3.2 software. A total of 1,161 pixels (three times the number of Sago pixels) were selected. Each of these pixels was individually checked to verify that they are not Sago palm locations, and that each of these pixels is not included in the training ROI sets. The accuracy ROIs were used to compute for the overall classification accuracy, and more importantly the Producer's and User's Accuracy of the Sago palm. The Producer's Accuracy determines how many of the "Sago" pixels were correctly classified as "Sago palm" while the User's Accuracy provides an indication of how accurate the classifier was in labeling a pixel in the image as "Sago". For example, if there were 100 of actual Sago pixels (as verified on the ground), a 90% Producer's Accuracy would mean that only 90 pixels were correctly classified as "Sago" ; the remaining 10 pixels were erroneously classified as Non-Sago. On the other hand, if 100 pixels classified as "Sago" were randomly chosen and checked on the ground, a 90% User's Accuracy would mean that only 90 of 100 pixels classified as "Sago" are actually "Sago" on the ground; the remaining 10 pixels were erroneously classified as "Sago" where in fact they are Non-Sago. The computation of the Producer's and User's Accuracy is made possible through the use of the classification error (confusion) matrix.

9.1.3 Input Band Combinations

Forty (40) combinations of the Landsat ETM+ reflectance bands 1-5 and 7, NDVI, TEMP and DEM were subjected to MLC. This was done to find the best combination that will yield the highest overall classification accuracy, as well as the Producer's and User's Accuracy for Sago palm. The combination with the highest values (> 85%) of these measures of accuracy is the one considered.

The 40 combinations were derived by starting with the first four bands of Landsat ETM+ image. The second combination includes bands 1-5, while the third includes bands 1-5 and 7. The next 2 (4^{th} and 5^{th}) combinations utilized the 2^{nd} and 3^{rd} combinations but removed the blue and green bands (bands 1 and 2). The next combinations are just a repeat of the first 5 combinations with individual additions of NDVI, TEMP and DEM. The same approach is repeated for the succeeding combinations wherein pairs of NDVI and TEMP, and NDVI and DEM are added. The last sets of combinations have all the NDVI, TEMP and DEM added to the first 5 combinations.

9.1.4 Classification Area of Interest

The classification area of interest (AOI) covers those portions of the image that was earlier determined to have potential presence of Sago palms (i.e., those areas with 86% or

more DOMAIN similarity index; see Chapter 8 for details). The AOI is further reduced to contain only those portions of the image with elevations less than or equal to 700 m which is the normal elevation range for Sago palm [**4**].

A further reduction of the AOI is done such that only vegetated portions of the image are retained. As earlier stated, the MLC is only applied to classify vegetation classes. To make this feasible, vegetated portion of the image (NDVI ≥ 0.6) were selected. The minimum NDVI value of 0.6 was chosen as it is the minimum NDVI of Sago palm based on the training data.

9.1.5 Classification Results and Discussion

Table 12 provides a summary of the Maximum Likelihood classification of the 40 combinations of Landsat 7 ETM+ reflectance bands, NDVI, TEMP and DEM. Graphical representations of the accuracies are presented in Figure 48, Figure 49 and Figure 50.

The results indicate that the use of combinations containing only the Landsat 7 ETM+ reflectance bands will yield not yield acceptable Producer's Accuracy for Sago palm; combination #3 (all the reflectance bands) can only yield a maximum of 61.76% producer's accuracy. This means that the first 5 combinations are not helpful in mapping all possible locations of Sago palms. In terms of User's Accuracy, the combinations yielded acceptable accuracy except for combination #1 which indicated high rate of falsely mapping non-Sago pixels as "Sago".

The addition of NDVI to the first 5 combinations appears to lessen the percentages of accuracy. The same can be said when TEMP was added. Relatively better overall classification and User's accuracies were obtained when DEM was added (> 90%) but the Producer's Accuracy remains to be unacceptable (<85%). No significant improvements to the Producer's Accuracy were found when NDVI and TEMP were both added to the first 5 combinations. The group addition of NDVI, TEMP and DEM significantly improved the classification accuracies. However, it is the combination when both TEMP and DEM were added that gave the acceptable results. Results of combinations #32, 33 and 34 are all acceptable. But the best result was obtained for combination #35 which included only the reflectance bands 3, 4 and 5, TEMP and DEM. This combination has overall classification accuracy of 96.19% and with 90.44% and 94.09% Producer's and User's Accuracies for Sago palm.

The classification map derived using combination #35 is shown in Figure 51 while the simplified Sago map is shown in Figure 52. Based on the result, a total of 3,717 hectares was classified as "Sago palm" within the classification area of interest.

Table 12. Summary of Maximum Likelihood classification results.

Combination Number	Bands Used	Overall Classification Accuracy (%)	Sago Palm Producer's Accuracy (%)	Sago Palm User's Accuracy (%)
1	1234	81.59	43.93	71.43
2	12345	88.05	58.66	90.08
3	123457	88.50	61.76	88.55
4	345	86.43	54.78	85.83
5	3457	87.34	58.40	86.59
6	1234+NDVI	79.39	44.19	62.41
7	12345+NDVI	86.76	58.66	83.46
8	123457+NDVI	86.56	58.40	82.78
9	345+NDVI	85.21	51.94	82.38
10	3457+NDVI	86.30	56.59	83.27
11	1234+TEMP	76.81	78.04	52.43
12	12345+TEMP	88.50	79.84	75.55
13	123457+TEMP	88.44	78.81	75.87
14	345+TEMP	88.37	79.84	75.18
15	3457+TEMP	89.99	81.65	79.00
16	1234+DEM	91.15	69.25	93.71
17	12345+DEM	93.99	78.55	96.82
18	123457+DEM	94.06	78.55	97.12
19	345+DEM	93.22	78.04	93.79
20	3457+DEM	93.73	78.81	95.31
21	1234+NDVI+TEMP	74.29	68.99	48.99
22	12345+NDVI+TEMP	86.69	78.29	71.29
23	123457+NDVI+TEMP	87.66	77.26	74.38
24	345+NDVI+TEMP	85.53	76.74	68.91
25	3457+NDVI+TEMP	87.40	76.49	74.00
26	1234+NDVI+DEM	89.53	63.82	91.82
27	12345+NDVI+DEM	92.76	73.90	96.30
28	123457+NDVI+DEM	93.09	74.16	97.62
29	345+NDVI+DEM	91.93	72.87	93.38
30	3457+NDVI+DEM	92.31	73.90	94.08
31	1234+TEMP+DEM	93.15	82.43	89.36
32	12345+TEMP+DEM	95.41	87.34	93.89
33	123457+TEMP+DEM	95.61	87.34	94.68
34	345+TEMP+DEM	95.03	87.86	91.89
35	**3457+TEMP+DEM**	**96.19**	**90.44**	**94.09**
36	1234+NDVI+TEMP+DEM	91.80	76.74	88.92
37	12345+NDVI+TEMP+DEM	94.19	83.20	92.80
38	123457+NDVI+TEMP+DEM	94.44	83.20	93.88
39	345+NDVI+TEMP+DEM	93.86	83.46	91.24
40	3457+NDVI+TEMP+DEM	94.57	84.75	92.92

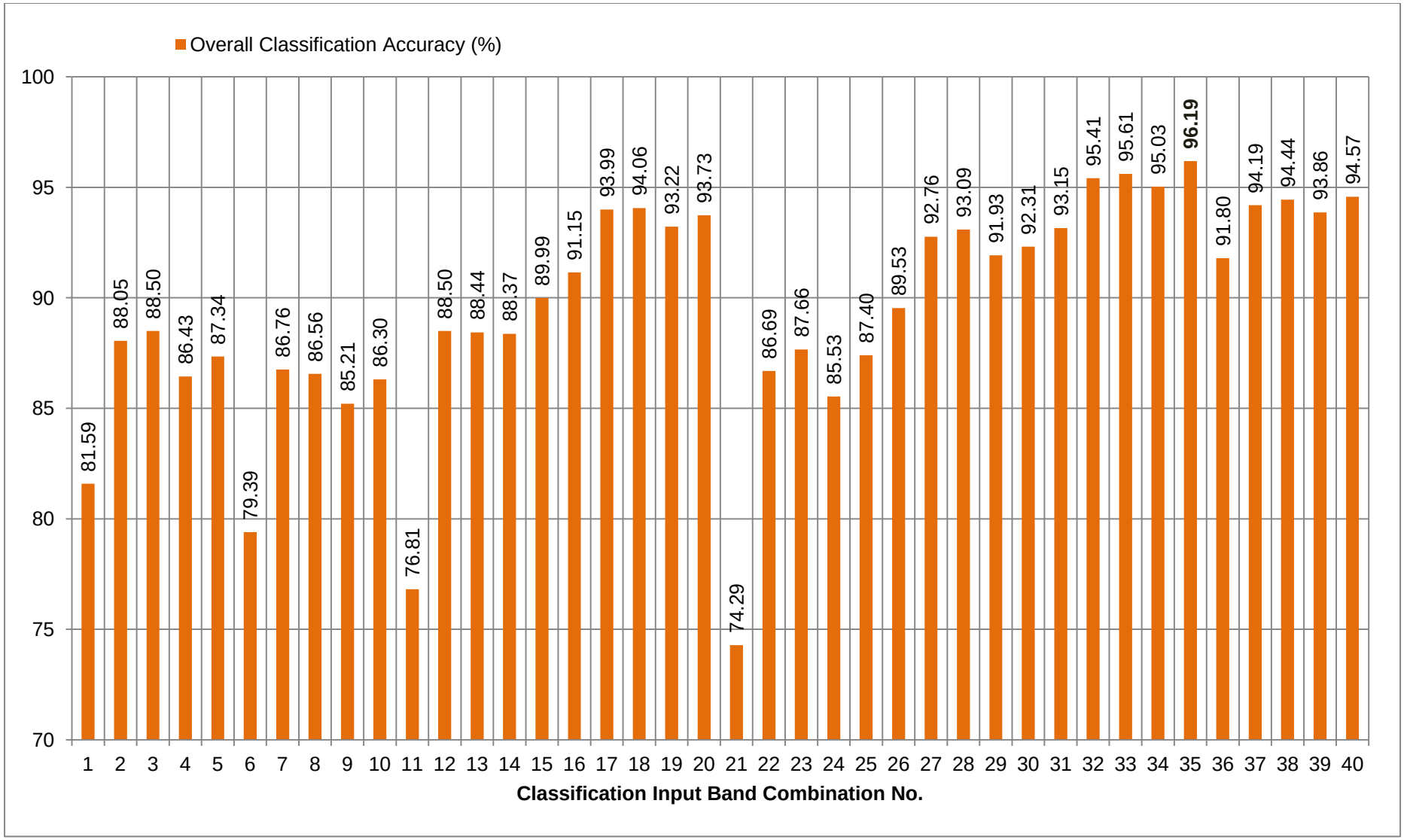

Figure 48. Graph showing the overall classification accuracy of different band combinations subjected to Maximum Likelihood classification.

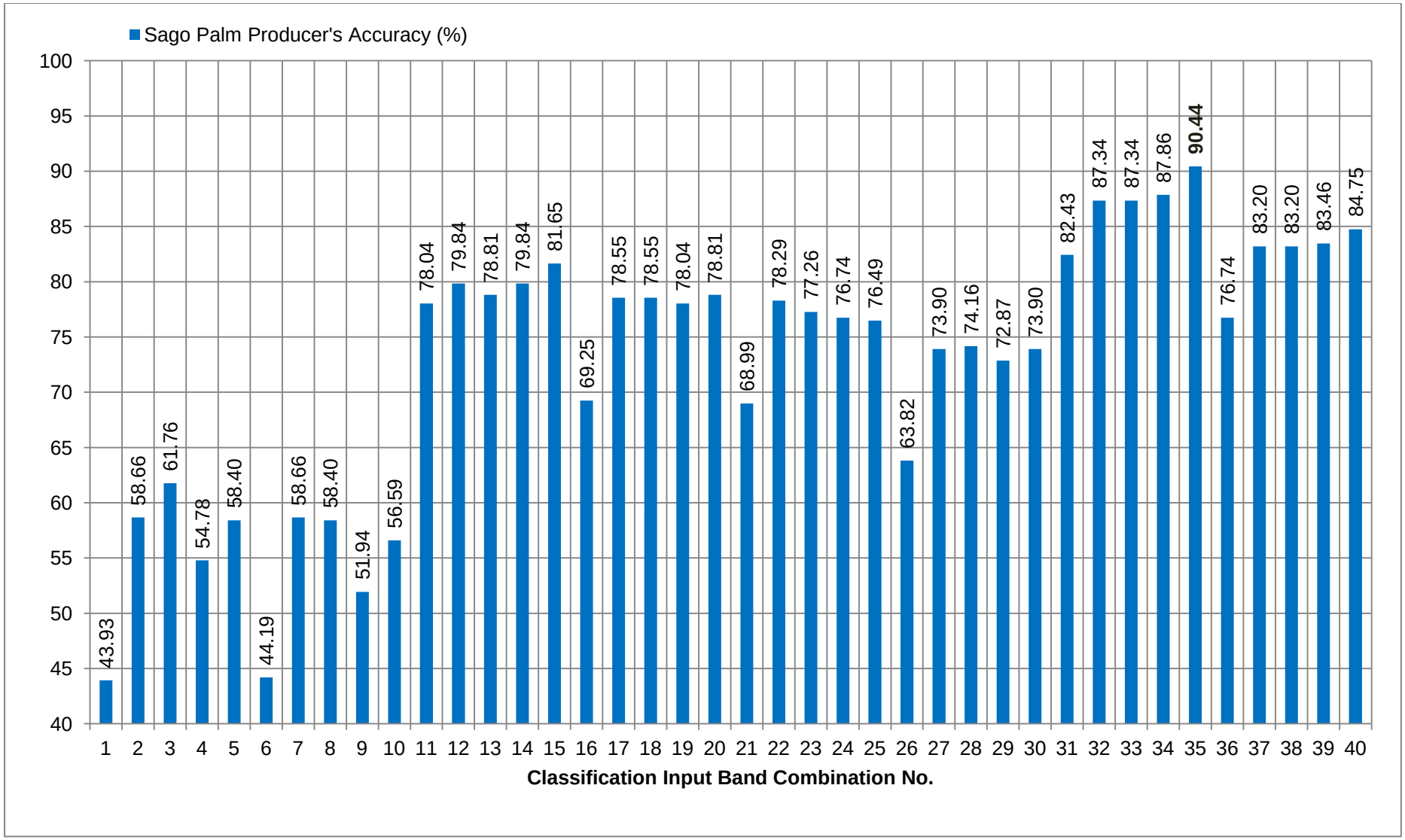

Figure 49. Graph showing the Producer's Accuracy of Sago palm according to different band combinations subjected to Maximum Likelihood classification.

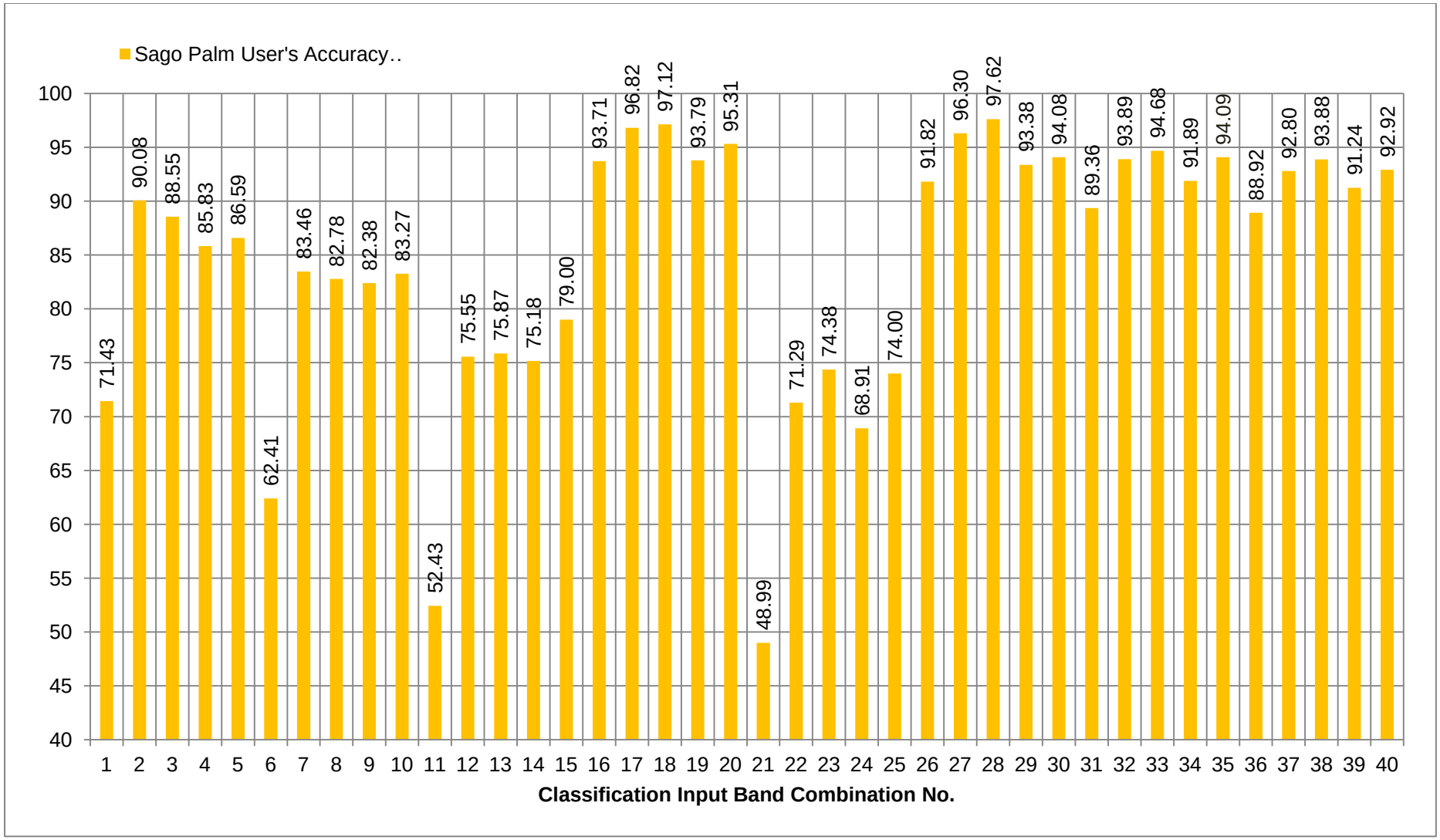

Figure 50. Graph showing the User's Accuracy of Sago palm according to different band combinations subjected to Maximum Likelihood classification.

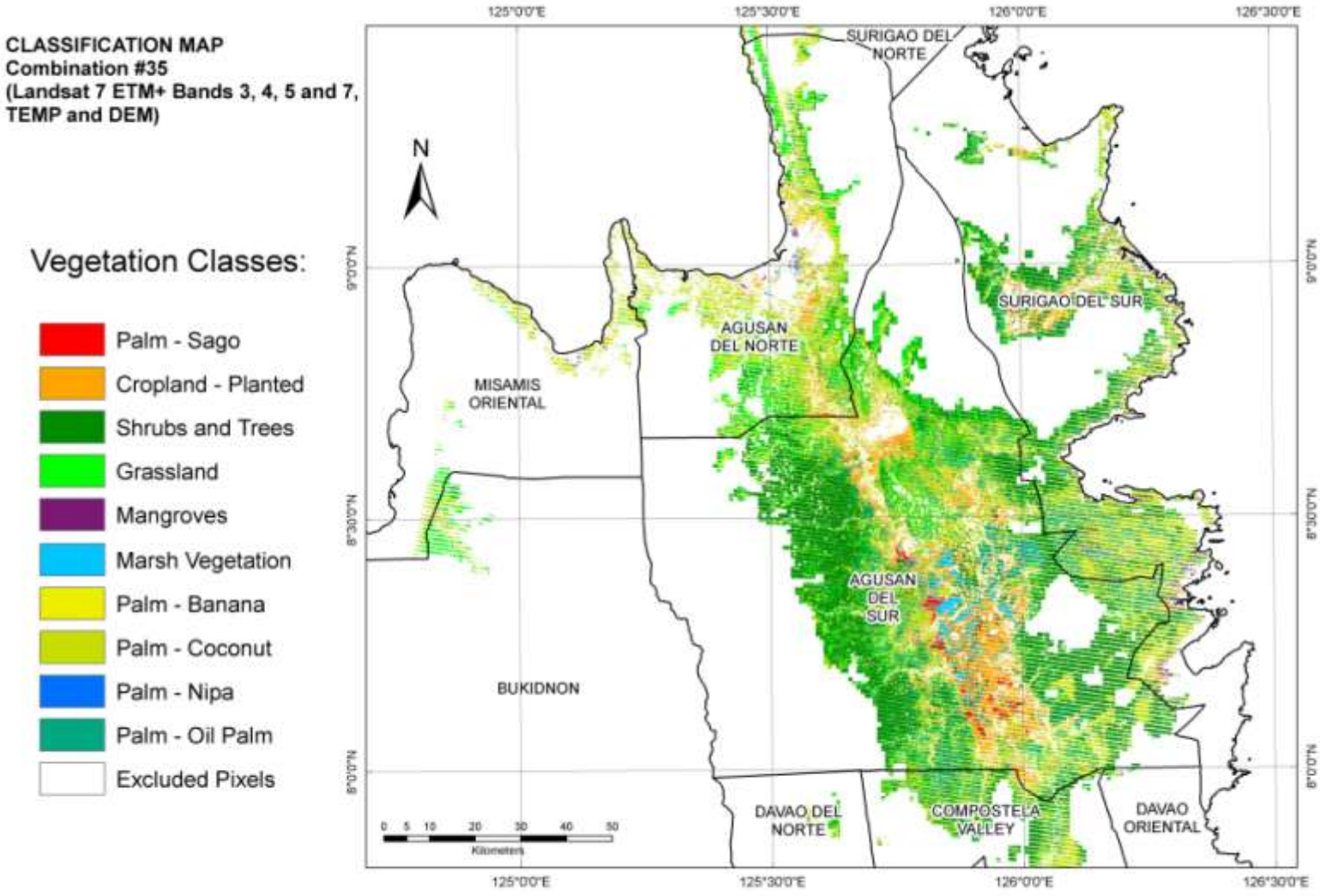

Figure 51. The classification map derived using combination #35.

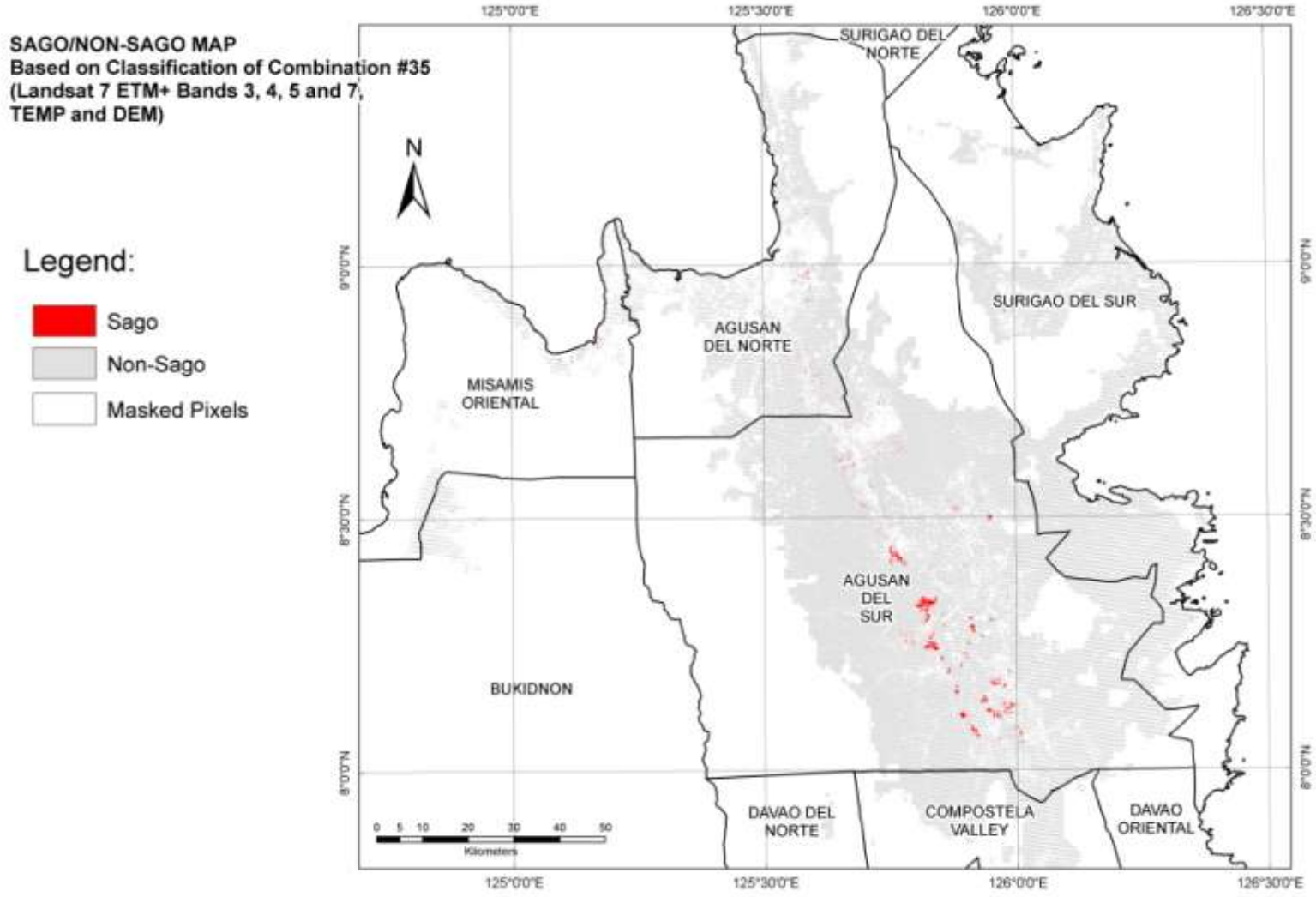

Figure 52. The Sago/Non-Sago map derived from classification of combination #35.

9.2 Application: Mapping Possible Locations of Sago Palms in Visayas and Mindanao using Landsat ETM+ Bands 3, 4, 5 and 7 with TEMP and DEM

With the acceptable classification results, the approach of Maximum Likelihood classification of Landsat 7 ETM+ bands 3, 4 and 5 together with TEMP and DEM can be adopted to map possible locations of Sago palms in other areas in Visayas and Mindanao. The parameters (mean vectors and covariance matrices) of the Maximum Likelihood classifier derived from the test image dataset will be re-used through the concept of "signature extension" - applying a signature obtained from one dataset to another dataset [**106**]. Here, the term "signature" is referred to as the mean vectors and covariance matrices. In this study, the use of signature extension assumes that spectral and brightness temperature characteristics of vegetation classes extracted from the radiometrically calibrated 14 Sept 2008 Landsat 7 ETM+ image are the same in radiometrically calibrated images of other areas acquired at different dates. Also, the topographic (elevation) characteristics of these vegetation classes are assumed to be same. This approach solves the problem of having no ground truth data of Sago palms in other areas.

9.2.1 Landsat ETM+ Images for Classification

A total of 14 Landsat 7 ETM+ scenes were subjected to classification (Table 13, Figure 53). Seven (7) scenes cover the Visayas and another 7 scenes cover Mindanao. Each scene is approximately 180 x 190 km. The images were acquired between the years 2008 and 2013. The images were obtained from the USGS through download from the GLOVIS. All the images have gaps due to the SLC error of the Landsat ETM+ sensor. Some portions of the image are also covered by clouds. All the images used here are the best possible ones in terms of date of acquisition (must be recent) and cloud coverage (< 20%) during the time when they were downloaded from GLOVIS. The image with scene id 112054 is the test image discussed in the previous sections.

All the images underwent the usual radiometric calibration to reflectance, atmospheric correction by dark object subtraction, and geometric correction. The computations of NDVI and TEMP bands were done for each image. The SRTM DEM tiles corresponding to all image scenes were downloaded. The DEM and TEMP pixel values were divided by 1000 in order to have the same data scale as that of the reflectance bands and NDVI. The NDVI, TEMP and DEM bands were then stacked and co-registered with the bands 1-5 and 7.

Similar to what has been done earlier, the classification area of interest for each image was limited only to those identified as having ≥ 86% DOMAIN similarity index, with elevation ranging from 0 to 700 m, and with NDVI > 0.6.

Table 13. List of Landsat 7 ETM+ images covering Visayas and Mindanao subjected to Maximum Likelihood Classification

Visayas		Mindanao	
Scene ID (path, row)	Date of Acquisition	Scene ID (path, row)	Date of Acquisition
115052	8/21/2009	114055	3/15/2012
114052	3/18/2013	113054	3/11/2013
114053	5/5/2013	113055	4/20/2010
113051	7/22/2009	112053	2/24/2010
113052	5/22/2010	112054	9/14/2008
113053	7/22/2009	112055	3/20/2013
114054	4/14/2011	112056	2/8/2010

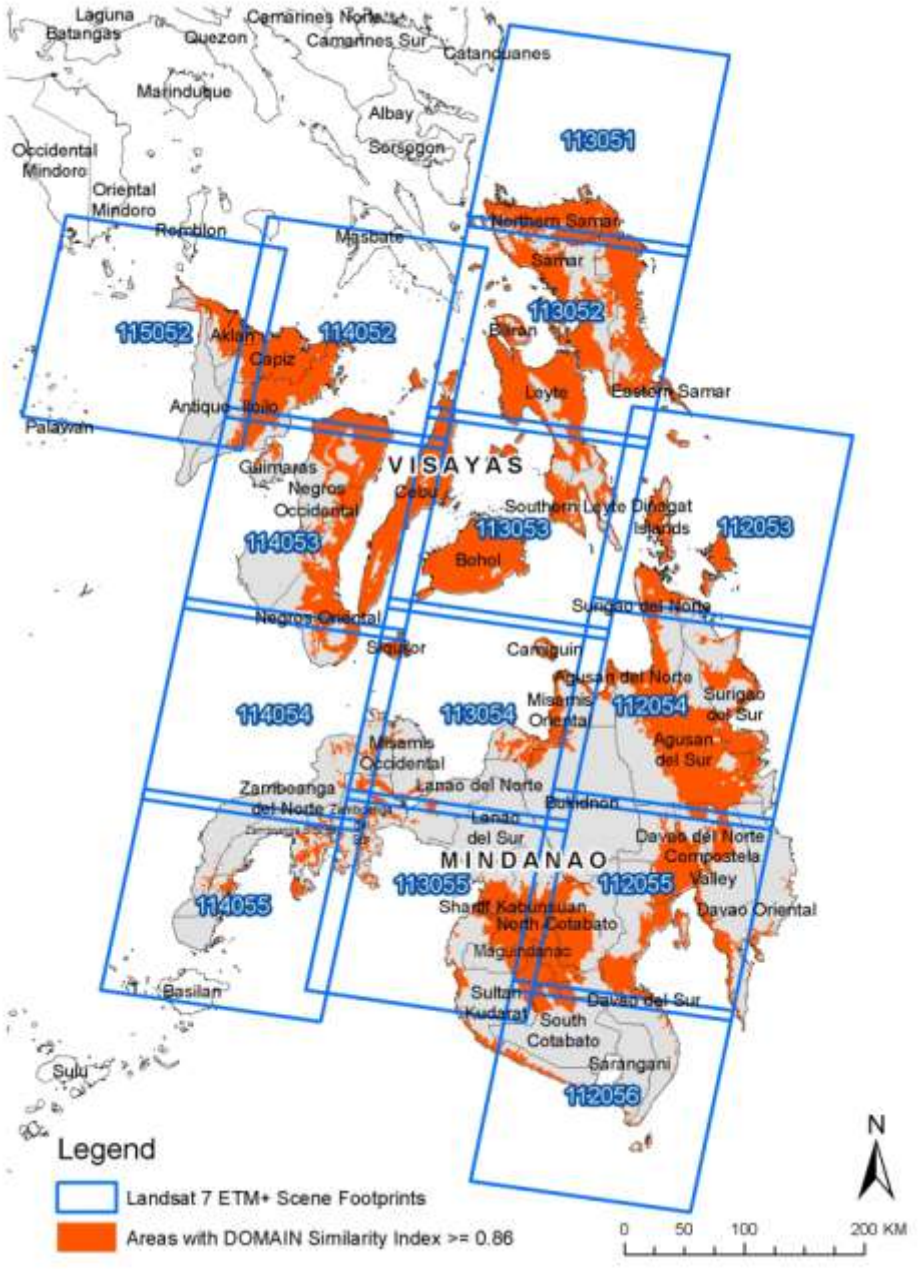

Figure 53. Map showing the footprints of the Landsat 7 ETM+ images subjected to classification to detection possible locations of Sago palms.

9.2.2 Classification Results and Detected Possible Sago Palms Locations

An example classification result after applying the Maximum Likelihood classifier on a combination of band 3, 4, 5, 7, TEMP and DEM for image id# 112055 is shown in Figure 54.

With the classification approach implemented in all the datasets, a total of 5,235 hectares in Mindanao, and 2,389 hectares in Visayas were detected to possibly contain Sago palms. The map showing the detected possible locations of Sago palms is shown in Figure 55.

In Visayas, the province of Leyte was found to have the largest area of possible locations (1,064 has), followed by Eastern Samar (497 has), Samar (212 has), Aklan (199 has), and Northern Samar (138 has). A total of 15 provinces in Visayas were found to have possible occurrences of Sago palms.

In Mindanao, the province of Agusan del Sur has the largest area of possible locations (3,211 has), followed by Sultan Kudarat (348 has), Maguindanao (340 has), Agusan del Norte (292 has), and Surigao del Norte (238 has). A total of 20 provinces in Mindanao were found to have possible occurrences of Sago palms.

The full statistics are shown in Table 14 and Table 15. In generating the statistics, the provincial boundaries were intersected with the polygons of the detected possible Sago palm locations. The administrative boundary GIS file used is the Global Administrative (GADM) Version 2 obtained from http://www.gadm.org/. (In this data, Shariff Kabunsuan is still considered a province although it was already nullified in 2008. To correct this error, the municipalities under Shariff Kabunsuan were merged with Maguindanao.)

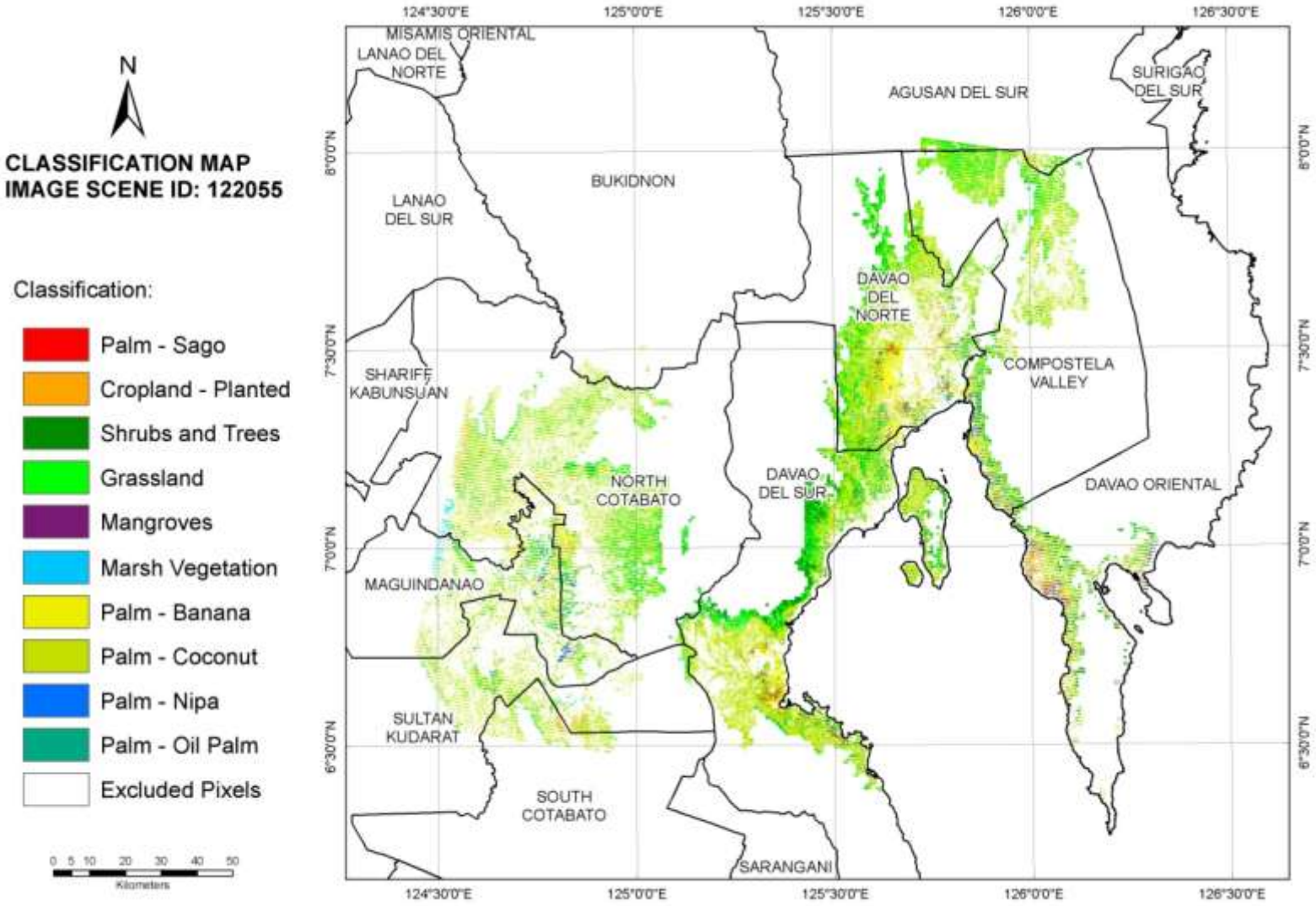

Figure 54. Example classification result for image id# 112055.

Figure 55. Possible Sago palm locations detected through Maximum Likelihood classification of Landsat ETM+ bands 3, 4, 5 and 7, TEMP and DEM.

Table 14. Number of hectares per province of detected possible locations of Sago palm in Visayas.

Rank	Province	Hectares
1	Leyte	1,064
2	Eastern Samar	497
3	Samar	212
4	Aklan	199
5	Northern Samar	138
6	Southern Leyte	107
7	Cebu	57
8	Capiz	35
9	Negros Oriental	30
10	Bohol	15
11	Antique	11
12	Iloilo	9
13	Siquijor	7
14	Negros Occidental	5
15	Biliran	3
Total		2, 389

Table 15. Number of hectares per province of detected possible locations of Sago palm in Mindanao.

Rank	Province	Hectares
1	Agusan del Sur	3,211
2	Sultan Kudarat	348
3	Maguindanao (incl. Shariff Kabunsuan)	340
4	Agusan del Norte	292
5	Surigao del Norte	238
6	North Cotabato	190
7	Surigao del Sur	157
8	Davao Oriental	130
9	Davao del Sur	111
10	Misamis Oriental	97
11	Davao del Norte	42
12	Compostela Valley	30
13	Dinagat Islands	16
14	South Cotabato	15
15	Camiguin	5
16	Zamboanga del Sur	4
17	Zamboanga del Norte	4
18	Lanao del Norte	2
19	Zamboanga Sibugay	2
20	Sarangani	1
Total		5,235

9.3 Chapter Conclusions

In this chapter, an evaluation on the use of readily-available and free Landsat 7 ETM+ images in detecting Sago palm locations has been presented. It was found that better detection of Sago palm locations can be achieved if only bands 3, 4, 5 and 7 of a Landsat 7 ETM+ image together with TEMP and DEM are used as input for Maximum Likelihood Classification. The Producer's and User's Accuracies for Sago palm using this combination were at acceptable levels of 90.44% and 94.09%, respectively based on 387 validation data points.

Using the signature extension approach, the Maximum Likelihood classifier that was trained based on spectral, brightness temperature, and elevation information extracted from the 14 Sept 2008 image reflectance bands, TEMP and DEM were utilized to map possible Sago palm locations in images covering Visayas and Mindanao. The classification detected a total of 5,230 hectares in Mindanao, and 2,394 hectares in Visayas to possibly contain Sago palms. The number of hectares presented in this chapter does not necessarily refer to the number of hectares of existing Sago palms. Certainly, the detected number of hectares may overestimate the actual distribution of Sago palms. There is also high possibility that

actual/existing Sago palm stands may have been excluded in the Sago palm classification map. These notions are stated in consideration of the classification errors and inadequacy of the image spatial resolution of 30 m for mapping Sago palms that are less than 30 x 30 m in size.

The detected locations of Sago palms were utilized as primary basis for the conduct of field surveys and ground validation, and for the acquisition of ALOS AVNIR-2, Envisat ASAR and high resolution Worldview-2 images for the refinement of the Sago palm classification map. In the next chapters, the Landsat-based Sago palm classification map is enhanced through field validation, and some parts of the maps are refined through analysis of 10-m spatial resolution ALOS-AVNIR 2 images together with Envisat ASAR data. The detected locations are also examined one-by-one with the aid of recent high resolution Worldview-2 images (purchased and those available in Google Earth) as a way to confirm if they are indeed Sago palms or just results of misclassifications.

Perhaps, an important contribution of this chapter (and some chapters before) in the task of mapping Sago palms is the ability to know where to look for Sago palms in Visayas and Mindanao. Earlier before this research was conducted, locations of Sago palms are merely based on reports. But with the potential distribution maps and the Landsat-based Sago palm classification map, the areas in Visayas and Mindanao to look for have been expanded but specific. While initially there is a need to analyze the whole of Visayas and Mindanao, at this point the coverage has been reduced. It is in this reduction of coverage that high resolution satellite images become of practical use to obtain very detailed and highly accurate maps and statistics of existing Sago palm stands.

Chapter 10. Evaluation of Envisat ASAR and ALOS AVNIR-2 Images in Land-cover Mapping and in Detection of Sago Palm Locations

10.1 Case Study 1: Multi-Temporal Approach of Mapping Palms Using Envisat ASAR AP Images

Using a single radar image for land-cover mapping is a hard task because of limited means to derive a land-cover map from this image. The most commonly used is through visual interpretation, and through the use of clustering algorithms. Both ways are difficult. For visual interpretation, appearance of a land-cover type is not as distinguishable as they were on an optical image. The use of clustering algorithms may automate the process but the hard part is to assign a specific land-cover type to the clusters of pixels.

Some studies have utilized a multi-temporal approach in land-cover mapping using the radar images. Images acquired at different dates are stacked together to form the input bands to a classifier. Others use a single radar image as additional band to an optical image for classification.

In this case study, Envisat ASAR images acquired in alternating polarization (AP) modes (HH, HV) at different dates were utilized in an attempt to map Sago palm locations in the images as alternative to using optical images. Horizontal Transmit - Horizontal Receive Polarization (HH) is a mode where the microwaves of the electric field are oriented in the horizontal plane for both signal transmission and reception by means of a radar antenna. In Horizontal Transmit - Vertical Receive Polarization (HV), the microwaves of the electric field are oriented in the horizontal plane for signal transmission, and where the vertically polarized electric field of the backscattered energy is received by the radar antenna.

The analysis was designed to be composed of two stages: (1) detect all kinds of palms of vegetation and test for classification accuracy; and (2) if the accuracy is acceptable (>85% for overall classification, Producer's and User's Accuracy for palm), then all pixels detected as "palm" are reclassified into different kinds of palms, one of which is Sago palm. The case study area is Butuan City, Agusan del Norte.

10.1.1 Related studies

Ahmed [**107**] investigated the capability of multi-temporal, multi-incidence angle, dual polarization Envisat ASAR imagery for extracting land use/land cover information in the rural-urban fringe of the Greater Toronto Area. Backscatter profiles were generated for selected land cover classes. Non-parametric classifiers such as K nearest Neighbor and Artificial Neural Network (ANN) were tested with some selected combinations of eleven (11) ASAR HH/HV imagery acquired at different dates. Prior to classification, each image was subjected to textural analysis to derive mean and standard deviation through computation of gray level co-occurrence matrix (GLCM) image. The window size used for the GLCM computation was 11 x 11. For each image, the HH and HV bands were subjected to textural analysis giving two mean bands (HH-mean, HV-mean), and two standard deviation bands

(HH-Std.dev, HV-Std. dev). The best kNN-classification was achieved with combined Mean and Standard Deviation with multi-incidence angle, dual polarization eleven date ASAR images. ANN further improved the classification results of the textured images. As for comparison of classifiers, it was found that, with complex combinations (dual polarization, multi-incidence angle), ANN performs significantly better than kNN. The overall accuracy was 9.6% higher than that of kNN.

One of the crucial parameter to set when computing GLCM of radar images is the window size to compute texture measures. In the study of Haack and Bechdol [**57**] where they used a SIR-C radar image to accurately locate areas of natural vegetation, scattered agricultural and settlements, classification of variance texture images computed with moving window size of 13x13 pixels gave the best result.

10.2.2 Envisat ASAR image preparation

The study used three (3) Alternating Polarization Precision (APP, in HH/HV polarizations) Envisat ASAR images of Butuan City, Agusan del Norte. The images were acquired on 2012 at the following dates: January 11, February 10, and March 11. These images were provided as a Level 1P product by the ESA under Category 1 Project No. 11044.

All the images were pre-processed using the Next ESA Tool Box (NEST) version 4C-1.1 in order to generate a radiometrically calibrated and orthorectified sigma nought, σ^0 image in UTM 51 WGS 1984 projection, and with spatial resolution of 12.5 x 12.5 m. The order of the steps employed are: (i.) refining the orbit state vectors in the product's metadata through application of the DORIS precise orbit file generated by the Centre for Traitement Doris Poseidon and Delft University; (ii.) radiometric calibration to convert the DN values (amplitude) to radar backscatter or sigma nought (σ^0) in linear scale; (iii.) de-speckling using the Enhanced/Refined Lee filter; (iv.) terrain correction using rigorous SAR simulation where a 3-arcsecond SRTM DEM was utilized; (v.) radiometric normalization. The images were geo-referenced using 6 ground control points obtained from 1:50,000 NAMRIA topographic map.

Using Envi 5 software, mean and variance textures were derived from the 3 APP images. Since a single image has two bands (HH and HV), two mean and two variance texture images were obtained. For the 3 APP images, a total of 12 texture images were derived and stacked together to form a single dataset. Each texture measure is assigned with band numbers (Table 16).

Table 16. Description of band numbers assigned to the stacked texture images.

Band No.	Assigned Texture Image
1	Mean_HV_Jan.11,2012
2	Var_HV_Jan.11,2012
3	Mean_HH_Jan.11,2012
4	Var_HH_Jan.11,2012
5	Mean_HV_Feb.10,2012
6	Var_HV_Feb.10,2012
7	Mean_HH_Feb.10,2012
8	Var_HH_Feb.10,2012
9	Mean_HV_March 11,2012
10	Var_HV_March 11,2012
11	Mean_HH_March 11,2012
12	Var_HH_March 11,2012

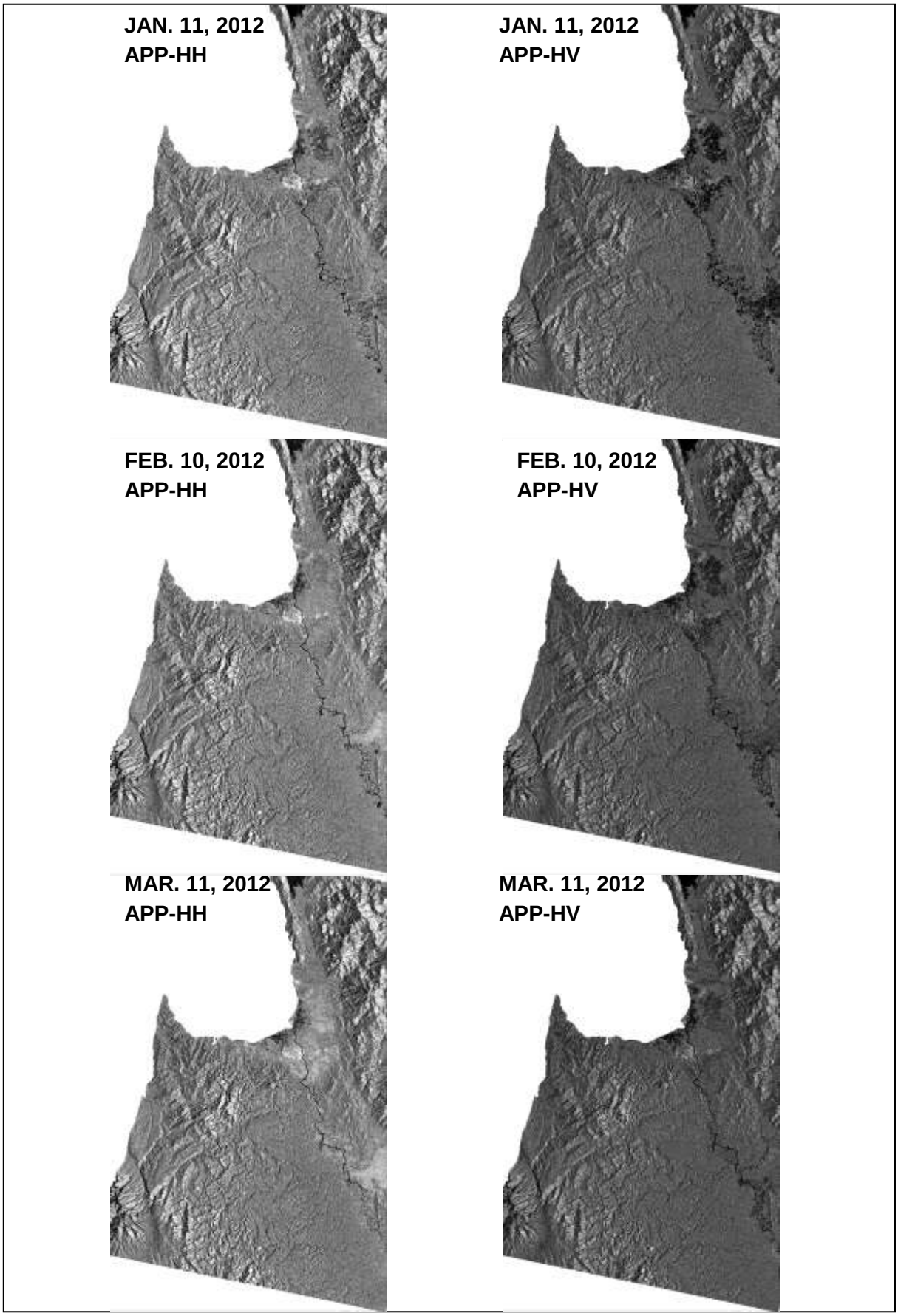

Figure 56. The Envisat ASAR image acquired in HH and HV polarizations.

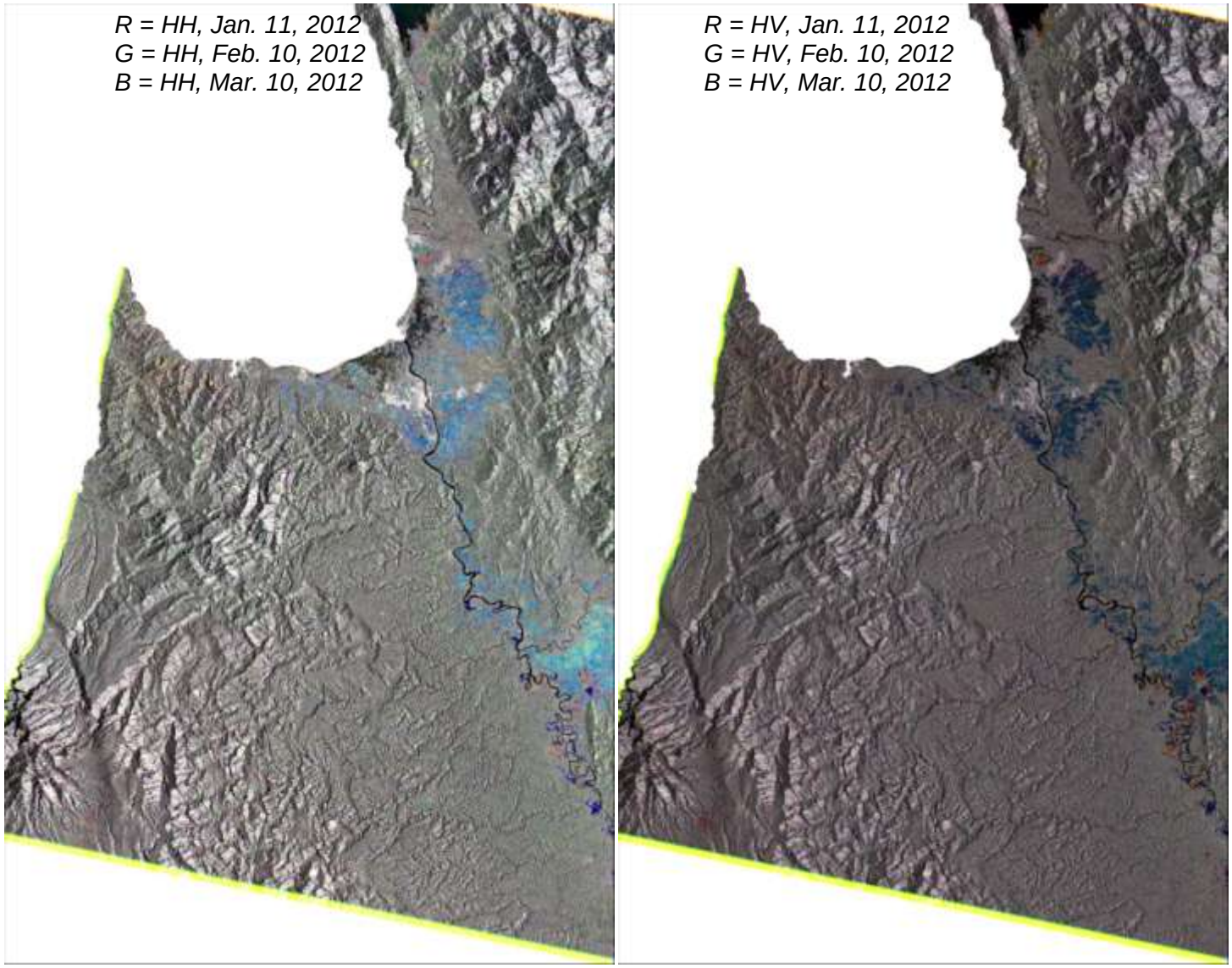

Figure 57. The Envisat ASAR APP HH and HV images shown in R-G-B combinations. Croplands have distinct colors.

10.2.3 Envisat ASAR image classification

Artificial Neural Network (ANN) and Support Vector Machine (SVM) were used to classify all the 12 texture bands. Both classifiers are non-parametric and have no assumptions about the probabilistic models of data, especially the assumption of normality which is required by parametric classifiers such as Maximum Likelihood. ANN and SVM have the ability to generalize in noisy environments and ability to learn complex patterns, especially if classifying multiple bands of data.

To train the classifiers, polygons representing barren land, built-up, cropland, dense vegetation, grassland, palm trees (all kinds), and water were digitized from high resolution Google Earth images and overlaid on the layer-stacked images. These were then converted into ROIS for classifier training in Envi 5. Figure shows the appearance of these land-cover classes in different band combinations of the texture bands. Another set (different from the training ROIs) was randomly selected for classification accuracy assessment. The number of training and accuracy ROIs are listed Table 18.

.

Table 17. Appearance of land-cover classes in different band combinations of the texture bands

Land Cover	Band Combinations						
	1-2-3	1-1-3	1-2-2	2-2-1	10-12-11	2-3-5	8-9-10
Barren land			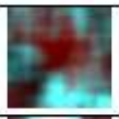	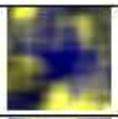	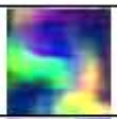		
Built-up		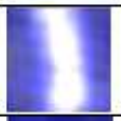					
Cropland							
Dense Vegetation			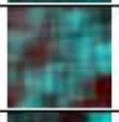				
Grassland							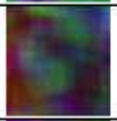
Palm Trees	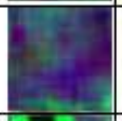		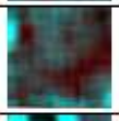				
Water							

Table 18. Number of ROIs for training and accuracy assessment of ANN and SVM classification.

Land-cover Class	Training	Accuracy Assessment
Barren Land	2,067	429
Built-up	8,075	7,632
Cropland	5,769	3,824
Dense Vegetation	16,266	9,364
Grassland	1,476	1,255
Palm trees	6,549	4,336
Water	29,036	9,753

10.2.3 Classification Results

Figure 58 shows the ANN and SVM classification results. The accuracies of the results are listed in Table 19.

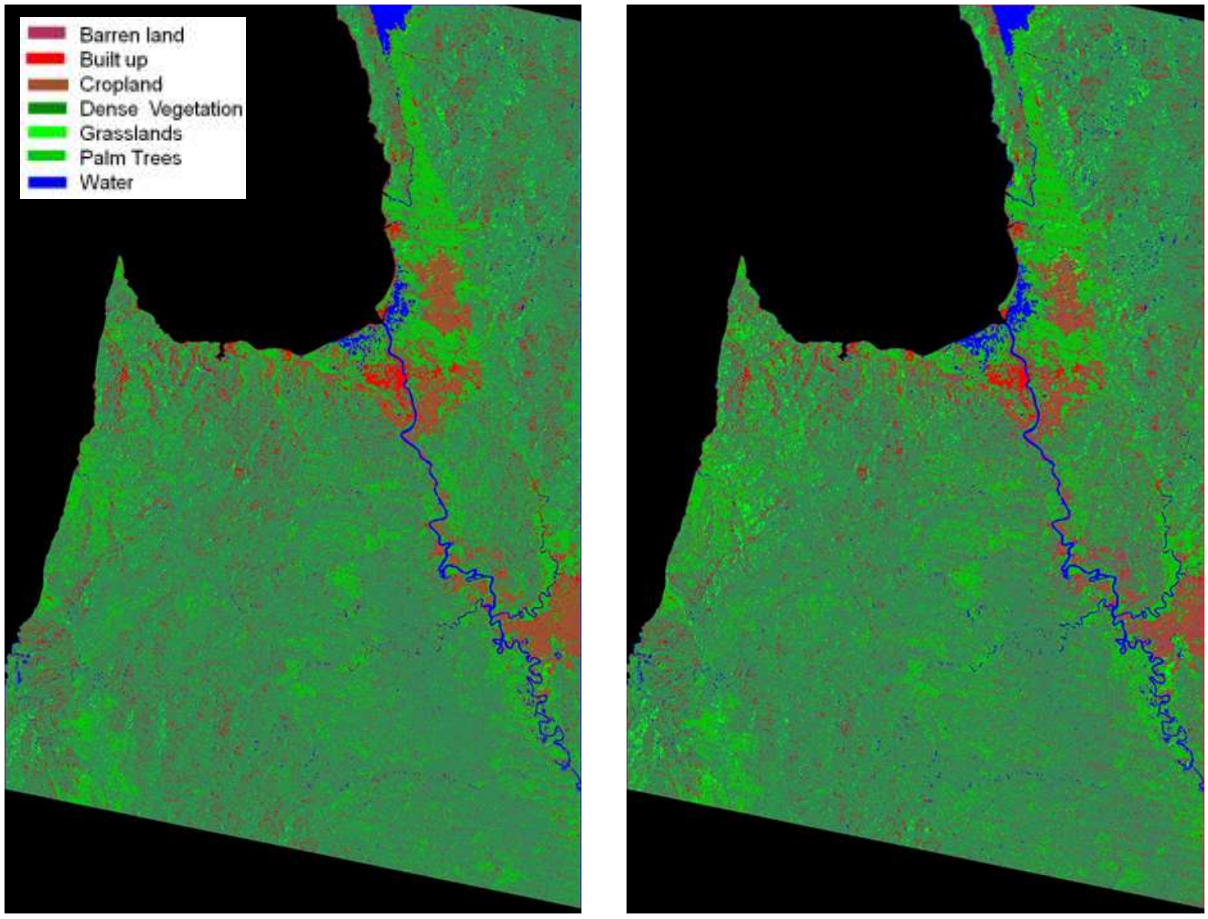

Figure 58. ANN and SVM classification results.

Table 19. Accuracy of ANN and SVM classifications.

Land-cover Class	ANN		SVM	
	Overall Accuracy: 86.23%		Overall Accuracy: 86.25%	
	Prod. Acc.(%)	User Acc.(%)	Prod. Acc.(%)	User Acc.(%)
Built-up	88.34	87.41	88.13	88.49
Barren land	6.76	3.66	14.92	5.82
Cropland	94.33	96.75	96.47	99.7
Grassland	1.99	20	0	0
Water	98.59	96.34	98.24	97.06
Palm trees	80.37	79.95	81.85	78.87
Dense vegetation	85.97	81.35	84.92	81.3

For ANN, the overall classification accuracy was at 86.23%. The Producer's and User's Accuracies for Palm trees are 80.37% and 79.95%, respectively, which means poor classification result. For SVM, the accuracy is similar to that of ANN. In both classification results, grassland have the lowest Producer's and User's Accuracies. This would mean that true grasslands are misclassified as other land-cover types, while other land-cover types are falsely classified as grasslands. Only cropland, built-up and water have good accuracies which indicate suitability of the multi-temporal APP images and of either ANN or SVM as classifier. This can be attributed to high separability of water, built-up and cropland. Grassland and barren land showed the poorest accuracy results due to low separability of these classes.

To check if Sago palm locations were accurately classified in both results as "Palm trees", 28 Sago palm locations in Butuan City were overlaid on the classification map the classification of the pixels at these locations were determined. The results are shown in . For ANN, only 17 of the 28 (60.71%) Sago palm locations were correctly classified as "Palm Trees". The remaining 11 locations were falsely classified as other land-cover types. For SVM, only 15 of the 28 (53..57%) Sago palm locations were correctly classified as "Palm Trees". The remaining 13 locations were falsely classified as other land-cover types.

Table 20. Results of comparison of Sago palm locations with the ANN and SVM classification.

Sago Palm Location Classified as:	No. of Pixels	
	ANN	SVM
Built-up	3	2
Barrenland	2	5
Cropland	0	0
Dense Vegetation (Non-Palm)	6	5
Grassland	0	1
Palm Trees	17	15
Water	0	0
Total	28	28

10.2.4 Case Study 1 Conclusions

The case study results showed that the approach of using multi-temporal Envisat ASAR APP images in land-cover mapping using ANN and SVM can only provide acceptable results for built-up, cropland and water. The results for mapping palm trees is low (<85%) and below the acceptable levels of accuracy. Comparing the classification results with actual Sago palm location revealed inadequacy in terms of mapping the location of Sago palms - only 50-60% of the Sago palm locations were accurately classified as "Palm trees". With these poor results, the stage 2 of the classification which is to detect Sago palms from all the pixels classified as "Palm trees" was no longer done. Moreover, the use of purely radar images as alternative to optical images for Sago palm detection was not longer pursued because there is high rate of omitting actual Sago palm locations, and high rate of misclassifying other vegetation as Sago palm.

With improvement in the classification approach and the use of more multi-date images, the accuracy of the results may be improved. This could be a subject of further research.

10.2 Case Study 2: Evaluation of ALOS AVNIR-2, NDVI, Envisat ASAR IM and ASTER GDEM in Mapping Sago Palms

For a given application it is often that spectral information acquired by a remote sensing sensor may not be sufficient to derive accurate information. Incorporation of additional or ancillary data sources in the process of remote sensing classification may result in better understanding and achievement of higher accuracy than utilizing spectral data from a remote sensing sensor alone [**103**]. For forested wetlands, visible and near-infrared satellite data have generally not produced adequate results because these data do not provide the sensitivity to soil moisture or to relatively small areas of inundation necessary to distinguish wetland vegetation from upland vegetation [**108**]. Synthetic aperture radar (SAR) data has proven its utility for mapping wetland and flooded forest extents not only because of its ability to penetrate the canopy and yield information about the ground but also because it is very sensitive to moisture which is a very useful characteristic for wetland mapping [**97**]. The integration of SAR data with visible and near-infrared satellite data has been found to bring a significant improvement to land-cover classification [**109**]. On the other hand, incorporation of a digital elevation model (DEM) and a normalized differenced vegetation index (NDVI) image as additional data sources has also been found to increase classification accuracy as these datasets account for the rugged topography so as to eliminate the presence or absence of certain classes in some elevation zones, and reduce the impact of shadows and to enhance the separability among various vegetation classes [**103**].

In this case study, the multi-source classification approach of mapping Sago palms by incorporating NDVI, Envisat ASAR and ASTER GDEM datasets to an ALOS AVNIR-2 image is evaluated. The study aims to investigate if the addition of these external datasets, either as an individual or as combined datasets, can improve the accuracy of identifying possible locations of Sago palms in an ALOS AVNIR-2 image using the MLC. Since the objective is to map all possible locations, the evaluation is geared towards assessment of the Sago palm's producer's accuracy (i.e., the accuracy to include all actual Sago palm locations in the classification result.

10.2.1 The multi-source classification approach

The stacked vector approach [**103**] is adapted to incorporate multi-source data into the Maximum Likelihood (ML) classification process. It is a straightforward approach where the data from each source are treated as augmented dimensions of an input data vector. In the stacked vector approach, a dataset consisting of four bands of ALOS AVNIR-2, an NDVI, a single-date Envisat ASAR, and an ASTER GDEM can be stacked together to form the input to the MLC.

10.2.2 Study area and multi-source datasets

The classification approach was tested to multi-source datasets (Table 21) of an area in Agusan del Sur, Mindanao, Philippines (Figure 59). A portion of the study area is within the Agusan Marsh Wild Life Sanctuary.

The study area was chosen because of the availability of multi-source datasets as well as ground truth datasets and high resolution Worldview-2 images (Figure 3) of Sago palm clusters that can be used to extract information necessary for classifier training and accuracy assessment. The areas with confirmed Sago palms are located in the municipalities of Bunawan and Veruela, Agusan del Sur.

Table 21. Datasets used in the multi-source detection of Sago palms.

Dataset Name	Description
ALOS AVNIR-2	Acquisition date: 14 September 2009; Level 1B (in digital numbers, DN) consisting of four bands (Blue, Green, Red and Near-infrared); Spatial resolution: 10 m. (Source: National Mapping and Resource Information Authority(NAMRIA))
NDVI	Normalized Difference Vegetation Index computed from radiometrically calibrated and atmospherically corrected ALOS AVNIR-2 bands 3 and 4 (Red and Near-infrared)
Envisat ASAR	Acquisition date: 15 November 2010; Level 1P, *C*-band (5.6 cm) SAR data acquired in image mode (IM), with HH polarization; Spatial resolution: 12.5 m. (Source: European Space Agency)
ASTER GDEM	30-m resolution elevation dataset, resampled to 10-m to conform with the resolution of ALOS AVNIR-2. (Source: NASA and METI; downloaded from http://reverb.echo.nasa.gov)

It can be noticed from Table 1 that the dates of acquisitions of the ALOS AVNIR-2 and Envisat ASAR are different, with the Envisat ASAR acquired one year later. This is because during the conduct of this case study, neither of the two datasets are available that were acquired in the same dates, or even in the same months.

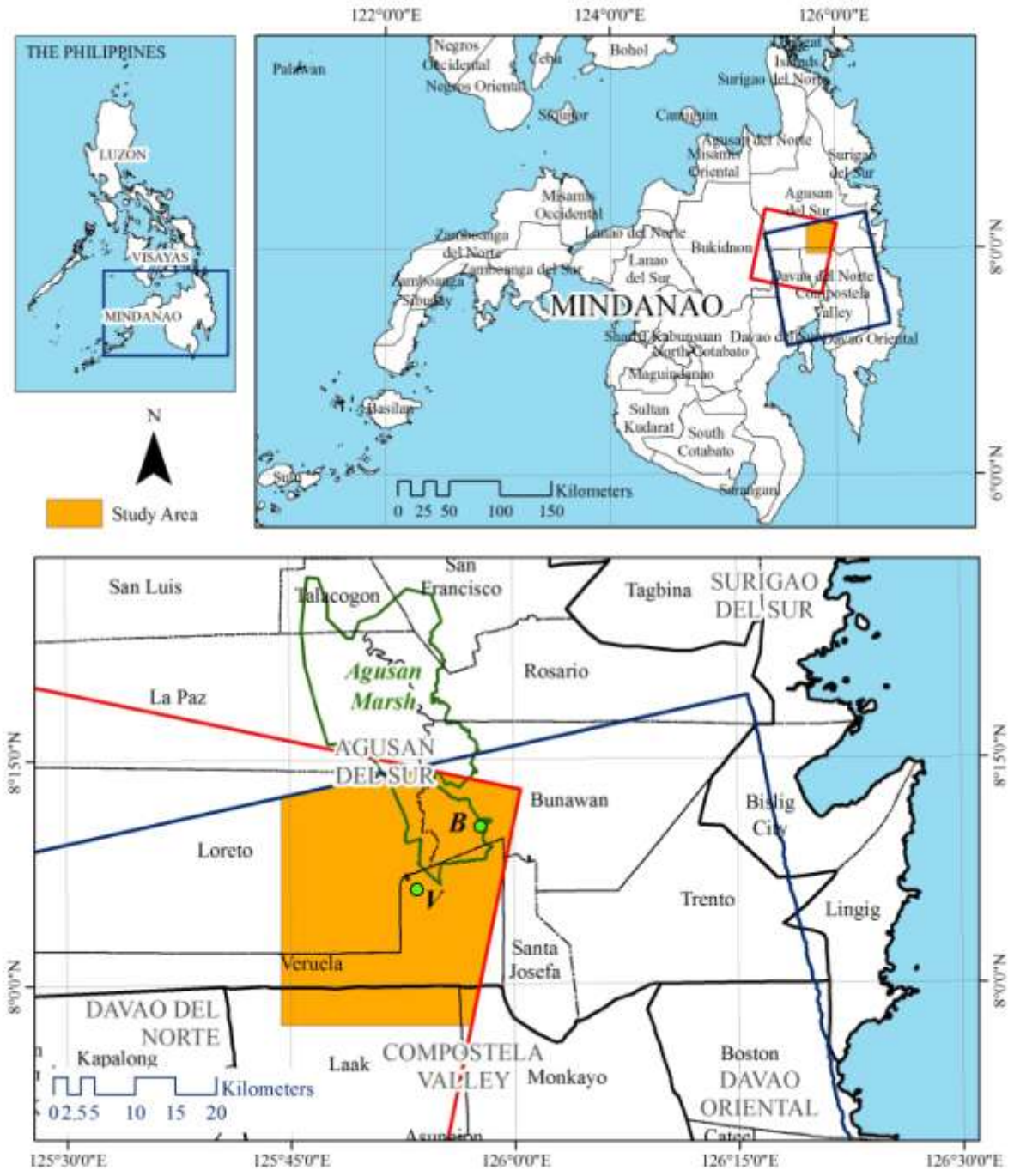

Figure 59. The case study area in Agusan del Sur, Mindanao, Philippines. Points B and V are the locations of Sago palm clusters in Bunawan and Veruela municipalities, respectively.

Figure 60. Worldview-2 images acquired on 29 March 2012 showing Sago palm clusters in Bunawan and Veruela, Agusan del Sur.

10.2.3 Data preparation

The raw ALOS AVNIR-2 dataset was calibrated to top-of-atmosphere radiance by applying gain and offset values. It was then subjected to atmospheric correction using the Fast Line-of-Sight Atmospheric Analysis of Spectral Hypercubes (FLAASH) as implemented in the ENVI 4.8 image processing software. FLAASH creates an image of surface reflectance, scaled into signed integers with a scale factor of 10,000 (i.e., a reflectance of 0.05 or 5% is shown in the image as a pixel value of 500). The NDVI band was then computed using the FLAASH-corrected bands 3 and 4. The calibrated dataset and NDVI were then georeferenced to UTM 51 WGS 1984 using ground control points collected from 1:50,000 NAMRIA topographic maps (total RMSE < 0.5 pixel).

The Envisat ASAR IM-HH Level 1P data product was processed using the Next ESA Tool Box (NEST) version 4C-1.1 in order to generate a radiometrically calibrated, orthorectified and normalized sigma nought (σ^0) image in linear scale and projected in UTM 51 WGS 1984. The order of the steps employed are: (i.) refining the orbit state vectors in the product's metadata through application of the DORIS precise orbit file generated by the Centre for Traitement Doris Poseidon and Delft University; (ii.) radiometric calibration to convert the DN values (amplitude) to radar backscatter or sigma nought (σ^0) in linear scale; (iii.) de-speckling using the Enhanced/Refined Lee filter; (iv.) terrain correction using rigorous SAR simulation where a 3-arcsecond SRTM DEM was utilized; and (v) radiometric normalization. The equations used in each step and other details are available in the NEST documentation available at http://nest.array.ca/web/nest/documentation. The resulting image was then co-registered to the ALOS AVNIR-2 dataset using 9 ground control points common to both images (total RMSE < 0.5 pixel). It was necessary to re-sample (using nearest neighbor) the processed Envisat ASAR image to 10-m to be compatible with the ALOS AVNIR-2 dataset.

The ASTER GDEM was also resampled to 10-m using bilinear interpolation.

10.2.4 Layerstacking

Although the stacked vector approach is straightforward and easy to implement, Watanachaturaporn et al. [**103**] pointed out that all data need to be normalized to bring them into the same scale especially if the approach is to be used with a parametric classifier such as the MLC. Unfortunately, in this study, normalization of the four datasets to a common scale - i.e., data stretching/shrinking such that dataset values are within a common range (e.g., 0 to 1) - seems to greatly degrade the pixel values especially for Envisat ASAR. Hence, normalization was not done and instead, a set of factors were chosen and multiplied to the NDVI (x10,000), Envisat ASAR (x10,000) and ASTER GDEM (x10). In this manner, the ranges of pixel values in these datasets are not very far from that of the calibrated ALOS AVNIR-2 dataset (which is in a scale of 10,000). After applying the scale factors, the four datasets were then stacked. The portion of the study area was extracted and used as input to the MLC. All these and subsequent processes were done in Envi 4.8. Figure 4 shows each band of the stacked datasets as well as their R-G-B combinations.

10.2.5 Maximum Likelihood Classification

Regions of interests (ROIs) of four vegetation classes namely, Sago palm, Shrubs & Trees, Marshland and Grassland, were collected in the stacked datasets for the estimation of the MLC parameters (class means and covariance matrices). The collection of this training dataset was done through image interpretation aided by information from field surveys (conducted on February-April 2012) and Worldview-2 images.

There were no ROIs specifically collected for Oil Palm, Banana, and Coconut because the ground truth data collected in the field for these classes are very few and were covered by clouds and shadows in the image. Initially, there were ROIs selected for these classes through visual interpretation but there is difficulty in correctly identifying them as either of the three. Hence, the ROIs selected were merged with Shrubs & Trees. It is assumed that during classification, pixels containing these palm vegetation may be classified as Shrubs &Trees.

For Sago palms, all the training ROIs were collected in the Bunawan area and none in the Veruela area.

During ROI selection, class statistics and test for divergence (using the Jeffries-Matusita Distance) were computed as initial assessment of the statistical separability of each vegetation class according to eight combinations of the stacked datasets. An independent validation set to be used for accuracy assessment was also collected randomly from the stacked datasets. Majority of the validation ROIs for Sago Palms were collected from the Veruela area and a few in the Bunawan area. Table 22 summarizes the training and validation sets.

Prior to classification, non-vegetation as well as cloud and shadow-covered areas were masked-out from the image by simple thresholding of the NDVI image. Only those pixels with NDVI > 0.3 were selected for classification (based on the minimum NDVI of Sago palms samples in the test image). All results were subjected to 3x3 majority analysis to remove isolated pixels and smoothen the classification map.

Table 22. Summary of training and validation sets for ML classification.

Set	Number of Pixels			
	Sago Palms	Shrubs & Trees (includes other palms)	Marshland	Grassland
Training	699	1,499	1,316	872
Validation	187	1,246	309	745

10.2.6 Class statistics and separability

Figure 61 shows the mean pixel values of training ROIs of the four vegetation classes in each band of the stacked datasets. Based on this figure, all classes have almost similar mean values in Band 1 while in Band 2, only grassland is distinguishable which could be due to the fact that Grassland is the greenest among the 4 classes. In Band 3, Marshland and Grassland are slightly distinguishable from Sago palms and Shrubs & Trees. It also appears that Sago palms' reflectance is very similar to that of Shrubs & Trees in Band 3. It is in Band 4 that all classes are distinguishable from each other due to greater differences in their class mean values. In terms of NDVI, Sago palm has the highest mean value followed by Shrubs & Trees, Marshland and Grassland. There is a big difference in NDVI values between Sago palm and Grassland. Looking at the Envisat ASAR class mean values, Shrubs & Trees has the highest backscattering coefficient and is distinguishable from the other classes. The mean backscattering coefficient (linear dB) of Sago palm is similar to that of Marshland and Grassland. In terms of elevation with the ASTER GDEM as basis, it shows that all four classes have distinct mean elevation values. As expected, Marshland has the lowest mean elevation while Shrubs & Trees have the highest mean elevation.

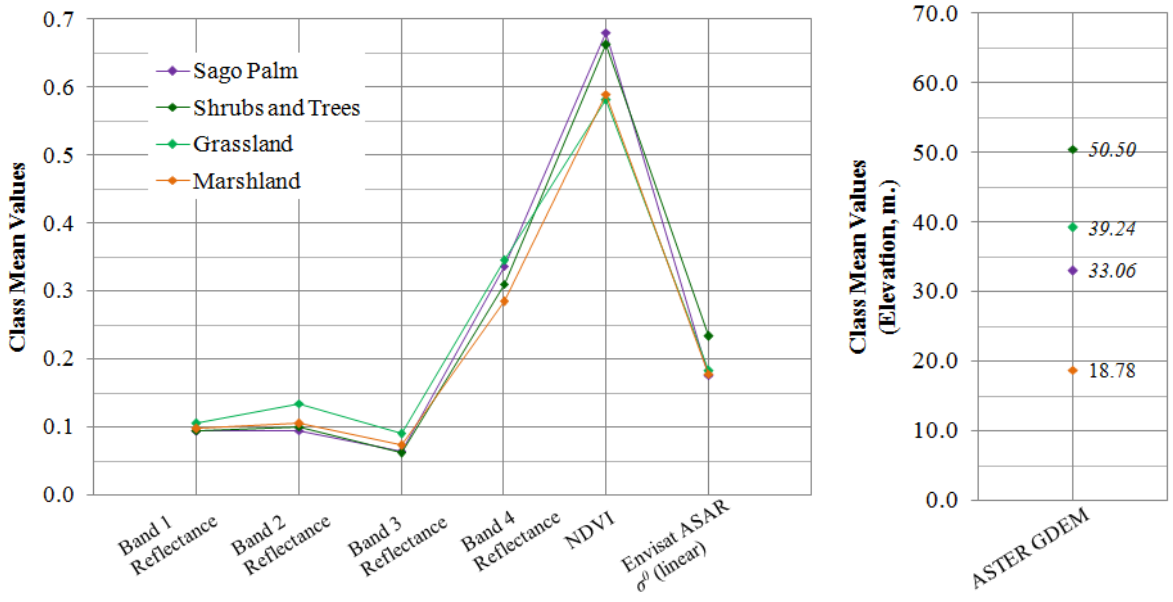

Figure 61. Class mean values of the four vegetation classes in each band of the ALOS AVNIR-2, NDVI, Envisat ASAR and ASTER GDEM stacked dataset. Note that the mean values are in their proper units.

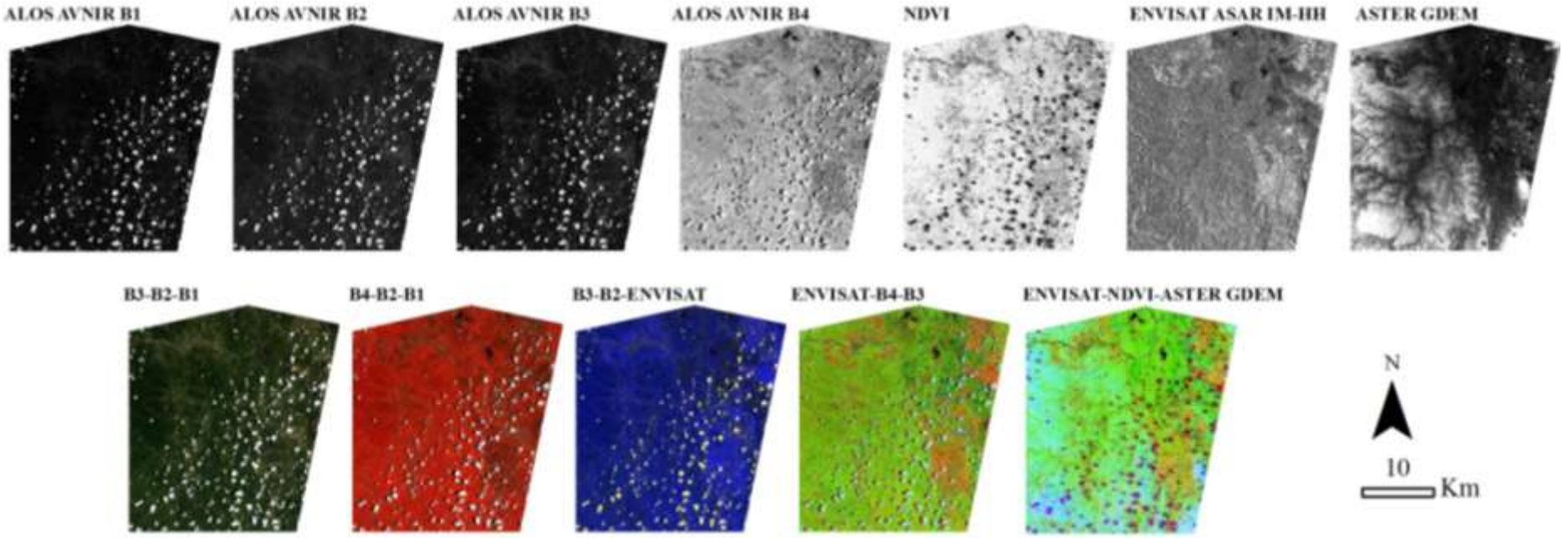

Figure 62. The 7 bands of the stacked dataset and some of their R-G-B combinations.

This simple graphical analysis of class mean values indicates that each data, in the exception of ALOS AVNIR-2 Band 1, has valuable information that could be used to distinguish the four vegetation classes. Clearly, Band 4 and ASTER GDEM have the most important information in distinguishing each class. While this is true, it could also be inferred that the use of other datasets will improve the discrimination as there are specific bands/data where one class is more distinguishable from one or more classes.

Since it is the interest of this study to accurately classify Sago palms from other vegetation classes, it is important to have basis on the statistical separability of Sago palm from other vegetation classes. Hence, Jeffries-Matusita Distances (JMD) were computed from 8 combinations of the ALOS AVNIR-2 bands, NDVI, Envisat ASAR and ASTER GDEM. The goal here is to determine if the addition of NDVI, Envisat ASAR and ASTER GDEM to the ALOS AVNIR-2 will have an effect on the separability of Sago palm from other classes. Depending on the combination, a JMD value nearer to 2 means Sago palm is highly separable to that class it is being compared to.

The results, shown in Figure 63, strongly indicates increase in separability of Sago palm with Shrubs & Trees as NDVI, Envisat ASAR and ASTER GDEM datasets are combined to the ALOS AVNIR-2 reflectance bands. There is very low separability between the two classes if relying only on the four ALOS AVNIR-2 bands. Individual addition of NDVI, Envisat ASAR and ASTER GDEM significantly increases separability. However, greatest separability is achieved when NDVI, Envisat ASAR and ASTER GDEM are all combined with ALOS AVNIR-2 dataset. What this imply is that when only the four ALOS AVNIR-2 bands are used in classification there is greater possibility that Shrubs and Trees will be confused by the classifier as Sago palm, and vice-versa. This will lead to high commission errors and consequently overestimation in the classification of Sago palms. But with the combination of additional datasets, confusions between Sago palm and Shrubs & Trees will decrease which may indicate better classification.

On the other hand, the JMD distances of Sago Palm with Marshland and Grassland are higher than those with Shrubs & Trees in all 8 combinations. This means that Sago palms are highly separable with Marshland and Grassland regardless of the combination of the datasets. But just like in the case of Shrubs & Trees, greatest separability is achieved when NDVI, Envisat ASAR and ASTER GDEM are all combined with ALOS AVNIR-2 dataset.

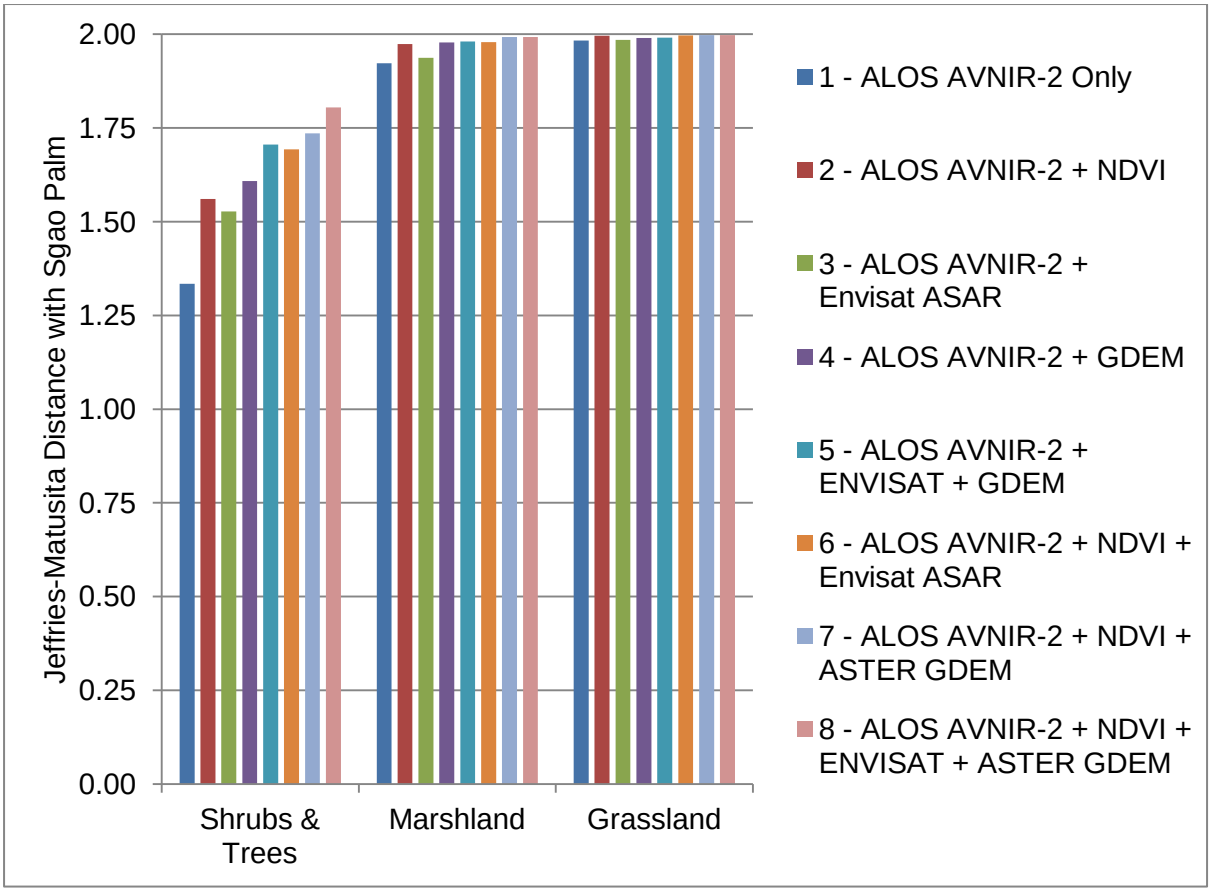

Figure 63. Separability of Sago palm with other vegetation classes based on the Jeffries-Matusita Distance that were computed from 8 combinations of the stacked datasets.

10.2.7 Classification results and accuracies

Figure 64 shows the results of the ML classification as applied to 8 combinations of ALOS AVNIR-2, NDVI, Envisat ASAR and ASTER GDEM. All the classifications were able to detect majority of the actual locations of Sago palms in both the Bunawan and Veruela areas. However, differences were found when accuracy of the classifications was assessed. The summary of overall classification accuracy, kappa statistic, Producer's and User's Accuracy for Sago Palm is shown in Figure 65. For convenience, the kappa statistics was plotted in percentage form.

Based on Figure 65, the use of MLC to all the 8 combinations produced more than 90% overall classification accuracies (OA). The highest OA of 96.42% was found when MLC was applied to the combination of ALOS-AVNIR2, Envisat ASAR and ASTER GDEM. When all the datasets are combined, a 95.82% OA was achieved. Lower OAs of ~92% were achieved when NDVI and ASTER GDEM are individually added to the ALOS AVNIR-2 image, as well as when both the NDVI and Envisat ASAR are added to it.

With regards to the classification of Sago Palm which is the interest of this study, all the 8 combinations produced more than 90% Producer's Accuracy which may indicate that more than 90% of all actual Sago palms in the study area have been correctly classified as such. Significant differences were found when the User's Accuracies (UA) of the classifications are taken into account. Only 77% UA was achieved when ALOS AVNIR-2

was used alone. This accuracy goes down to 69.72% when NDVI is added. The addition of both the NDVI and Envisat ASAR also shows poor UA (70.66%). This means that for these classifications, commission errors are high and there are overestimations in Sago palm classification. When the error matrices of these classifications were examined, many Shrubs and Trees were incorrectly classified as Sago palms. However, the best result was achieved when incorporating NDVI, Envisat ASAR and ASTER GDEM datasets to the ALOS AVNIR-2 image. A UA of 91.37% for this classification results indicate low commission errors, and that overestimation in Sago palm classification is lower than when other datasets are used.

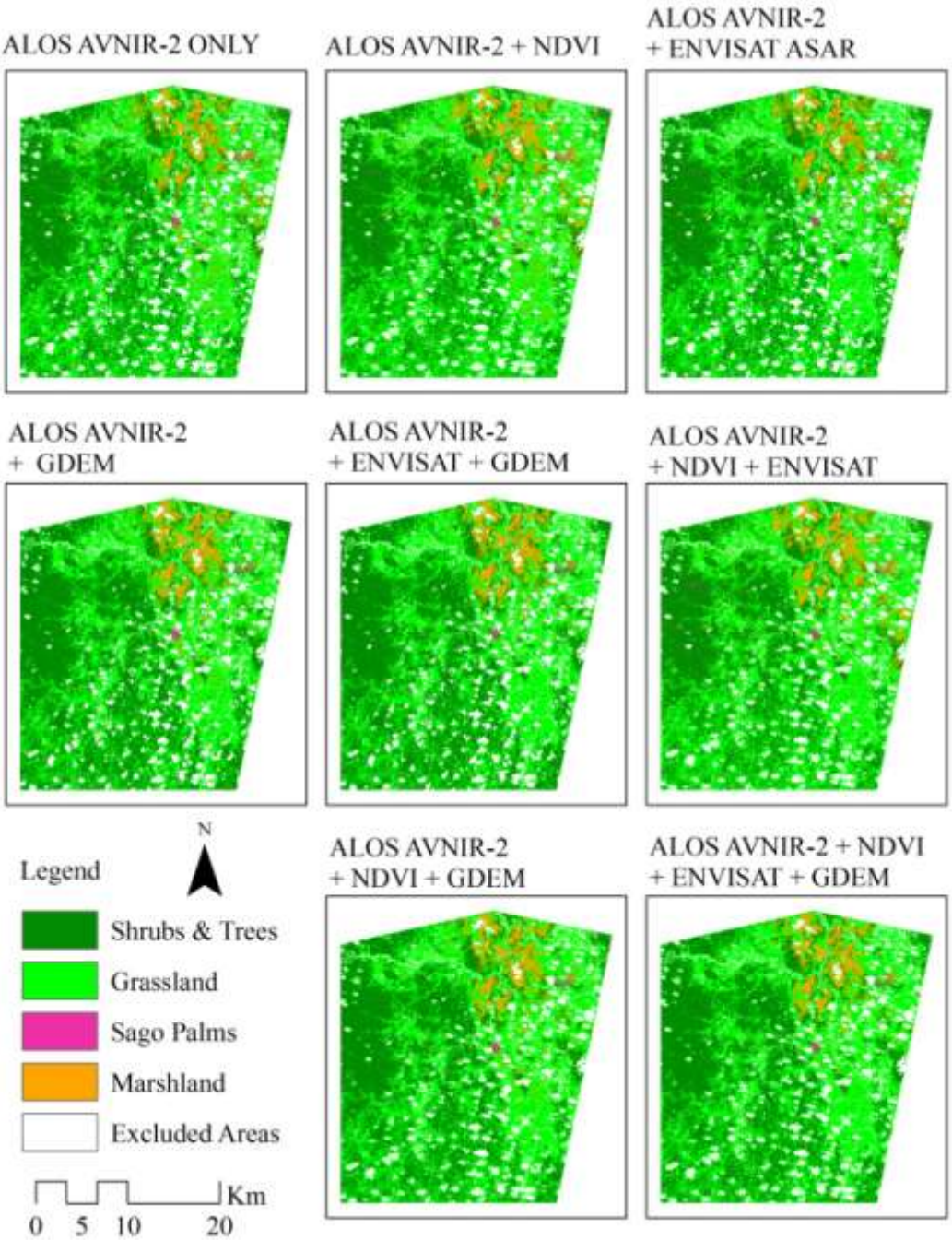

Figure 64. Results of the ML classification of 8 combinations of ALOS AVNIR-2, NDVI, Envisat ASAR and ASTER GDEM. (Due to the scale in which the above results are displayed, the classified Sago palms clusters may not be very visible especially that Sago palms in the study area are significantly fewer than other vegetation classes.)

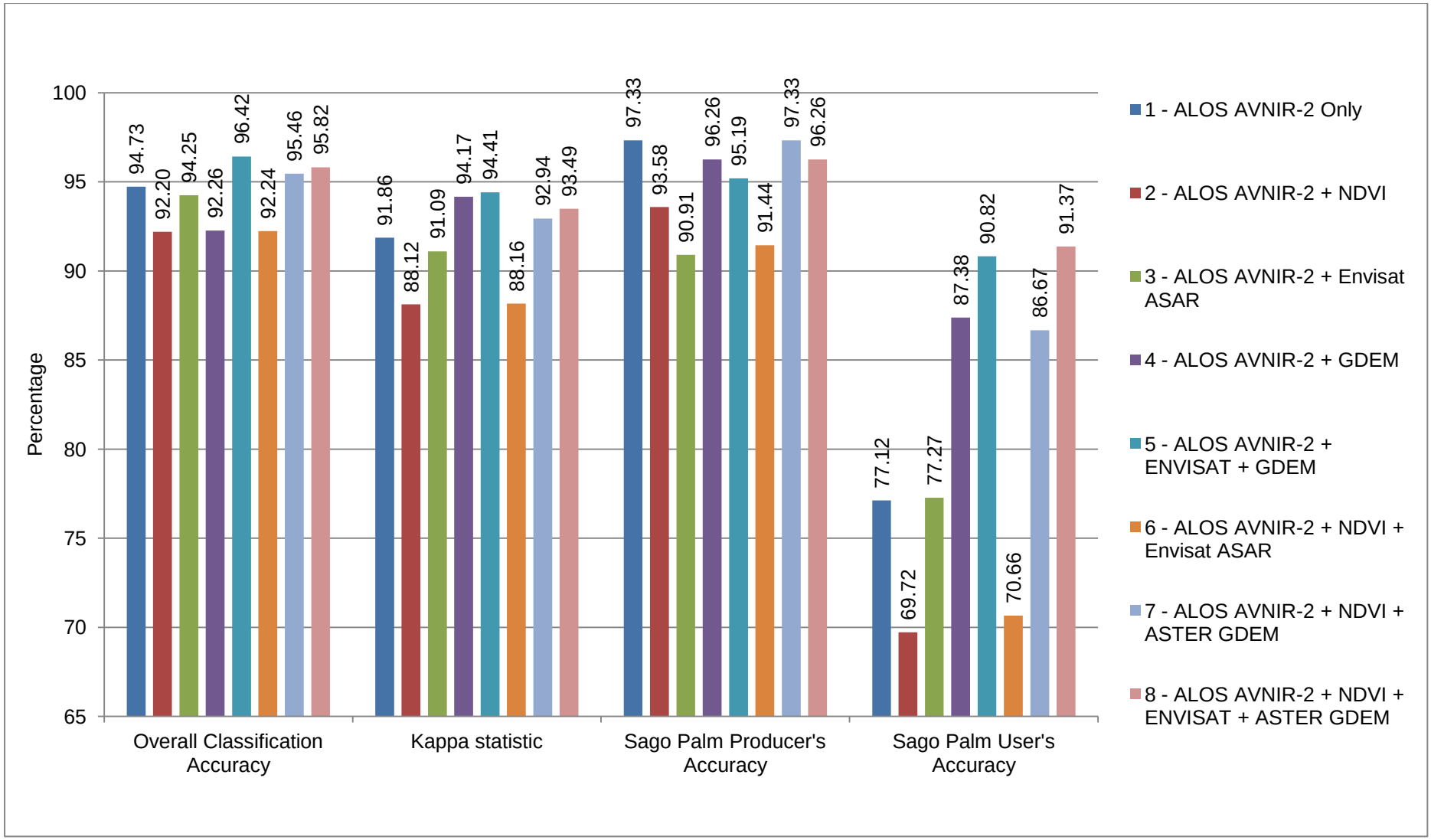

Figure 65. Summary of overall classification accuracy, kappa statistic, Producer's and User's Accuracy for Sago Palm.

Although not shown, it is also remarkable to note that the Producer's and User's Accuracy (PA/UA) for the other vegetation classes in all the classifications are more than 85% with majority of them surpassing 90%. The lowest PA was found for Shrubs & Trees (87.56%) when the MLC was applied on the combination of ALOS AVNIR-2 and NDVI; the lowest UA was found for Marshland (88.82%) when the MLC was applied on the combination of ALOS AVNIR-2, NDVI, Envisat ASAR and ASTER GDEM.

Using the result of the classification incorporating NDVI, Envisat ASAR and ASTER GDEM datasets to the ALOS AVNIR-2 image, about 256 hectares were found to contain possible locations of Sago palms in the case study area.

10.2.8 Case Study 2 Conclusions and Recommendation

The major finding in this case study is that incorporating NDVI, Envisat ASAR and ASTER GDEM datasets to an ALOS AVNIR-2 image can improve the accuracy of classifying Sago palms using MLC. It was clearly shown by both the separability analysis and the accuracy of the classifications that in the study area, spectral information alone acquired by ALOS AVNIR-2 sensor was not sufficient to accurately map Sago palms in such a way that there is no overestimation. The procedure of applying MLC to a combination of these multi-source datasets shows potential in mapping possible Sago palms locations in other areas in the Philippines.

However, there are issues that needs to be considered when the procedure is to be applied for mapping in other areas, which are

- availability of ALOS AVNIR-2 images
- availability of Envisat ASAR images co-incident with the ALOS AVNIR-2 images, preferably acquired in the same dates

During the time when this study was conducted, not all of Visayas and Mindanao are covered by Envisat ASAR IM and ALOS AVNIR-2 images. In some portions, there are ALOS AVNIR-2 images but the corresponding Envisat ASAR images are lacking.

In cases when ALOS AVNIR-2 images are the only available images, then the next best classification approach would be applying MLC to a stack of ALOS AVNIR-2 and ASTER GDEM. Looking back to Figure 65, this combination (#4) has acceptable Producer’s and User’s Accuracy for Sago palm (96.26% and 87.38%).

10.3 Application: Mapping Possible Locations of Sago Palms in portions of Visayas and Mindanao using ALOS AVNIR-2, ASTER GDEM and Envisat ASAR

Based on the results of the case study, mapping of possible locations of Sago palms in some portions of Visayas and Mindanao was conducted by applying MLC to a stack of ALOS AVNIR-2, ASTER GDEM, and Envisat ASAR (if available).

The aim of this analysis is to refine and complement the Sago palm locations that were detected through Landsat image analysis, specifically in portions where ALOS AVNIR-2 images are available. In these portions, the locations detected through ALOS AVNIR-2 analysis replace those obtained using Landsat.

Similar to the Landsat image analysis, signature extension was also utilized to apply the parameters (class mean vectors and covariance matrices) of the MLC derived from the stacked datasets of the case study area to the same datasets of other areas. The MLC parameters were updated by collection of additional training ROIs. Instead of merging other palms with “Shrubs and Trees”, specific ROIs were collected for coconut, nipa, oil palm and banana. This became necessary because the original MLC parameters appear to overestimate Sago palms when applied in other images.

10.3.1 ALOS AVNIR-2 Images for Classification

Ten (10) ALOS AVNIR-2 images covering portions of Visayas and Mindanao (Table 23, Figure 66) were subjected to Sago palm detections using MLC. The images were obtained from NAMRIA. Four of these images (P42, Q43, Q44 and R44) were classified in combination with Envisat ASAR IM images (acquired 15 November 2010) and ASTER GDEM. The remaining images were classified in combination with ASTER GDEM only. Prior to classification, the images and ASTER GDEM underwent the usual pre-processing procedures (radiometric calibration, atmospheric correction, geometric correction, DEM resampling, and layerstacking).

The classification area of interest for each image was limited only to those identified as having ≥ 86% DOMAIN similarity index, with elevation ranging from 0 to 700 m, and with NDVI > 0.3.

Table 23. List of ALOS AVNIR-2 images.

Image Scene ID	Date of Acquisition
M40	January 6, 2010
O36	June 5, 2010
O39	June 5, 2010
O43	June 5, 2010
P42	October 4, 2010
P45	February 16, 2010
P47	February 16, 2010
Q43	September 14, 2009
Q44	September 14, 2009
R44	July 16, 2010

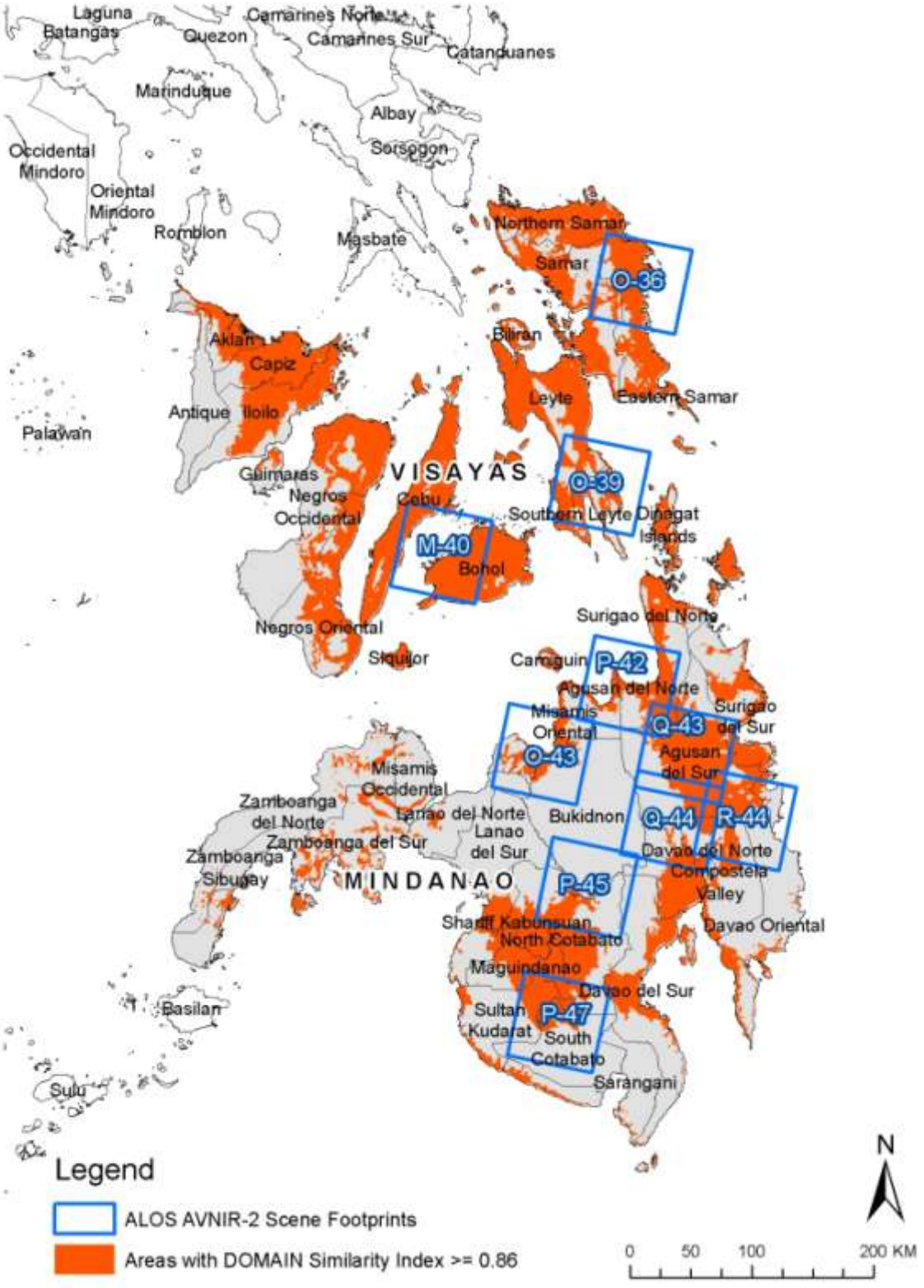

Figure 66. Map showing the footprints of the ALOS AVNIR-2 images subjected to Sago palm classification.

10.3.2 Classification results

Some of the results of the classification to detect possible Sago palm locations are shown in Figure 67 - Figure 71. The detected locations within the ALOS AVNIR-2 images are shown in Figure 72. The total number of hectares per image is listed in Table 24. Overall, a total of 5,238 hectares were mapped in the 10 images.

Table 24. Number of hectares of detected possible Sago palm locations in ALOS AVNIR-2 image scenes.

Image Scene ID	Area of Detected Possible Locations of Sago Palms, in hectares
M40	221
O39	535
O43	157
O46	412
P42	361
P45	497
P47	576
Q43	1,210
Q44	601
R44	666
Total	5,238

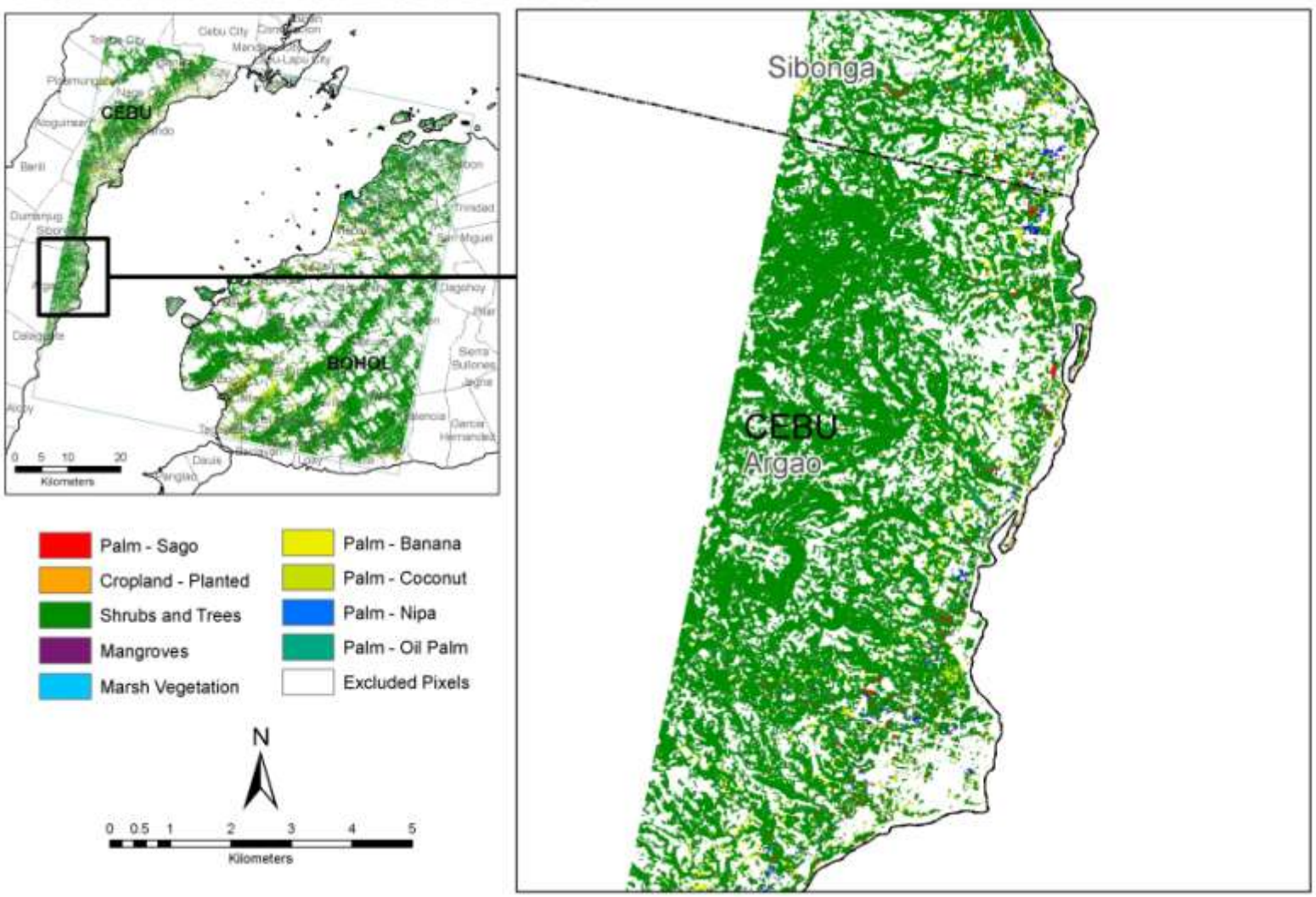

Figure 67. Classification result for image with scene id = M40.

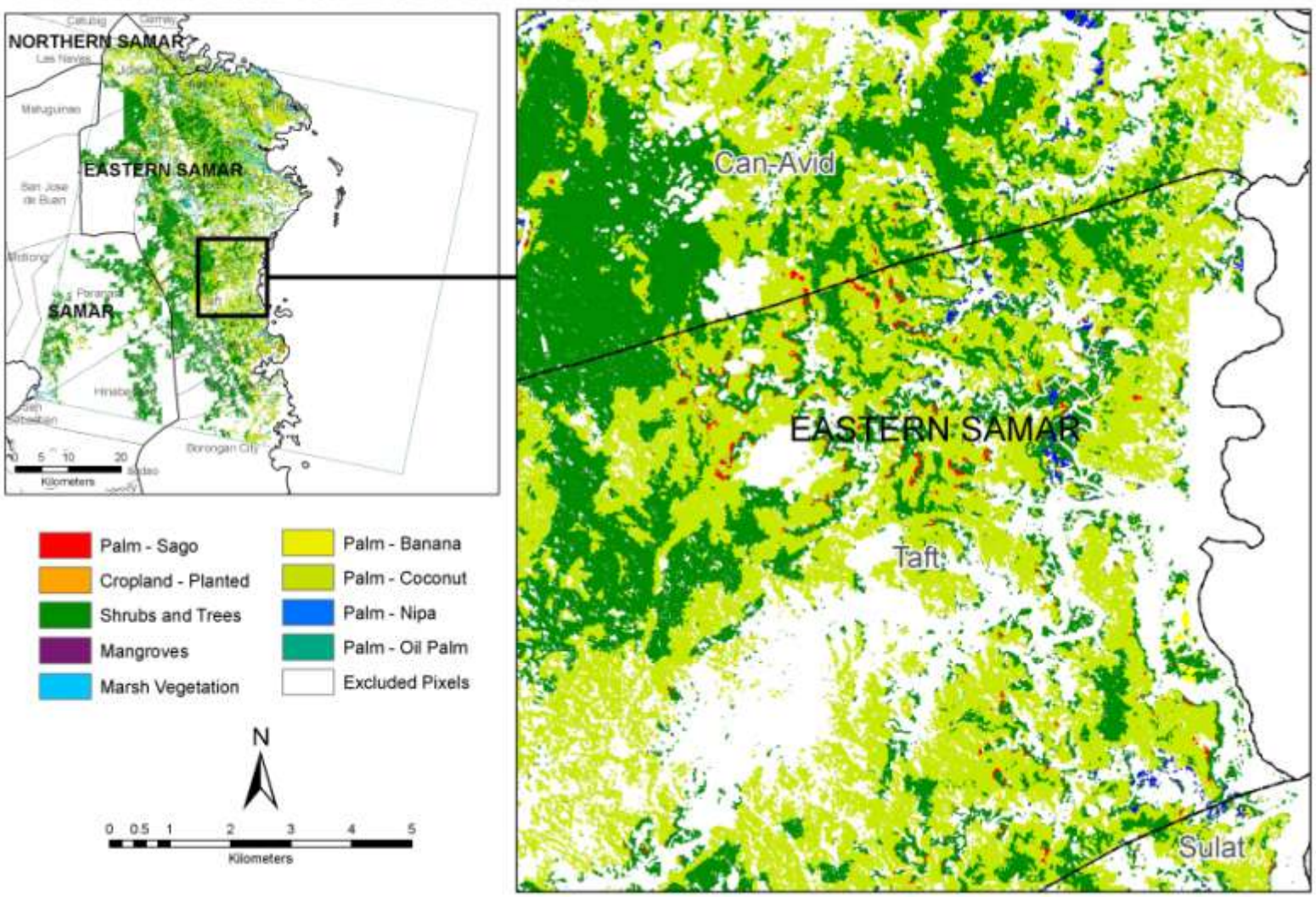

Figure 68. Classification result for image with scene id = O36.

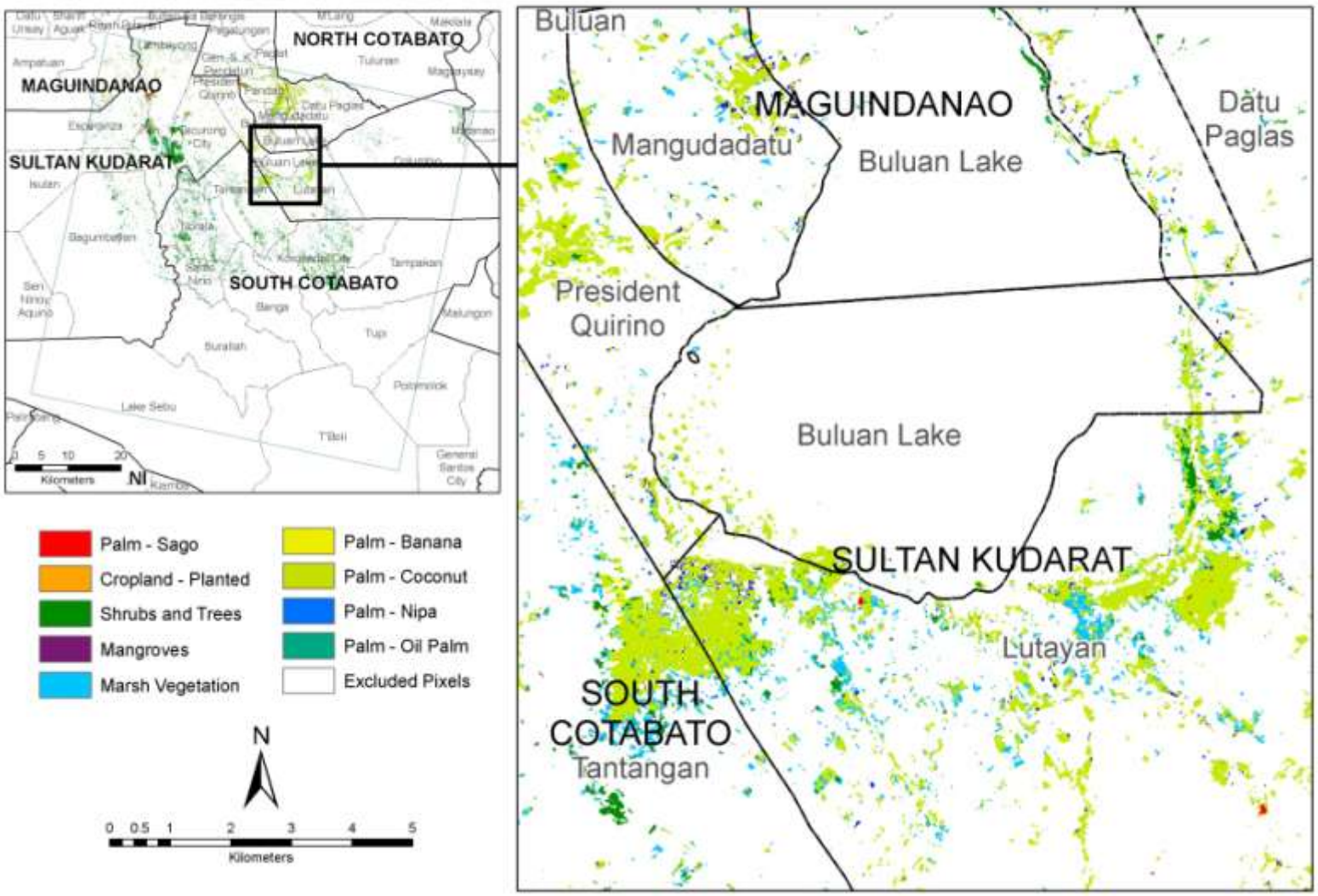

Figure 69. Classification result for image with scene id = P47.

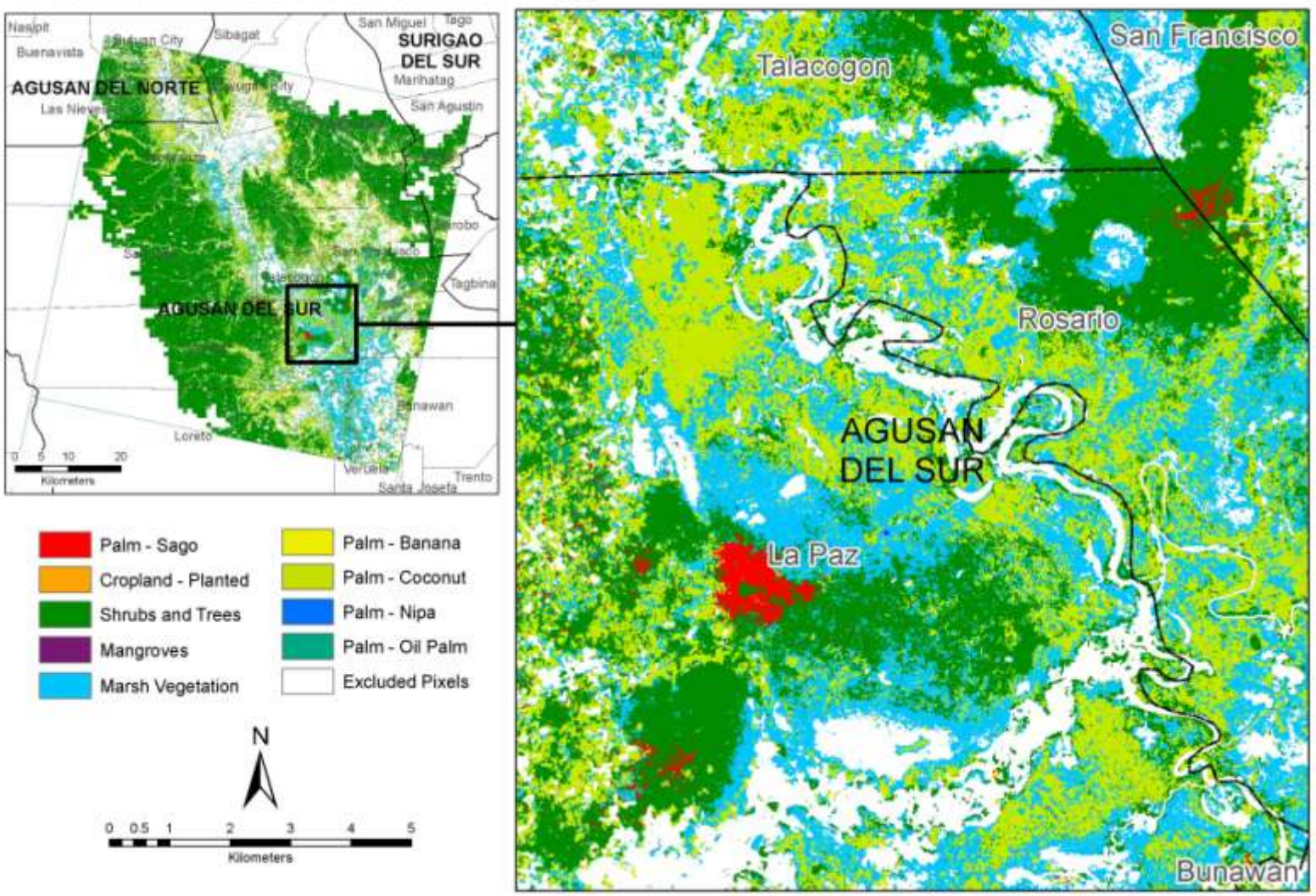

Figure 70. Classification result for image with scene id = Q43.

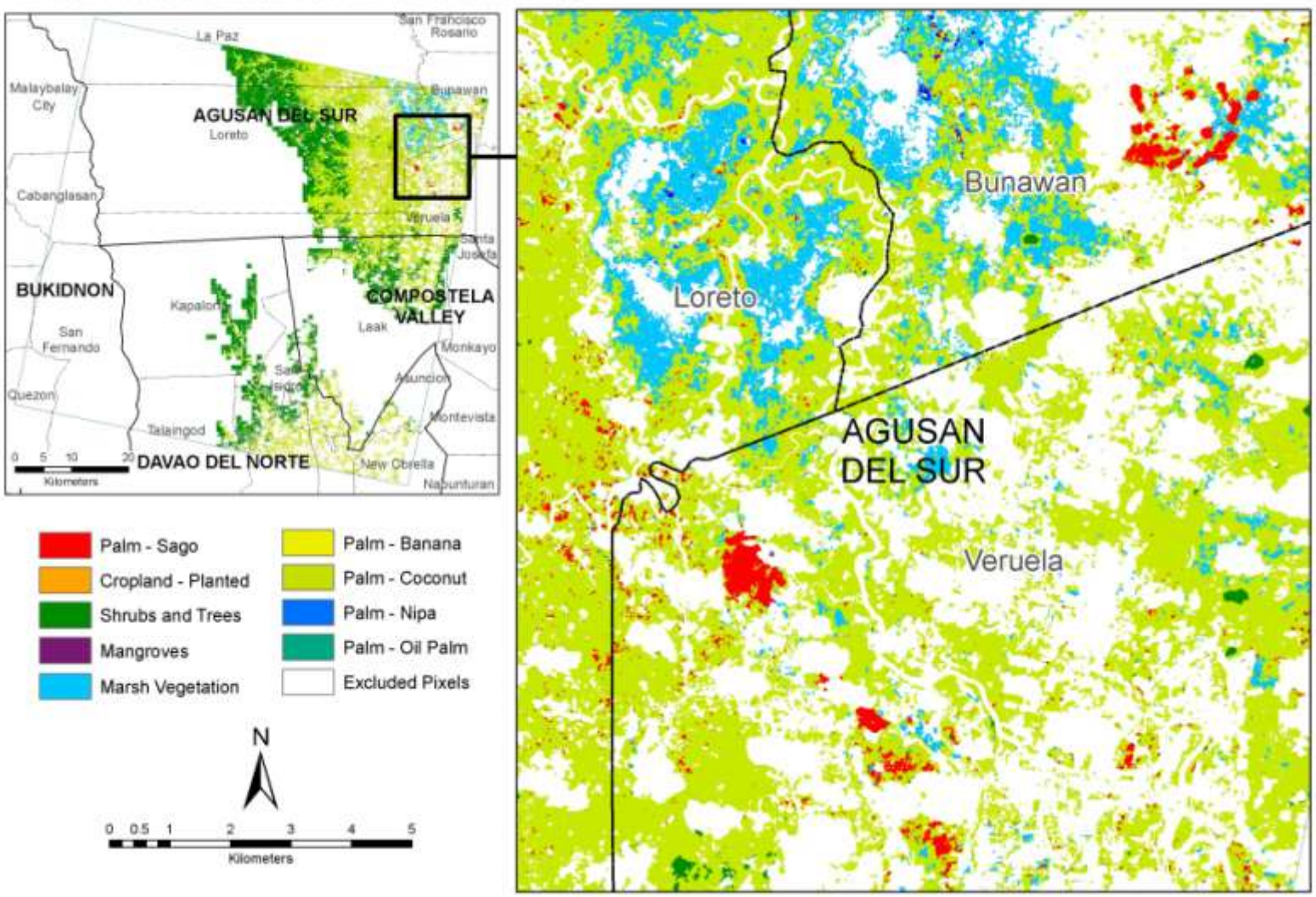

Figure 71. Classification result for image with scene id = Q44.

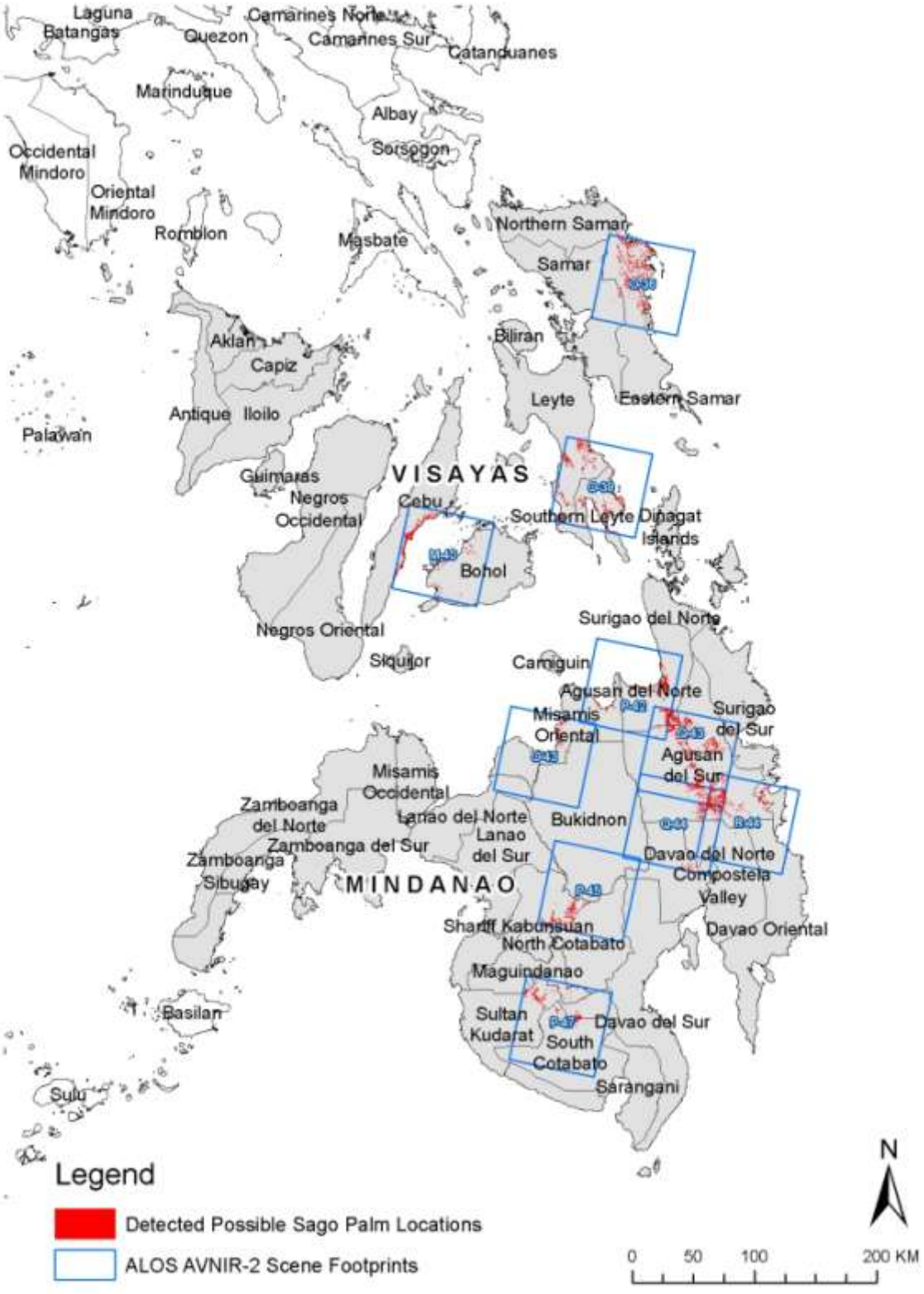

Figure 72. Possible Sago palm locations detected through Maximum Likelihood classification of ALOS AVNIR-2 images combined with ASTER GDEM and Envisat ASAR (in some scenes).

10.4 Mapped Possible Sago Palm Location in Visayas and Mindanao Based on Medium Resolution Optical and Radar images

The locations of the Sago palms detected using the ALOS AVNIR images were used to replace those detected from the Landsat images. The updated map of detected Sago palm location in Visayas and Mindanao is shown in Figure 73. The updated statistics of detected locations per province are show in Table 25 and Table 26.

Table 25. Updated number of hectares per province in Visayas that have been determined to possibly contain Sago palms.

Rank	Province	Hectares
1	Leyte	1,174
2	Eastern Samar	477
3	Southern Leyte	272
4	Cebu	228
5	Samar	221
6	Aklan	199
7	Northern Samar	137
8	Bohol	47
9	Capiz	35
10	Negros Oriental	30
11	Antique	11
12	Iloilo	9
13	Siquijor	7
14	Negros Occidental	5
15	Biliran	3
Total		2,855

Table 26. Updated number of hectares per province in Mindanao that have been determined to possibly contain Sago palms.

Rank	Province	Hectares
1	Agusan del Sur	7,986
2	Sultan Kudarat	720
3	North Cotabato	664
4	Agusan del Norte	605
5	Maguindanao (incl. Shariff Kabunsuan)	394
6	Surigao del Sur	333
7	Surigao del Norte	238
8	Misamis Oriental	224
9	Davao Oriental	130
10	Davao del Sur	111
11	South Cotabato	67
12	Davao del Norte	65
13	Compostela Valley	38
14	Dinagat Islands	16
15	Bukidnon	15
16	Camiguin	5
17	Zamboanga del Sur	4
18	Zamboanga del Norte	4
19	Lanao del Norte	2
20	Zamboanga Sibugay	2
21	Sarangani	1
Total		11,624

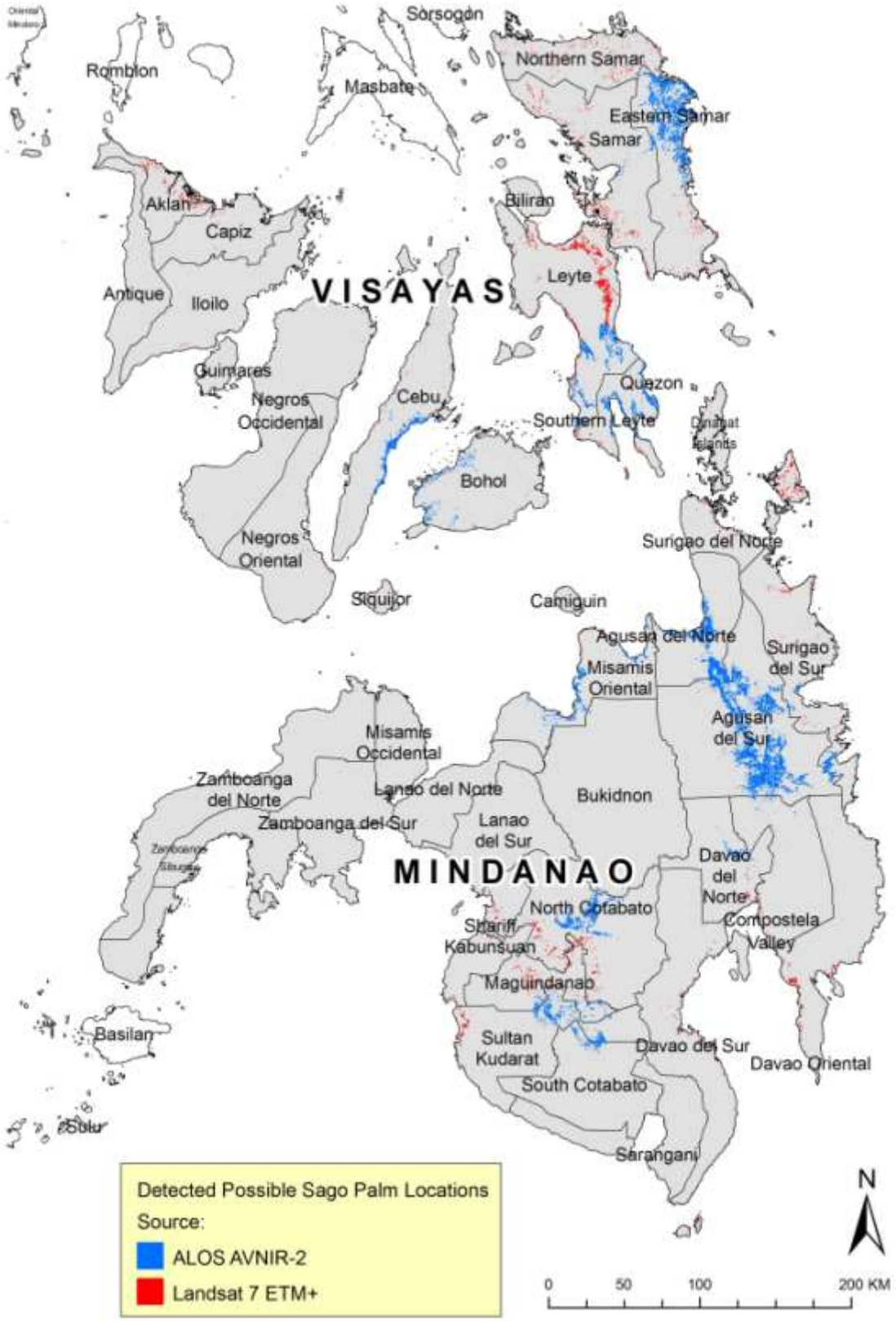

Figure 73. Updated map of detected possible locations of Sago palms.

Chapter 11. Confirmation and Refinements of Detected Sago Palm Locations through Field Surveys and High Resolution Optical Satellite Image Analysis

11.1 Overview

The detected possible locations of Sago palms in Visayas and Mindanao were examined with the aid of data from field surveys, and recent high resolution Worldview-2 images (purchased and those available in Google Earth) for their confirmation if they are indeed Sago palms or just results of misclassifications. Refinements in the extents of Sago palm stands were done during this stage.

In some provinces, confirmation and refinements of the detected locations were done through combined actual field visits and use of high resolution images (e.g., in some municipalities of Antique, Aklan, Agusan del Norte, Agusan del Sur, Misamis Oriental, Cebu and Leyte). The coordinates of the verified locations of Sago palm stands were overlaid on the high resolution images and manual digitizing aided by image interpretation keys was done to refine the Sago palm polygons.

In other provinces, confirmation and refinements were done through field surveys only. In confirmed locations, perimeter surveys using a mapping grade, hand-held GPS was used to obtain the extent of the verified Sago palm stands. These were done in the provinces of Bohol, Surigao del Norte, Surigao del Sur, Bukidnon, Davao Oriental, Compostela Valley, Davao del Norte and Davao del Sur.

In Visayas, confirmation surveys were not conducted in Capiz, Iloilo, Negros Occidental, Negros Oriental, western part of Leyte, Southern Leyte, and all Samar provinces. In Mindanao, due to security related concerns, surveys were not conducted in Zamboanga provinces, Misamis Occidental, Lanao del Norte, Lanao del Sur, North and South Cotabato, Maguindanao (incl. Shariff Kabunsuan), Sultan Kudarat, and Sarangani. Most of the confirmation and refinements of detected Sago palm locations in these provinces relied on visual interpretation of high resolution satellite images available in Google Earth.

11.2 Perimeter survey of Sago palm stands

In confirmed locations, a Garmin Oregon 550 handheld GPS receiver was used to collect points delineating the exterior boundary of a Sago palm stand. At each point, the GPS was set to get the average UTM 51 WGS 1984 coordinates with 1-2 minutes observation time. The positional accuracy displayed in the GPS receiver ranges from 3-5 meters during the observation period. The coordinates were downloaded from the GPS and processed in GIS software to create polygons of the Sago palm stand.

Perimeter surveys were conducted in Aklan, Cebu, Bohol, Leyte, Agusan del Norte, Agusan del Sur, Misamis Oriental, Surigao del Norte, Surigao del Sur, Bukidnon, Davao Oriental, Compostela Valley, Davao del Norte and Davao del Sur. The results of the perimeter surveys (polygons of Sago stands) were used in tandem with high resolution images to confirm and refine detected possible locations of Sago palm stands. In areas where images were not available (as mentioned earlier), the perimeter survey results were used as the final polygons of confirmed Sago palm stands.

Figure 74. Using the Garmin Oregon 550 GPS to get the perimeter of a Sago palm stand.

11.3 Visual Interpretation and Analysis of Worldview-2 Images

11.3.1 Images used

High resolution Worldview-2 images were purchased covering potential Sago locations in Cebu (Alegria, Argao), Agusan del Norte (portion of Butuan City, Magallanes), Agusan del Sur (portions of Bunawan, Prosperidad, La Paz, San Francisco and Veruela), and Leyte (portions of Alangalang, Burauen, Dagami, Dulag, Jaro, Julita, La Paz, Mayorga, Sta. Fe, and Tabontabon). The date of acquisitions of these images are listed in Table 27. Maps showing the coverage of these images, including zoomed-in views (displayed in true color RGB combination) are shown in Figure 75- Figure 87.

The images covering portions of municipalities of Cebu, Leyte (Alangalang and Sta Fe), Agusan del Norte and Agusan del Sur (Bunawan) were acquired with the full 8 multispectral bands while the remaining images were acquired in 4 bands only (visible and

NIR). Each image dataset consist of the multi-spectral bands with 2 m spatial resolution and one panchromatic (“black and white”) band with 0.5-m spatial resolution. Prior to visual interpretation and analysis, the multi-spectral and panchromatic bands of the images were subjected to radiometric calibration and orthorectification. Then, the panchromatic band was fused with the multispectral bands through Gram-Schmidt Spectral Sharpening to enhance the spatial detail of the multi-spectral bands by increasing its spatial resolution to 0.5-m.

Table 27. List of purchased Worldview-2 images including dates of field surveys.

Image ID	Covered Province	Covered Municipalities (portions)	Date of Acquisition
CEB-1	Cebu	Alegria	September 15, 2011
CEB-2	Cebu	Argao	April 29, 2011
LYT-1	Leyte	Dagami, Tabontabon	November 10, 2010
LYT-2	Leyte	Dulag, Julita, La Paza, Mayorga	November 10, 2010
LYT-3	Leyte	Burauen, Julita, La Paz	April 18, 2011
LYT-4	Leyte	Alangalang, Jaro	January 4, 2010
LYT-5	Leyte	Alangalang, Sta. Fe	January 4, 2010
LYT-6	Leyte	Alangalang, Jaro	February 11, 2010
ADN-1	Agusan del Norte	Butuan City, Magallanes	April 10, 2011
ADS-1	Agusan del Sur	Prosperidad, San Francisco	March 29, 2012
ADS-2	Agusan del Sur	La Paz	September 10, 2011
ADS-4	Agusan del Sur	Bunawan, Veruela	March 29, 2012
ADS-4	Agusan del Sur	Veruela	March 29, 2012

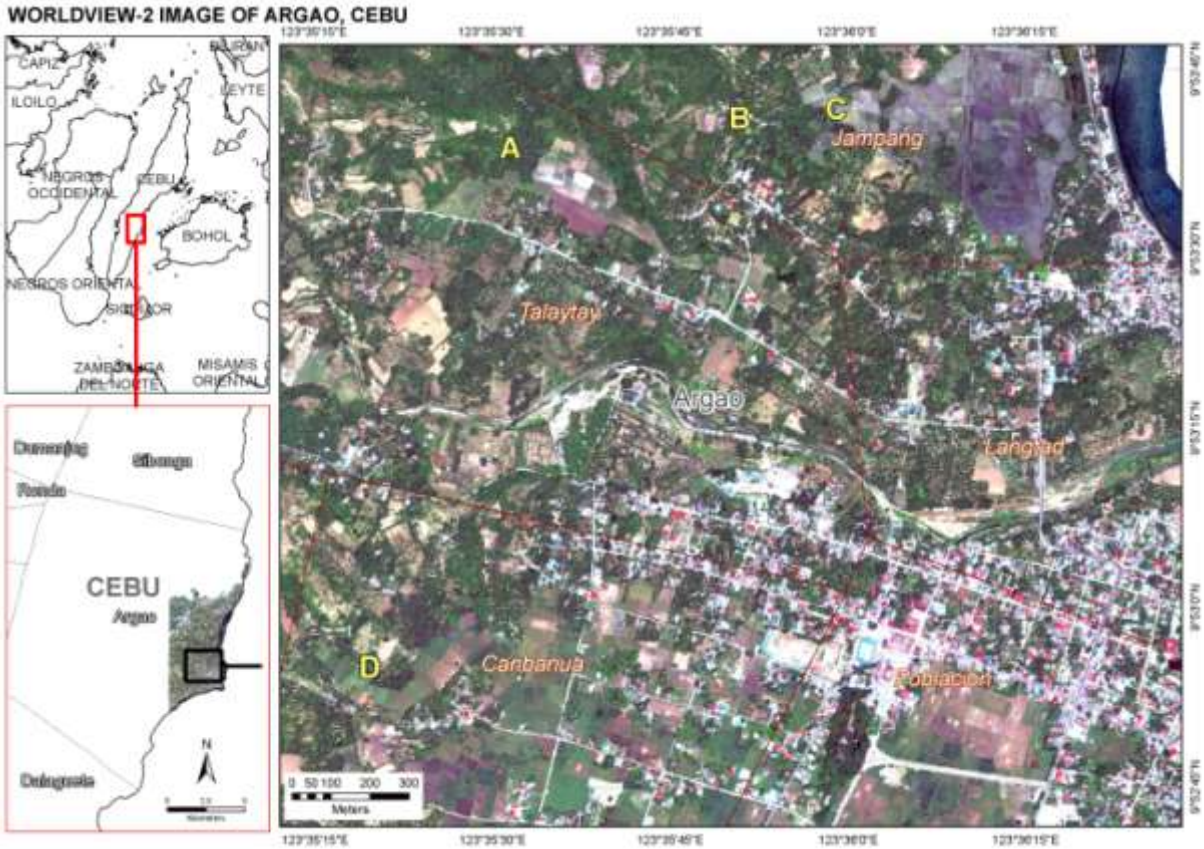

Figure 75. A zoomed-in view of the 0.5-m resolution Worldview-2 image of a portion of Argao, Cebu. Letters A, B, C and D are some of the verified locations of Sago palm stands (see Figure 76 for their pictures).

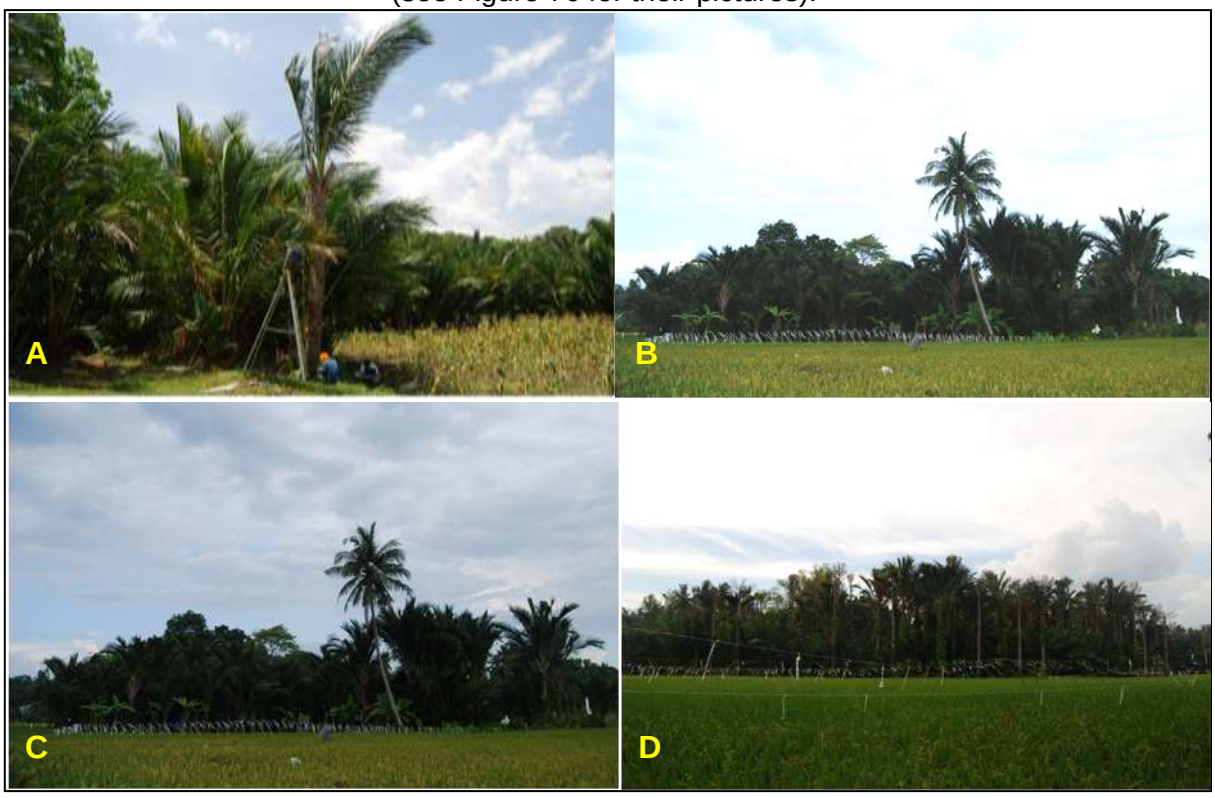

Figure 76. Pictures of Sago palms stands in Argao, Cebu with their locations indicated in Figure 75.

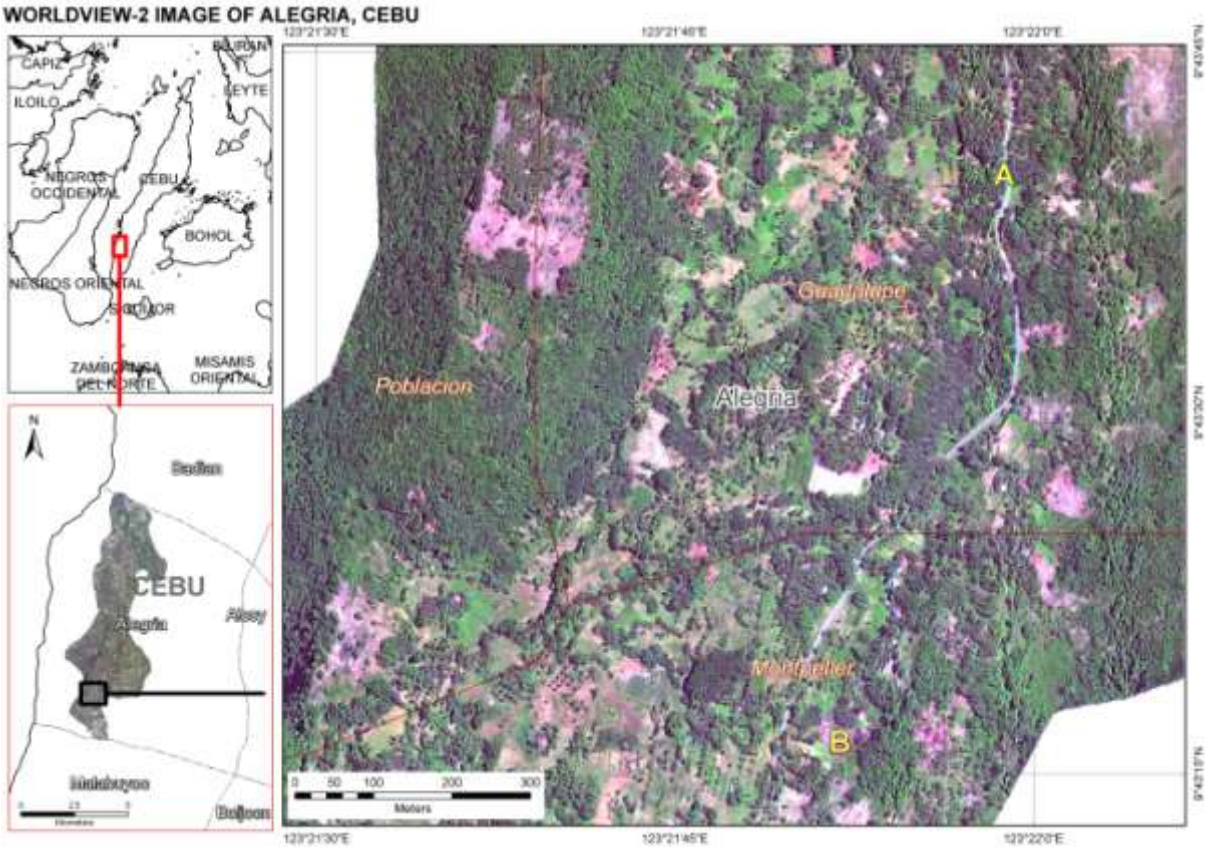

Figure 77. A zoomed-in view of the 0.5-m resolution Worldview-2 image of a portion of Alegria, Cebu. Letters A and B are some of the verified locations of Sago palm stands (see Figure 78 for their pictures).

Figure 78. Pictures of Sago palms stands in Alegria, Cebu with their locations indicated in Figure 77.

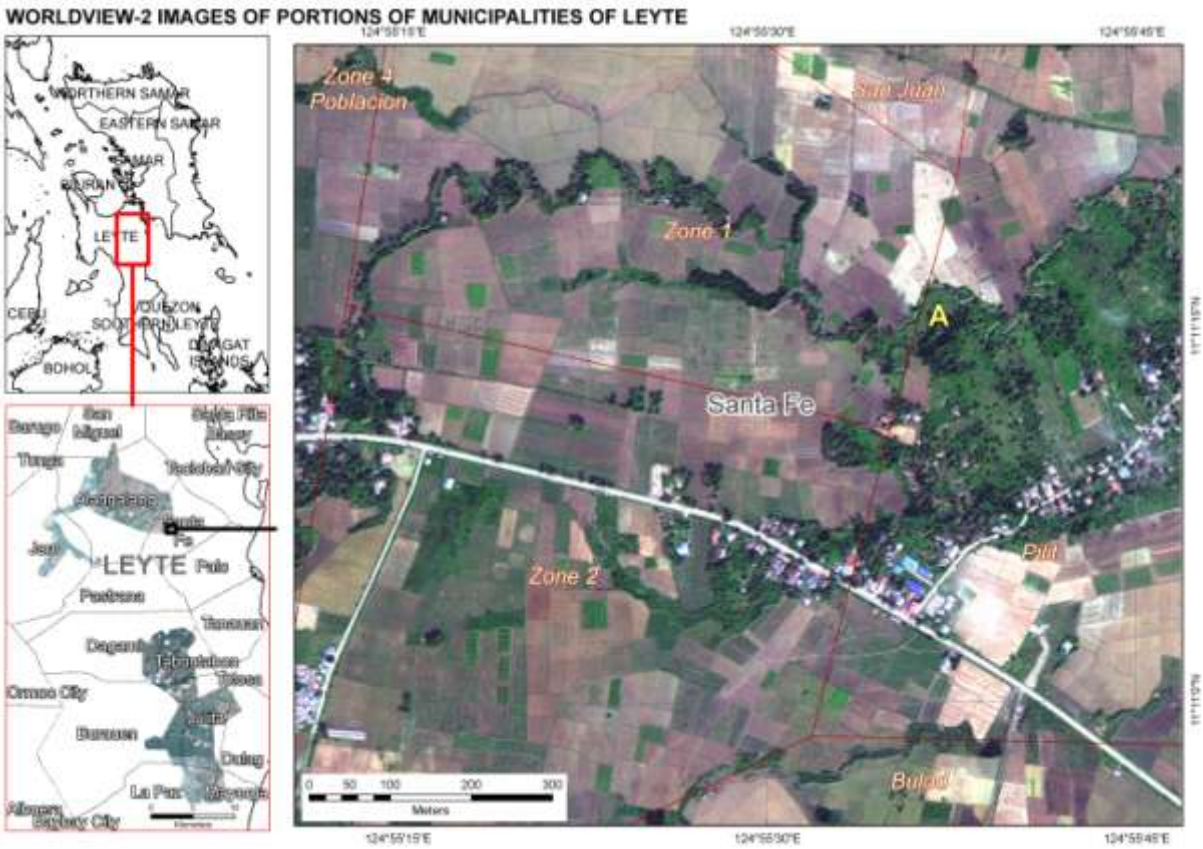

Figure 79. A zoomed-in view of the 0.5-m resolution Worldview-2 image of a portion of Sta. Fe, Leyte. Letter A is just one of the verified locations of Sago palms in this municipality (see Figure 80 for its picture).

Figure 80. Picture of a Sago palm stand in Sta. Fe, Leyte with its location indicated in Figure 79.

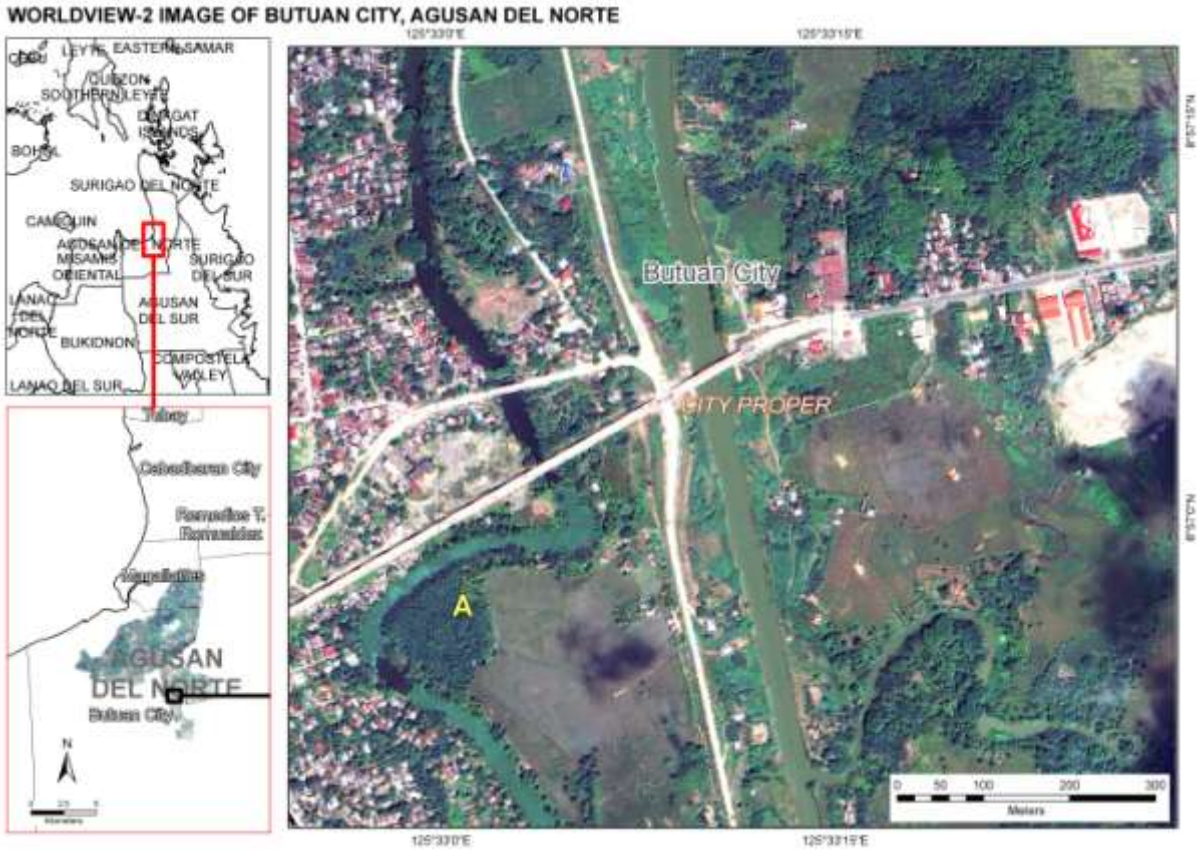

Figure 81. A zoomed-in view of the 0.5-m resolution Worldview-2 image of a portion of Butuan City, Agusan del Norte. Letter A is just one of the verified locations of Sago palms in this municipality (see Figure 81 for its picture).

Figure 82. Picture of a Sago palm stand in Butuan City, Agusan del Norte with its location indicated in Figure 81.

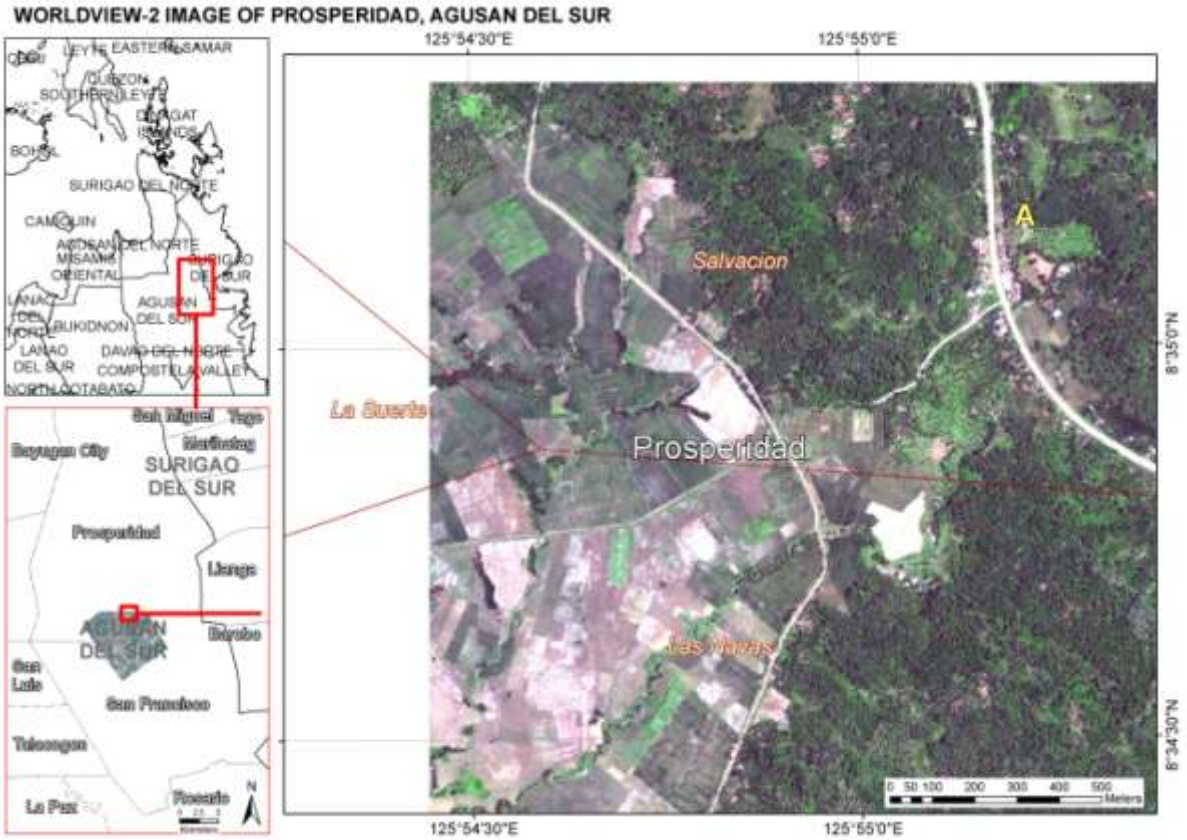

Figure 83. A zoomed-in view of the 0.5-m resolution Worldview-2 image of a portion of Prosperidad, Agusan del Sur. Letter A is just one of the verified locations of Sago palms in this municipality (see Figure 84 for its picture).

Figure 84. Picture of a Sago palm stand in Prosperidad, Agusan del Sur with its location indicated in Figure 83.

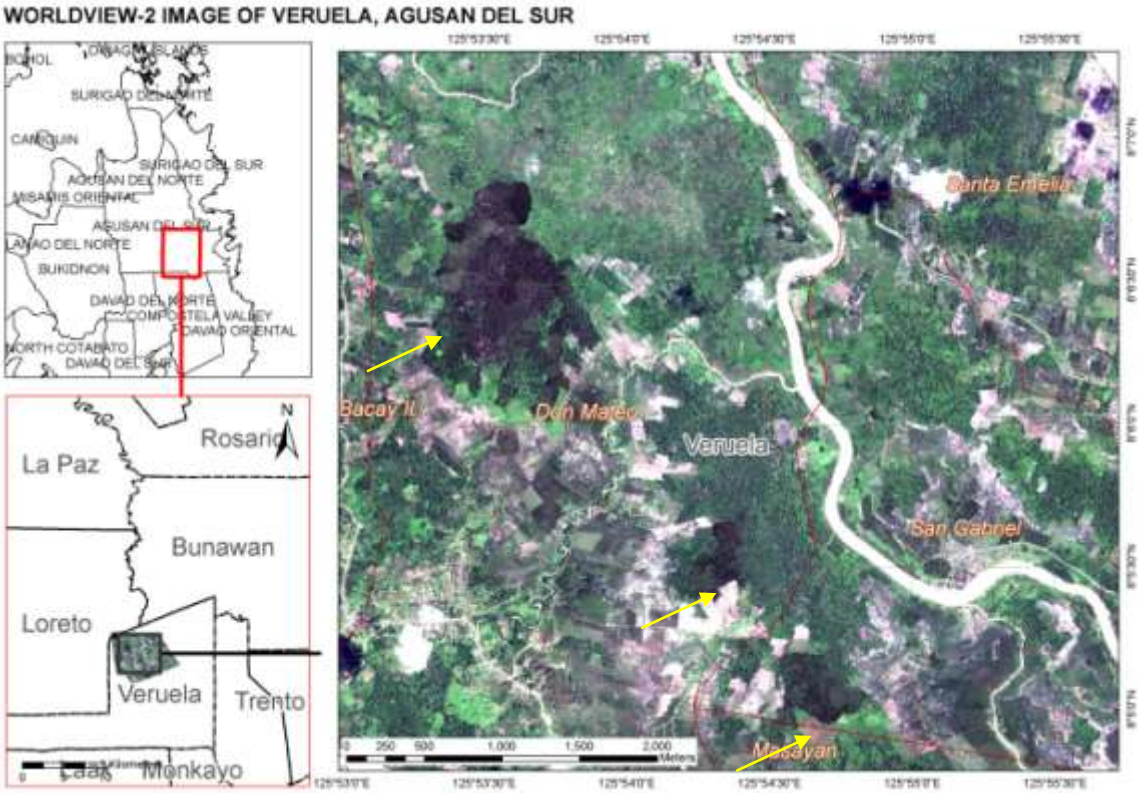

Figure 85. A zoomed-in view of the 0.5-m resolution Worldview-2 image of a portion of Veruela, Agusan del Sur.The dark-colored vegetations indicated by yellow arrows are Sago palms stands.

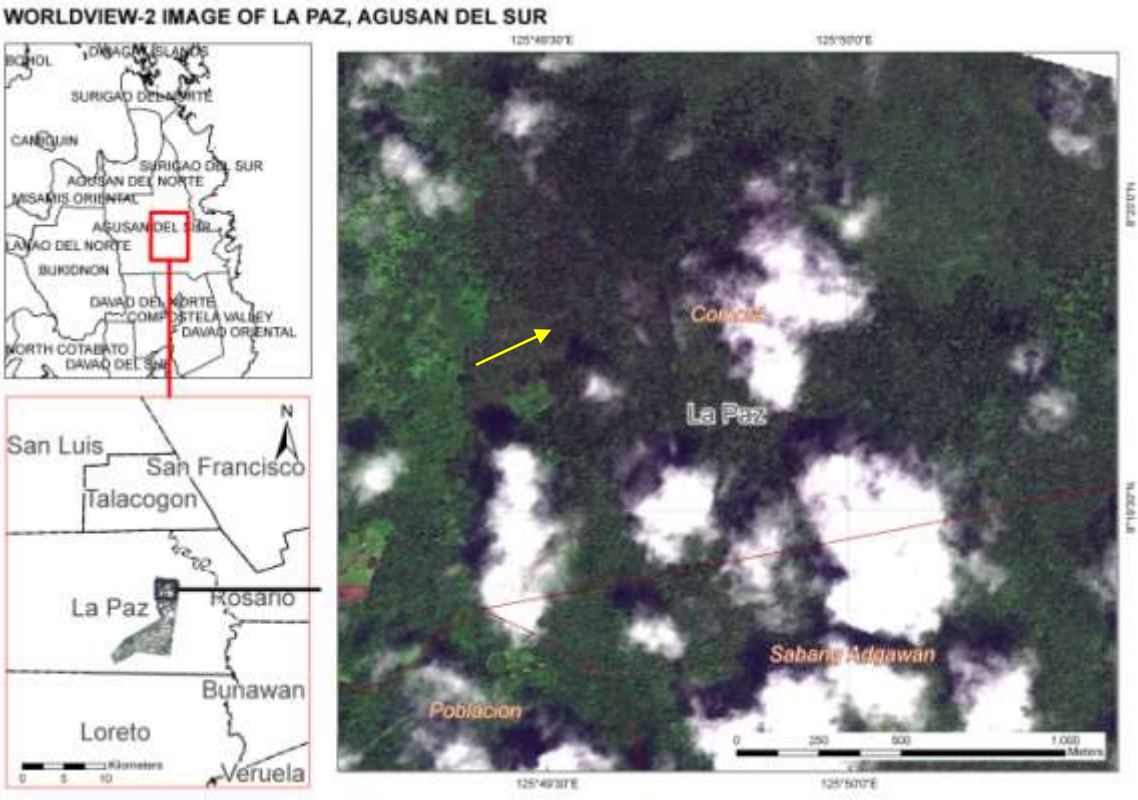

Figure 86. A zoomed-in view of the Worldview-2 image of a portion of La Paz, Agusan del Sur.The dark-colored vegetations indicated by a yellow arrow are Sago palms stands.

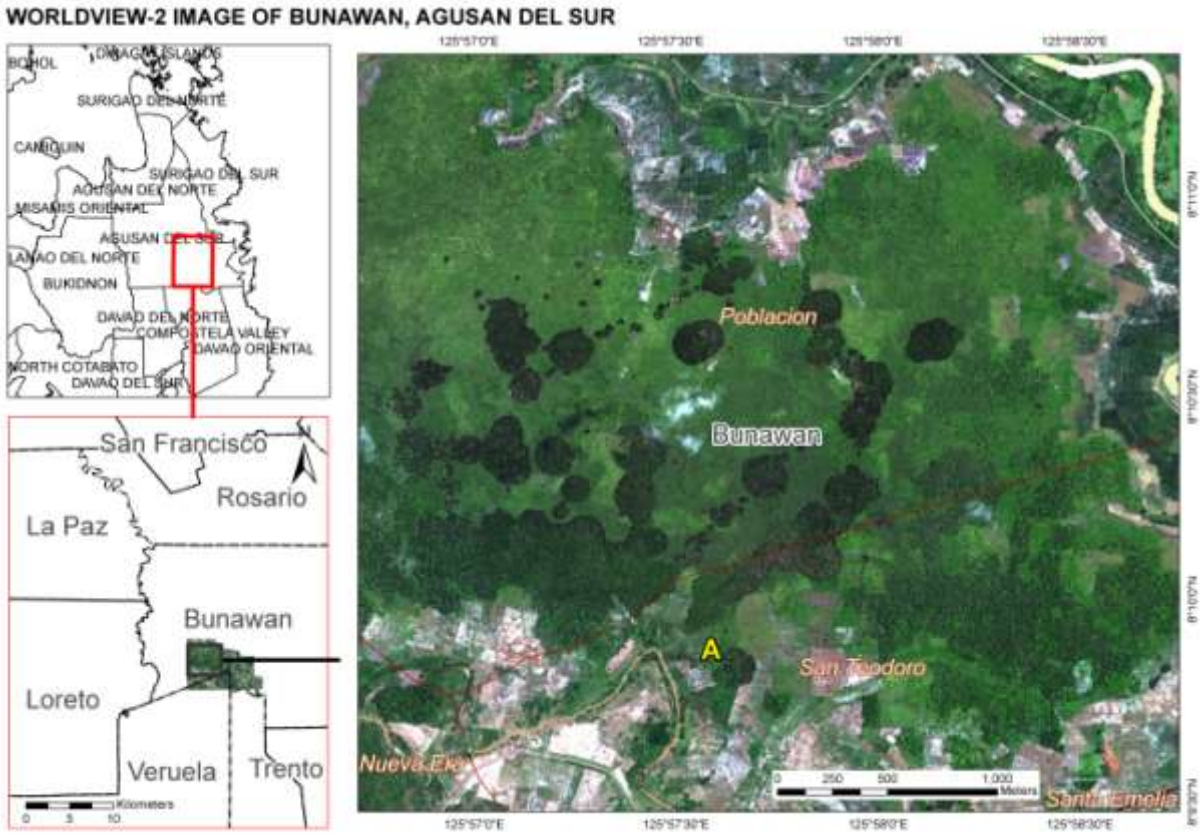

Figure 87. A zoomed-in view of the 0.5-m resolution Worldview-2 image of a portion of Bunawan, Agusan del Sur. Letter A is just one of the verified locations of Sago palms in this municipality (see Figure 88 for its picture).

Figure 88. Picture of a Sago palm stand in Butuan City, Agusan del Norte with its location indicated in Figure 87.

11.3.2 Image Interpretation Keys

In order to confirm and refine using the Worldview-2 images all those locations detected as Sago palms, it was necessary to create interpretation keys that can be used to analyze the images. The development of the interpretation keys was done by finding in the images the location of confirmed locations of Sago palms and other land-cover types. The keys consisted of imagettes indicating appearance of Sago palms and other vegetation types in different combinations of the Worldview-2 images. Combinations containing Bands 1, 6, 7 and 8 were specifically made as it was revealed during the in-situ reflectance analysis (Chapter 5) that large differences in reflectance values between different palms exist in these bands.

Shown in Figure 89 is the Worldview-2 image of Bunawan, Agusan del Sur wherein various land-cover classes are labeled using ground truth information collected during the field surveys. Imagettes in various band combinations were extracted from this image, as well as from that of Butuan City, Agusan del Norte, to serve as interpretation keys and shown in Table 28.

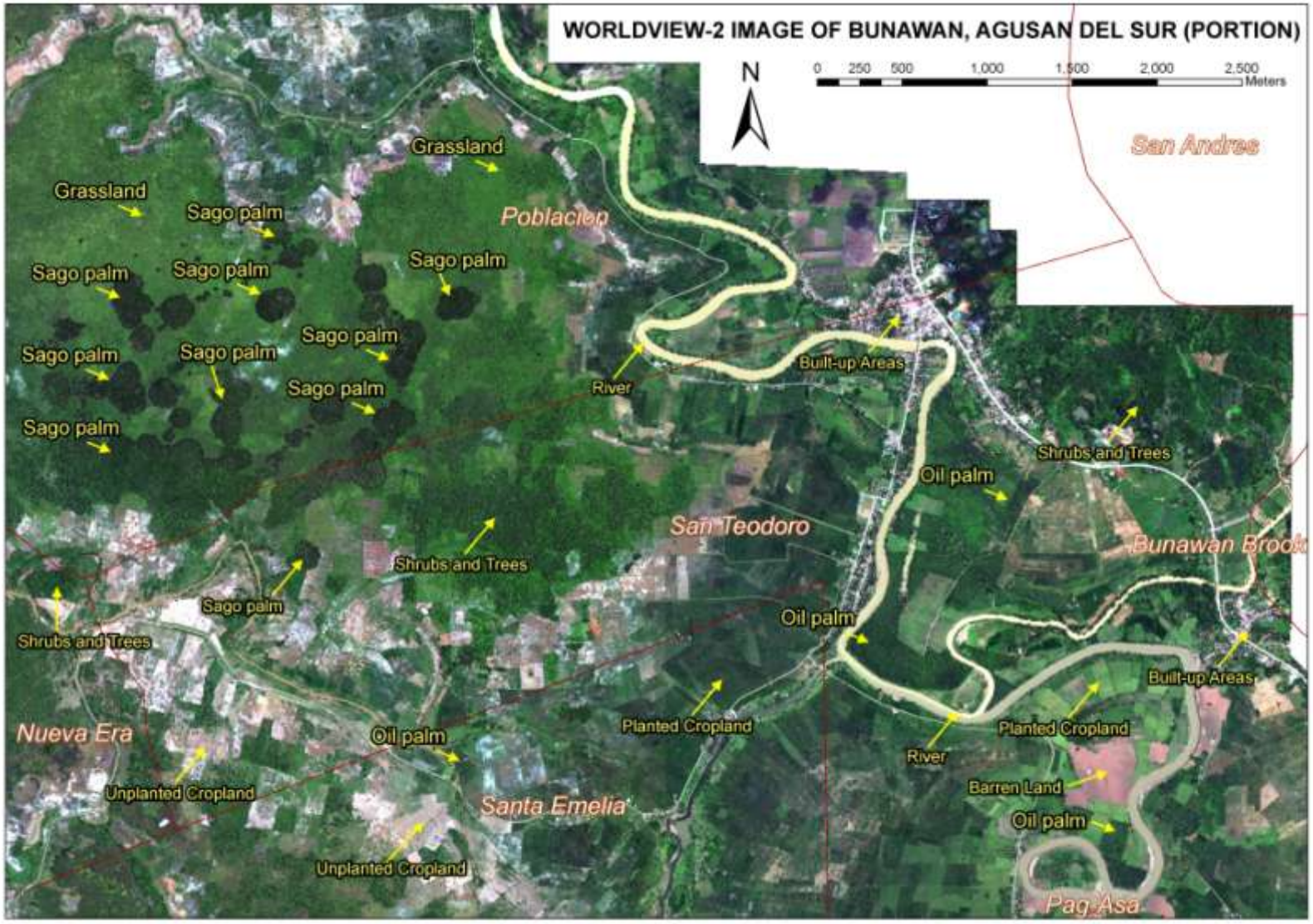

Figure 89. Worldview-2 image (displayed in true color RGB) of Bunawan, Agusan del Sur shown with labels of various land-cover types.

Table 28. Worldview-2 image interpretation keys.

Land-cover	Appearance in Different Band Combinations							
	5-3-2 (True Color	1-6-8	1-7-6	3-5-4	6-3-2	7-4-3	8-6-1	8-7-6
Sago Palm								
Other Palm – Banana								
Other Palm – Coconut	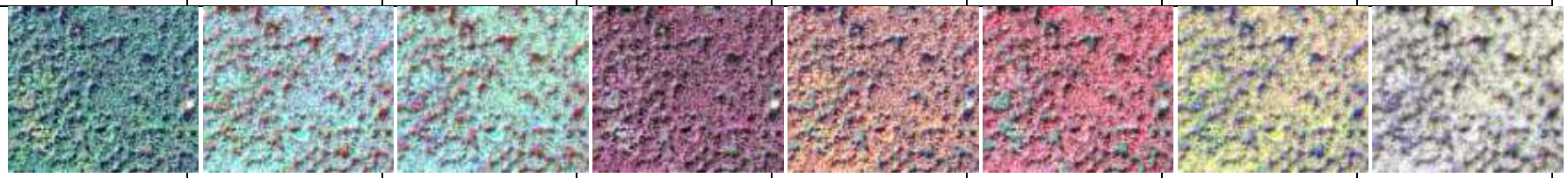							
Other Palm – Nipa								

Other Palm – Oil Palm		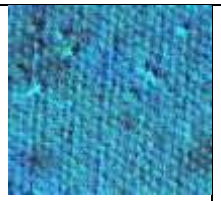	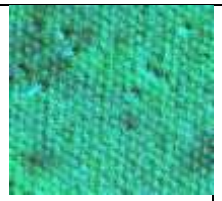		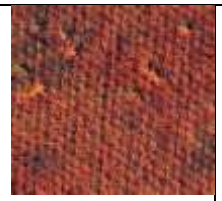		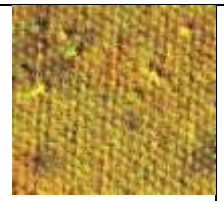	
Cropland, Planted		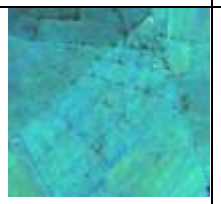	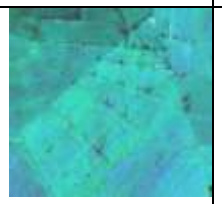				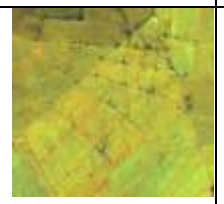	
Crop-land, Un-planted		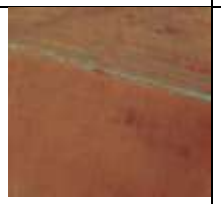		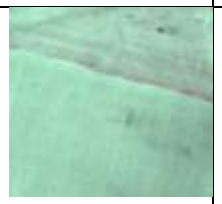		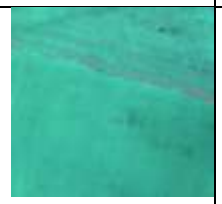		
Grass-land			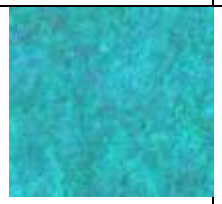					
Shrubs and Trees		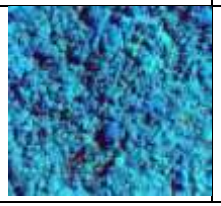	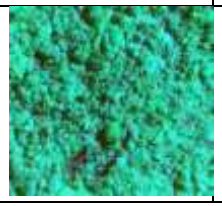	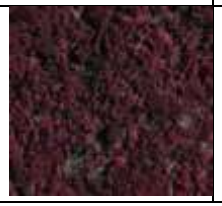				

11.3.3 Confirmation and Refinement of Detected Sago Palm Locations using Worldview-2 Images

The detected possible Sago palms locations were overlaid in the images and were checked if they are actual Sago palm stands or not using the interpretation keys (and in some provinces, ground truth information). Aside from the differences in color, Sago palms were also identified based on their shape, texture, tone, pattern and context. It can be seen from the interpretation keys that Sago palms are different from Oil palm and coconut as the latter have defined patterns due to their nature of being planted. In terms of context, Sago palms are usually located in swampy areas (with stagnant water) and near sources of water (e.g., rivers, irrigation canals).

If a detected Sago palm location is confirmed, the polygons were refined through digitizing. Example confirmations and refinements are shown in Figure 90-Figure 95.

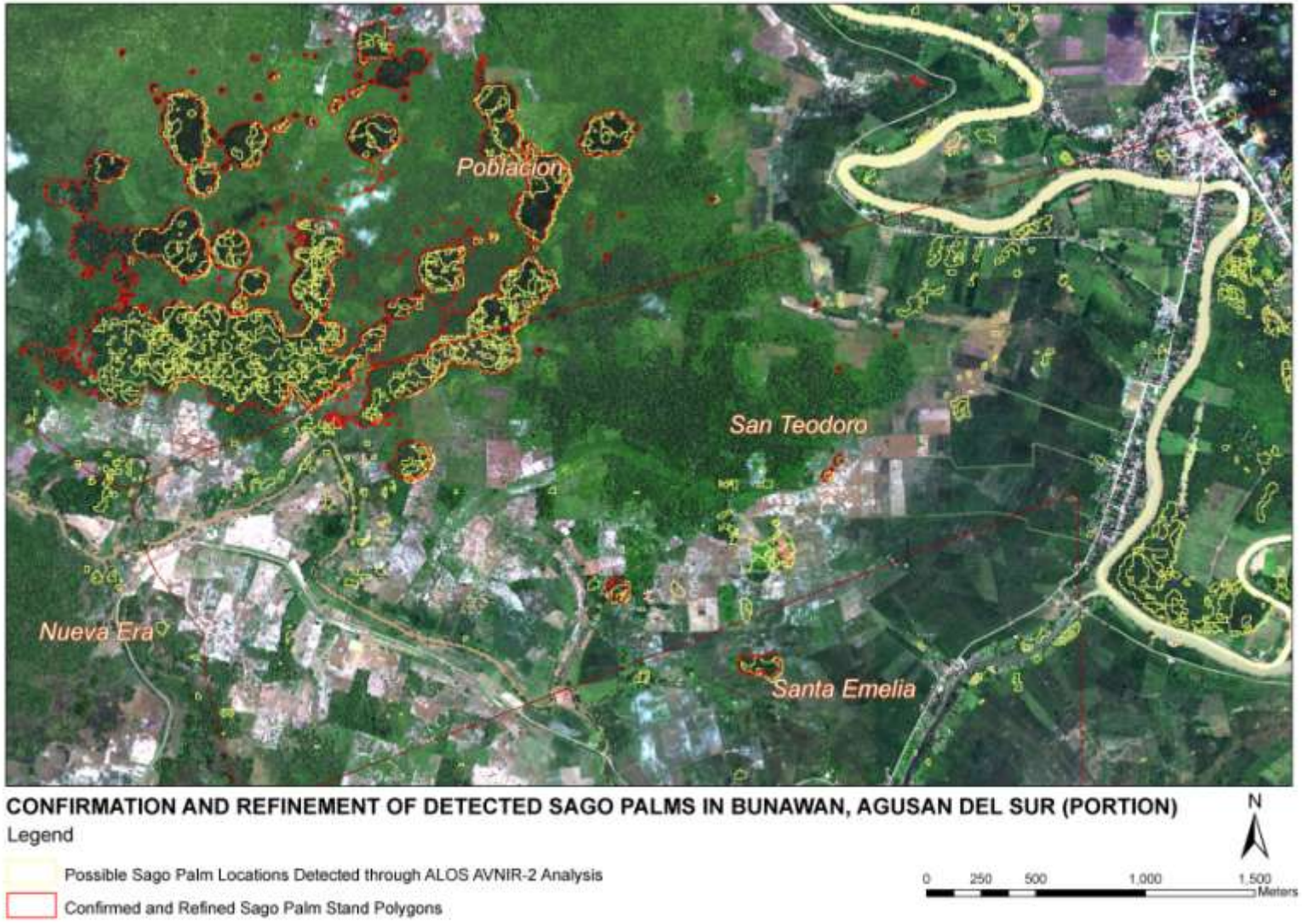

Figure 90. Example result of confirmation and refinement of detected possible Sago palm locations in Bunawan, Agusan del Sur through the use of Worldview-2 images.

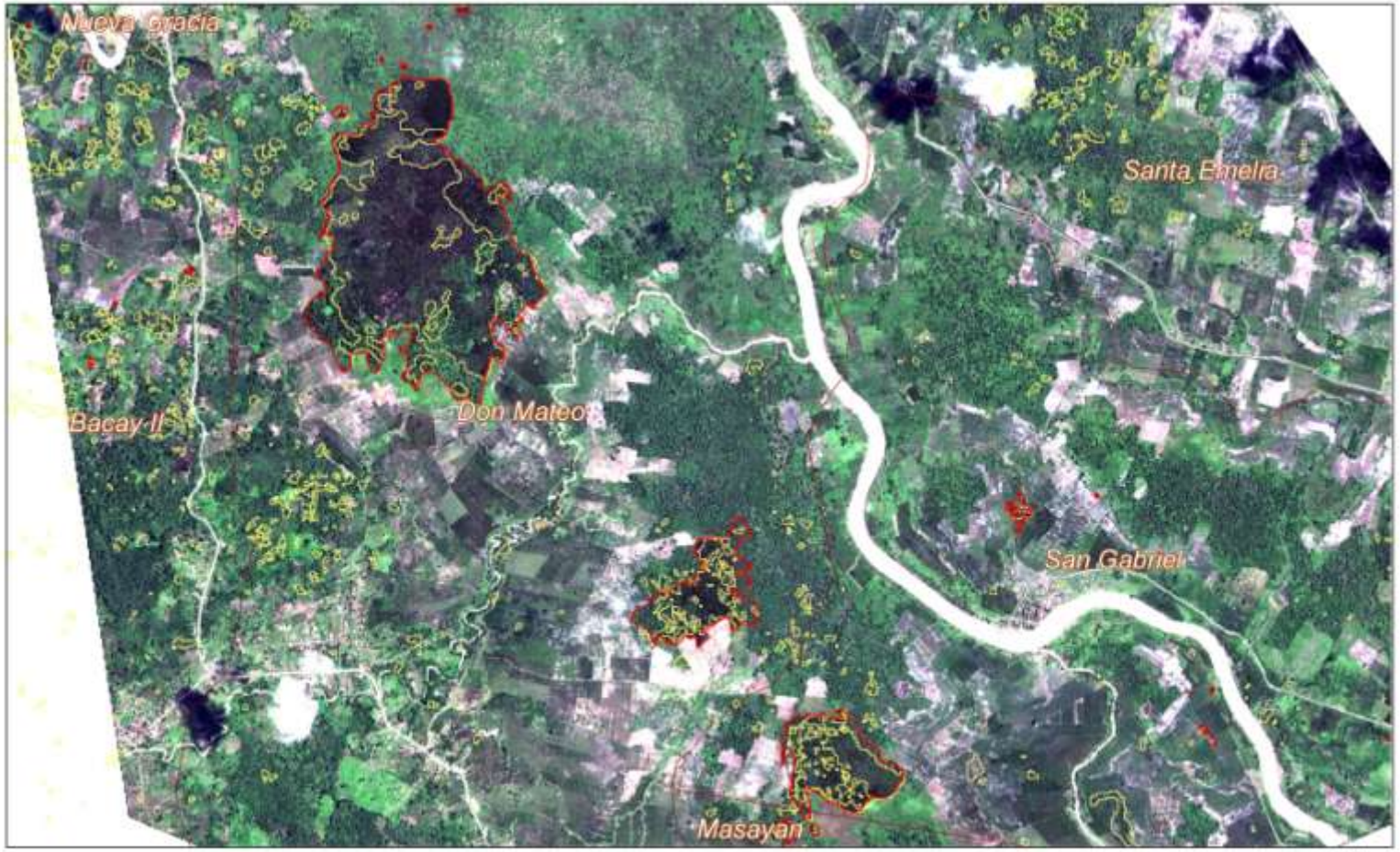

Figure 91. Example result of confirmation and refinement of detected possible Sago palm locations in Veruela, Agusan del Sur through the use of Worldview-2 images.

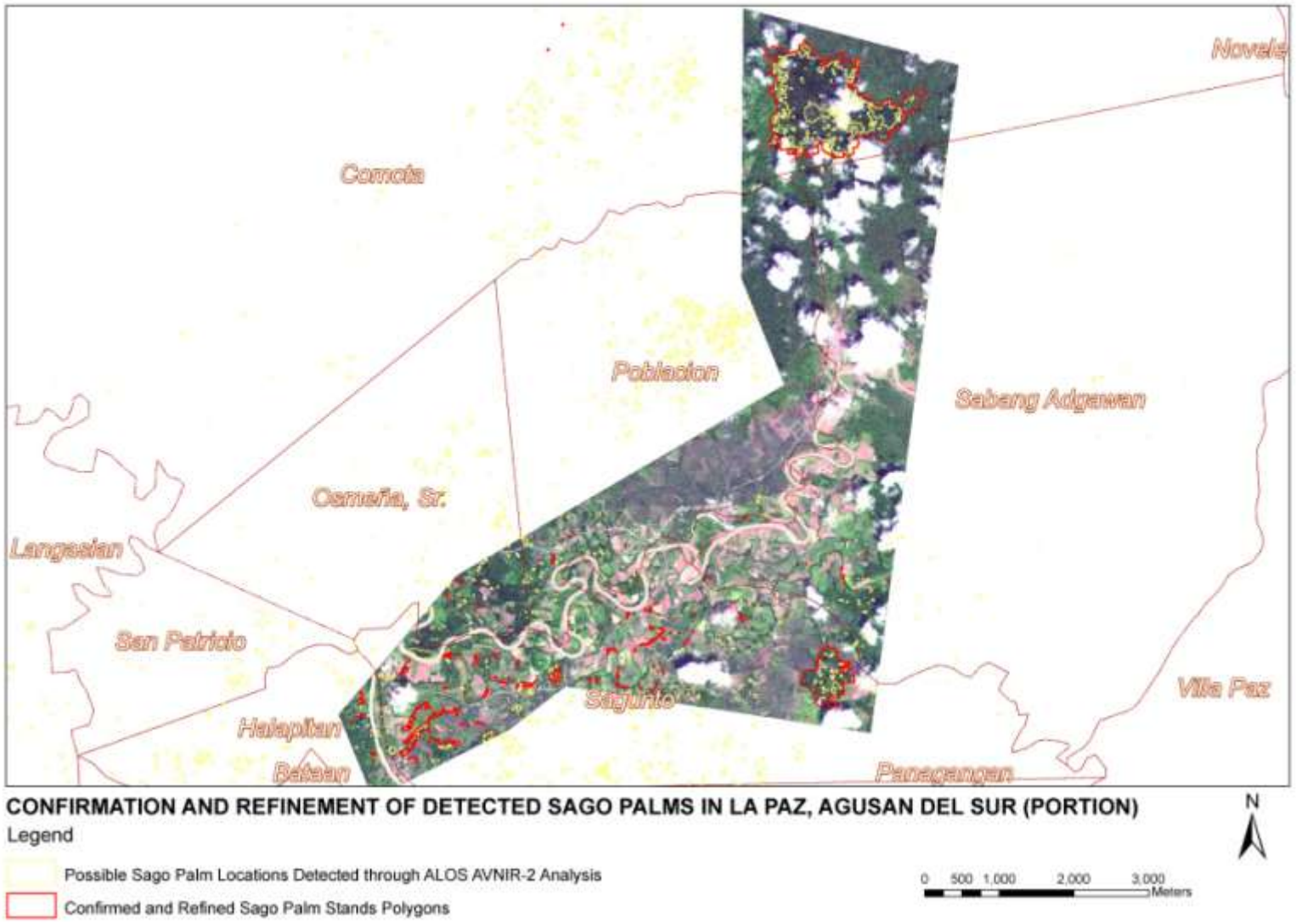

Figure 92. Example result of confirmation and refinement of detected possible Sago palm locations in La Paz, Agusan del Sur through the use of Worldview-2 images.

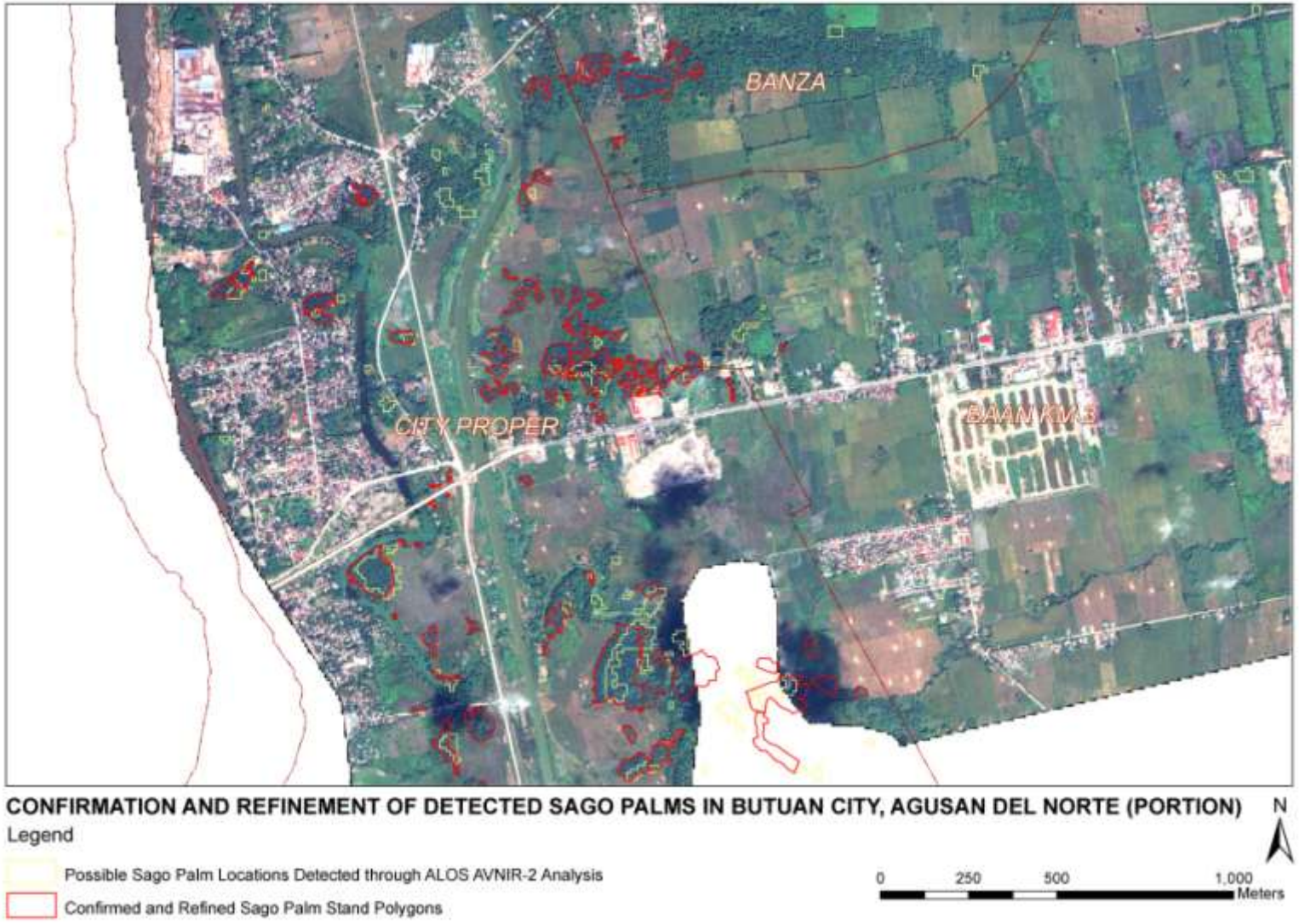

Figure 93. Example result of confirmation and refinement of detected possible Sago palm locations in Butuan City, Agusan del Norte through the use of Worldview-2 images. (Confirmed polygons without Worldview-2 images were obtained through perimeter surveys).

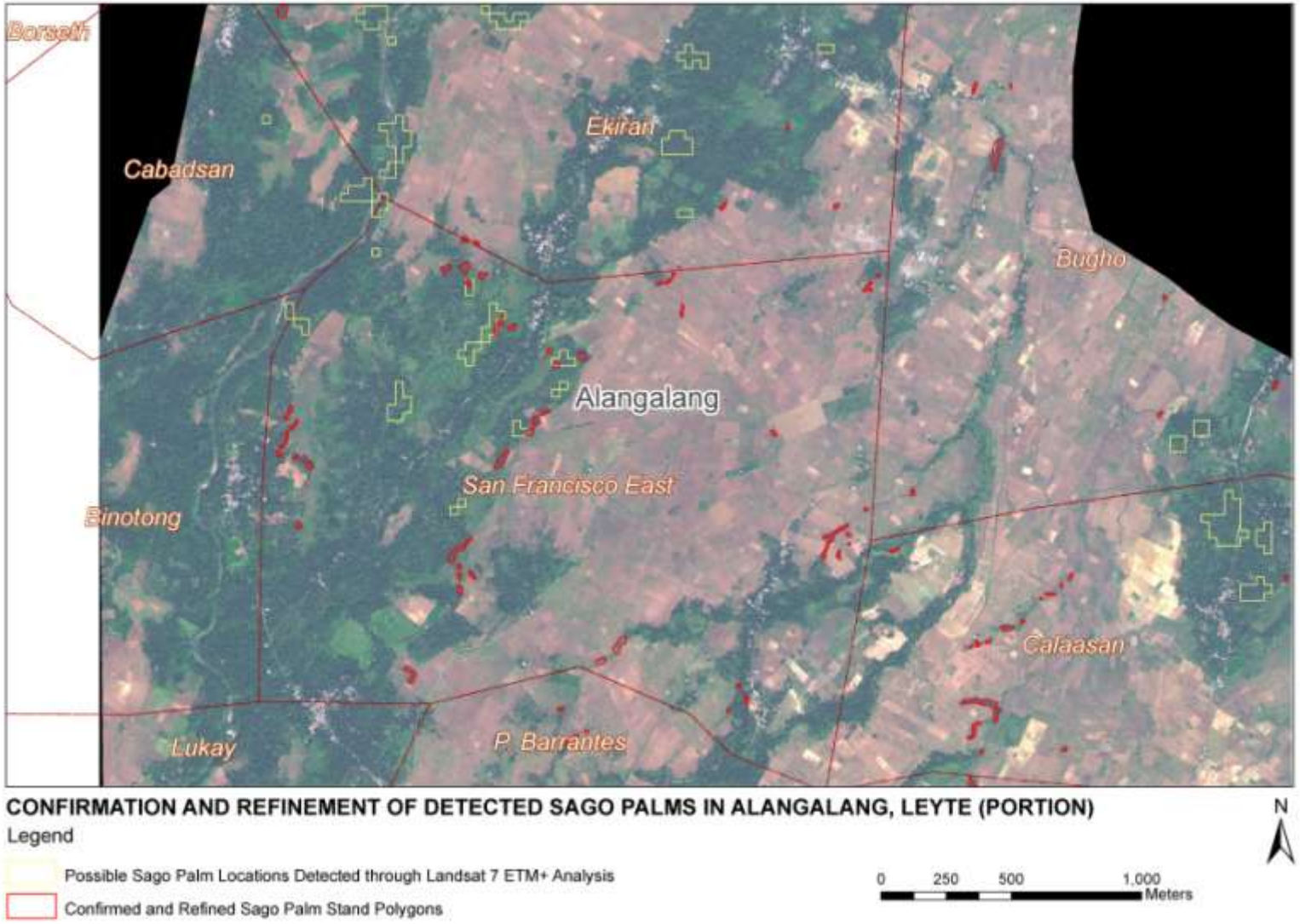

Figure 94. Example result of confirmation and refinement of detected possible Sago palm locations in Alangalang, Leyte through the use of Worldview-2 images. Note that the low spatial resolution of Landsat 7 ETM+ was not able to detect Sago palm stands which are very small in area.

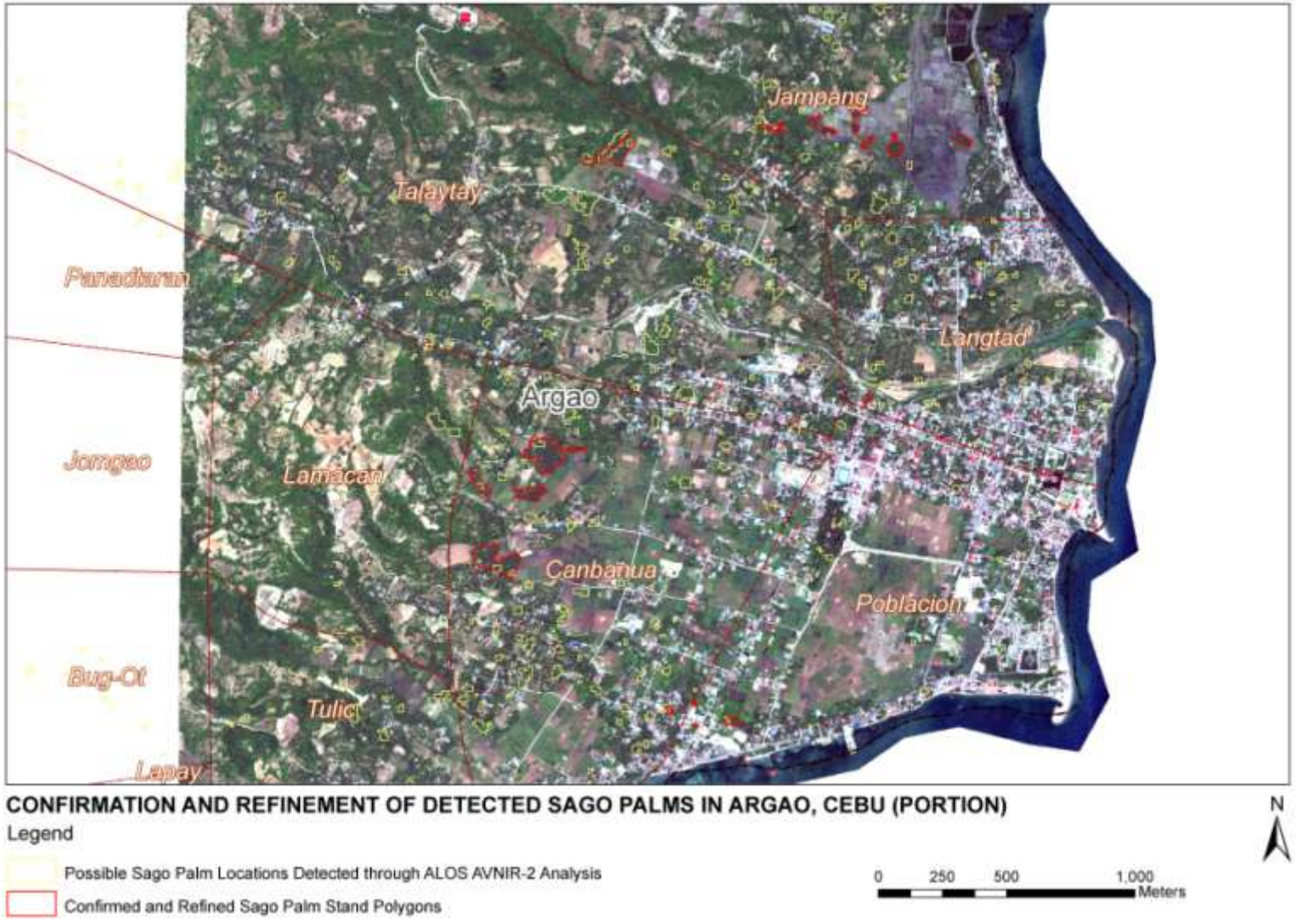

Figure 95. Example result of confirmation and refinement of detected possible Sago palm locations in Argao, Cebu through the use of Worldview-2 images.

11.3.4 Confirmation and Refinement of Detected Sago Palm Locations using High Resolution Images Displayed in Google Earth

In some municipalities, purchase of Worldview-2 images was not done due to limited budget. Fortunately, high resolution images in Google Earth are available to be used for confirmation and refinements of detected Sago palm locations. These municipalities are listed in Table 29. The list includes municipalities with purchased Worldview-2 images but with limited coverage. Since the Google Earth images are displayed only in true color, the interpretation keys for RGB = 5-3-2 were the ones used, together with comparison between tone, texture, pattern and context.

In the municipalities of Kitcharao, Jabonga and Santiago, there were no detected possible locations from the ALOS AVNIR-2 images because of cloud coverage in these portions. But during the initial survey conducted in July 2012, several Sago palm stands were observed. The observed locations were located in Google Earth wherein more stands were detected. A second survey was conducted in June 2013 to validate the detected locations.

An example of the visual interpretation of the Google Earth images is shown in Figure 96.

Table 29. List of municipalities where Google Earth images were utilized to confirm and refine detected possible Sago palm locations.

Province	Municipality	Acquisition Date of Images Displayed in Google Earth	Remarks
Aklan	Altavas	May 25, 2010 August 27, 2010	Image analysis supplemented by data from field surveys conducted on Dec. 15-21, 2012
	Balete		
	Banga		
	Lezo		
	Libacao		
	Madalag		
	Makato		
	Malinao		
Leyte	Dulag	September 12, 2006	
	Julita	November 10, 2010 April 18, 2011; February 23, 2012	
	Dagami	March 28, 2003	
	La Paz	September 12, 2006	
	Mayorga	November 10, 2010	
	Palo	February 23, 2012	Image analysis supplemented by data from field surveys conducted on Sept. 30 – Oct. 6, 2012
	Pastrana	April 5, 2003	

	Sta. Fe	February 23, 2012	Image analysis supplemented by data from field surveys conducted on Sept. 30 – Oct. 6, 2012
	Tabontabon	February 23, 2012	
	Tacloban City	February 23, 2012	Image analysis supplemented by data from field surveys conducted on Sept. 30 – Oct. 6, 2012
	Tanauan	February 23, 2012	
	Tolosa	February 23, 2012	
Agusan del Norte	Jabonga	May 18, 2012	Image analysis supplemented by data from field surveys conducted on July 24-25, 2012 and June 12-19, 2013.
	Kitcharao		
	Santiago		
	Las Nieves	April 8, 2005	
Agusan del Sur	Sta. Josefa	June 17, 2012	
Misamis Oriental	Jasaan	April 24, 2010	Image analysis supplemented by data from field surveys conducted on June 9-25, 2012.
	Villanueva		
	El Salvador City		
	Alubijid		
Maguindanao	Datu Odin Sinsuat	October 15, 2011	
	Cotabato City		
	Northen Kabuntalan	July 23, 2007	
	Sultan Kudarat	October 15, 2011	

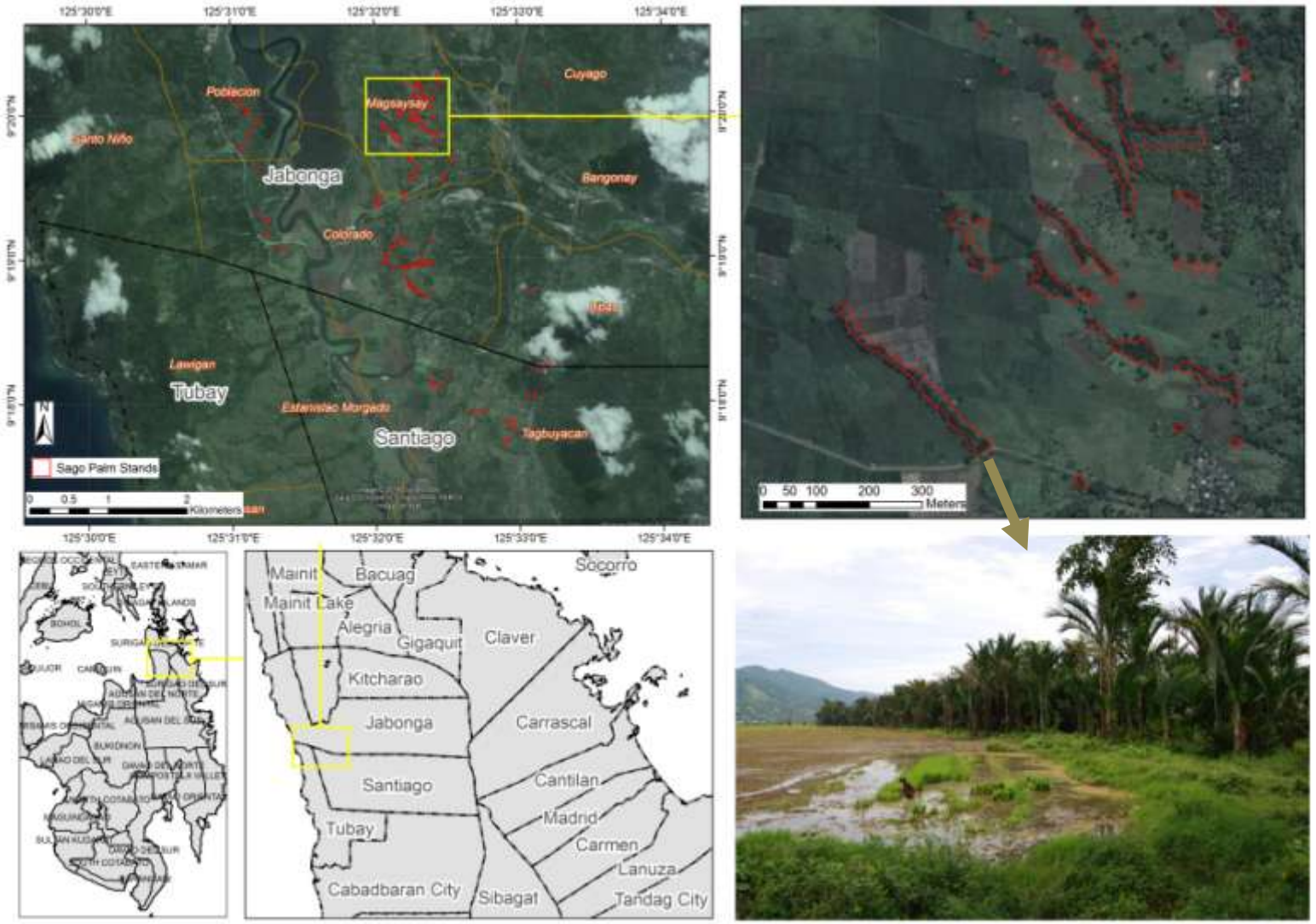

Figure 96. Example result of detecting Sago palm stands in Jabonga, Agusan del Norte through the use of high resolution Google Earth images.

11.3.5 Detection of Sago Palms in Jolo, Sulu

The island provinces of Mindanao were not included both in the analysis of satellite images and in the conduct of field surveys to map Sago palm locations. Through visual interpretation of Google Earth images aided by the knowledge learned in detecting Sago palms in high resolution images, an aggregated area of 19.67 hectares were detected in Jolo, Sulu. The Google Earth image (acquired on February 3, 2013) overlaid with the detected Sago palm stands is shown in Figure 97.

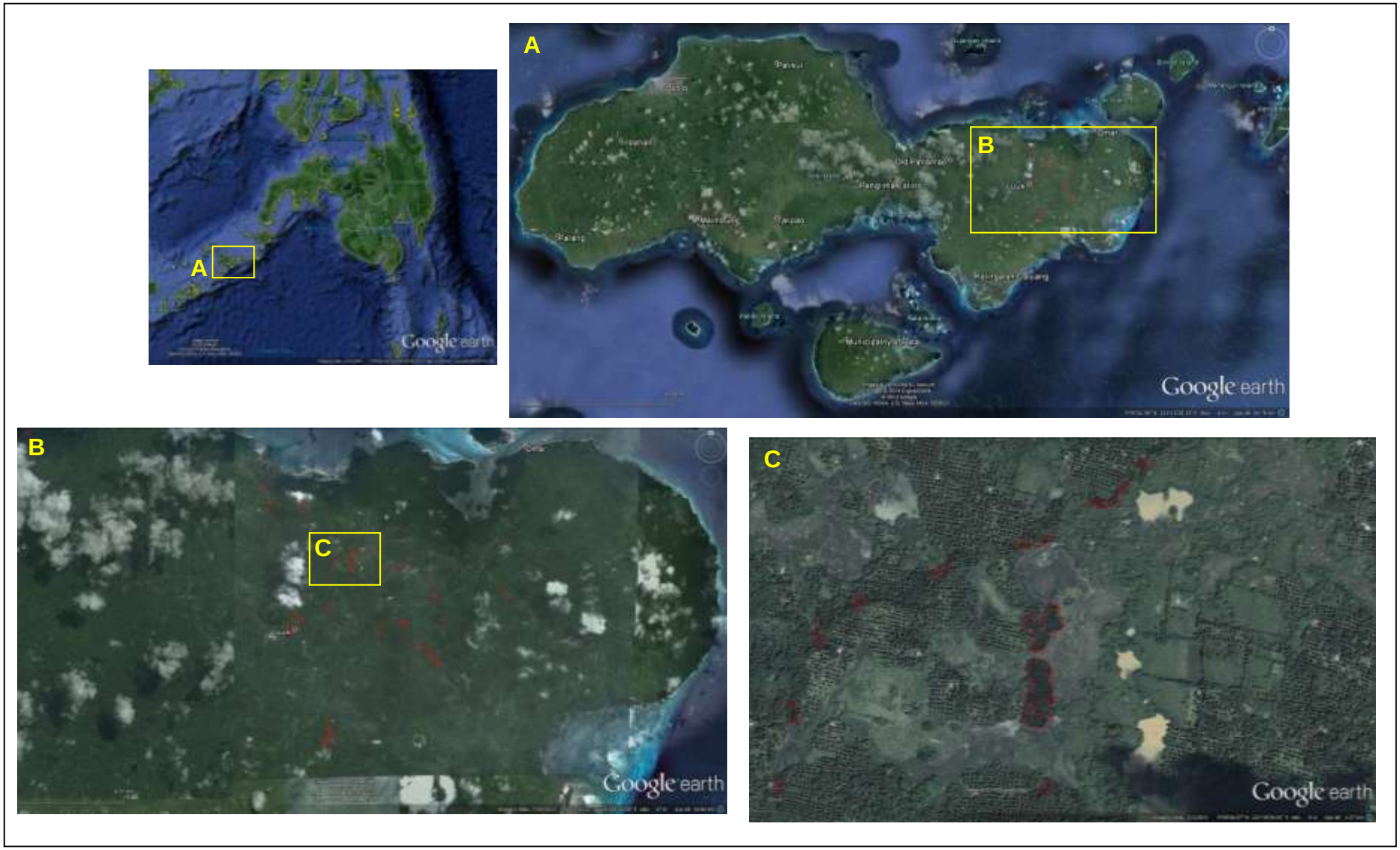

Figure 97. Google Earth image of Jolo, Sulu shown with the detected Sago palm stands. (Image Data: Google, Digital Globe).

11.4 Statistics of Confirmed Sago Palms Stands in Visayas and Mindanao

Sago palm stands were confirmed in 4 provinces in Visayas (Table 30) and 13 provinces in Mindanao (Table 32). The locations of these confirmed stands are shown in Figure 98. In Figure 99, the confirmed Sago palm stands are shown together with the boundaries of protected areas. Note that Sago palm stands confirmed in Bohol and Bukidnon were no longer included in the statistics because the area is negligible (less than 10 m^2). The total area of confirmed Sago palm stands in Visayas and Mindanao is 914.04 hectares.

In Visayas, all the confirmed Sago palm stands have an aggregated area of 252.87 hectares. Sago palms were found to be abundant in Leyte (215.70 has.), followed by Cebu (19.54 has) and Aklan (17.59 has). Very few Sago palms were found in Antique. Among the 30 municipalities in Visayas, Julita (in Leyte) has the highest aggregated area of confirmed Sago palms at 71.18 hectares. None of the confirmed Sago palms in Visayas are within protected areas.

In Mindanao, all the confirmed Sago palm stands have an aggregated area of 661.17 hectares. Of this, 337.92 hectares are within protected areas, majority of which is found in Agusan del Sur, specifically in the La Paz and Bunawan municipalities. In these municipalities, 337.87 hectares of Sago palm stands are within the Agusan Marsh Wild Life Sanctuary.

At the provincial level, Agusan del Sur has the highest total aggregated area of confirmed Sago palm stands (570.29 has), followed by Agusan del Norte (44.81 has), Sulu (19.67 has), Maguindanao (17.68 has), and Davao Oriental (2.72 has). The municipalities of La Paz, Bunawan and Veruela (all from Agusan del Sur) are the top 3 municipalities with the largest aggregated area of Sago palm stands (Table 33). They are followed by Butuan City, Prosperidad, Cotabato City, Jabonga, San Francisco and Sultan Kudarat.

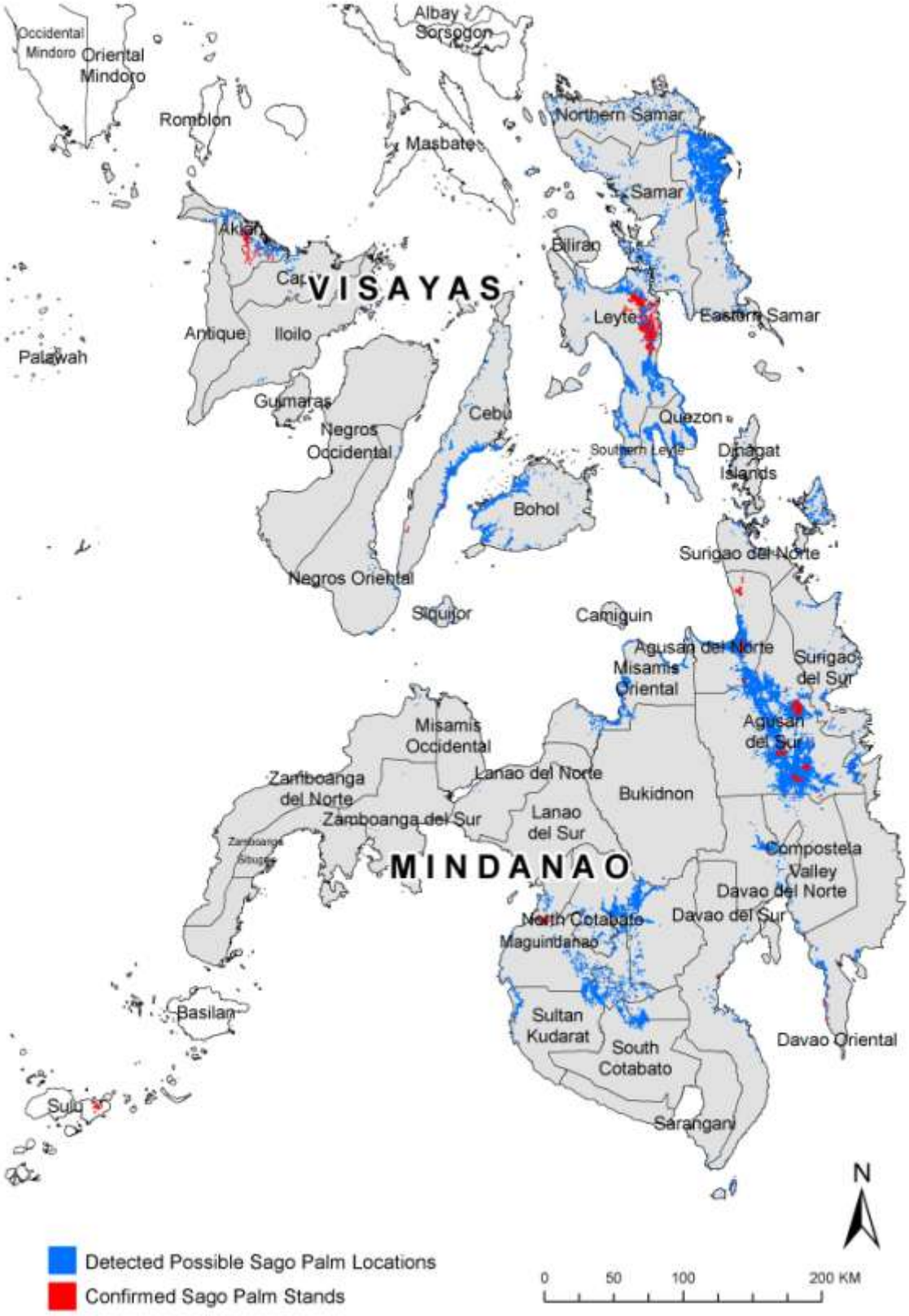

Figure 98. Map showing the confirmed Sago palm stands in Visayas and Mindanao.

Figure 99. Map of confirmed Sago palm stands shown together with the boundaries of protected areas.

Table 30. Aggregated area of confirmed Sago palm stands in Visayas provinces.

Rank	Province	Aggregated Area of Sago palm stands, in has.	Within Protected Area, in has.
1	Leyte	215.70	-
2	Cebu	19.54	-
3	Aklan	17.59	-
4	Antique	0.04	-
Total		252.87	-

Table 31. Aggregated area of confirmed Sago palm stands by municipalities of Visayas provinces.

Rank	Municipality	Province	Aggregated area, in has.
1	Julita	Leyte	71.18
2	Alangalang	Leyte	33.26
3	Dagami	Leyte	21.13
4	Dulag	Leyte	14.34
5	Pastrana	Leyte	12.78
6	Tabontabon	Leyte	12.30
7	Tanauan	Leyte	10.99
8	La Paz	Leyte	9.89
9	Palo	Leyte	9.30
10	Malinao	Aklan	9.22
11	Argao	Cebu	7.65
12	Santa Fe	Leyte	7.29
13	Samboan	Cebu	4.53
14	Alegria	Cebu	4.23
15	Libacao	Aklan	3.33
16	Mayorga	Leyte	3.22
17	Tolosa	Leyte	3.06
18	Jaro	Leyte	2.87
19	Burauen	Leyte	2.07
20	Tacloban City	Leyte	1.90
21	Sibonga	Cebu	1.74
22	Carcar	Cebu	1.40
23	Lezo	Aklan	1.04
24	Banga	Aklan	0.92
25	Balete	Aklan	0.82
26	Madalag	Aklan	0.81
27	Makato	Aklan	0.78
28	Altavas	Aklan	0.67
29	San Miguel	Leyte	0.11
30	Pandan	Antique	0.04

Table 32. Aggregated area of confirmed Sago palm stands in Mindanao provinces.

Rank	Province	Aggregated Area of Sago palm stands, in has.	Within Protected Area, in has.	Outside Protected Area, in has.
1	Agusan Del Sur	570.29	337.87	232.42
2	Agusan Del Norte	44.81	-	44.81
3	Sulu	19.67	-	19.67
4	Maguindanao	17.68	-	17.68
5	Davao Oriental	2.72	-	2.72
6	Surigao Del Sur	2.29	-	2.29
7	Misamis Oriental	2.27	-	2.27
8	Davao Del Sur	1.03	-	1.03
9	Compostela Valley	0.21	-	0.21
10	Surigao Del Norte	0.08	-	0.08
11	Davao Del Norte	0.05	-	0.05
12	South Cotabato	0.05	0.05	0
13	Zamboanga Sibugay	0.02	-	0.02
Total		661.17	337.92	323.25

Table 33. Aggregated area of confirmed Sago palm stands by municipalities of Mindanao provinces.

Rank	Municipality	Province	Aggregated Area of Sago palm stands, in has.	Within Protected Area, in has.	Outside Protected Area, in has.
1	La Paz	Agusan Del Sur	231.84	186.08	45.76
2	Bunawan	Agusan Del Sur	154.55	151.78	2.77
3	Veruela	Agusan Del Sur	145.88	-	145.88
4	Butuan City	Agusan Del Norte	28.23	-	28.23
5	Prosperidad	Agusan Del Sur	24.69	-	24.69
6	Luuk	Sulu	19.26	-	19.26
7	Cotabato City	Maguindanao	13.83	-	13.83
8	Jabonga	Agusan Del Norte	13.02	-	13.02
9	San Francisco	Agusan Del Sur	10.44	-	10.44
10	Sultan Kudarat	Maguindanao	2.15	-	2.15
11	Governor Generoso	Davao Oriental	2.13	-	2.13
12	Santiago	Agusan Del Norte	1.78	-	1.78
13	Rosario	Agusan Del Sur	1.65	-	1.65
14	Tagbina	Surigao Del Sur	1.34	-	1.34
15	El Salvador City	Misamis Oriental	1.20	-	1.20
16	Santa Cruz	Davao Del Sur	0.99	-	0.99
17	Datu Odin Sinsuat	Maguindanao	0.93	-	0.93
18	Las Nieves	Agusan Del Norte	0.90	-	0.90
19	Kitcharao	Agusan Del Norte	0.79	-	0.79
20	Bislig City	Surigao Del Sur	0.78	-	0.78
21	Santa Josefa	Agusan Del Sur	0.58	-	0.58
22	Talacogon	Agusan Del Sur	0.55	--	0.55
23	Lagonglong	Misamis Oriental	0.50	-	0.50
24	Northern Kabuntalan	Maguindanao	0.47	-	0.47
25	Old Panamao	Sulu	0.41	-	0.41
26	Datu Blah T. Sinsuat	Maguindanao	0.31	-	0.31
27	Mati City	Davao Oriental	0.29	-	0.29
28	Alubijid	Misamis Oriental	0.27	-	0.27
29	Mabini	Compostela Valley	0.21	-	0.21
30	Jasaan	Misamis Oriental	0.18	-	0.18
31	Lianga	Surigao Del Sur	0.17	-	0.17
32	Baganga	Davao Oriental	0.14	-	0.14
33	Villanueva	Misamis Oriental	0.12	-	0.12
34	Loreto	Agusan Del Sur	0.10	-	0.10
35	Mainit Lake	Agusan Del Norte	0.09	-	0.09
36	San Isidro	Davao Oriental	0.09	-	0.09
37	Placer	Surigao Del Norte	0.07	-	0.07

38	Banaybanay	Davao Oriental	0.06	-	0.06
39	Carmen	Davao Del Norte	0.05	-	0.05
40	Surallah	South Cotabato	0.05	0.05	0.00
41	Davao City	Davao Del Sur	0.04	-	0.04
42	Diplahan	Zamboanga Sibugay	0.02	-	0.02
43	Gigaquit	Surigao Del Norte	0.01	-	0.01
Total			661.17	337.92	323.25

11.5 Chapter Conclusions

In this chapter, the confirmation and refinement of the possible Sago palm locations detected using Landsat 7 ETM+ and ALOS AVNIR-2 images was presented. The confirmation and refinement consisted of integrating ground truth information with the interpretation and analysis of high resolution Worldview-2 images, including images available in Google Earth. A total of 914.04 hectares of Sago palms were confirmed in Visayas and Mindanao. Detailed maps and statistics of the confirmed Sago palm stands can be found in Annex 2 of this report.

Chapter 12. Habitat Suitability Analysis of Sago Palms in Visayas and Mindanao[3]

Habitat suitability analysis was conducted primarily to search for lands in Visayas and Mindanao where Sago palms can grow based on biophysical and bioclimatic factors. The suitability analysis utilized information on the biophysical and bioclimatic conditions at the confirmed Sago palm locations.

A one hectare (100 m x 100 m) mapping unit was utilized upon the assumption that 1 ha corresponds to the unit of decision making for agricultural or forestry management [**91**].

The suitability analysis consisted of two steps:

- Step 1: Finding suitable areas based on biophysical characteristics
- Step 2: Finding suitable areas based on bioclimatic characteristics

The results of both steps are raster grids, with pixel resolution of 1 hectare (100 x 100 m). Each pixel is coded as 0 and 1: 0 is “not suitable” and 1 is “suitable”. The final suitability map is then obtained by multiplying the two raster grids. The following sections provide details of each step.

12.1 Datasets used

12.1.1 Sago Palm Samples

Samples used in habitat suitability analyses were obtained from a GIS database of confirmed Sago palm stands. Samples were randomly generated within the polygons of confirmed Sago stand using the Random Point Generator v. 1.3 extension [**110**] of Arcview GIS 3.2. The selection was done in such a way that there is at least one sample per polygon of Sago stand.

From the total number of generated samples, 80% were selected for exploratory statistical and habitat suitability analysis while the remaining 20% were used for validating the habitat suitability maps. The number of samples generated for Visayas and Mindanao are summarized in Table 34 with their locations depicted in Figure 100.

Table 34. Number of samples representing actual Sago palm locations in Visayas and Mindanao used for exploratory statistical and habitat suitability analysis.

Locality	Number of Training Samples (80%)	Number of Validation Samples (20%)	Total Number of Samples
Visayas	404	103	507
Mindanao	1,008	252	1,260
Total	1,412	355	1,767

[3] *This chapter was prepared together with Sago Project II.2. Majority of this chapter can also be found in Sago Project II.2’s terminal report.*

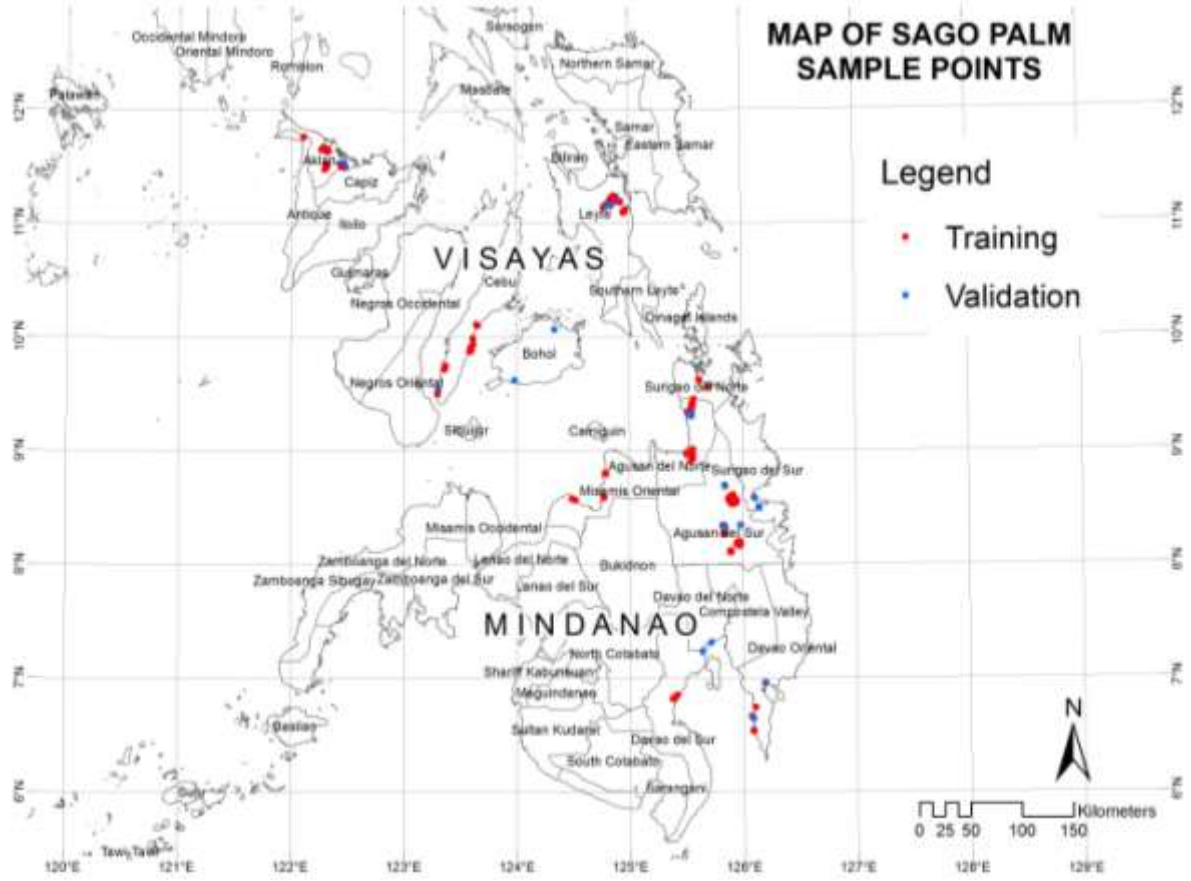

Figure 100. Map of samples representing actual Sago palm locations in Visayas and Mindanao used for habitat suitability analysis.

12.1.2 Biophysical Datasets

Biophysical data used in the analyses include elevation (ELEV), slope (SLOPE), and soil texture (SOIL). These datasets are summarized in Table 35 and illustrated in Figure 101 and Figure 102.

Table 35. Biophysical datasets used for exploratory statistical and habitat suitability analysis.

Biophysical Data	***Symbology***	***Description***	***Source***
Elevation	ELEV	Raster dataset containing elevation values at 90x90 m spatial resolution	Shuttle Radar Topography Mission Digital Elevation Model (SRTM DEM), http://gdex.cr.usgs.gov/gdex/
Slope	SLOPE	Raster dataset that provides a measure of flatness or steepness of the terrain calculated in percent (%) using the SRTM DEM	SRTM DEM
Soil Texture	SOIL	GIS shapefile containing information on the type of soil texture (loam, silt, clay, silty clay, clay loam, etc.)	Bureau of Soils and Water Management – Department of Agriculture (BSWM-DA)

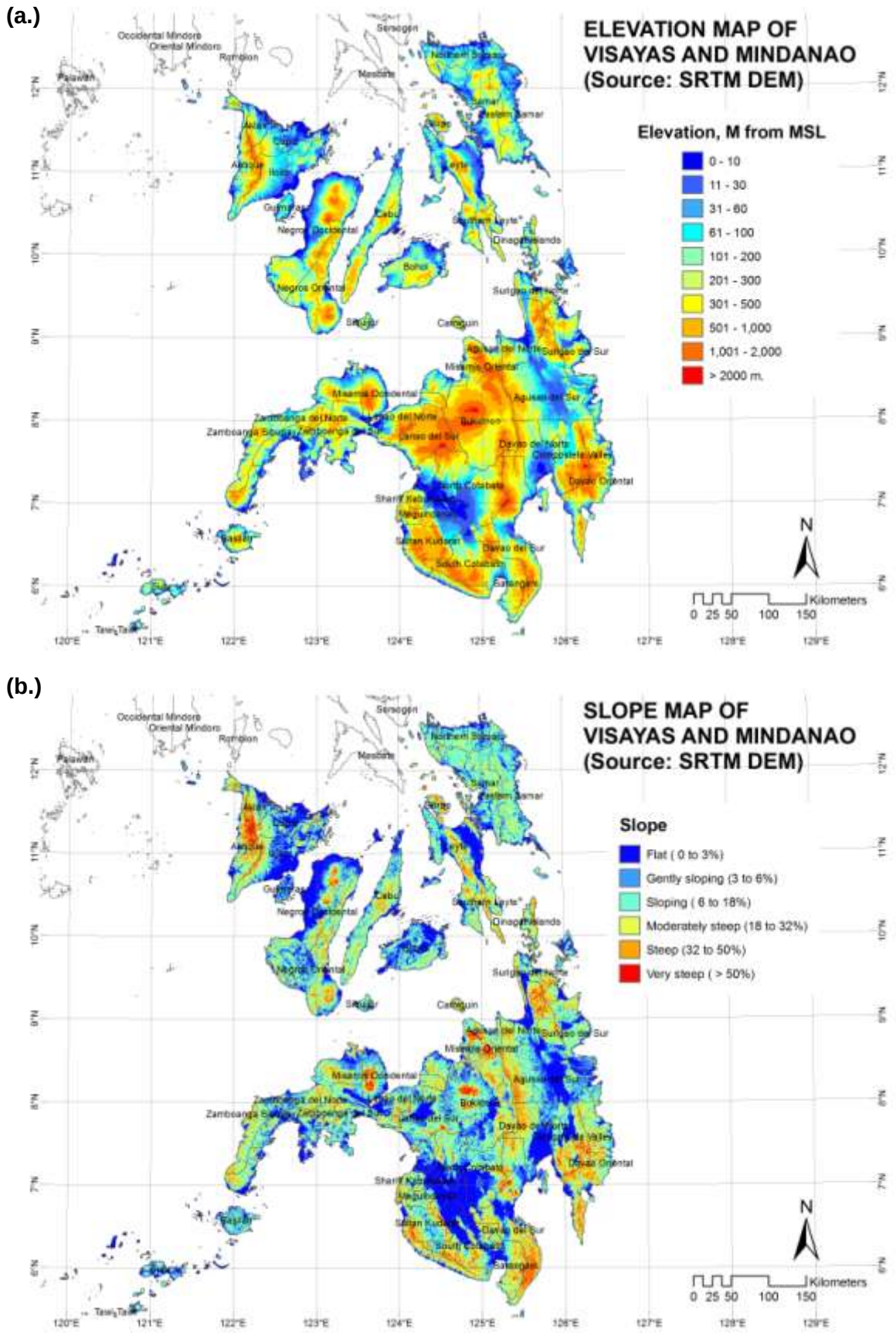

Figure 101. Elevation (a) and slope (b) maps derived from the SRTM DEM.

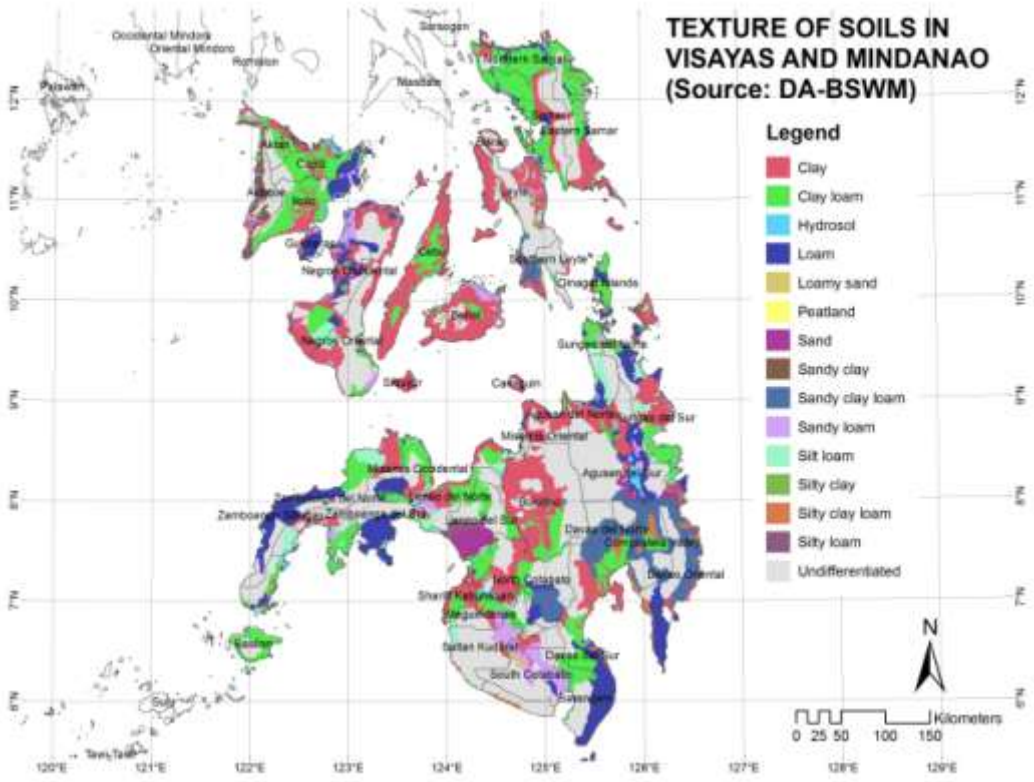

Figure 102. Map showing the soil textures in Visayas and Mindanao. Undifferentiated soils are mostly mountain soils.

12.1.3 Bioclimatic Datasets

Global climate surfaces interpolated using time series of temperature and rainfall data measured between 1950 – 2000 at different meteorological stations throughout the world with a 30 arc-second spatial resolution (approximately 1 km x 1 km) called *WorldClim* were used in the analyses. WorldClim, which can be obtained at http://www.worldclim.org/, is a set of 19 global climate layers (climate grids) depicting temperature and precipitation that can be used for mapping and spatial modeling in a GIS or with other computer programs. This dataset is well documented in [**99**] and has been used in a variety of plant species distribution and habitat suitability modeling studies (e.g., [**111**]; [**90**]; [**112**]; [**113**]; [**114**]).

In the analyses, we used the most recent version (ver. 1.4) of WorldClim. The 19 climate layers, symbolized as BIO1 to BIO19, are listed in Table 36 and illustrated in Figure 103 and Figure 104.

Table 36. The 19 climate layers in WorldClim.

Temperature Layers	***Symbology***
Annual mean temperature	BIO1
Mean diurnal range	BIO2
Isothermality	BIO3
Temperature seasonality	BIO4
Max temperature of warmest month	BIO5
Min temperature of coldest month	BIO6
Temperature annual range	BIO7
Mean temperature of wettest quarter	BIO8
Mean temperature of driest quarter	BIO9
Mean temperature of warmest quarter	BIO10
Mean temperature of coldest quarter	BIO11
Precipitation Layers	
Annual precipitation	BIO12
Precipitation of wettest month	BIO13
Precipitation of driest month	BIO14
Precipitation seasonality	BIO15
Precipitation of wettest quarter	BIO16
Precipitation of driest quarter	BIO17
Precipitation of warmest quarter	BIO18
Precipitation of coldest quarter	BIO19

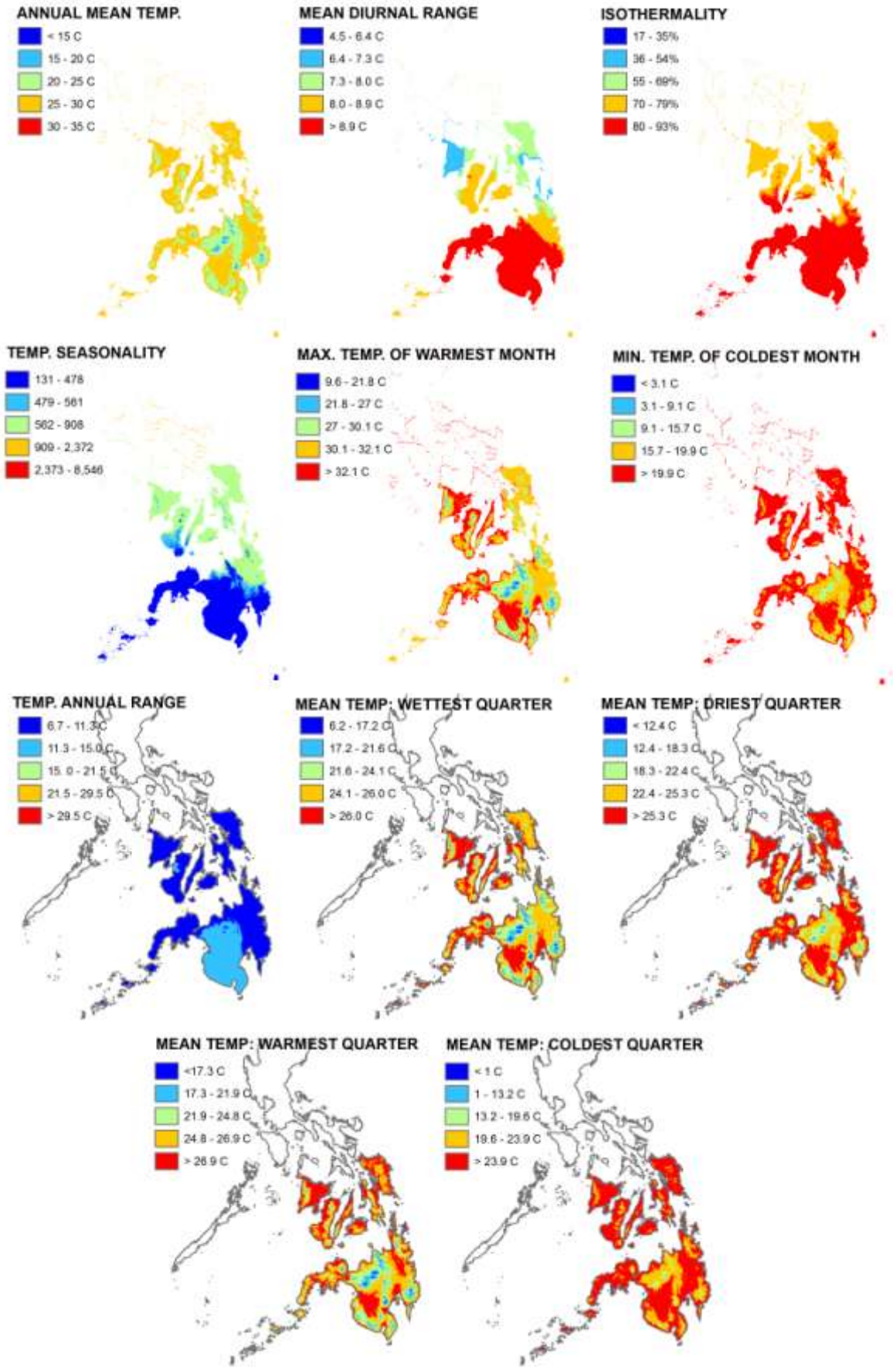

Figure 103. Maps of the 11 WorldClim temperature layers.

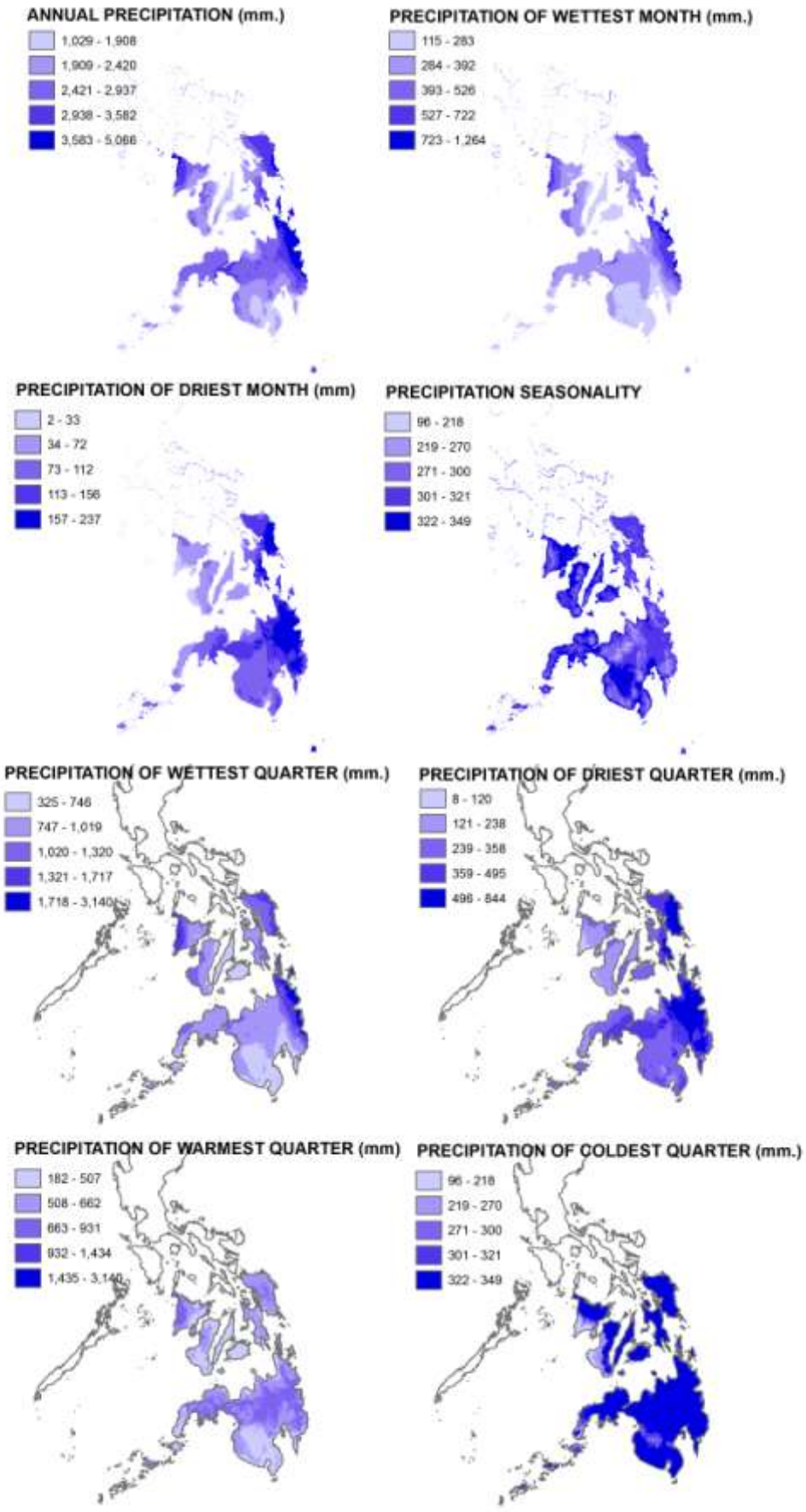

Figure 104. Maps of the 8 WorldClim precipitation layers.

12.2 Methods

12.2.1 Finding suitable areas based on biophysical characteristics

Step 1 of the suitability analysis uses the ranges of elevation and slope values and the type of soil textures of the Sago palm training samples in order to create the biophysical habitat suitability map ($SUIT_{BIOPHYSICAL}$). The required information are obtained through exploratory statistical analysis

The following decision rule is implemented in each pixel of ELEV, SLOPE and SOIL raster grids:

$$SUIT_{BIOPHYSICAL} = \begin{Bmatrix} 1 & \text{if} \quad \min_{ELEV} \le ELEV_i \le \max_{ELEV} \ \text{AND} \\ & \quad \min_{SLOPE} \le SLOPE_i \le \max_{SLOPE} \ \text{AND} \\ & \quad SOIL = \left(SOIL_1 \ \text{OR} \ SOIL_2 \ \text{OR} \ SOIL_3 ... \ \text{OR} \ SOIL_n\right) \\ & \text{else} \\ 0 & \end{Bmatrix}$$

In the above equation, *i* is a 100x100m pixel in a layer stack of ELEV, SLOPE and SOIL. The variables min_{ELEV}, max_{ELEV}, min_{SLOPE} and max_{SLOPE} are the minimum and maximum values of elevation and slope in the Sago sample locations or as obtained from the Sago palm literature. $SOIL_1$, $SOIL_2$, $SOIL_3$, $SOIL_n$ are the soil textures in the Sago sample locations.

The basis for the above rule is simple: the fact that a Sago palm stand has been found in a location within the elevation and slope ranges and with the soil texture as determined through overlay analysis is a good indication that Sago palm can grown in other areas with the same biophysical characteristics.

12.2.2 Finding suitable areas based on bioclimatic characteristics and suitability models

In Step 2, existing habitat suitability models such as Bioclim and Domain, were used. The goal here is to find those areas where Sago palms can grow in a manner that they could tolerate temperature (hotness and coldness) and precipitation (dryness and wetness). Description of the model including their suitability rules are discussed as follows. DIVA GIS version 7 [**98**] was used in this analysis.

All the 19 bioclimatic variables were used inputs in these 2 models based upon the argument by Nix [**76**] that that inclusion of further variables (instead of a just a selection) provides for a more useful discrimination of potentially suitable habitat. Also, all the 19 variables are considered to be relevant and effectively represents correlates of physiological tolerance of Sago palms, as described in McClatchey et al. [**115**] and as listed in the Ecrocrop Datasheet for *Metroxylon sagu* [**116**].

The Bioclim Model

Bioclim is a model that is used to describe the environment in which a plant or animal species has been recorded, and then utilizes these descriptions to identify other locations where the species may currently reside, or could be grown ([**76**]; [**117**]). As a range-based model, it uses bioclimatic data (e.g., temperature and precipitation) to interpolate a species' bioclimatic envelope as a rectilinear volume, which is a summary of the climate at locations from where the species has been recorded. This climatic envelope suggests that a species can tolerate locations where values of all climatic parameters fit within the extreme values determined by the set of known locations [**77**]. To state it simply, Bioclim assumes that climate restricts species distribution.

In order to predict the potential distribution of a Sago palm, Bioclim interpolates the climate within each grid cell and comparing it to the climatic profile of the species. Locations with values of all climatic parameters within the range of the species profile are classified by Bioclim as climatically suitable [**82**]. The concept behind Bioclim and how it identifies as a location as suitable or not suitable is illustrated in Figure 105. The model is similar to the parallelepiped classifier that is implemented in remote sensing image analysis. In the figure, dots represent values of mean annual temperature and mean annual precipitation at each known location of a hypothetical species. In predicting a species' potential distribution, Bioclim could classify all locations with values within the extremes of the species envelope (unbroken line) as suitable. The dashed box represents those areas where climatic values outside of the 5–95th percentiles of the species envelope are excluded. Locations where the values of all the parameters lie outside the species envelope are classified by Bioclim as not suitable [**82**].

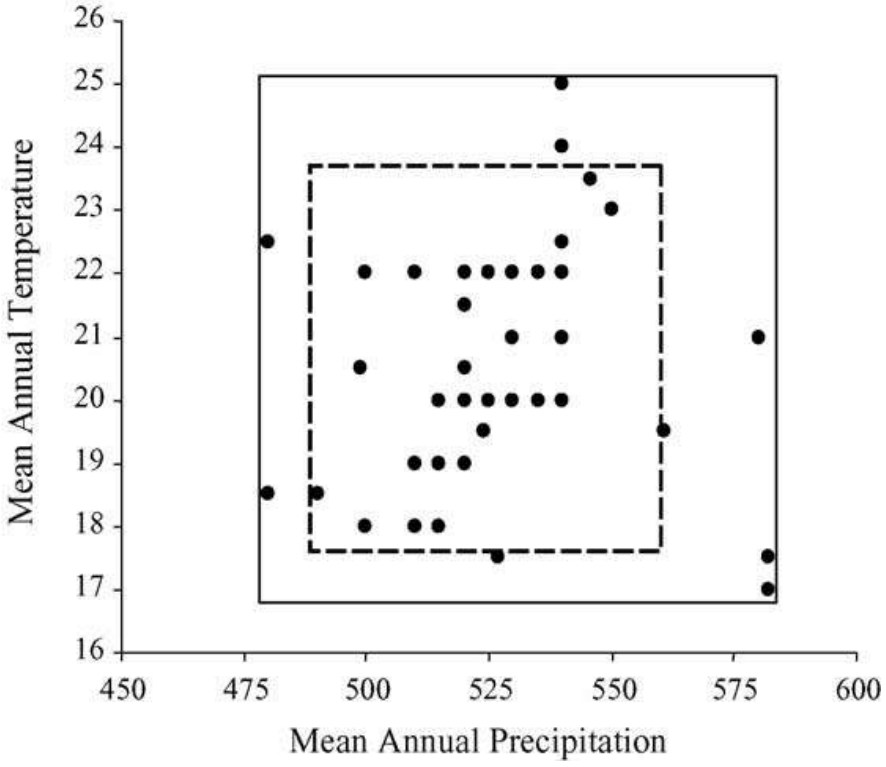

Figure 105. A diagrammatic representation of a hypothetical two dimensional bioclimatic envelope generated by Bioclim. (Diagram and explanation from Beaumont et al. [**82**]).

In predicting a Sago palm's potential distribution, Bioclim could classify all locations with values within the extremes of the species envelope (unbroken line) as suitable. Multiple levels of classification can be achieved by removing the extreme values of each parameter, and identifying locations with climatic values that lie within different percentile limits. For example, locations where the values of all parameters lie within the 5–95th percentiles of the species envelope may be classified as 'core' regions (Figure 105). On the other hand, locations where the values of all the parameters lie outside the species envelope are classified by Bioclim as not suitable.

The Bioclim model is available as a built-in function of Diva GIS software. To implement the model, one just needs to prepare the 19 bioclimatic grid files and the Sago palm training dataset (presence only data). With the Bioclim tool, data can be extracted from the climate database for point locations, make graphs of these data and use the extracted data to predict where a species is likely to occur, or would survive if it was brought there.

Four types of areas are mapped. Areas completely outside the 0-100 percentile envelope for one or more climate variables get a code "0". The cells within the 5 -95 percentile get a code "3", those outside this range but within the 2.5-97.5 percentile get a code "2", and the ones outside this but within the 0 -100 percentile for all climate variables get a code "1" [**98**]. This four types could then be translated as 0 - not suitable, 1 – low suitability, 2 - medium suitability, and 3 - high suitability. A simple suitability map ($SUIT_{BIOCLIMATIC\text{-}BIOCLIM}$) can then be created by aggregating types 1 to 3 as "suitable" and 0 as not suitable.

The Domain Model

Domain [**77**] derives a point-to-point similarity metric to assign a classification value to a potential site based on its proximity in environmental space to the most similar occurrence. The Gower metric, which is the sum of the standardized distance between two points for each predictor variable, is used to quantify the similarity between two sites. The standardization is achieved using the predictor variable range at the presence sites to equalize the contribution from each predictor variable. Similarity is then calculated by subtracting the distance from 1. The maximum similarity between a candidate point and the set of known occurrences is assigned to each grid cell within the study area; these similarity values are degrees of classification confidence.

In DIVA GIS, the Domain procedure calculates the Gower distance (d_{AB}) statistic between each cell on the map and each point, using the values of the 19 climate variables [**98**]. The distance between point A and grid cell B for a single climate variable is calculated as the absolute difference in the values of that variable divided by the range of the variable across all points. The Gower distance is then the mean over all climate variables and computed as follows:

$$d_{AB} = \frac{1}{p}\sum_{k=1}^{p}\frac{|A_k - B_k|}{range(k)}$$

The Domain similarity index is calculated as $D = 1 - d_{AB}$. The maximum similarity between a grid cell and all points is mapped. In DIVA GIS, this value is then multiplied by 100. A good match is thus a high number, e.g., above 95 [**98**].

Using the Domain model, potential distribution grids for Sago palms were created and then reclassified to values of zero or one for unsuitable or suitable using the similarity index cutoff of 0–0.95 and 0.95– 1.0, respectively as have been done in Vargas et al [**87**]. By eliminating all areas below 95% similarity we are assuming the 'core bioclimate' would contain those locations between 95 and 100 percentile limits and those locations whose grid value fall outside these limits would be considered areas of 'marginal bioclimate'. The cutoff point of 0.95 is based on other studies testing the DOMAIN model for plant and animal distributions [**77**]; [**86**]; [**118**]. The output suitability map is referred to as $SUIT_{BIOCLIMATIC\text{-}DOMAIN}$.

12.2.3 Sago Palm Habitat Suitability Map Generation and Accuracy Assessment

In order to generate the final habitat suitability maps, the $SUIT_{BIOPHYSICAL}$ map (result of Step 1) was multiplied with the two resulting maps under Step 2 which are $SUIT_{BIOCLIMATIC\text{-}BIOCLIM}$ and $SUIT_{BIOCLIMATIC\text{-}DOMAIN}$. This will result to two maps indicating Sago habitat suitable areas:

$$SUIT_{BIOPHYSICALxBIOCLIM} = SUIT_{BIOPHYSICAL} \times SUIT_{BIOCLIMATIC\text{-}BIOCLIM}$$

$$SUIT_{BIOPHYSICALxDOMAIN} = SUIT_{BIOPHYSICAL} \times SUIT_{BIOCLIMATIC\text{-}DOMAIN}$$

The resulting maps were then subjected to accuracy assessment by overlaying the 355 validation samples (as described in Table 34 and shown in Figure 98. Map showing the confirmed Sago palm stands in Visayas and Mindanao.). Each of these samples are checked if they are correctly classified in the habitat suitability maps as "suitable" (i.e., pixel value = 1). The percentage accuracy is then computed by dividing the number of correctly classified samples with the total number of samples.

12.3 Results and Discussions

12.3.1 Biophysical and bioclimatic habitat characteristics of Sago palms: comparison with published reports

Table 37 shows a comparison of Sago palm habitat characteristics as reported in McClatchey et al. [**115**] and as determined in this study. It shows that biophysical and bioclimatic characteristics of Sago palm habitats in Visayas and Mindanao are near or within the range of reported or published values. This means that Sago palm habitats in the Philippines are similar to habitats found in other areas of the world (e.g., Malaysia, Indonesia and Papua New Guinea).

Table 37. Sago palm habitat characteristics as reported in McClatchey et al. [**115**] and as determined in this study.

Biophysical and bioclimatic characteristics	***McClatchey et al. (2006)***	***In this study***
Topography	1 – 700 m above MSL	2 – 437 m above MSL
Soil	Wide variety of soils, including well drained, poor quality sand, clay or lava; prefers medium and heavy soils.	clay, clay loam, hydrosol, loam, sandy loam, silt loam and silty clay loam
Mean Annual Temperature	25^{o}C	27^{o}C (BIO1)
Mean maximum temperature of warmest period	>30^{o}C	32^{o}C (BIO5)
Mean minimum temperature of coldest period	17^{o}C	22^{o}C (BIO6)
Minimum temperature tolerated	17^{o}C	22^{o}C (BIO6)
Mean Annual Rainfall	2,000 – 5,000 mm	2,972 mm. (BIO12)

The bioclimatic characteristics of Visayas and Mindanao Sago palm habitats obtained in this study was also compared with temperature and precipitation ranges defined by the Food and Agriculture Organization (FAO) which is integrated in the FAO Ecocrop model [**116**]. These values are shown in Table 38. It shows that all Sago habitat locations used in the analysis are within the tolerable ranges of temperature and rainfall as defined in FAO Ecocrop datasheet for Sago palm. It was also found that the annual rainfall values of the Sago habitat locations are within the optimum range (i.e., for Sago palm to grow in a productive manner). However, the observed average minimum temperature is not within the optimum range although there are habitat locations in Visayas and Mindanao that have minimum temperature equal or greater than 25^{o}C.

Table 38. Sago palm habitat bioclimatic characteristics according to the FAO Ecocrop database, and as determined in this study.

Biophysical and bioclimatic characteristics		***FAO Ecocrop Database Values (FAO, 2007)***	***In this study***
Temperature	Absolute Temperature Range (Tolerable)	18^{o}C – 40^{o}C	22^{o}C – 32^{o}C (average min. and max. temperatures, i.e., BIO6 and BIO5)
	Optimum Temperature Range	25^{o}C – 36^{o}C	
	Killing Temperature	10^{o}C	
Rainfall	Absolute Annual Precipitation Range (Tolerable)	2,100 – 5,800 mm	2,972 mm (average annual rainfall, i.e., BIO12)

12.3.2 Habitat suitability mapping results

Basic suitability requirements based on field data and published literature

The results of the exploratory statistical analysis of biophysical and bioclimatic characteristics of Sago palm habitats in Visayas and Mindanao provided important information on deriving a very basic relationship to determine if the biophysical and bioclimatic characteristics of a certain locality are suitable for Sago palm to grow. Using the field data combined with information from published Sago palm literature [**115**]; [**116**], a set of Sago palm suitability requirements was developed, and this is summarized in Table 39. This table can be used as a preliminary assessment in determining a locality's suitability for Sago palm if all the constraints are met.

Table 39. Sago palm suitability requirements based on field data combined with information from published Sago palm literature.

Biophysical and bioclimatic characteristics		***Suitability Constraints (min and max)***	***Corresponding Biophysical or Bioclimatic Variable***	***Reference***
BIOPHYSICAL	Elevation	1 – 700 m	ELEV	*McClatchey et al. (2006); this study.*
	Slope	0 – 31%	SLOPE	*This study.*
	Soil	clay, clay loam, hydrosol, loam, sandy loam, silt loam and silty clay loam	SOIL	*This study.*
BIOCLIMATIC	Temperature	$18^{o}C$ – $40^{o}C$	BIO6, BIO5	*FAO, 2007*
	Rainfall/Precipitation	2,100 – 5,800 mm	BIO12	*FAO, 2007*

Sago biophysical suitability map

Using the information listed in Table 39, the decision rule for step 1 of the Sago suitability mapping was parameterized as follows:

$$SUIT_{BIOPHYSICAL} = \begin{cases} 1 & \text{if} \quad 1 \le ELEV_i \le 700 \text{ AND} \\ & \quad 0 \le SLOPE_i \le 31 \text{ AND} \\ & \quad SOIL = \begin{pmatrix} clay \text{ OR } clay\ loam \text{ OR } hydrosol \text{ OR } loam \\ \text{OR } sandy\ loam \text{ OR } silt\ loam \text{ OR } silty\ clay\ loam \end{pmatrix} \\ & \text{else} \\ 0 & \end{cases}$$

The resulting suitability map is shown in Figure 106 and depicts areas in Visayas and Mindanao that satisfy the biophysical requirements (as listed in Table 39) for growing Sago palms. Note that the Sulu Archipelago (containing the provinces of Sulu and Tawi-Tawi) was excluded in the suitability map generation due to unavailability of soil information for these areas.

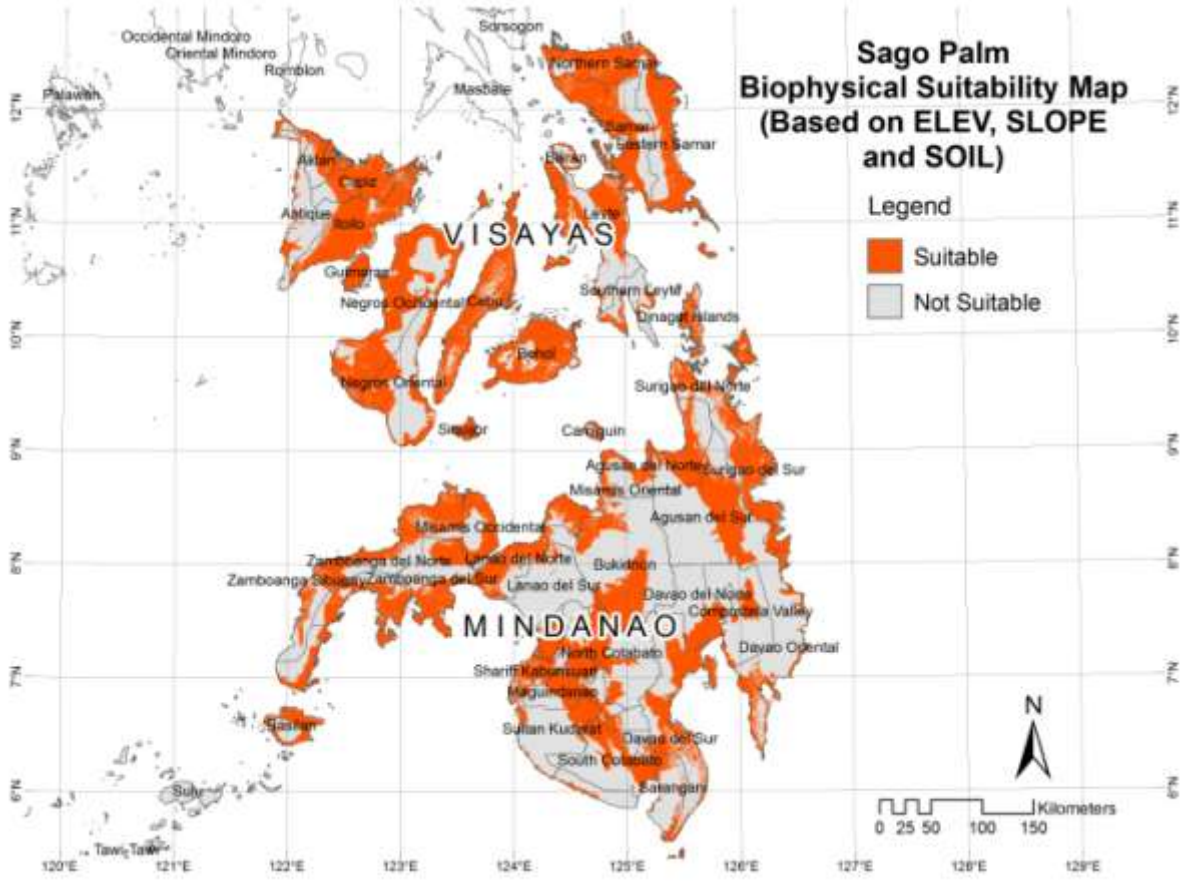

Figure 106. The Sago suitability map based on biophysical requirements ($SUIT_{BIOPHYSICAL}$).

Sago bioclimatic suitability map based on Bioclim and Domain

Figure 107 and Figure 108 show the step 2 suitability maps based on bioclimatic suitability models, Bioclim and Domain. The maps depict areas in Visayas and Mindanao that are computed by the models as having the bioclimatic characteristics (temperature and rainfall) suitable for Sago palm to grow.

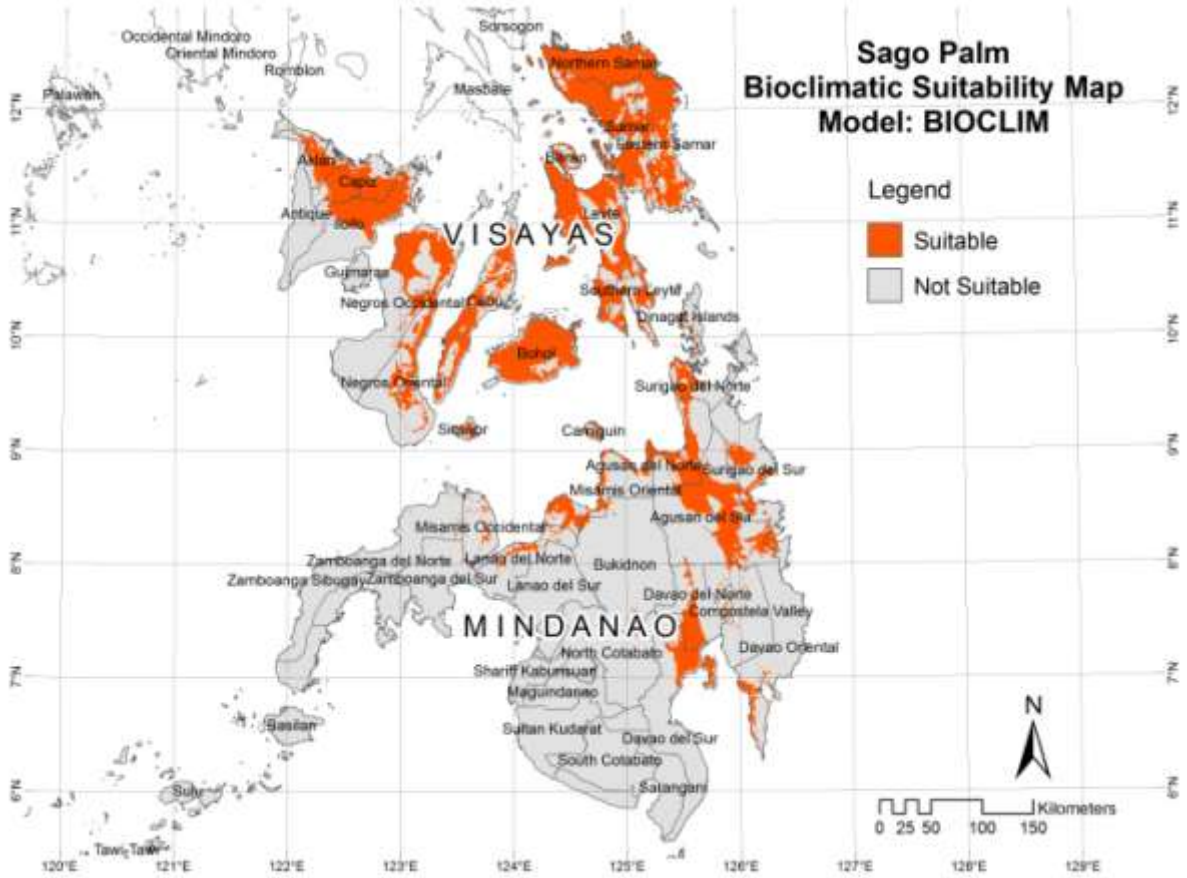

Figure 107. The Sago bioclimatic suitability map ($SUIT_{BIOCLIMATIC\text{-}BIOCLIM}$) derived using the Bioclim model.

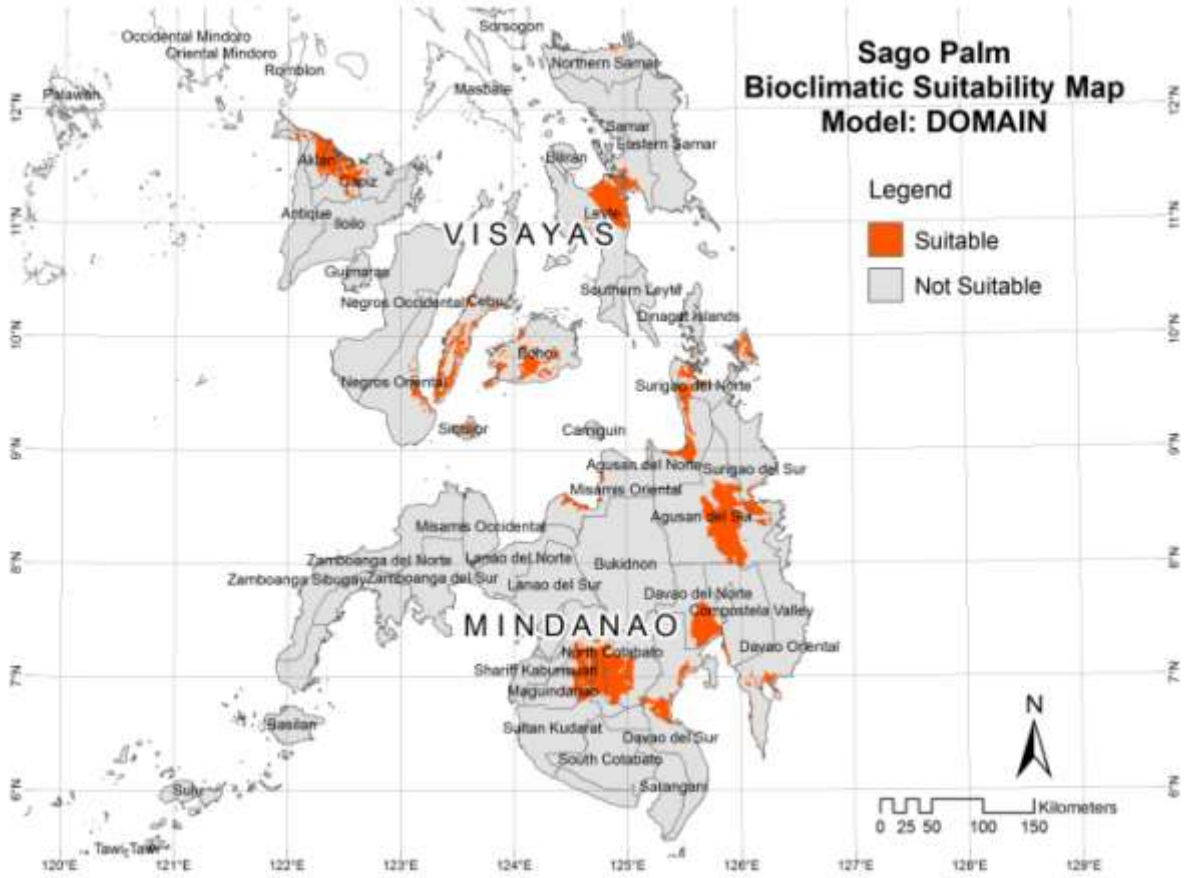

Figure 108. The Sago bioclimatic suitability map ($SUIT_{BIOCLIMATIC\text{-}DOMAIN}$) derived using the Domain model.

Sago suitability maps based on combined $SUIT_{BIOPHYSICAL}$ and $SUIT_{BIOCLIMATIC}$ results

Figure 109 and Figure 110 shows the results of multiplying the $SUIT_{BIOPHYSICAL}$ map (result of Step 1) with the two resulting maps under Step 2 which are $SUIT_{BIOCLIMATIC\text{-}BIOCLIM}$ and $SUIT_{BIOCLIMATIC\text{-}DOMAIN}$. These two maps indicate Sago habitat suitable areas that satisfy biophysical requirements, as well as bioclimatic conditions set by the model.

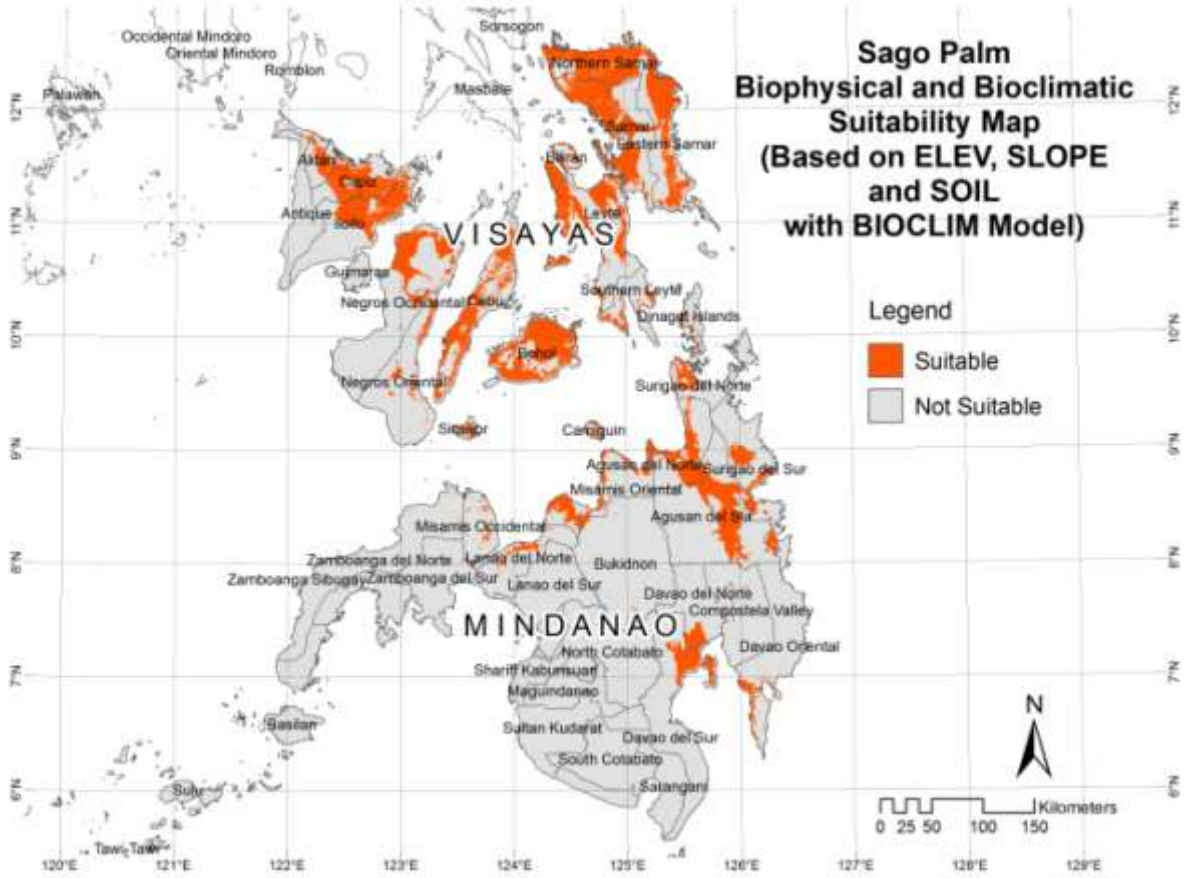

Figure 109. The Sago suitability map based on $SUIT_{BIOPHYSICALxBIOCLIM}$.

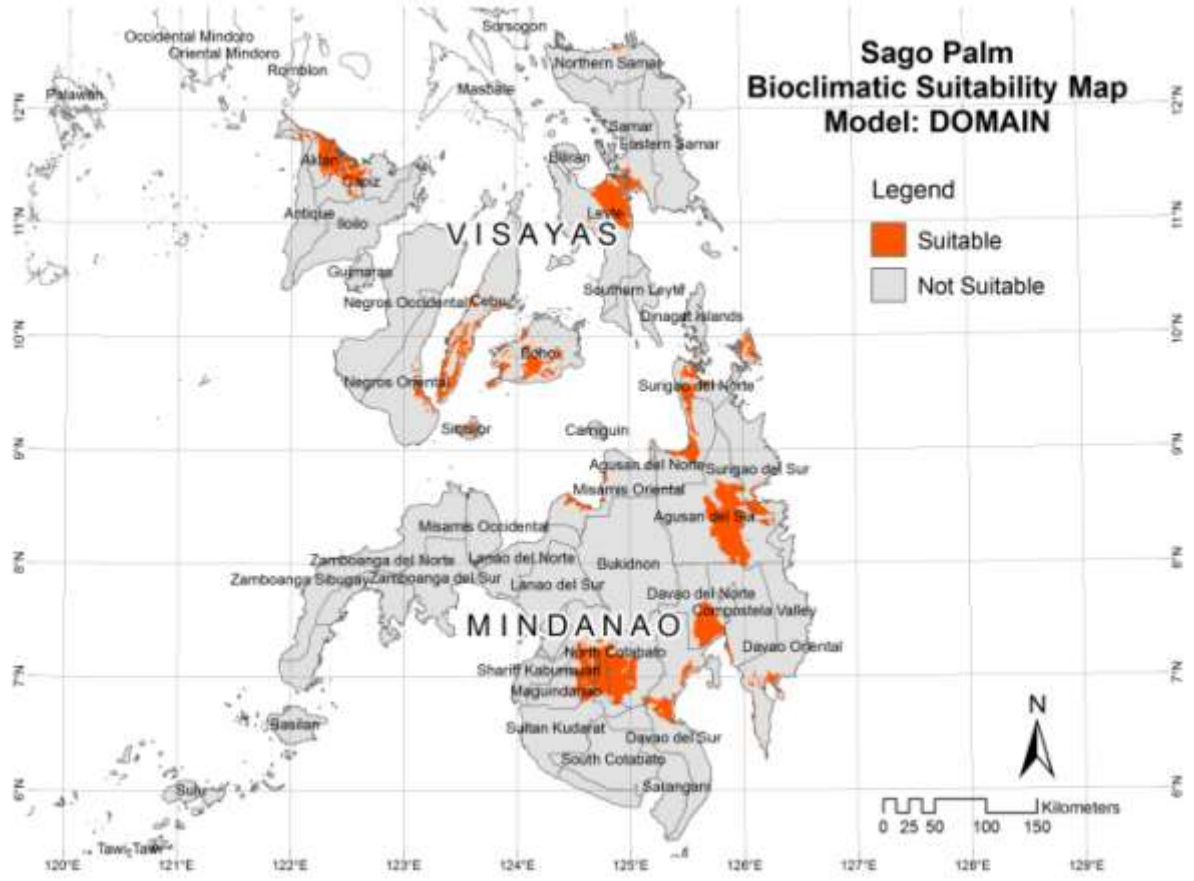

Figure 110. The Sago suitability map based on $SUIT_{BIOPHYSICALxDOMAIN}$.

Suitability map based on Sago palm basic biophysical and bioclimatic requirements

A suitability map can also be produced by utilizing the information listed in Table 39 into a basic Sago palm suitability rule ($SUIT_{BASIC}$). This can be done by updating the $SUIT_{BIOPHYSICAL}$ equation through addition of bioclimatic variables BIO5 (max. temperature of warmest month), BIO6 (min. temperature of coldest month) and BIO12 (annual precipitation). The resulting equation will be:

$$SUIT_{BASIC} = \begin{cases} 1 \quad \text{if} \quad 1 \le ELEV_i \le 700 \text{ AND} \\ \qquad 0 \le SLOPE_i \le 31 \text{ AND} \\ \qquad SOIL = \begin{pmatrix} clay \text{ OR } clay\ loam \text{ OR } hydrosol \text{ OR } loam \\ \text{OR } sandy\ loam \text{ OR } silt\ loam \text{ OR } silty\ clay\ loam \end{pmatrix} \text{ AND} \\ \qquad BIO5 \le 40°C \text{ AND} \\ \qquad BIO6 \ge 18°C \text{ AND} \\ \qquad 2100 \le BIO12 \le 5800 \\ \quad \text{else} \\ 0 \end{cases}$$

The generation of this map is similar to $SUIT_{BIOPHYSICAL\ x\ BIOCLIM}$ except that only the 3 bioclimatic variables are included, and the bioclimatic minimum and maximum range is not based on the training dataset but based on published Sago palm literature. The resulting suitability map is shown in Figure 111.

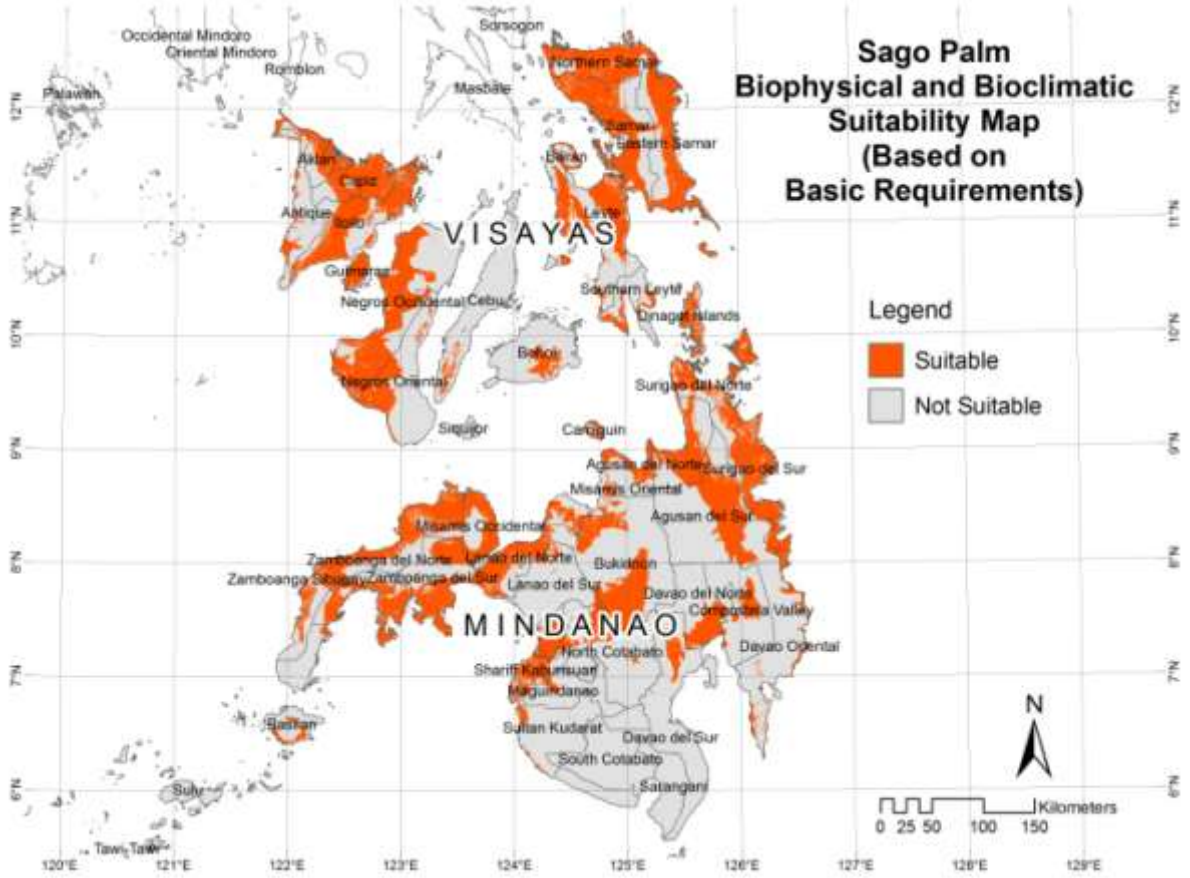

Figure 111. The suitability map based on Sago palm basic biophysical and bioclimatic requirements ($SUIT_{BASIC}$).

Accuracy of the Sago suitability maps

Table 40 summarizes the accuracy of the three suitability maps generated in this study. It can be observed that the accuracy is more than 80%. These relatively good accuracies of the three maps suggest that the biophysical and bioclimatic variables included in the generation of these maps are important and sufficient enough to determine the distribution patterns of Sago palms at the spatial scales examined in this study.

Of the three suitability maps that were generated, $SUIT_{BIOPHYSICALxDOMAIN}$ was found to be the most accurate. As listed in Table 40, 332 of 355 validation samples were correctly classified in this map. This translates to 93.52% accuracy. This map has the least error of 6.48% compared to $SUIT_{BASIC}$ (9.58%) and $SUIT_{BIOPHYSICALxBIOCLIM}$ (16.34%).

The higher accuracy of the Domain-based suitability map can be explained by its ability to determine the similarity of bioclimatic conditions in a locality to those of known Sago

palm habitats. The low accuracy of the Bioclim-based result can be explained by the way it was constructed. Because a subset of point locations is used, Bioclim do not always include all areas where the Sago palm is known to be present. This is evident by the failure of the model to correctly classify as "suitable" the 58 validation points. In these locations, the value(s) of one or more of the 19 bioclimatic variables are not within the range across all locations determined in the training dataset.

Table 40. Summary of Sago suitability maps accuracy assessment.

Suitability Map	No. of Correct Classifications (out of 355)	No. of Incorrect Classifications (out of 355)	Accuracy	Error
$SUIT_{BIOPHYSICALxBIOCLIM}$	297	58	83.66%	16.34%
$SUIT_{BIOPHYSICALxDOMAIN}$	332	23	93.52%	6.48%
$SUIT_{BASIC}$	321	34	90.42%	9.58%

Discussion

Aside from accuracy of classifications, the three suitability maps generated in this study can be further differentiated by looking into the areas they classify as suitable for growing Sago palms, and how realistic these classifications are.

All the three maps show areas that passed the biophysical requirements. The difference is on which areas the bioclimatic requirements are fulfilled. The $SUIT_{BIOPHYSICALxBIOCLIM}$ result indicates the areas that have values of all climatic parameters within the range of the species profile computed from the training samples used in the analysis. This means that each 100x100 m pixel in the map coded as "suitable" has all values of the 19 bioclimatic variables within the minimum and maximum values of the training dataset. The $SUIT_{BIOPHYSICALxDOMAIN}$ result indicates the areas that have the bioclimatic conditions similar to the bioclimatic conditions of the training samples used in the analysis. The $SUIT_{BASIC}$ result generally shows the areas where the biophysical and bioclimatic conditions are fulfilled, specifically the defined ranges of ELEV, SLOPE, SOIL, BIO5, BIO6 and BIO12.

All of the 3 maps indicate that there are additional tracts of potential suitable habitat beyond the known occupied habitat for Sago palms. Table 41 shows that $SUIT_{BASIC}$ has the highest total area classified as suitable. All the provinces in Visayas and Mindanao, except for South Cotabato and Sarangani, have suitable areas in this map. The $SUIT_{BIOPHYSICALxBIOCLIM}$ map is a reduced version of $SUIT_{BASIC}$. In this map, more than half of areas classified by $SUIT_{BASIC}$ as "suitable" have been classified as "unsuitable". The suitable areas did not include the Zamboanga peninsula as well as the provinces of Bukidnon, Maguindanao, North Cotabato and Sultan Kudarat.

The $SUIT_{BIOPHYSICALxDOMAIN}$ has the least total area classified as "suitable". The map is more specific than the other two maps, classifying only selected areas in the provinces of Aklan, Capiz, Negros Oriental, Cebu, Bohol, Leyte, Northern Samar, Samar, Misamis

Oriental, Agusan del Norte, Agusan del Sur, Surigao del Norte, Surigao del Sur, the Davao provinces, North Cotabato, and Maguindanao. The map is notable because it was able to classify as "suitable" some portions of Liguasan Marsh (located near North Cotabato). This marsh has been reported to have wild Sago palm stands but these stands were undetected based on satellite image analysis.

Table 41. Summary of Sago palm suitable areas[4].

Suitability Map	Suitable Areas in Visayas (has.)	Suitable Areas in Mindanao (has.)	Total (has.)
$SUIT_{BIOPHYSICALxBIOCLIM}$	2,065,932	754,367	2,820,299
$SUIT_{BIOPHYSICALxDOMAIN}$	392,809	606,682	999,491
$SUIT_{BASIC}$	2,546,616	3,002,273	5,548,890

Among the three suitability maps, the $SUIT_{BIOPHYSICALxDOMAIN}$ map is more realistic because the depicted suitability patterns are most consistent with the known ecology of the species [**77**]. The result is more logical and most appropriate for findings suitable areas than the other maps because the map specifically informs the user that all areas indicated as "suitable" have greater similarities to the biophysical and bioclimatic characteristics of actual Sago palm habitats. Hence, this map can is recommended among the three as the final Sago palm habitat suitability map.

12.4 Suitability Ranking Using the FAO *EcoCrop* Model

The $SUIT_{BIOPHYSICALxDOMAIN}$ map does not indicate the degree of suitability of a particular area. One way to rank the suitability is through the use of the FAO *EcoCrop* model. In a sense, the *EcoCrop* is also a suitability model but does not use the actual biophysical and bioclimatic conditions at the training sample locations. Instead, it uses expert-based temperature and rainfall ranges data reported in the FAO-EcoCrop database (http://ecocrop.fao.org) as inputs to determine the main niche of a crop and then produces a suitability score as output.

In the *EcoCrop* model, each of the temperature and rainfall ranges is defined by the absolute range (minimum and maximum absolute temperatures and rainfall at which the crop can grow) and by the optimum range (minimum and maximum optimum temperatures and rainfall). Using a gridded data of temperature and rainfall, the model's algorithm determines the conditions over the growing season at a particular place. When the conditions are beyond the absolute thresholds, the suitability index is zero (not suitable); when they are between absolute and optimum thresholds, the suitability score ranges from 1 to 99, and when they are within the optimum conditions the suitability score is 100% (excellent suitability). The model performs two different calculations separately, one for rainfall and the other for temperatures and then calculates the interaction by multiplying them. The final suitability scores are then grouped to indicate suitability types: very marginal

[4] *The area statistics shown here have been recomputed and updated and will differ from those reflected in the Sago Project II.2 terminal report.*

(1-20%), marginal (20-40%), suitable (40-60%), very suitable (60-80%), and excellent (80-100%).

Because of the model's capability to group suitability scores into suitability types, it was used to re-classify all areas identified as "suitable" in the $SUIT_{BIOPHYSICALxDOMAIN}$. The suitability scores of all the pixels in the $SUIT_{BIOPHYSICALxDOMAIN}$ were computed both for rainfall (R_{SUIT}) and temperature (T_{SUIT}) using the algorithms reported in [**82**].

DIVA GIS Version 7.5 was used to implement the *EcoCrop* model. This software has a built-in function for the *EcoCrop* model, including the FAO database of crop temperature and rainfall ranges. Based on the database, the Sago palm's absolute temperature range is from 18 – 40^0C, with 25 – 36^0C as the optimum range. The absolute total annual rainfall range is from 2100 – 5800 mm, with 3000 – 4500 mm as the optimum range. The growing season is 1 year (365 days). The WorldClim climate layers depicting minimum and maximum temperatures and total annual rainfall were used in the *EcoCrop* modeling.

In essence, the final suitability scores (R_{SUIT} x T_{SUIT}) indicates the degree of bioclimatic suitability of an area. While $SUIT_{BIOPHYSICALxDOMAIN}$ suitability map identifies areas where Sago palms can grow, the ranking by the *EcoCrop* model indicates if the areas have the necessary rainfall and temperature conditions for Sago palms to grow productively. The re-classified $SUIT_{BIOPHYSICALxDOMAIN}$ map is shown in Figure 112. The updated statistics of suitable areas according to type of suitability are listed in Table 42.

Based on the updated statistics, a total of 415,260 hectares in Visayas and Mindanao have excellent suitability for Sago palm. In Visayas, these areas are located in the provinces of Aklan, Capiz and Leyte. In Mindanao, they are located in Agusan del Norte, Agusan del Sur, Surigao del Norte and Surigao del Sur. If Sago palms are to be mass propagated, then the municipalities in these provinces that have excellent suitability should be targeted. Further prioritization can be made by focusing first on the municipalities that have confirmed Sago palm stands since in these municipalities there is proof that Sago palms can actually grow. If areas with "very suitable to excellent" suitability are to be targeted, there will be an increase in number of municipalities and in area for mass propagation. For Visayas, these municipalities are listed in Table 43 and Table 44. The list of municipalities for Mindanao can be found in Table 45 and Table 46.

Table 42. Summary of Sago palm suitable areas derived from $SUIT_{BIOPHYSICALxDOMAIN}$ that has been ranked according to suitability types.

Suitability Class	Visayas (has.)	Mindanao (has.)	Total (has.)
Excellent	134,828	280,432	415,260
Very suitable	57,390	46,630	104,020
Suitable	44,111	44,217	88,328
Marginal	47,716	224,211	271,927
Very Marginal	108,764	11,192	119,956
Total	392,809	606,682	999,491

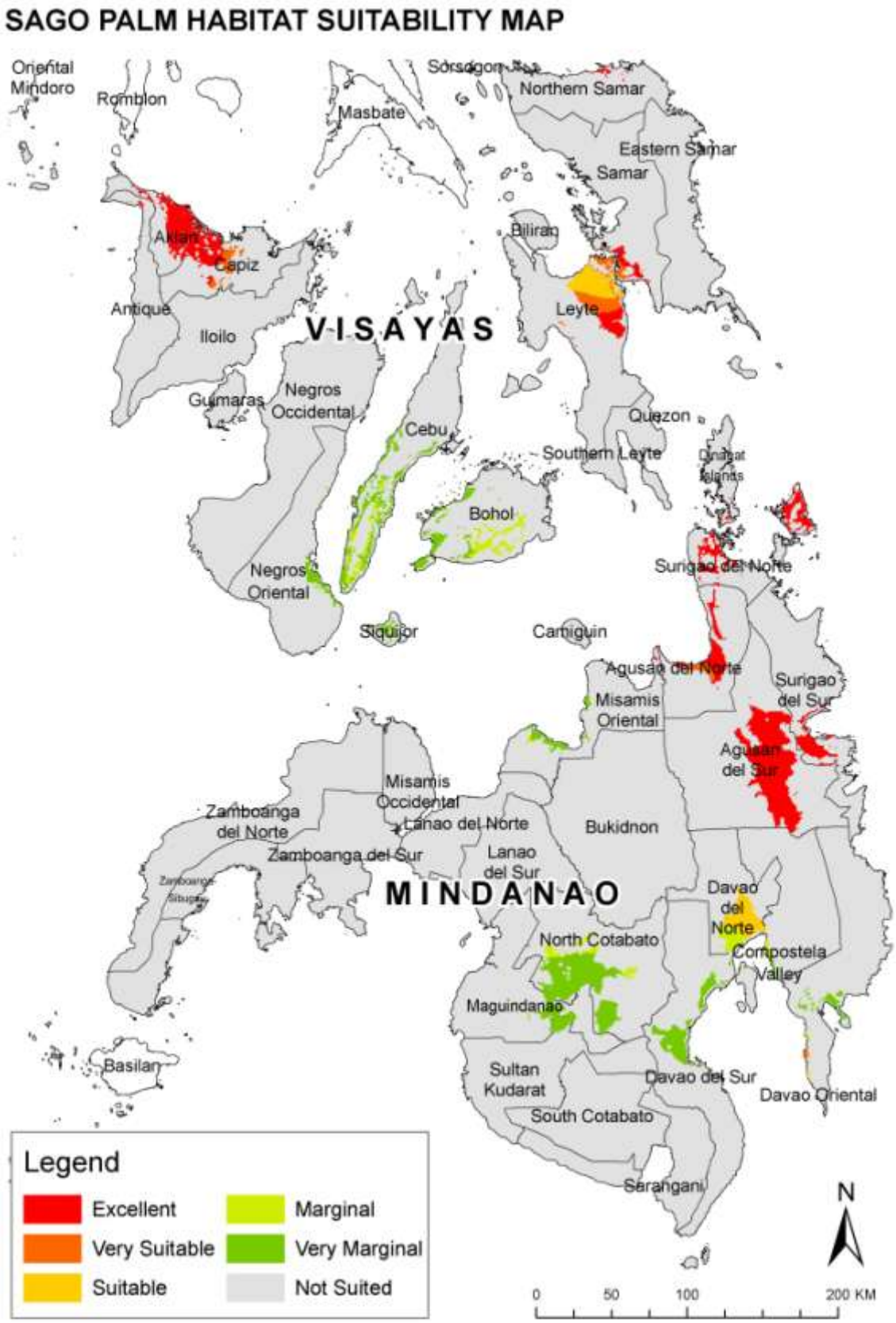

Figure 112. The final Sago palm habitat suitability map.

Table 43. List of Visayas municipalities, with excellent suitability and with confirmed Sago palm stands, which can be prioritized for mass propagation.

Rank (based on confirmed Sago stands)	Municipality	Province	Area of Confirmed Sago Palm Stands, in hectares	Area with Excellent suitability, in hectares
1	Julita	Leyte	71.18	4,152
2	Dagami	Leyte	21.13	5,793
3	Dulag	Leyte	14.34	3,246
4	Tabontabon	Leyte	12.30	1,835
5	Tanauan	Leyte	10.99	4,315
6	Malinao	Aklan	9.22	8,794
7	Libacao	Aklan	3.33	6,121
8	Tolosa	Leyte	3.06	116
9	Burauen	Leyte	2.07	2,474
10	Lezo	Aklan	1.04	1,938
11	Banga	Aklan	0.92	6,548
12	Balete	Aklan	0.82	10,040
13	Madalag	Aklan	0.81	5,376
14	Makato	Aklan	0.78	4,794
15	Altavas	Aklan	0.67	8,569
16	Pandan	Antique	0.04	1,150
Total			152.70	75,261

Table 44. List of Visayas municipalities, with “very suitable to excellent” suitabilities and with confirmed Sago palm stands, which can be prioritized for mass propagation.

Rank (based on confirmed Sago stands)	Municipality	Province	Area of Confirmed Sago Palm Stands, in hectares	Area with “Very Suitable to Excellent” suitability, in hectares
1	Julita	Leyte	71.18	4,152
2	Alangalang	Leyte	33.26	2,441
3	Dagami	Leyte	21.13	7,343
4	Dulag	Leyte	14.34	3,246
5	Pastrana	Leyte	12.78	6,895
6	Tabontabon	Leyte	12.30	1,835
7	Tanauan	Leyte	10.99	4,816
8	Palo	Leyte	9.30	5,356
9	Malinao	Aklan	9.22	8,794
10	Santa Fe	Leyte	7.29	2,069
11	Libacao	Aklan	3.33	6,121
12	Tolosa	Leyte	3.06	116
13	Jaro	Leyte	2.87	8,791
14	Burauen	Leyte	2.07	2,474
15	Tacloban City	Leyte	1.90	2,401
16	Lezo	Aklan	1.04	1,938
17	Banga	Aklan	0.92	6,548
18	Balete	Aklan	0.82	10,040

19	Madalag	Aklan	0.81	5,376
20	Makato	Aklan	0.78	4,794
21	Altavas	Aklan	0.67	8,569
22	San Miguel	Leyte	0.11	827
23	Pandan	Antique	0.04	1,150
Total			220.21	106,092

Table 45. List of Mindanao municipalities, with excellent suitability and with confirmed Sago palm stands, which can be prioritized for mass propagation.

Rank (based on confirmed Sago stands)	Municipality	Province	Area of Confirmed Sago Palm Stands, in hectares	Area with Excellent suitability, in hectares
1	La Paz	Agusan del Sur	231.84	17,915
2	Bunawan	Agusan del Sur	154.55	16,628
3	Veruela	Agusan del Sur	145.88	14,343
4	Butuan City	Agusan del Norte	28.23	15,379
5	Prosperidad	Agusan del Sur	24.69	28,541
6	Jabonga	Agusan del Norte	13.02	2,368
7	San Francisco	Agusan del Sur	10.44	33,486
8	Santiago	Agusan del Norte	1.78	1,904
9	Rosario	Agusan del Sur	1.65	15,372
10	Tagbina	Surigao del Sur	1.34	12,041
11	Kitcharao	Agusan del Norte	0.79	327
12	Santa Josefa	Agusan del Sur	0.58	9,588
13	Talacogon	Agusan del Sur	0.55	11,888
14	Lianga	Surigao del Sur	0.17	3,179
15	Loreto	Agusan del Sur	0.10	8,599
16	Placer	Surigao del Norte	0.07	3,888
17	Gigaquit	Surigao del Norte	0.01	725
Total			615.69	196,171

Table 46. List of Mindanao municipalities, with “very suitable to excellent” suitabilities and with confirmed Sago palm stands, which can be prioritized for mass propagation.

Rank (based on confirmed Sago stands)	Municipality	Province	Area of Confirmed Sago Palm Stands, in hectares	Area with “Very Suitable to Excellent” suitability, in hectares
1	La Paz	Agusan del Sur	231.84	17,915
2	Bunawan	Agusan del Sur	154.55	16,628
3	Veruela	Agusan del Sur	145.88	14,343
4	Butuan City	Agusan del Norte	28.23	21,618
5	Prosperidad	Agusan del Sur	24.69	28,541
6	Jabonga	Agusan del Norte	13.02	2,371
7	San Francisco	Agusan del Sur	10.44	33,494
8	Governor Generoso	Davao Oriental	2.13	1,383
9	Santiago	Agusan del Norte	1.78	1,904
10	Rosario	Agusan del Sur	1.65	15,372
11	Tagbina	Surigao del Sur	1.34	12,041
12	Kitcharao	Agusan del Norte	0.79	327
13	Santa Josefa	Agusan del Sur	0.58	9,588
14	Talacogon	Agusan del Sur	0.55	11,888
15	Lianga	Surigao del Sur	0.17	3,179
16	Loreto	Agusan del Sur	0.10	8,599
17	Placer	Surigao del Norte	0.07	3,888
18	Gigaquit	Surigao del Norte	0.01	725
Total			617.82	203,804

12.5 Chapter Summary and Conclusions

In this study, we have conducted habitat suitability analysis of Sago palms in Visayas and Mindanao. The suitability analysis was aided by exploratory statistical analysis that determined the biophysical and bioclimatic characteristics of known Sago palm habitats. The information derived from the statistical analysis was then used in conjunction with bioclimatic models to create suitability rules that are then used to search for lands in Visayas and Mindanao where Sago palms can grow at a spatial resolution of one hectare (100 m x 100 m).

Of the three suitability maps that were generated, $SUIT_{BIOPHYSICALxDOMAIN}$ was found to be the most accurate at 93.52%. The relatively good accuracy of the suitability map generated in this study suggests that the biophysical and bioclimatic variables included in the generation of this map are sufficient enough to determine the distribution patterns of Sago palms at the spatial scales examined in this study. However, this hypothesis should be

further evaluated by field survey and by expert opinion of botanists and ecologists familiar with the Sago palm.

The degree of suitability was determined through the use of the FAO *EcoCrop* model. Based on the suitability map, a total of 999,491 hectares of lands in Visayas and Mindanao were found to be biophysically and bioclimatically “suitable” for growing Sago palms. Of this, 415,260 hectares have “excellent” suitability while 104,020 hectares are “very suitable”. The list of municipalities with confirmed Sago palm stands and with “excellent” and “very suitable” suitability were also identified in Visayas and Mindanao. If Sago palms are to be mass propagated, then these municipalities should be targeted since in these municipalities there is proof that Sago palms can actually grow. In Visayas, majority of these municipalities are in Leyte and Aklan. In Mindanao, majority are found in Agusan del Sur, Agusan del Norte, Surigao del Sur and Surigao del Norte.

Chapter 13. Summary of Findings, Conclusions and Recommendations

13.1 In-situ Spectral Reflectance Analysis

Important information with regards to differences in spectral reflectance of Sago and other palms in the visible to near infra-red region of the electromagnetic spectrum was revealed through analysis of in-situ reflectance spectra. The analysis showed that the blue and red regions are the best portions, especially those at the 400-500 nm and at 650-700, in distinguishing growth stages of Sago palm. The two groups of growth stages: rosette-bole formation and inflorescence-fruit ripening can be at 770 nm. Further analysis of reflectance spectra showed that in general, Sago, coconut, nipa and oil palms have lower reflectance in the blue and red regions but higher reflectance in the green region. There were several portions of the electromagnetic spectrum where Sago palm is distinguishable from other palms. The NIR region, specifically at 770, 800 and 875 nm, provides the best wavelengths where Sago palm can be distinguished from other palms.

The resampling of the in-situ reflectance spectra to match the spectral response of optical sensors namely, Landsat 7 ETM+, Landsat 8 OLI, ASTER VNIR, ALOS AVNIR-2 and Worldview-2 made possible the analysis of the differences in reflectance values of Sago and other palms in different bands of the sensors. Results showed if images acquired by either Landsat 7 ETM+, Landsat 8 OLI, ALOS AVNIR-2 and even ASTER VNIR are to be used to detect Sago palms, the use of single band may not provide good results. The use of all bands (and maybe some derivatives such as NDVI) may be helpful to successfully detect Sago palms by discriminating them from other palm vegetation. A more interesting result was obtained with the analysis of Worldview-2 reflectance values of Sago and other palms. Compared to the other 3 sensors, there were four bands that appear to be useful in discriminating Sago from other palms: Bands 1, 6, 7 and 8. It is in these bands that the large differences in reflectance values were obtained.

The knowledge learned was useful in the actual analysis of optical satellite images, specifically in determining which band to include or to exclude, or whether to use all bands of a sensor in discriminating and mapping Sago palms using the images.

13.2 Image-based Spectral Reflectance Analysis

The average image-based reflectance values derived from ALOS AVNIR-images are higher than what was derived from Landsat 7 ETM+ image. Also, the differences in reflectance values are more apparent in ALOS AVNIR-2 than in Landsat 7 ETM+. One factor that may have contributed to this is the higher spatial resolution of the ALOS AVNIR-2 images which is 10x10 m. Because of this, the reflectance values extracted were more precise because the inclusion of other land-cover types in pixel is minimized. In a Landsat 7 ETM+ image pixel of 30x30 m, several land-cover classes may exist other than the target land-cover type. This in turn affected the reflectance values. Another factor is the differences

in locations of the samples used, and the differences in the dates of acquisitions of the images.

13.3 Radar backscattering of Sago palms and other land-cover types

The appearance of Sago palms in an Envisat IM image was found to be darker than other vegetation types such as cropland, shrubs and trees, grassland, mangroves, coconut and oil palm. What makes it darker is perhaps the presence of standing water underneath its canopy which has been observed during the field surveys in Bunawan, Agusan del Sur (the location of the samples used in the analysis). It has been reported that for *C*-band radar, high backscattering should be expected for a vegetation with high moisture (due to humid or saturated soil) and rough canopy structure. But for wetlands with no woody plants the increase in specular scattering caused by standing water tends to decrease radar backscattering [**97**]. Visually, Sago palm stands have a rough canopy structure due to presence of many fronds and leaves, with young Sago palms having the most number of the fronds and leaves. Only Sago palms in bole formation and later stages have woody materials that when compared to younger palms (rosette stage) is not significant in terms of quantity. Moreover, standing water is an ordinary characteristic of Sago palm stands. This perhaps explains the low backscattering of Sago palms in an Envisat Image.

The basic statistics and the ANOVA analysis of extracted backscattering coefficients of Sago palms and other land-cover types revealed that it is possible to identify land-cover types according their backscattering values in an Envisat ASAR IM image. The statistics suggest better discrimination of Sago palm from other land-cover types due to its relatively low but unique mean backscattering value which is significantly different from those of other land-cover types.

13.4 Potential Distribution Modelling of Sago Palm

It was shown that employing SDM using the DOMAIN model can be a valuable procedure prior to employing remote sensing image analysis to map uncommon vegetation species such as the Sago palm. The SDM approach was found to considerably reduce areal coverage of image analysis while maintaining acceptable accuracy of detecting actual locations of Sago palm. As the approach only targets locations where there is high likelihood of occurrence of a species, it reduces the number of images to analyze and can save time and resources. The similarity index map with 86% cut-off was utilized in mapping Sago palms using Landsat 7 ETM+, ALOS AVNIR-2, and Envisat ASAR.

13.5 Detection of Possible Sago Palm Locations through Landsat 7 ETM+ Image Analysis

The results of the Maximum Likelihood classification of the 14 September 2008 Landsat 7 ETM+ test image indicate that the use of combinations containing only the reflectance bands can only yield a maximum of 61.76% Producer's accuracy. In terms of User's Accuracy, the combinations yielded acceptable levels accuracies. The addition of NDVI appears to lessen the percentages of accuracy. The same can be said when TEMP was added. Relatively better overall classification and User's accuracies were obtained

when DEM was added (> 90%) but the Producer's Accuracy remains to be unacceptable (<85%). No significant improvements to the Producer's Accuracy were found when NDVI and TEMP were both added to the first 5 combinations. The group addition of NDVI, TEMP and DEM significantly improved the classification accuracies. However, it is the combination when both TEMP and DEM were added that gave the acceptable results. The best result was obtained for combination which included reflectance bands 3, 4 and 5, TEMP and DEM. This combination has an overall classification accuracy of 96.19% and with 90.44% and 94.09% Producer's and User's Accuracies for Sago palm.

With the acceptable classification results, the approach of Maximum Likelihood classification of Landsat 7 ETM+ bands 3, 4 and 5 together with TEMP and DEM can be adapted to map possible locations of Sago palms in other areas in Visayas and Mindanao. The classification detected a total of 5,230 hectares in Mindanao, and 2,394 hectares in Visayas to possibly contain Sago palms. The number of hectares presented does not necessarily refer to the number of hectares of existing Sago palms in consideration of the classification errors and inadequacy of the image spatial resolution of 30 m for mapping Sago palms that are less than 30 x 30 m in size.

The detected locations of Sago palms were utilized as primary basis for the conduct of field surveys and ground validation, and for the acquisition of ALOS AVNIR-2, Envisat ASAR and high resolution Worldview-2 images for the refinement of the Sago palm classification map.

With the potential distribution maps and the Landsat-based Sago palm classification map, the areas in Visayas and Mindanao to look for Sago palms have been expanded but specific. While initially there is a need to analyze the whole of Visayas and Mindanao, the coverage has been reduced. It is in this reduction of coverage that high resolution satellite images become of practical use to obtain very detailed and highly accurate maps and statistics of existing Sago palm stands.

13.6 Multi-Temporal Approach of Mapping Palms Using Envisat ASAR AP Images

The case study of using multi-temporal Envisat ASAR APP images in land-cover mapping using ANN and SVM showed that the approach can only provide acceptable results for built-up, cropland and water. The results for mapping palm trees is low (<85%) and below the acceptable levels of accuracy. Comparing the classification results with actual Sago palm location revealed inadequacy in terms of mapping the location of Sago palms - only 50 to 60% of the Sago palm locations were accurately classified as "Palm trees". With these poor results, the detection of Sago palms from all the pixels classified as "Palm trees" was no longer done. Moreover, the use of purely radar images as alternative to optical images for Sago palm detection was not longer pursued because there is high rate of omitting actual Sago palm locations, and high rate of misclassifying other vegetation as Sago palm.

With improvement in the classification approach and the use of more multi-date images, the accuracy of the results may be improved. This could be a subject of further research.

13.7 Evaluation of ALOS AVNIR-2, NDVI, Envisat ASAR IM and ASTER GDEM in Mapping Sago Palms

Incorporating NDVI, Envisat ASAR and ASTER GDEM datasets to an ALOS AVNIR-2 image can improve the accuracy of classifying Sago palms using MLC. It was clearly shown by both the separability analysis and the accuracy of the classifications that in the study area, spectral information alone acquired by ALOS AVNIR-2 sensor was not sufficient to accurately map Sago palms in such a way that there is no overestimation. The procedure of applying MLC to a combination of these multi-source datasets shows potential in mapping possible Sago palms locations in other areas in the Philippines.

However, there are issues that needs to be considered when the procedure is to be applied for mapping in other areas, which are

- availability of ALOS AVNIR-2 images
- availability of Envisat ASAR images co-incident with the ALOS AVNIR-2 images, preferably acquired in the same dates

During the time when this study was conducted, not all of Visayas and Mindanao are covered by Envisat ASAR IM and ALOS AVNIR-2 images. In some portions, there are ALOS AVNIR-2 images but the corresponding Envisat ASAR images are lacking.

In cases when ALOS AVNIR-2 images are the only available images, then the next best classification approach would be applying MLC to a stack of ALOS AVNIR-2 and ASTER GDEM. This combination has acceptable Producer's and User's Accuracy for Sago palm (96.26% and 87.38%).

Using 10 scenes of ALOS AVNIR-2 together with Envisat ASAR (in some scenes) and ASTER GDEM covering portions of several provinces in Visayas and Mindanao, a total of 5,238 hectares of possible Sago palm locations were mapped. The locations of the Sago palms detected using the ALOS AVNIR images were used to replace those detected from the Landsat images. This resulted to 2,855 hectares of detected possible Sago palm locations in Visayas and 11,624 hectares in Mindanao, that were subjected to confirmation and refinement.

13.8 Confirmation and refinement of detected possible locations of Sago palms

The detected possible locations of Sago palms in Visayas and Mindanao were examined with the aid of data from field surveys, and recent high resolution Worldview-2 images (purchased and those available in Google Earth) for their confirmation if they are indeed Sago palms or just results of misclassifications. Refinements in the extents of Sago palm stands were done during this stage.

Sago palm stands were confirmed in 4 provinces in Visayas and 13 provinces in Mindanao, with an aggregated total area of 914.04 hectares. In Visayas, all the confirmed Sago palm stands have an aggregated area of 252.87 hectares. Sago palms were found to be abundant in Leyte (215.70 has.), followed by Cebu (19.54 has) and Aklan (17.59 has). Very few Sago palms were found in Antique. Among the 30 municipalities in Visayas, Julita

(in Leyte) has the highest aggregated area of confirmed Sago palms at 71.18 hectares. None of the confirmed Sago palms in Visayas are within protected areas.

In Mindanao, all the confirmed Sago palm stands have an aggregated area of 661.17 hectares. Of this, 337.92 hectares are within protected areas, majority of which is found in Agusan del Sur, specifically in the La Paz and Bunawan municipalities. In these municipalities, 337.87 hectares of Sago palm stands are within the Agusan Marsh Wild Life Sanctuary. At the provincial level, Agusan del Sur has the highest total aggregated area of confirmed Sago palm stands (570.29 has), followed by Agusan del Norte (44.81 has), Sulu (19.67 has), Maguindanao (17.68 has), and Davao Oriental (2.72 has). The municipalities of La Paz, Bunawan and Veruela (all from Agusan del Sur) are the top 3 municipalities with the largest aggregated area of Sago palm stands (Table 33). They are followed by Butuan City, Prosperidad, Cotabato City, Jabonga, San Francisco and Sultan Kudarat.

There were provinces that confirmation and refinements were not done. In Visayas, confirmation surveys were not conducted in Capiz, Iloilo, Negros Occidental, Negros Oriental, western part of Leyte, Southern Leyte, and all Samar provinces. In Mindanao, due to security related concerns, surveys were not conducted in Zamboanga provinces, Misamis Occidental, Lanao del Norte, Lanao del Sur, North and South Cotabato, Maguindanao, Sultan Kudarat, and Sarangani. In Maguindanao, South Cotabato and Zamboanga Sibugay, the confirmation and refinements of detected Sago palm locations in these provinces relied on visual interpretation of high resolution satellite images available in Google Earth. This same method was used in the province of Sulu to map Sago palms although it was excluded during the process of Sago palm detection using Landsat 7 ETM+ and ALOS AVNIR-2 images. In all these mentioned province, confirmation and refinement of the detected Sago palms is necessary.

13.9 Habitat Suitability Analysis

Habitat suitability analysis of Sago palms in Visayas and Mindanao was aided by exploratory statistical analysis that determined the biophysical and bioclimatic characteristics of known Sago palm habitats. The information derived from the statistical analysis was then used in conjunction with bioclimatic models to create suitability rules that are then used to search for lands in Visayas and Mindanao where Sago palms can grow at a spatial resolution of one hectare (100 m x 100 m).

Of the three suitability maps that were generated, $SUIT_{BIOPHYSICALxDOMAIN}$ was found to be the most accurate at 93.52%. The relatively good accuracy of the suitability map generated in this study suggests that the biophysical and bioclimatic variables included in the generation of this map are sufficient enough to determine the distribution patterns of Sago palms at the spatial scales examined in this study. However, this hypothesis should be further evaluated by field survey and by expert opinion of botanists and ecologists familiar with the Sago palm.

The degree of suitability was determined through the use of the FAO *EcoCrop* model. Based on the suitability map, a total of 999,491 hectares of lands in Visayas and Mindanao were found to be biophysically and bioclimatically “suitable” for growing Sago palms. Of this, 415,260 hectares have “excellent” suitability while 104,020 hectares are “very suitable”. The municipalities with confirmed Sago palm stands and with "very suitable" to

“excellent” suitabilities were also identified in Visayas and Mindanao. If Sago palms are to be mass propagated, then these municipalities should be targeted since in these municipalities there is proof that Sago palms can actually grow. In Visayas, majority of these municipalities are in Leyte and Aklan. In Mindanao, majority are found in Agusan del Sur, Agusan del Norte, Surigao del Sur and Surigao del Norte.

While the study was able to identify specific locations of Sago palm suitable areas, the locations identified as should be interpreted as areas that have the biophysical and bioclimatic conditions suited for growing Sago palm. Factors such as existing land-uses/land-cover in the suitable areas, and socioeconomic conditions are not yet accounted. These factors must be accounted in order to narrow down the suitable areas only to those locations where it is indeed possible to grow Sago palms (e.g., you cannot grow Sago palms in built-up areas). An example of this would be determining whether a “suitable” area in the map has other land-uses (e.g., forest, protected area, cropland, grassland, etc.), and determining whether these suitable areas have favorable conditions for Sago palms to be propagated at plantation scale (i.e., nearness to water supply, roads, processing plants, etc.).

Problems Encountered

1. Problems in accessing the locations of Sago palm stands

The problems encountered by Sago Project II.2 are the same problems encountered by Sago Project II.3 with regards to accessing the locations of Sago palm stands.

A. The Sago Palm Environment

The location itself of the Sago area is a disadvantage because most of the Sago clusters are situated within marshy lands, wet lands and peat lands, hence, the trail leading to the Sago areas is muddy and most of the time very difficult to access (see for example, Figure 113). Also, it hindered the team to be at the exact location of Sago area.

As experienced in Brgy. Maharlika, Talacogon, Agusan del Sur, the project teams was not able to penetrate the Sago forest in the area because the local hires (guides) chose the route where the team has to pass through peat lands. Local hires of Brgy. Mambalili, Bunawan, Agusan del Sur also led the teams to a longer and muddy route to access the Sago area in the said municipality. But, after the conduct of the reconnaissance survey, the researchers identified a better route within the adjacent barangay to access the same Sago area. With this, the project teams strategized to remedy this problem for a smooth conduct of their subsequent fieldworks. Part of the goals of conducting reconnaissance survey before conducting on-site measurements then was the identification of best routes to access the Sago areas to save valuable time and efforts.

Figure 113. Some pictures showing difficulties in accessing the Sago palm areas.

B. Health Hazards

The prevalence of schistosomiasis was confirmed in most of the visited Sago palms stands (e.g., in Bunawan, Agusan del Sur; Jabonga, Agusan del Norte; and in all visited stands in Leyte). Safety precautions were carried out always by the survey teams to be safe from Schistosomiasis and from mosquitoes that are carrier of Malaria. The team made it as a safety rule to wear boots and appropriate safety suits at all times during fieldworks.

C. Security Considerations

Most of the Sago palms are thriving wild in remote areas where danger of including “rebel-infested” territories is high. Some of the reported vast Sago areas that were supposed to be part of the survey sites were already dropped from the list for security reasons. An example of this is the Liguasan Marsh and some provinces in Western Mindanao (Maguindanao, North Cotabato, Zamboanga provinces) which are also known for its unstable security condition. Hence, the project teams opted to make use of remotely-sensed data to confirm or locate these Sago areas.

There were also a number of survey areas which were safely penetrated by the project teams but were identified by locales to be nestled by insurgents. These areas are in the provinces of Davao Oriental, Compostela Valley, and Agusan del Sur (especially in Loreto).

2. Delay in the delivery of ALOS AVNIR-2 satellite images

Major delays were encountered in Sago palm detection and in habitat suitability analysis due to the delayed procurement and delivery of ALOS AVNIR-2 satellite images. It was only in late December 2012 that the satellite images. Aside from using them for Sago palm detection, the images are supposed to be processed to derive land-cover maps needed by Sago Project II.3 for their exploratory statistical analysis of Sago palm locations. The maps became available to Project II.2 beginning April 2013. Only after the availability of land-cover maps that the Project II.3 and Project II.2 jointly started working on the habitat suitability analyses.

Bibliography

[1] M. Flach, "Metroxylon Sagu Rottb. - Promoting the Conservation and Use of Underutilized and Neglected Crops," Institute of Plant Genetics and Crop Plant Research, Gatesleben/International Plant Genetic Resources, Rome, Italy, 1997.

[2] S Abd-Azis, "Sago starch and its utilization," *Journal of Bioscience and Bioengineering*, vol. 94, no. 6, pp. 526-529, 2002.

[3] K.B. Bujang, "Potentials of Bioenergy from the Sago Indistries in Malaysia," in *Biotechnology*, Malaysia, 2008.

[4] W McClatchey, H I Manner, and C R Elevitch, "Metroxylon amicarum, M. paulcoxii, M. sagu, M. salomonense, M. vitiense, and M. warburgii (sago palm)," in *Species Profiles for Pacific Island Agroforestry*, C R Elevitch, Ed. Hōlualoa, Hawaii, 2006, www.traditionaltree.org.

[5] R. S. Singhal et al., "Industrial productions, processing, and utilization of sago palm-derived products," *Carbohydrate Polymers*, pp. 1-20, 2008.

[6] W. R. Stanton, "Long-Term and Ancillary Environmental Benefits from Sago Agroforestry Systems," in *Fourth International Sago Symposium*, Kuching, Sarawak, Malaysia, 1991, pp. 24-35.

[7] T Acuna, S Concepcion, A J Fedillaga, N Laorden, and B Ramoneda, "Issues and challenges in the establishment of Sago plantation in the Philippines," in *2013 Biennial Convention of the Philippine Agricultural Economics and Development Association (PAEDA)*, Davao City, Philippines, 2013.

[8] D S Boyd and F M Danson, "Satellite remote sensing of forest resources: three decades of research," *Progress in Physical Geography*, vol. 29, no. 1, pp. 1-26, 2005.

[9] P J Pinter et al., "Remote sensing for crop management," *Photogrammetric Engineering and Remote Sensing*, vol. 69, no. 6, pp. 647-664, 2003.

[10] A R Josue and M Okazaki, "Sago cultivation in Northern Mindanao, Philippines," *Sago palm*, pp. 43-50, 2002.

[11] V C Calag and L S Maquinano, "Program I: Conservation of a Bioresource, Project I.1 Assessing the Sago Bioresource in Mindanao Using Remote Sensing Technology," Davao City, 2009.

[12] H. Ehara, "Potency of sago palm as carbohydrate resource for strengthening food security program," *Journal Agronomi Indonesia*, vol. 37, no. 3, 2010.

[13] W. J. Jang, A. D. Powell, and C. G. Oates, "Sago starch as a biomass source: raw sago starch hydrolysis by commercial enzymes," *Bioresource Technology*, vol. 55, pp.

55-61.

[14] A. Mohamed, B. Jamilah, K. A. Abbas, R. A. Rahman, and K. Roselina, "A review on physicochemical and thermorheological properties of sago starch," *American Journal of Agriculture and Biological Sciences*, vol. 3, no. 4, pp. 639-648, 2008.

[15] A. Kjær, A. S. Barford, C. B. Asmussen, and O. Seberg, "Investigation of genetic and morphological variation in the sago palm (Metroxylon sagu: Arecaceae) in Papua New Guinea," *Annals of Botany*, vol. 95, no. 1, p. 109, 2004.

[16] H. Ehara, S. Susanto, C. Mizota, S. Hirose, and T. Matsuno, "Sago palm (Metroxylon sagu, Arecaceae) production in the eastern archipelago of Indonesia: Variation in morphological characteristics and pith dry-matter yield," *Economic Botany*, vol. 54, no. 2, pp. 197-206, 2000.

[17] R. O. Ellen, "“Local knowledge and management of sago palm (Metroxylon sagu Rottboell) diversity in South Central Seram, Maluku, Eastern Indonesia," *Journal of Ethnobiology*, vol. 26, no. 2, pp. 258-298, 2006.

[18] Y. Kobayashi, "Local utilization of the sago palm (Metroxylon sagu) in southern Thailand," *Tropical Forestry*, no. 47, pp. 52-58, 2000.

[19] A. R. Josue and M. Okazi, "Stands of sago palms in Northern Mindanao, Philippines," *Sago Palm*, vol. 6, no. 1, pp. 24-27, 1998.

[20] L. L. Celiz, M. Okazaki, A. R. Josue, and K. Toyota, "Sago production and income analysis in Northern Mindanao," *Sago Palm*, vol. 10, no. 1, pp. 1-6, 2001.

[21] K. Toyota and M. Okazaki, "Sago in Cebu, Philippines - its growing area and utilization," *Sago Palm*, vol. 11, no. 1, pp. 18-20, 2003.

[22] L. L. Celiz, "Income analysis of sago (Metroxylon sagu) starch production in the municipality of Dulag, Leyte, Philippines," *Sago Palm*, vol. 12, no. 1, pp. 14-20, 2005.

[23] M. A. Quevedo, A. Loreto, A. M. Mariscal, O. Masanori, and K. Toyota, "Distribution and traditional uses of sago palms (Metroxylon sagu Rottb) in the Eastern and Central Visayas regions of the Philippines," *Sago Palm*, vol. 13, no. 2, pp. 17-25, 2005.

[24] Y. Yanai et al., "Sago in Aklan, Panay, Philippines - its growing area and utilization," *Sago Palm*, vol. 12, no. 1, pp. 21-23, 2005.

[25] A. Loreto, M. A. Quevedo, A. M. Mariscal, M. Okazaki, and K. Toyota, "Improvement of the traditional sago starch processing in the Philippines through mechanization," *Sago Palm*, vol. 14, no. 1, pp. 4-9, 2006.

[26] R. E. Kennedy et al., "). Remote sensing change detection tools for natural resource managers: Understanding concepts and tradeoffs in the design of landscape monitoring projects," *Remote Sensing of Environment*, vol. 113, no. 7, pp. 1382-1396,

2009.

[27] D. O. Fuller and R. R. Chowdhury, "Monitoring and modelling tropical deforestation: Introduction to the Special Issue," *Singapore Journal of Tropical Geography*, vol. 27, pp. 1-3, 2006.

[28] J. T. Kerr and M. Ostrovsky, "From space to species: ecological applications for remote sensing," *Trends in Ecology and Evolution*, vol. 18, no. 6, pp. 299-305, 2003.

[29] F. Yuan, K. E. Sawaya, B. C. Loeffelholz, and M. E. Bauer, "Land cover classification and change analysis of the Twin Cities (Minnesota) Metropolitan Area by multitemporal Landsat remote sensing," *Remote Sensing of Environment*, vol. 98, no. 2-3, pp. 317-328, 2005.

[30] G. M. Foody, "Remote sensing of tropical forest environments: towards the monitoring of environmental resources for sustainable development," *International Journal of Remote Sensing*, vol. 24, no. 20, pp. 4035-4046, 2003.

[31] S. R. Freitas, M. Mello, and C. Cruz, "Relationships between forest structure and vegetation indices in Atlantic Rainforest," *Forest Ecology and Management*, vol. 218, no. 1-3, pp. 353-362, 2005.

[32] J. C. Ingram, T. P. Dawson, and R. J. Whittaker, "Mapping tropical forest structure in southeastern Madagascar using remote sensing and artificial neural networks," *Remote Sensing of Environment*, vol. 94, no. 4, pp. 491-507, 2005.

[33] M. Wulder, "Optical remote-sensing techniques for the assessment of forest inventory and biophysical parameters," *Progress in Physical Geography*, vol. 22, no. 4, p. 449, 1998.

[34] S. Frolking, X. Xiao, Y. Zhung, W. Salas, and C. Li, "Agricultural land-use in China: a comparison of area estimates from ground-based census and satellite-borne remote sensing," *Global Ecology and Biogeography*, vol. 8, no. 5, pp. 407-416, 1999.

[35] S. K. Seelan, S. Laguette, G. M. Casady, and G. A. Seielstad, "Remote sensing applications for precision agriculture: A learning community approach," *Remote Sensing of Environment*, vol. 88, no. 1-2, pp. 157-169, 2003.

[36] T. A. Tsiligirides, "Remote sensing as a tool for agricultural statistics: a case study of area frame sampling methodology in Hellas," *Computers and Electronics in Agriculture*, vol. 20, no. 1, pp. 45-77, 1998.

[37] K. E. Sawaya, L. G. Olmanson, N. J. Heinert, P. L. Brezonik, and M. E. Bauer, "Extending satellite remote sensing to local scales: land and water resource monitoring using high-resolution imagery," *Remote Sensing of Environment*, vol. 88, no. 1-2, pp. 144-156, 2003.

[38] M. S. Chubey, S. E. Franklin, and M. A. Wulder, "Object-based analysis of Ikonos-2 imagery for extraction of forest inventory parameters," *Photogrammetric Engineering*

and Remote Sensing, vol. 72, no. 4, p. 383, 2006.

[39] S. J. Goetz, R. J. Wright, A. J. Smith, E. Zinecker, and E. Schaub, "IKONOS imagery for resource management: Tree cover, impervious surfaces, and riparian buffer analyses in the mid-Atlantic region," *Remote Sensing of Environment*, vol. 88, no. 1-2, pp. 195-208, 2003.

[40] I. Ozdemir and A. Karnieli, "Predicting forest structural parameters using the image texture derived from WorldView-2 multispectral imagery in a dryland forest, Israel," *International Journal of Applied Earth Observation and Geoinformation*, vol. 13, no. 5, pp. 701-710, 2011.

[41] L. Wang, W. P. Sousa, and G. S. Biging, "Comparison of IKONOS and QuickBird images for mapping mangrove species on the Caribbean coast of Panama," *Remote Sensing of Environment*, vol. 91, no. 3-4, pp. 432-440, 2004.

[42] C. D. Lelong and A. Thong-Chane, "Application of textural analysis on very high resolution panchromatic images to map coffee orchards in Uganda," *Geoscience and Remote Sensing Symposium*, vol. 2, pp. 1007-1009, 2003.

[43] Y. Tian, B. Wu, W. Xu, J. Huang, and W. Xu, "An effective field method of crop proportion survey in China based on GVG integrated system," *Geoscience and Remote Sensing Symposium*, vol. 6, pp. 4028-4030, 2004.

[44] J. Shen, J. Liu, X. Lin, R. Zhao, and S. Xu, "Cropland Extraction from Very High Spatial Resolution Satellite Imagery by Object-Based Classification Using Improved Mean Shift and One-Class Support Vector Machines," *Sensor Letters*, vol. 9, no. 3, pp. 997-1005, 2011.

[45] I. L. Castillo-Gonzalez et al., "Object-and pixel-based analysis for mapping crops and their agro-environmental associated measures using QuickBird imagery," *Computers and Electronics in Agriculture*, vol. 68, no. 2, pp. 207-215, 2009.

[46] M. S. Moran, Y. Inoue, and E. M. Barnes, "Opportunities and limitations for image-based remote sensing in precision crop management," *Remote Sensing of Environment*, vol. 61, no. 3, pp. 319-346, 1997.

[47] Y. Lehahn, "Recovering missing data in cloudy high resolution ocean color images using kriging," *Geophysical Research Abstracts*, vol. 9, pp. 53-64, 2007.

[48] F. Melgani, "Contextual reconstruction of cloud-contaminated multitemporal multispectral images," *IEEE Transactions on Geoscience and Remote Sensing*, vol. 44, no. 2, pp. 442-455, 2006.

[49] F. M. Henderson and A. J. Lewis, *Introduction, in Principles and Applications of Imaging Radar*. Canada: John Wiley & Sons, 1998.

[50] T. Le Toan et al., "Relating radar remote sensing of biomass to modelling of forest

carbon budgets," *Climatic Change*, vol. 67, no. 2, pp. 379-402, 2004.

[51] M. Moghaddam, S. Durden, and H. Zebker, "Radar measurement of forested areas during OTTER," *Remote Sensing of Environment*, vol. 47, no. 2, pp. 154-166, 1994.

[52] J. Hyyppa et al., "Accuracy comparison of various remote sensing data sources in the retrieval of forest stand attributes," *Forest Ecology and Management*, vol. 128, no. 1-2, pp. 109-120, 2000.

[53] S. L. Durden, J. J. Van Syl, and H. A. Zebker, "Modeling and observation of the radar polarization signature of forested areas," *IEEE Transactions on Geoscience ans Remote Sensing*, vol. 27, no. 3, pp. 290-301, 1989.

[54] T. Kurosu, M. Fujita, and K. Chiba, "Monitoring of rice crop growth from space using the ERS-1 C-band SAR," *IEEE Transactions on Geoscience and Remote Sensing*, vol. 33, no. 4, pp. 1092-1096, 1995.

[55] H. McNairn and B. Brisco, "The application of C-band polarimetric SAR for agriculture: a review," *Canadian Journal of Remote Sensing*, vol. 30, no. 3, pp. 525-542, 2004.

[56] G. Simone, A. Farina, F. C. Morabito, S. B. Serpico, and L. Bruzzone, "Image fusion techniques for remote sensing applications," *Information Fusion*, vol. 3, no. 1, pp. 3-15, 2002.

[57] B. Haack and M. Bechdol, "Integrating multisensor data and RADAR texture measures for land cover mapping," *Computers & Geosciences*, vol. 26, no. 4, pp. 411-421, 2000.

[58] E. Rignot, W. A. Salas, and D. L. Skole, "Mapping deforestation and secondary growth in Rondonia, Brazil, using imaging radar and thematic mapper data," *Remote Sensing of Environment*, vol. 59, no. 2, pp. 167-179, 1997.

[59] D. G. Leckie, "Synergism of synthetic aperture radar and visible/infrared data for forest type discrimination," *Photogrammetric Engineering & Remote Sensing*, vol. 56, no. 9, pp. 1237-1246, 1990.

[60] H. McNairn, C. Champagne, J. Shang, D. Holmstrom, and G. Reichert, "Integration of optical and Synthetic Aperture Radar (SAR) imagery for delivering operational annual crop inventories," *ISPRS Journal of Photogrammetry adn Remote Sensing*, vol. 64, no. 5, pp. 434-449, 2009.

[61] D. Lu, "The potential and challenge of remote sensing-based biomass estimation," *Journal of Remote Sensing*, vol. 27, no. 7, pp. 1297-1328, 2006.

[62] J. M. Chen and J. Cihlar, "Retrieving leaf area index of boreal conifer forests using Landsat TM images* 1," *Remote Sensing of Environment*, vol. 55, no. 2, pp. 153-162, 1996.

[63] F. M. Danson, C. S. Rownland, S. E. Plummer, and P.R. J. North, "Comparison of models for simulating forest canopy reflectance," *Physical measurements &*

Signatures in remote sensing, pp. 475-480, 2001.

[64] J. Franklin, "Predictive vegetation mapping: geographic modelling of biospatial patterns in relation to environmental gradients," *Progress in Physical Geography*, vol. 19, no. 4, pp. 474-499, 1995.

[65] NOAA Center for Coastal Monitoring And Assessment. Global Change Master Directory. [Online]. http://gcmd.nasa.gov/KeywordSearch/Metadata.do?Portal=GCMD_Services&KeywordPath=ServiceParameters|MODELS|DYNAMIC+VEGETATION%2FECOSYSTEM+MODELS&EntryId=NOAA_HSM&MetadataView=Full&MetadataType=1&lbnode=mdlb3

[66] R. Store and J. Kangas, "Integrating spatial multi-criteria evaluation and expert knowledge for GIS-based habitat suitability modelling," *Landscape and Urban Planning*, vol. 55, no. 2, pp. 79-93, 2001.

[67] A. H. Hirzel and G. Le Lay, "Habitat suitability modelling and niche theory," *Journal of Applied Ecology*, vol. 45, no. 5, pp. 1372-1381, 2008.

[68] A. H. Hirzel, G. Le Lay, V. Helfer, C. Randin, and A. Guisan, "Evaluating the ability of habitat suitability models to predict species presences," *Ecological Modelling*, vol. 199, no. 2, pp. 142-152, 2006.

[69] A. H. Hirzel, J. Hausser, D. Chessel, and N. Perrin, "Ecological-niche factor analysis: how to compute habitat-suitability maps without absence data?," *Ecology*, vol. 83, no. 7, pp. 2027-2036, 2002.

[70] H. Padalia, R. R. Bharti, Y. P. S. Pundir, and K. P. Sharma, "Geospatial Multiple Logistic Regression Approcah for Habitat Characterization of Scarce Plant Population: A Case Study of Pittosporum Eriocarpum Royle (An Endemic Soecies of Uttarakhand, India)," *Journal of Indian Society of Remote Sensing*, vol. 38, pp. 513-521, 2010.

[71] L. B. Prasetyo, "Distribution of Sago Palm (Metroxylon spp) and Habitat Distribution Prediction at Pulau Seram, Maluku Province," 2010.

[72] Jeffrey T. Morisette et al., "A tamarisk habitat suitability map for the continental United States," *Frontiers in Ecology and the Environment*, vol. 4, no. 1, pp. 11-17, 2006.

[73] J. N. Stokland, R. Halvorsen, and B. Stoa, "Species distribution modelling - Effect of design and sample size of pseudo-absence observations," *Ecological Modelling*, vol. 222, no. 11, pp. 1800-1809, 2011.

[74] D. I. Warton and L. C. Shepherd, "Poisson point process model solve the "pseudo-absence problem" for prsence-only data in ecology," *The Annals of Applied Statistics*, vol. 4, no. 3, pp. 1383-1402, 2010.

[75] J. VanDerWal, L. P. Shoo, C. Graham, and S. E. Williams, "Selecting pseudo-absence data for presence-only distribution modeling: How far should you stay from what you

now?," *Ecological modelling*, vol. 220, no. 4, pp. 589-594, 2009.

[76] H. Nix, "A biogeographic analysis of Australian elapid snakes. - In Longmore, R. (ed), Atlas of elapid snakes of Australia, Bureau of flora and Fauna," *Canberra*, pp. 4-15, 1986.

[77] G Carpenter, A N Gillison, and J Winter, "DOMAIN: a flexible modeling procedure for mapping potential distributions of plants and animals," *Biodiversity and Conservation*, vol. 2, pp. 667-680, G. Carpenter, A.N. Gillison and J. Winter 1993.

[78] A. Hirzel and A. Guisan, "Which is the optimal sampling strategy for habitat suitability modeling," *Ecological Modelling*, vol. 157, no. 2, pp. 331-341, 2002.

[79] S. J. Phillips, "A maximum entropy approach to species distribution modeling. - In Brodley, C.E. (ed), Machine learning.," in *Twenty-first Century International Conference on Machine Learning*, Banff, Canada, 2004.

[80] S. J. Phillips, "Maximum entropy modeling of species geographic distributions," *Ecol. Modell.*, vol. 190, pp. 231-259, 2006.

[81] P. A. Hernandez, C. H. Graham, L. L. Master, and D. L. Albert, "The effect of sample size and species characteristics on performance of different species distribution modeling methods," *Ecography*, vol. 29, no. 5, pp. 773-785, 2006.

[82] L. J. Beaumont, L. Hughes, and M. Poulsen, "Predicting species distributions: use of climatic parameters in BIOCLIM and its impact on predictions of species' current and future distributions," *Ecological Modelling*, vol. 186, no. 2, pp. 251-270, 2005.

[83] P. A. Stankowski and w. H. Parker, "Species distribution modelling: Does one size fit all? A phytogeographic analysis of< i> Salix in Ontario," *Ecological Modelling*, vol. 221, no. 13, pp. 1655-1664, 2010.

[84] A. Guisan and N. E. Zimmerman, "Predictive habitat distribution models in ecology," *Ecological Modelling*, vol. 135, pp. 147-186, 2000.

[85] F. Skov, "Potential plant distribution mapping based on climatic similarity," *Taxon.*, vol. 49, pp. 503-515, 2000.

[86] V. A. Funk and K. S. Richradson, "Systematic data in biodiversity studies: use it or lose it.," *Systematic Biology*, vol. 51, pp. 303-316, 2002.

[87] J. H. Vargas, T. Consiglio, P. M. Jorgensen, and T. B. Croat, "Modelling distribution patterns in a species-rich plant genus, Anthurium (Araceae), in Ecuador," *Diversity and Distributions*, vol. 10, no. 3, pp. 211-216, 2004.

[88] B. W. Heumann, S. J. Walsh, and P. M. McDaniel, "Assessing the application of a geographic presence-only model for land suitbaility mapping," *Ecological informatics*, vol. 6, no. 5, pp. 257-269, 2011.

[89] P. H. Evangelista, S. Kumar, T. J. Stohlgren, and N. E. Young, "Assessing forest vulnerability and the potential distribution of pine beetles under current and future climate scenarios in the Interior West of the US.," *Forest Ecology and Management*, vol. 262, no. 3, pp. 307-316, 2011.

[90] S. Kumar and T. J. Stohlgren, "Maxent modeling for predicting suitable habitat for threatened and endangered tree Canacomyrica monticola in New Caledonia," *Joournal of Ecology and Natural Environment*, vol. 1, no. 4, pp. 94-98, 2009.

[91] A. M. Van Doorn and M. M. Bakker, "The destination of arable land in a marginal agricultural landscape in South Portugal: an exploration of land use change determinants," *Landscape ecology*, vol. 22, no. 7, pp. 1073-1087, 2007.

[92] ESA. (2012, May) ESA declares end of mission for Envisat. [Online]. http://www.esa.int/Our_Activities/Observing_the_Earth/Envisat/ESA_declares_end_of_mission_for_Envisat

[93] ESA. ASAR. [Online]. https://earth.esa.int/web/guest/missions/esa-operational-eo-missions/envisat/instruments/asar

[94] A C Tamhane, "Multiple comparisons in model I one-way ANOVA with unequal variances," *Communications in Statistics-Theory and Methods*, vol. 6, no. 1, pp. 15-32, 1977.

[95] CRISP. (2001) Interpreting SAR Images. [Online]. http://www.crisp.nus.edu.sg/~research/tutorial/sar_int.htm

[96] X Wang, Q Wang, F Ling, X Zhu, and h Jiang, "Principal component analysis and its application on banana fields mapping using ENVISAT ASAR data in Zhangzhou, Fujian province," *Geo-spatial Information Science*, vol. 12, no. 2, pp. 142-145, 2009.

[97] P Maillard, T Alencar-Silva, and D A Clausi, "An evaluation of RADARSAT-1 and ASTER data for mapping veredas (palm swamps)," *Sensors*, vol. 8, no. 9, pp. 6055-6076, 2008.

[98] R. J. Hijmans, L. Guarino, and P. Mathur. (2012) DIVA GIS Version 7.5 Manual. [Online]. http://www.diva-gis.org/docs/DIVA-GIS_manual_7.pdf

[99] R J Hijmans, S E Cameron, J L Parra, P G Jones, and A Jarvis, "Very high resolution interpolated climate surfaces for global land areas," *International Journal of Climatology*, vol. 25, no. 15, pp. 1965-1978, 2005.

[100] S M Davis et al., *Remote Sensing: The Quantitative Approach*. New York: McGraw-Hill, 1978.

[101] A Shalaby and R Tateishi, "Remote sensing and GIS for mapping and monitoring land-cover and land-use changes in the Northwestern coastal zone of Egypt," *Applied Geography*, vol. 27, pp. 28-41, 2007.

[102] J A Richards and X Jia, *Remote Sensing Digital Image Analysis*. Berlin: Springer-Verlag, 1999.

[103] P Watanachaturaporn, M K Arora, and P K Varshney, "Multisource classification using support vector machines: an empirical comparison with decision tree and neural network classifiers," *Photogrammetric Engineering and Remote Sensing*, vol. 74, pp. 239-246, 2008.

[104] A Elumnoh and R P Shrestha, "Application of DEM data to Landsat image classification: evaluation in a tropical wet-dry landscape of Thailand," *Photogrammetric Engineering & Remote Sensing*, vol. 66, no. 3, pp. 297-304, 2000.

[105] J R Jensen, *Introductory Digital Image Processing: A Remote Sensing Perspective*, 2nd ed.: Prentice-Hall, 1996.

[106] A G Laborte, A A Maunahan, and R J Hijmans, "Spectral signature generalization and expansion can improve the accuracy of satellite image classification," *Plos One*, vol. 5, no. 5, p. e10516, 2010.

[107] K I Ahmed, "Envisat ASAR for Land Cover Mapping and Change Detection," Royal Institute of Technology, Stockholm, Sweden, MS Thesis 2006.

[108] M W Lang, E S Kasischke, S D Prince, and K W Pittman, "ssessment of C-band synthetic aperture radar data for mapping and monitoring Coastal Plain forested wetlands in the Mid-Atlantic Region, USA," *Remote Sensing of Environment*, vol. 112, pp. 4120-4130, 2008.

[109] L D Pereira, C D Freitas, S J Sant'Anna, D Lu, and E F Moran, "Optical and radar data integration for land use and land cover mapping in the Brazilian Amazon," *GIScience and Remote Sensing*, vol. 50, pp. 301-321, 2013.

[110] J. Jenness. (2005) Random point generator (randpts.avx) extension for ArcView 3.x, v. 1.3. [Online]. http://www.jennessent.com/arcview/random_points.htm

[111] B. A. Loiselle et al., "Predicting species distributions from herbarium collections: does climate bias in collection sampling influence model outcomes?," *Journal of Biogeography*, vol. 35, no. 1, pp. 105-116, 2008.

[112] A. Lane and Andrew Jarvis, "Changes in climate will modify the geography of crop suitability: agricultural biodiversity can help with adaptation," *Journal of Semi-arid Tropical Agricultural Research*, vol. 4, no. 1, pp. 1-12, 2007.

[113] W. H. Maes, A. Trabucco, W. M. Achten, and B. Muys, "Climatic growing conditions of Jatropha curcas, L.," *Biomass and bioenergy*, vol. 33, no. 10, pp. 1481-1485, 2009.

[114] R. T. Belote, S. Prisley, R. H. Jones, M. Fitzpatrick, and K. de Beurs, "Forest productivity and tree diversity relationships depend on ecological context within mid-Atlantic and Appalachian forests (USA)," *Forest Ecology and Management*, vol. 261,

no. 7, pp. 1315-1324, 2011.

[115] Will McClatchey, Harley I. Manner, and Craig R. Elevitch, "Metroxylon amicarum, M. paulcoxii, M. sagu," *Species Profiles for Pacific Island Agroforestry*, 2006.

[116] FAO. (2007) Ecocrop Dataset for Metroxylon sagu. [Online]. http://ecocrop.fao.org/ecocrop/srv/en/dataSheet?id=1466

[117] D. Houlder, M. Hutchinson, H. Nix, and J. McMahon, "ANUCLIM," in *Centre for Resource and Environment Studies*, Canberra.

[118] B. A. Loiselle et al., "Avoiding pitfalls of using species distribution models in conservation planning," *Conservation biology*, vol. 17, no. 6, pp. 1591-1600, 2003.

[119] J.B. Avé, "Sago in Insular South-East Asia: Historical Aspects and Contemporary Use," in *1st International Sago Symposium*, Kuching, Malaysia, 1977, pp. 21-30.

[120] D. M. Flores, "The Versatile Sago (Metroxylon Sagu) and Its Green Potential for Mindanao," *Banwa: The Multidisciplinary Journal of UP Mindanao*, pp. 8-15, 2008.

[121] J. Avé, "Safo in Insular South-East Asia: Historical Aspects and Contemporary Use," in *1st International Sago Symposium*, Kuching, Malaysia, 1997.

[122] M. Flach, "Metroxylon Sagu Rottb. - Promoting the Conservation and Use of Underutilized and Neglected Crops," in *International Plant Genetic Resources*, Rome, Italy, 1997.

[123] K. Bujang, "Potentials of Bioenergy from the Sago Industries in Malaysia," *Biotechnology*, 2008.

[124] R. J. Hijmans, L. Guarino, M. Cruz, and E. Rojas, "Computer tools for spatial analysis of plant genetic resources data," *Plant Genetic Resources Newsletter 127*, pp. 15-19, 2001.

[125] R. F. Isbell, "The Australian Soil Classification," Melbourne, Australia, 1996.